

DIALLYL POLYSULFIDES FROM GARLIC

MODE OF ACTION AND APPLICATIONS IN AGRICULTURE

Miriam Arbach

A thesis submitted for the degree of Doctor of Philosophy



University of East Anglia

School of Pharmacy

July 2014

© "This copy of the thesis has been supplied on condition that anyone who consults it is understood to recognise that its copyright rests with the author and that use of any information derived there from must be in accordance with current UK Copyright Law. In addition, any quotation or extract must include full attribution."

Declaration

This thesis is submitted to the University of East Anglia for the Degree of Doctor of Philosophy and has not been previously submitted at this or any university assessment or for any other degree. Except where stated, and reference and acknowledgment is given, this work is original and has been carried out by the author alone.

Miriam Arbach

Published work within this thesis

Sharma, S. V., Arbach, M., Roberts, A. A., Macdonald, C. J., Groom, M., and Hamilton, C. J. (2013) Biophysical Features of Bacillithiol, the Glutathione Surrogate of *Bacillus subtilis* and other Firmicutes, *ChemBioChem* 14, 2160-2168.

Acknowledgements

I would like to thank my supervisors Dr. Chris Hamilton, Dr. Murree Groom and Prof. Nick Le Brun for giving me the opportunity to work with great freedom on this exciting and extremely diverse project. Thank you for your support and advice and especially your enthusiasm, never-ending stream of ideas and great interest in my work. Thank you, Chris, for seeing the connection between garlic and thiols, for welcoming a plant-biologist in your lab and being so open minded to new ideas and research areas. For all the time you spent discussing my work, paying attention to detail and thinking about clever experiments to do. Murree, it was a pleasure working with you, thanks for the insights in crop protection, plant pathogens and field trial design from a very practical perspective and for your colourful explanations.

Special thanks to Dr. Sunil Sharma and Dr. Alex Roberts who guided me through my PhD journey from the beginning and from whom I learned so much. Thank you for all your patience, the good time we had together and for creating such a good working and learning atmosphere in the lab. I remember very well how I started off nearly four years ago, not even knowing what an NMR machine is good for. All the chemistry-specific techniques and equipment were new to me, but thanks to Sunil's endless patience in explaining and being able to simplify things, slowly it started to make sense. Thanks to Alex who worked so hard, but still managed to keep her good mood and always took the time to share her widespread knowledge. It was a great experience working with the two of you.

I would also like to thank ECOspray Ltd. , especially David Sadler-Bridge, Dr. Awais Anwar and Stephen Silvester, for the opportunity to work with them and get insights in the company. It is fascinating to see a small company with few people achieving such great things. Thank you for the funding which enabled me to bring the work to a good finish.

Thanks to everyone who was involved in the RedCat Network, especially Prof. Claus Jacob who coordinated the project so well and Prof. Alan Slusarenko and his lab members who supported me in the first few challenging months. It was a great opportunity to work and learn in a multidisciplinary and international environment and the numerous meetings we had were very inspiring and enjoyable.

Thanks to Dr. Colin Fleming, who enabled me to work on root-knot nematodes, shared his experience, and performed soil sample analyses for this project.

Thanks to the great HPLC expert, Dr. Charles Brearley, who always helped with spare HPLC parts, suggestions and repair skills on the few occasions when we experienced HPLC breakdowns.

In addition, all the groups in the School of Pharmacy, School of Chemistry and School of Biology, and in particular the Medicinal Chemistry groups, who lent me chemicals, equipment and a sympathetic ear. Thank you all for making my time at UEA so enjoyable.

My final thanks go to my family and friends who have always been supportive. Special thanks to Martin for listening to all my worries or excitements, for not complaining about never-ending evenings in the lab or the library, and for cooking all the food and washing all the dishes during the write-up period, I could get used to that...

Abstract

Garlic (*Allium sativum*) contains a wide range of organosulfur compounds which show a variety of biological effects including broad spectrum antibacterial, antifungal and antiviral activity, as well as selective anticancer activity. One highly bioactive class of compounds from garlic are diallyl polysulfides (DAS), containing one to six sulfur atoms in a linear chain. The bioactivity of DAS has been shown to increase with increasing sulfur chain length up to DAS4 and in this study the even higher bioactivity of DAS5 and DAS6 was demonstrated.

The bioactivity of DAS is believed to be initiated following initial reaction with intracellular low molecular weight (LMW) and protein thiols. In this study the interaction between DAS and LMW thiols was investigated and for the first time the reduced DAS metabolites allyl hydrodisulfides have been detected *in vitro* and *in vivo* in the Gram positive bacterium *Bacillus subtilis*. Additionally, formation of mixed polysulfides between DAS and LMW thiols with up to five sulfur atoms was observed *in vitro*. Proteomic studies revealed a large number of proteins in *B. subtilis* that formed mixed di- and trisulfides with DAS. Therefore multiple points of DAS attack have been proven and the disturbance of the cellular redox status through lowering the pool of reduced LMW thiols was established in two different organisms (*B. subtilis* and the nematode *Steinernema feltiae*).

To exploit the polysulfide chemistry for the development of a “green” nematicide, the nematicidal activity of DAS was investigated in bioassays as well as the efficacy of DAS formulations towards plant pathogenic nematodes (*Meloidogyne* spp. and *Globodera* spp.) in potato and carrot field trials. It was demonstrated that the DAS derived nematicides form an equally effective alternative compared to synthetic nematicides at a much lower environmental and health risk.

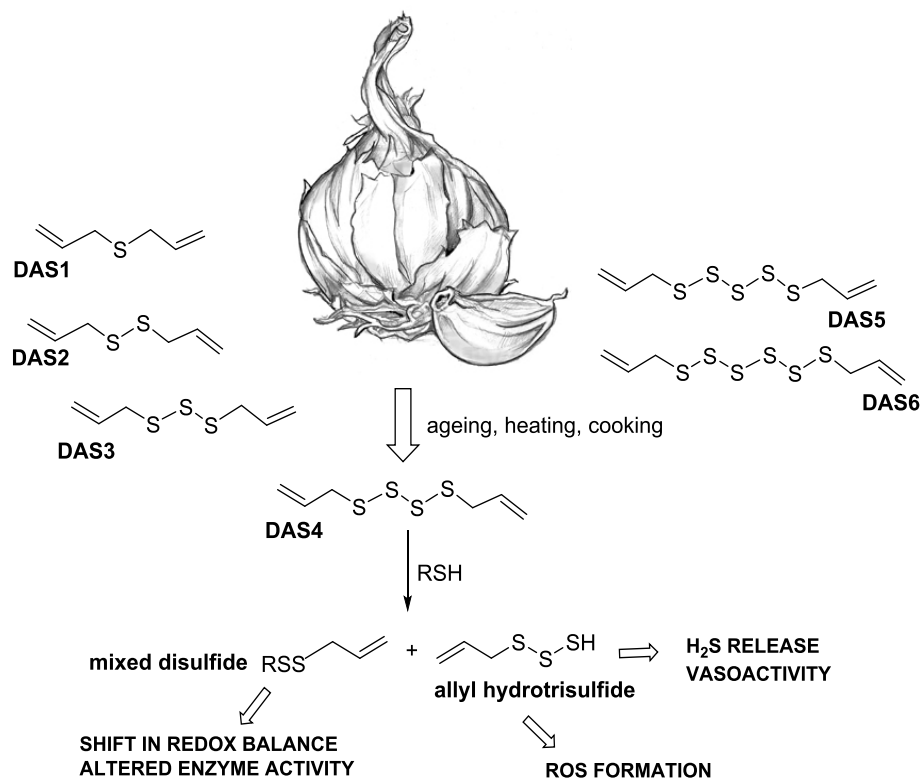


Table of Contents

Acknowledgements	3
Abstract	4
Table of Contents	5
List of Figures	9
List of Tables	13
Abbreviations	15
1 Introduction	19
1.1 Organosulfur compounds occurring in garlic	20
1.1.1 Overview	20
1.1.2 Organosulfur storage compounds of whole garlic cloves	21
1.1.3 Allicin and related sulfinates	22
1.1.4 Allicin transformations	23
1.2 Diallyl polysulfides (DAS)	26
1.2.1 Formation of DAS	26
1.2.2 Dietary uptake of DAS through garlic oil or cooked garlic	27
1.2.3 Bioactivity of DAS	27
1.2.4 Mode of action of DAS	29
1.3 Low molecular weight thiols and redox systems in different organism	35
1.3.1 Overview	35
1.3.2 Glutathione	36
1.3.3 Bacillithiol	38
1.3.4 Cysteine	40
1.3.5 Coenzyme-A	40
1.3.6 Interaction between DAS and LMW and protein thiols	41
1.4 Objectives and strategy of this project	43
2 Diallyl polysulfides and their reactivity with low molecular weight thiols	45
2.1 Synthesis, purification and characterisation of diallyl polysulfides	45
2.1.1 Synthesis of DAS	45
2.1.2 Purification and isolation of DAS3 to DAS6	46
2.1.3 Characterisation of DAS	47
2.2 Stability of DAS	51
2.3 Reactivity of DAS with low molecular weight thiols	54
2.4 The reduced form of DAS	54
2.4.1 Formation of allyl perthiol (AS ₂ H)	54
2.4.2 Formation of allyl hydrotrisulfide (AS ₃ H)	58
2.5 Formation of mixed allyl-glutathione sulfides (AGS(2-5))	60

2.5.1	DAS2 and GSH form mixed disulfide	60
2.5.2	DAS3 and GSH form mixed di- and trisulfide and liberate AS ₂ H	62
2.5.3	DAS3 to DAS6 all form mainly mixed di- and trisulfide upon reaction with GSH	66
2.6	Formation of mixed allyl-bacillithiol sulfides (ABS(2-4))	67
2.6.1	DAS2 and BSH form mixed disulfide	67
2.6.2	DAS5 and BSH form a mixture of mixed di- to tetrasulfide (ABS(2-4)).....	68
2.7	Formation of mixed allyl-cysteine sulfides (ACS(2-4)).....	70
2.7.1	DAS2 and Cys form mixed disulfide (ACS ₂) and cystine (CySS)	70
2.7.2	DAS5 and Cys form a mixture of CySS and mixed di- to tetrasulfide (ACS(2-4)).	73
2.8	Reactivity of DAS5 towards different thiols	74
2.8.1	Comparison of the reactivity of DAS5 with GSH vs. Cys	74
2.8.2	Comparison of the reactivity of DAS5 with BSH vs. Cys.....	75
2.9	Initial product formation upon DAS reacting with GSH	76
2.9.1	Experimental methods to measure product formation over time	76
2.9.2	Initial product formation upon reaction of DAS3 with GSH	78
2.9.3	Initial product formation upon reaction of DAS4 with GSH	81
2.9.4	Initial product formation upon reaction of DAS5 with GSH	82
2.9.5	Reaction rates of different DAS with GSH.....	84
2.10	Summary and Conclusions	86
3	Structure-activity relationship and mode of action of diallyl polysulfides – investigated on the model organism <i>Bacillus subtilis</i>	88
3.1	Introduction	88
3.1.1	Aims and overview of this chapter	88
3.1.2	Model organism: <i>Bacillus subtilis</i>	88
3.2	Structure-activity relationship of DAS determined through <i>B. subtilis</i> growth experiments.....	88
3.2.1	Methodology.....	89
3.2.2	MIC determinations of DAS towards the <i>B. subtilis</i> WT and the <i>bshA</i> ⁻ mutant..	91
3.2.3	DAS induced dose dependent growth inhibition of <i>B. subtilis</i>	93
3.2.4	BSH helps <i>B. subtilis</i> to recover from DAS stress	94
3.3	Hypothesis for the interaction of DAS with cellular thiols	95
3.4	LMW thiol and disulfide levels in <i>B. subtilis</i>	97
3.4.1	Methodology.....	97
3.4.2	LMW thiol and disulfide levels in <i>B. subtilis</i> under non-stress conditions.....	97
3.4.3	Influence of DAS3 on thiol and disulfide levels in the <i>B. subtilis</i> WT and the <i>bshA</i> ⁻ mutant.....	100
3.4.4	Influence of DAS4 on LMW thiol and disulfide levels in the <i>B. subtilis</i> WT	104

3.5	Posttranslational modification of protein thiols as a consequence of DAS treatment	108
3.5.1	Bacillithiolation of proteins.....	108
3.5.2	S-Allylation of proteins after DAS4 treatment	110
3.6	Summary and Conclusions	112
4	Influence of diallyl polysulfides on (plant pathogenic) nematodes and applications in crop protection	114
4.1	Plant pathogenic nematodes	114
4.1.1	Root-knot nematodes (<i>Meloidogyne</i> spp.)	115
4.1.2	Potato cyst nematodes (<i>Globodera</i> spp.)	116
4.1.3	Crop protection against pathogenic nematodes in the UK - practices and challenges	118
4.1.4	Nematicidal effects of garlic	119
4.1.5	Glutathione redox system in nematodes.....	119
4.2	<i>In vitro</i> nematicidal activity of DAS	120
4.2.1	Nematicidal activity of DAS against <i>Steinernema feltiae</i>	120
4.2.2	Nematicidal activity of DAS against <i>Meloidogyne minor</i>	122
4.3	Mode of action of nematicidal activity of DAS	123
4.3.1	LMW thiol concentrations in <i>S. feltiae</i> under non-stress conditions.....	123
4.3.2	Influence of DAS3 on LMW thiol and disulfide levels in <i>S. feltiae</i>	124
4.3.3	Intra- and extracellular DAS levels detected in <i>S. feltiae</i>	126
4.3.4	Summary and proposed MOA.....	127
4.4	Field trials	129
4.4.1	From <i>in vitro</i> nematicidal activity in bioassays to an effective nematicide	129
4.4.2	Garlic formulations from ECOSpray Ltd.	130
4.4.3	Carrot Field Trials – Control of Root-knot nematodes.....	131
4.4.3.1	Trial design	131
4.4.3.2	Nematode	131
4.4.4	Potato field trial - Control of potato cyst nematodes.....	135
4.5	Summary and Conclusions	141
5	Conclusions and Outlook.....	143
6	Materials and Methods.....	146
6.1	Materials and general experimental methods	146
6.2	Synthesis, purification and characterisation	147
6.2.1	Synthesis, purification and characterisation of diallyl polysulfides (DAS) ⁽⁸³⁾ ...	147
6.2.2	Synthesis and purification of thiol-monobimane (thiol-mB) standards	148

6.2.3	Synthesis and characterisation of mixed polysulfides	154
6.3	Analytical Methods	158
6.3.1	HPLC	158
6.3.2	LC-MS	159
6.4	<i>In vitro</i> reactions between DAS and LMW thiols	159
6.4.1	Formation of reduced DAS.....	159
6.4.2	Formation of mixed polysulfides	160
6.5	<i>In vivo</i> experiments	163
6.5.1	Bacteria	163
6.5.2	Nematodes.....	168
6.6	Field trials	170
6.6.1	Carrot trial.....	170
6.6.2	Potato trial	171
6.6.3	Statistical analysis	172
Appendix 1 : Methodology to quantify LMW thiols and disulfides in cell extracts of <i>B. subtilis</i> and <i>S. feltiae</i>		173
1.1	Methodology overview.....	173
1.2	Synthesis and characterisation of fluorescent thiol adducts as HPLC standards ..	175
1.2.1	Preparation of qualitative standards	176
1.2.2	Preparation of quantitative standards.....	176
1.3	LMW thiol labelling of cell extracts of. <i>B. subtilis</i>	177
1.4	Disulfide analysis of cell extracts from <i>B. subtilis</i>	180
1.4.1	Original protocol for disulfide analysis in cell extracts (Method 1)	181
1.4.2	Improved protocol for disulfide analysis in cell extracts (Method 2) ⁽¹⁶¹⁾	184
1.4.3	Development of disulfide analysis Method 3	186
1.4.4	<i>In vivo</i> comparison of disulfide Methods 1,2 and 3.....	188
1.5	Method development for thiol and disulfide analysis in <i>S. feltiae</i>	190
References		190
Publications		

List of Figures

Chapter 1

Figure 1.1: Overview of produced organosulfur compounds upon crushing of garlic.

Figure 1.2: Chemical structures of organosulfur compounds produced in garlic.

Figure 1.3: Structures of S-alkylcysteine sulfoxides found in garlic.

Figure 1.4: Transformation of the main thiosulfinates from garlic.

Figure 1.5: Suggested mechanism for the formation of DAS from alliin.

Figure 1.6: Different biological activities of DAS from garlic.

Figure 1.7: Possible reactions of DAS3 and their physiological consequences.

Figure 1.8: Reaction of DAS2 and DAS3 with thiols.

Figure 1.9: DAS induced reactive oxygen species (ROS) production indirectly leads to thiol oxidation.

Figure 1.10: Superoxide radical formation and hydrogen sulfide liberation induced by allyl perthiol.

Figure 1.11: LMW thiols produced by different organisms.

Figure 1.12: The main cellular functions of low molecular weight thiols.

Figure 1.13: Oxidation of Cys residues of proteins to sulfenic acid by oxidants (e.g. H₂O₂) can have damaging or regulatory effects.

Figure 1.14: Biosynthesis of bacillithiol.

Figure 1.15: Overview of the functions of bacillithiol.

Figure 1.16: General mechanism for thiol disulfide exchange reactions.

Figure 1.1: Hypothesised interaction of DAS with cellular LMW and protein thiols leading to ROS formation and a disturbance of the cellular redox status.

Chapter 2

Figure 2.1: Synthesis of polysulfides through reaction of thiols with dichlorosulfanes.

Figure 2.2: Synthesis of DAS mixture from DAS2 and elemental sulfur.

Figure 2.3: HPLC analysis of diallyl sulfides.

Figure 2.4: NMR characterisation of diallyl sulphides.

Figure 2.5: Mass spectra of DAS4 and DAS5 coordinated with silver.

Figure 2.6: Formation of DAS mixtures from pure, single molecule samples.

Figure 2.7: Suggested mechanism for the disproportionation of DAS.

Figure 2.8: Reduction of DAS3 by TCEP leads to formation of allyl mercaptan (ASH) and allyl perthiol (AS2H).

Figure 2.9: Reaction between 100 mM DAS3 and 10 mM TCEP.

Figure 2.10: Confirmation of allyl perthiol formation.

Figure 2.11: Analysis of product formation over time after reaction of 100 mM DAS3 with 10 mM GSH.

Figure 2.12: HPLC traces of reaction mixture after reacting a 100 mM DAS4 with 10 mM GSH.

Figure 2.13: Formation of thiol (ASmB), perthiol (AS2mB) and hydro trisulfide (AS3mB) products after reaction of 100 mM DAS4 or 100 mM DAS5 with 10 mM GSH.

Figure 2.14: DAS2 and GSH form mixed allyl-glutathione disulfide (AGS2).

Figure 2.15: $^1\text{H-NMR}$ of AGS2 compared to the symmetric disulfides DAS2 to DAS4 and GSSG.

Figure 2.16: The reaction of a 10-fold excess of DAS3 with GSH forms a mixture of mixed di- to pentasulfide and a mixture of DAS2 to DAS6.

Figure 2.17: Comparison of $^1\text{H-NMR}$ spectra of AGS2, AGS3 and product mixture from reaction of DAS3+GSH.

Figure 2.18: Formation of DAS4 and AGS4 after initial reaction of DAS3 with GSH.

Figure 2.19: Distribution of different AGS_n and distribution of different DAS after overnight incubation of 100 mM DAS with 10 mM GSH.

Figure 2.20 Reaction between BSH and a 10-fold excess of DAS2 forms pure mixed disulfide.

Figure 2.21: Reaction of BSH with a 10-fold excess of DAS5 forms mixed allyl-bacillithiol di- and polysulfides.

Figure 2.22: HPLC analysis of reaction mixtures before and after workup.

Figure 2.23: Product formation after reaction of 27 mM DAS5 with 2.7 mM BSH.

Figure 2.24: Cysteine and DAS2 form a mixture of mixed allyl-cysteine disulfide and cystine.

Figure 2.25: $^1\text{H-NMR}$ spectrum of the reaction mixture after reacting a 10-fold excess of DAS2 with Cys.

Figure 2.26: HPLC analysis of the reaction mixtures from cysteine reacted with DAS2.

Figure 2.27: Reaction between Cys and a five-fold excess of DAS5 leads to formation of mixed di- and polysulfides, cystine and DAS2-DAS6.

Figure 2.28: HPLC analysis of product mixture after reaction and work-up of DAS5 with Cys.

Figure 2.29: Competition reaction between GSH, Cys and DAS5.

Figure 2.30: Competition reaction between BSH, Cys and DAS5.

Figure 2.31: Example of $^1\text{H-NMR}$ time course, done for the reaction with DAS3 and GSH.

Figure 2.32: $^1\text{H-NMR}$ of a standard mixture of DAS and a reaction mixture of DAS3+GSH.

Figure 2.33: Initial reaction of DAS3 with GSH.

Figure 2.34: Different pathways and products for the reaction of DAS4 with GSH.

Figure 2.35: Initial reaction of DAS4 with GSH.

Figure 2.36: Different pathways and products for the reaction of DAS5 with GSH.

Figure 2.37: Initial reaction of DAS5 with GSH.

Figure 2.38: Relative reactivity of different sulfur atoms in DAS3, DAS4 and DAS5 for nucleophilic attack from GSH.

Chapter 3

Figure 3.1: Overview of different methods to investigate the influence of DAS towards the growth of *B. subtilis*.

Figure 3.2: Summary of the results of MIC determination for DAS1 to DAS6 (mg/L) against the *B. subtilis* WT and the *bshA*⁻ mutant.

Figure 3.3: Influence of different concentrations of DAS2 to DAS6 on the growth of *B. subtilis* WT.

Figure 3.4: Growth comparison of *B. subtilis* WT and *bshA*⁻ mutant after DAS treatment.

Figure 3.5: BSH redox system and hypothesised DAS interference.

Figure 3.6: Thiol levels and thiolate levels in *B. subtilis*.

Figure 3.7: Comparison of thiol levels in *B. subtilis* grown in different media.

Figure 3.8: Comparison of thiol and disulfide levels and redox ratios in *B. subtilis*.

Figure 3.9: Thiol levels in *B. subtilis* WT after treatment with 100 μ M DAS3.

Figure 3.10: Disulfide levels and redox ratios in *B. subtilis* after treatment with 100 μ M DAS3.

Figure 3.11: Thiol and disulfide levels in *B. subtilis bshA*⁻ after treatment with 100 μ M DAS3.

Figure 3.12: Cellular concentrations of allyl di- and polysulfides and allyl mercaptan after treatment of *B. subtilis* with 100 μ M of DAS3.

Figure 3.13: Thiol levels in *B. subtilis* up to 1.5 hours after DAS4 (92 μ M) treatment.

Figure 3.14: Thiol levels in *B. subtilis* up to 6 hours after DAS4 (92 μ M) treatment.

Figure 3.15: Disulfide levels in *B. subtilis* after DAS4 (92 μ M) treatment.

Figure 3.16: Diallyl polysulfide metabolites detected in *B. subtilis* after DAS4 (92 μ M) treatment.

Figure 3.17: Proposed reactions of DAS4 with LMW and protein thiols.

Figure 3.18: Bacillithiolation and overoxidation of proteins.

Figure 3.19: Western Blot analysis and protein gel of DAS2 and DAS3 treated *B. subtilis* WT.

Chapter 4

Figure 4.1: Schematic cross section of a nematode.

Figure 4.2: Life cycle and symptoms of root-knot nematodes (*Meloidogyne* spp.).

Figure 4.3: A: Life cycle and symptoms of potato cyst nematodes (*Globodera* spp.).

Figure 4.4: Chemical structures of nematicides used in the UK in 2012.

Figure 4.5: *S. feltiae* observed using a binocular at 45x magnification.

Figure 4.6: *In vitro* nematicidal activity of DAS towards *Steinernema feltiae*.

Figure 4.7: Thiol levels, disulfide levels and redox ratios measured in *S. feltiae* 5 min before and 40 and 195 min after treatment with 750 μ M DAS3.

Figure 4.8: Comparison of GSH levels in nematodes treated with 1 mM DAS3 and an untreated control.

Figure 4.9: Proposed mode of action for the interaction of DAS3 with a nematode.

Figure 4.10: Penetration of a nematicide to a target molecule.

Figure 4.11: Carrot trial design.

Figure 4.12: Visual carrot comparison between different nematicide treatments.

Figure 4.13: Aerial photograph of PCN damaged field during the summer.

Figure 4.14: Potato trial designs.

Figure 4.15: Potato yields of the paired trial.

Figure 4.16: Potato yield comparison of different treatments from the randomised trial.

Chapter 6

Figure 6.1: Synthesis of dibimane-disulfide.

Appendix 1

Figure 1.1: Overview of experimental steps involved in thiol and disulfide quantification of cell samples.

Figure 1.2: Fluorescent labelling of thiols with mBBr.

Figure 1.3: Disulfide analysis through irreversible alkylation of thiols, reduction of disulfides and mBBr labelling of reduced disulfides.

Figure 1.4: Chemical structures of thiols (RSH) reacted with mBBr to use as HPLC standards.

Figure 1.5: Synthesis of thiol-mB standards.

Figure 1.6: Thiol quantification through thiol-disulfide exchange reaction of DTNB with a thiolate.

Figure 1.7: Calibration curves for thiol-mB standards recorded by fluorescence HPLC.

Figure 1.8: MBBBr labelling of pure, DTNB quantified samples of BSH and Cys.

Figure 1.9: Correlation between residual dry weight (rdw) per volume (mg/mL) at different culture densities (OD_{600}).

Figure 1.10: Schematic overview of disulfide labelling.

Figure 1.11: Chemical reactions for disulfide analysis.

Figure 1.12: Efficiency of BSSB reduction by DTT.

Figure 1.13: Reduction of mixed polysulfides by DTT.

Figure 1.14: *In vitro* verification of disulfide Method 1.

Figure 1.15: β -mercaptoethanol (ME) can be alkylated by NEM and ME reduces disulfides to thiols.

Figure 1.16: *In vitro* test of disulfide Method 2.

Figure 1.17: Reaction speed of ME with NEM and ABS2 under assay conditions.

Figure 1.18: Disulfide analysis method for cell samples.

Figure 1.19: Comparison of different disulfide analyses methods in *B. subtilis* cell extracts.

Figure 1.20: Disulfide analysis of *E. coli* using three different methods.

Figure 1.21: Overview of thiol and disulfide analysis methods for DAS treated nematodes.

List of Tables

Chapter 1

Table 1.1: Quantities of different storage precursors of thiosulfates found in whole garlic cloves.

Table 1.2: Thiosulfate content in garlic clove homogenates.

Table 1.3: Minimum Inhibitory concentrations (MIC) (mg/L) of DAS and allicin against some bacteria and fungi.

Table 1.4: Thiol redox potentials and pK_a values.

Chapter 2

Table 2.1: Reaction speed of DAS3, DAS4 and DAS5 with GSH.

Chapter 3

Table 3.1: Thiol concentrations ($\mu\text{mol/g rdw}$) in *B. subtilis* WT CU1065.

Table 3.2: Overview of allylated proteins found in *B. subtilis* after DAS4 (92 μM) treatment categorised according to their functions.

Chapter 4

Table 4.1: Thiol and disulfide levels in nematodes.

Table 4.2: Intra- and extracellular reduced (ASH) and oxidised (ASSnR) DAS3 metabolites in *S. feltiae*.

Table 4.3: Enzyme kinetics for different substrates of glutathione disulfide reductase (GR).

Table 4.4: Plant pathogenic nematode species in the soil of the trial site seven weeks after carrot drilling.

Table 4.5: Carrot root damage and carrot premium yields for different treatments 23 weeks after planting.

Table 4.6: Initial PCN distribution (P_i , eggs/g soil) in the potato field at the different sampling positions of the paired trial just before drilling and application of the nematicides.

Table 4.7: P_f/P_i values in the potato field at different sampling positions. P_i (initial PCN populations) were measured before drilling and P_f (final PCN populations) were measured at the time of harvest.

Table 4.8: Initial egg numbers (P_i , eggs/g soil) in different plots of the randomised potato trial before drilling and application of nematicides.

Table 4.9: Initial (P_i) and final (P_f) mean PCN egg numbers in eggs/g and calculated P_f/P_i values.

Chapter 5

Table 1.1: pH-independent formation rate of mixed polysulfides (AGS2, AGS3 and AGS4) after reaction of diallyl polysulfides (DAS3, DAS4 and DAS5) with GSH.

Chapter 6

Table 6.1: Coordination Ion Spray Mass Spectrometry (CIS-MS) of diallyl sulfides.

Table 6.2: ^1H -NMR and ^{13}C -NMR characterisation of DAS.

Table 6.3: ^1H -NMR and ^{13}C -NMR data for allyl mercaptan-bimane (ASmB).

Table 6.4: ^1H -NMR and ^{13}C -NMR characterisation for allyl glutathione disulfide (AGS2).

Table 6.5: ^1H -NMR and ^{13}C -NMR characterisation of allyl-glutathione trisulfide (AGS3).

Table 6.6: ^1H -NMR data of allyl-bacillithiol disulfide (ABS2).

Table 6.7: Reactant concentrations for reactions between DAS3 to DAS5 with GSH.

Table 6.8: Different mBBR labelling conditions used for thiol labelling of *B. subtilis* cell extracts.

Abbreviations

ABS2	Allyl-bacillithiol disulfide
ABS3	Allyl-bacillithiol trisulfide
ABS4	Allyl-bacillithiol tetrasulfide
ABS_n	Allyl-bacillithiol sulfides
ACS2	Allyl-cysteine disulfide
ACS3	Allyl-cysteine trisulfide
ACS4	Allyl-cysteine tetrasulfide
ACS_n	Allyl-cysteine sulfides
AgBF₄	Silver tetrafluoroborate
AGS2	Allyl-glutathione disulfide
AGS3	Allyl-glutathione trisulfide
AGS4	Allyl-glutathione tetrasulfide
AGS5	Allyl-glutathione pentasulfide
AGS_n	Allyl-glutathione sulfides
AMS2	Allyl-methyl disulfide
AMS3	Allyl-methyl trisulfide
AMS4	Allyl-methyl tetrasulfide
ARS1	Mixed allyl monosulfide
ARS2	Mixed allyl disulfide
ARS3	Mixed allyl trisulfide
AS2H	Allyl perthiol
AS3H	Allyl hydrotrisulfide
ASH	Allyl mercaptan
AS_nH	Allyl hydrosulfides
AS_nmB	Allyl hydrosulfides-monoimane
Bca	Bacillithiol-S-conjugate amidase
BCIP	5-bromo-4-chloro-3'-indolyphosphate p-toluidine salt
BMM	Belitsky Minimal Media
BR	Bacillithiol disulfide reductase
Brx	Bacilliredoxin
BSH	Bacillithiol

BSSB	Bacillithiol disulfide
BST	Bacillithiol-S-transferase
CIS-MS	Coordination ion spray-mass spectrometry
Cm	Chloramphenicol
CoA	Coenzyme-A
CoADR	Coenzyme-A disulfide reductase
Cys	Cysteine
CysGly	Cysteinylglycine
CysNAc	<i>N</i> -Acetyl-cysteine
CySS	Cystine
DAS	Diallyl sulfides
DAS1	Diallyl monosulfide
DAS2	Diallyl disulfide
DAS3	Diallyl trisulfide
DAS4	Diallyl tetrasulfide
DAS5	Diallyl pentasulfide
DAS6	Diallyl hexasulfide
DAS7	Diallyl heptasulfide
DAS10	Diallyl decasulfide
DCM	Dichloromethane
dd	Doublet of doublets
ddt	Doublet of doublet of triplets
DMS2	Dimethyl disulfide
DMS3	Dimethyl trisulfide
DMS4	Dimethyl tetrasulfide
DMS_n	Dimethyl sulfide
DMSO	Dimethyl sulfoxide
DTNB	5,5'-dithiobis-(2-nitrobenzoic acid)
DTT	Dithiothreitol
EDTA	Ethylenediaminetetraacetic acid
ESH	Ergothioneine
ESI	Electrospray ionisation
EtOH	Ethanol

Et₂O	Diethyl ether
GO	Garlic oil
Gpx	Glutathione peroxidase
GR	Glutathione disulfide reductase
Grx	Glutaredoxin
GSH	Glutathione
GSSG	Glutathione disulfide
GSSH	Glutathione perthiol
GSSSG	Glutathione trisulfide
GST	Glutathione-S-transferase
HCys	Homocysteine
Hepes	4-(2-hydroxyethyl)-1-piperazineethanesulfonic acid
HPLC	High performance liquid chromatography
IC₅₀	Half maximal inhibitory concentration
IgG	Immunoglobulin G
J (J1-J4)	Nematode juvenile (Juvenile stages 1 to 4)
LB	Luria broth
LC	Liquid chromatography
LC₅₀	Half lethal concentration
LC-MS	Liquid chromatography-mass spectrometry
LMW thiol	Low molecular weight thiol
logP	Logarithm of the octanol-water coefficient
mB	Monobimane
mBBr	Monobromobimane
mBOH	Hydrolysed monobromobimane
ME	β-mercaptoethanol
MeOH	Methanol
MeSO₃H	Methanesulfonic acid
MetE	Methionine synthase
MIC	Minimum inhibitory concentration
MOA	Mode of action
MS	Mass spectrometry
MSH	Mycothioli

NAD(P)H	Nicotinamide adenine dinucleotide (phosphate)
NBT	Nitro-blue tetrazolium chloride
NEM	<i>N</i> -Ethylmaleimide
NMR	Nuclear magnetic resonance spectroscopy
NP	Normal phase
OD	Optical density
OSC	Organosulfur compound
OSH	Ovothiol
PCN	Potato cyst nematode
P_f	Final population
P_i	Initial population
pK_a	Negative logarithm of the acid/thiol dissociation constant
Prx	Peroxiredoxin
rdw	Residual dry weight
RKN	Root knot nematode
ROS	Reactive oxygen species
RP	Reverse phase
rpm	Revolutions per minute
RSH	Thiol
RT	Room temperature
rt	Retention time
SDS	Sodium dodecyl sulfate
T(SH)₂	Ttrypanothione
TBAP	Tetrabutylammonium phosphate
TCEP	Tris(2-carboxyethyl)phosphine
TNB	2-nitro-5-thiobenzoate
Tris	Tris(hydroxymethyl)amino methane
Trx	Thioredoxin
UV	Ultraviolet
wPCN	White potato cyst nematode
WT	Wild-type
γ-GC	γ-glutamylcysteine
yPCN	Yellow potato cyst nematode

1 Introduction

With a history going back over 4000 years ⁽¹⁾, garlic (*Allium sativum*) is well known as a herb and spice and is a fundamental component in many dishes of various regions around the globe. Garlic belongs to the genus of *Alliums* that also includes other well-known plants like onion, leek and chive. For many centuries folk medicine has considered garlic and its products, such as garlic oil (GO), as powerful therapeutic agents which are used all over the world, because of their antibacterial, antifungal and antiviral activities. Sulfur containing compounds derived from garlic are a fascinating (and complex) area of research as still many questions of the chemistry and biochemistry of garlic derived compounds remain unanswered. By using modern research methods it may be possible to bring the mode of action (MOA) of compounds to light which have been used for centuries to cure diseases. Increasing knowledge about the MOA and biochemical interactions of the garlic compounds may open doors to further exploit the garlic plant or specific isolated compounds and improve and expand their use in medicine and agriculture.

This project particularly focusses on the application of a certain class of molecules, diallyl polysulfides (DAS) found in garlic, as a nematicide to combat the threat of important plant pathogenic nematodes in the UK and other (European) countries. For maximum exploitation of the complex chemistry provided by DAS it is important to understand their MOA and affected biochemical pathways, which is another important research area of this study. In the introduction different bioactive sulfur compounds produced in garlic are presented, with a special focus on DAS. The current knowledge concerning the bioactivities and MOA of DAS molecules is summarised. An introduction for the more applied part of the study, which deals with plant pathogenic nematodes, their control in general and prospects of DAS for nematode control follows in chapter 4.

1.1 Organosulfur compounds occurring in garlic

1.1.1 Overview

Typical for the genus of *Alliums* is their high content of organosulfur compounds (OSCs) and, as a result, their characteristic taste and smell. The most abundant organosulfur metabolite produced by garlic plants is the non-protein amino acid alliin (*S*-allyl-L-cysteine sulfoxide) which is stored in large amounts in the cytosol of the garlic cells (5-15 mg/g fresh weight ⁽¹⁾, Figure 1.1 and Figure 1.2).

Interestingly, garlic in its intact form, is odourless until it is crushed or cells become otherwise damaged. Upon damaging the cellular structure of the plant, the enzyme alliin-lyase (alliinase E.C.4.4.1.4.) is released from the vacuoles and catalyses the rapid conversion of alliin into the chemically very reactive molecule alliin (diallyl thiosulfinate), which was first isolated and identified in 1944 by Cavallito ⁽²⁾.

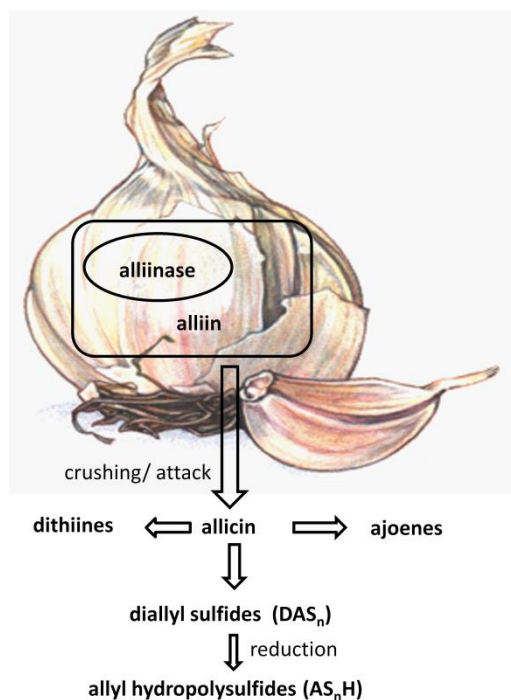


Figure 1.1: Overview of produced organosulfur compounds upon crushing of garlic.

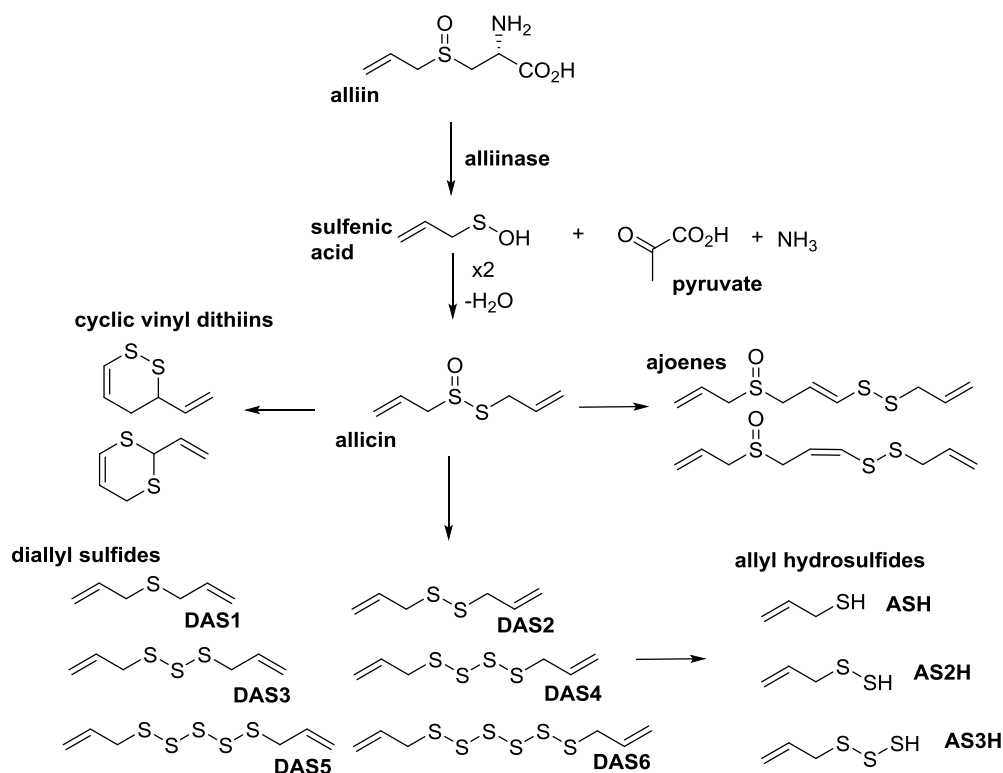


Figure 1.2: Chemical structures of organosulfur compounds produced in garlic upon enzymatic conversion of alliin to alliin induced by the crushing of garlic and chemical conversion of alliin to different compound classes.

Alliin is an extraordinary bioactive molecule and is also ultimately responsible for the characteristic smell of freshly cut garlic. From the perspective of the plant, this is a very effective defense mechanism against attacking pathogens. The formation of the active compound upon cell damage ensures that there is only a local formation of the active for a short period of time which avoids alliin-induced toxicity for the plant itself ⁽³⁾. Because of its high chemical reactivity alliin undergoes a cascade of further chemical rearrangements leading to other organosulfur molecules such as DAS, dithiines and ajoene (Figure 1.1 and Figure 1.2).

1.1.2 Organosulfur storage compounds of whole garlic cloves

The total content of *S*-alkylcysteine sulfoxides (alliin, methiin, isoalliin, Figure 1.3) in garlic cloves is approximately equal to the total amount of γ -glutamyl-*S*-alkylcysteines (Table 1.1). γ -glutamyl-*S*-alkylcysteines are stored as precursors of the corresponding sulfoxides. During sprouting of the garlic plant γ -glutamyl-*S*-alkylcysteines get converted into *S*-alkylcysteine sulfoxides via two enzymatic reactions involving a hydrolysis of the peptide bond by γ -glutamyl transpeptidase enzymes followed by an enzyme catalysed oxidation to the corresponding sulfoxide ⁽⁴⁾.

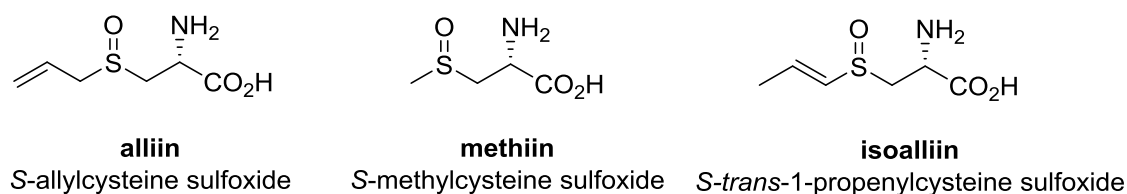


Figure 1.3: Structures of *S*-alkylcysteine sulfoxides found in garlic, which are the storage precursors of the reactive thiosulfinates.

Alliin is the major sulfoxide found in garlic (~80%, Table 1.1) and it is exclusively found in garlic, e.g. onion (*Allium cepa*) produces methiin, isoalliin and *S*-propylcysteine sulfoxide (propiin) ⁽⁵⁾.

Table 1.1: Quantities of different storage precursors of thiosulfinates found in whole garlic cloves according to Lawson *et al.* ⁽⁴⁾.

Storage precursors	Amount (mg/g fresh weight) in whole garlic cloves	% of total in category
Cysteine sulfoxides		
S-allylcysteine sulfoxide (alliin)	7.0-14.0	83
S-methylcysteine sulfoxide (methiin)	0.5-2.0	10
S- <i>trans</i> -1-propenylcysteine sulfoxide (isoalliin)	0.1-2.0	8
Total	12.6	100
γ-glutamylcysteines		
γ -glutamyl-S- <i>trans</i> -1-propenylcysteine	3.0-9.0	59
γ -glutamyl-S-allylcysteine	2.0-6.0	39
γ -glutamyl-S-methylcysteine	0.1-0.4	2
Total	10.3	100

Two different pathways for the biosynthesis of alliin have been described ⁽⁶⁾: 1) Serine can combine with an allyl thiol source to give *S*-allylcysteine which is oxidised to alliin. 2) Alternatively glutathione (GSH) can combine with an allyl source to form *S*-allylglutathione followed by loss of glycine and glutamate and ultimately oxidation of *S*-allylcysteine to alliin. In tissue culture of *A. sativum*, labelled sulfur was found in γ -glutamyl-cysteine peptides and GSH before accumulating in *S*-alkylcysteine sulfoxides, supporting the proposed pathway via GSH ^(5, 7). The allyl group was suggested to derive from methacrylic acid, which can be converted into allyl, propenyl or propyl (not found in garlic) groups ⁽⁶⁾.

The enzyme alliinase is stored in the vacuoles and upon release from the vacuole through cell damage, it rapidly catalyses the reaction from *S*-alkylcysteine sulfoxides (which are stored in the cytosol) to their corresponding thiosulfinates (Figure 1.2). Alliinase accounts for up to 10% of total garlic clove protein and belongs to a family of glycoproteins containing about 6% carbohydrate and has been fully characterised by X-ray crystallography as a dimer with two equal subunits, each consisting of 448 amino acids ⁽⁸⁾. The enzymatic reaction involves cleavage of the alliin carbon-sulfur bond on the amino acid side, releasing 2-propenesulfenic acid, which has never been isolated. Two molecules of 2-propenesulfenic acid rapidly self-condense with water to form allicin without enzymatic involvement (Figure 1.2). As by-products pyruvate and ammonia are formed. The formation of allicin is instant and the reactivity of alliin and isoalliin towards alliinase is about 10-fold faster compared to methiin. As the alliin concentration in the garlic clove is one to two orders of magnitude higher than the isoalliin concentration, the major product formed is allicin.

1.1.3 Allicin and related sulfinates

Allicin gives its characteristic taste and smell to freshly cut garlic. It is formed through condensation of two molecules of 2-propenesulfenic acid derived from sulfoxides (i.e. alliin, Figure 1.2). Due to the fact that garlic contains three different cysteine sulfoxides, nine different thiosulfinates could be formed, of which seven have been detected (Table 1.2). Allicin is the most abundant thiosulfinate and makes up nearly 70% of the produced thiosulfinates.

Table 1.2: Thiosulfinate content in garlic clove homogenates. Ranges and mean of six samples purchased from three different stores at two different time points ⁽⁹⁾.

Thiosulfinates	Amount (mg/g fresh weight)	Mean amount (mg/g fresh weight)	% of total thiosulfinates
Allicin	2.3-4.6	3.72	69.0
Allyl methyl	0.4-0.8	0.50	9.3
Methyl allyl	0.2-0.4	0.23	4.3
1-Propenyl allyl	0.2-0.6	0.35	6.5
Allyl 1-propenyl	0.1-0.5	0.34	6.3
Methyl 1-propenyl	0.1-0.2	0.14	2.6
Dimethyl	0.1	0.11	2.0
Total	4.6-6.7	5.37	100

Allyl-S-thiosulfinates (allicin, allyl-SS(O)-methyl and allyl-SS(O)-trans-1-propenyl) are the least stable of garlic's thiosulfinates, which was attributed to their ability to form thioacrolein and allyl mercaptan (ASH) as reaction intermediates. In ether allicin and allyl-SS(O)-methyl have a half-life of three hours whereas methyl-SS(O) allyl shows no measurable loss after 6 days⁽⁴⁾.

The bioactivity of allicin is attributed to its ability to undergo thiol-disulfide exchange reactions with thiol groups of proteins. One mole of allicin reacts with two moles of cysteine (Cys) to form two moles of allyl-cysteine disulfide (ACS2, Figure 1.4 e)⁽⁴⁾. It therefore inhibits numerous enzymes which contain Cys residues at their active sites⁽¹⁰⁾. The biological activity is not only due to allicin's potential in thiol-disulfide exchange reactions but it is also able to alter the redox status of the cell and ultimately induce apoptosis⁽¹¹⁾. Allicin is very effective as an antibiotic, antioxidant and anticancer agent *in vitro*. It easily penetrates biological membranes and it disappears from the circulation shortly after injection⁽¹⁾. Therefore *in vivo* exploitation of antibiotic and cytotoxic effects are limited. Development of an antibody-directed enzyme prodrug therapy which ensures allicin formation at the tumour site has been explored to deal with the short half-life of allicin⁽¹²⁾. According to allicin's short half-life it decomposes to numerous other molecules that are biologically active as well (Figure 1.2 and Figure 1.4).

1.1.4 Allicin transformations

Allicin and related thiosulfinates are very reactive molecules and form a variety of secondary sulfur metabolites. The nature of these metabolites depends on the temperature, pH and solvent conditions at which allicin is transformed (Figure 1.4). The main transformation products of allicin in water are diallyl trisulfide (DAS3) and diallyl disulfide (DAS2). The rate of formation of sulfides is greatly accelerated by heat, such as during steam distillation, which is used to produce GO. Kinetic studies indicated that during steam distillation of garlic homogenates trisulfides are formed first, followed by formation of other sulfides with $S_n = 1-6$ (Figure 1.4 b)⁽⁴⁾. Upon incubation of allicin or allyl methanethiosulfinate in low-polarity solvents (e.g. ether, hexane or vegetable oil, Figure 1.4 c) vinyl dithiines (70%), ajoene (12%) and sulfides (18%) are formed. Incubation of thiosulfinates in alcohol gave variable results depending on the use of pure allicin or garlic homogenate. Garlic homogenate in ethanol (EtOH) produces mainly DAS3 (73%), some DAS2 (8%) and ajoene (8%) whereas pure allicin in ethanol leads to formation of mainly ajoene (55%) and vinyl dithiines (34%) and low amounts of DAS (11%) (Figure 1.4 d). At extreme alkaline pH (>10) thiosulfinates can undergo alkaline hydrolysis to form disulfides and sulfur dioxide (Figure 1.4 a)⁽⁴⁾.

The impact of different methods of cooking was summarised by Lawson⁽⁴⁾. Upon chopping or crushing of garlic, most of the cysteine sulfoxides are transformed into thiosulfinates. Heating the crushed garlic at boiling temperature for 20 min in a closed container leads to complete conversion of thiosulfinates to mainly DAS3 and lower amounts of DAS2 and allyl methyl trisulfide (AMS3). Cooking in an open container for 20 min retained 7% of the thiosulfinates, but 97% of the sulfides evaporated. Stir-frying chopped and smashed garlic cloves in hot oil for one min retained 16% of the sulfides in the oil, but no thiosulfinates were detected. Therefore, through consumption of cooked garlic, mainly sulfides are taken up, but prolonged cooking times in open containers lead to evaporation and loss of these volatile compounds.

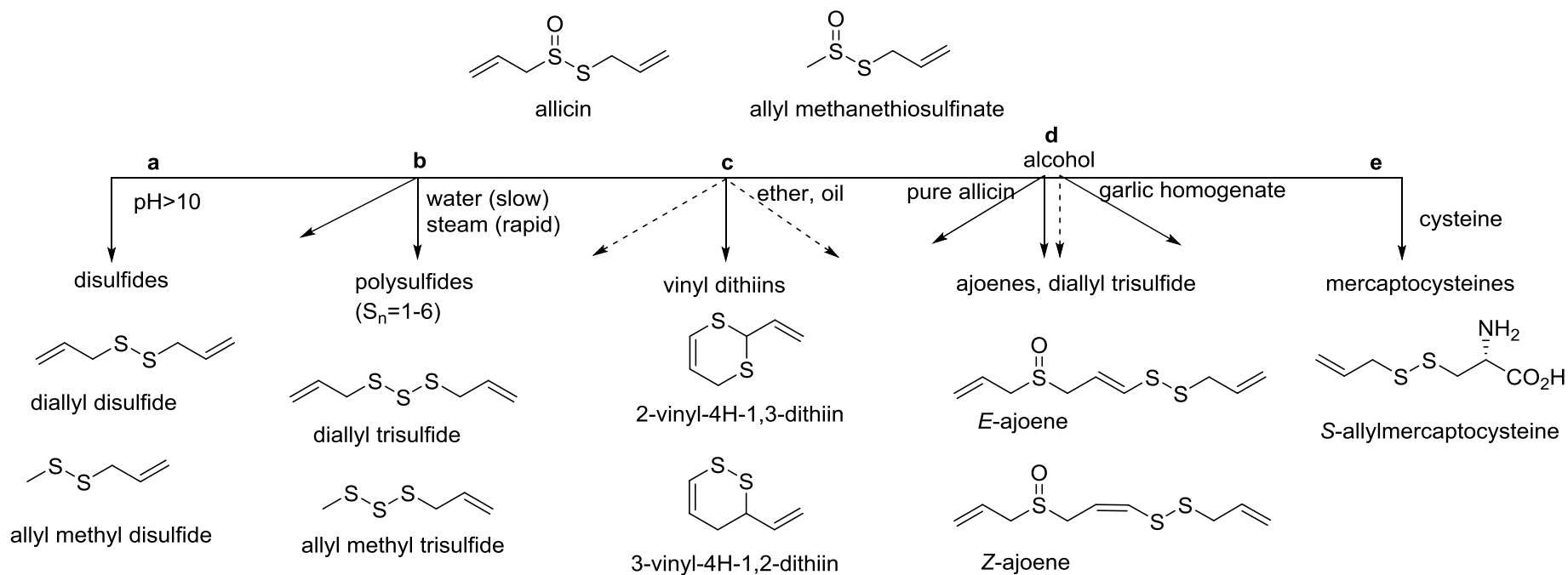


Figure 1.4: Transformation of the main thiosulfinates from garlic (allicin and allyl methanethiosulfinate) depending on the solvent, temperature and pH ⁽⁴⁾.

1.1.4.1 Physiological fate of allicin and allicin-derived compounds

Allicin has never been detected in human blood after consumption of garlic, showing that it is quickly converted into other compounds. ASH was the dominant sulfur compound in human breath after garlic consumption. In an attempt to detect allicin, ajoene, dithiins or sulfides, Lawson fed 25 g of fresh garlic to volunteers, but none of the OSCs were subsequently detected in the blood or urine⁽⁴⁾. In another experiment it was shown that allicin quickly reacts with protein in blood plasma, as allicin was detected in the plasma only when it was deproteinated before adding allicin. Incubation of allicin, ajoene, dithiines and sulfides with blood leads to the quantitative formation of ASH⁽⁴⁾, which suggests an important role for ASH, but concentrations of ASH would need to be quantified *in vivo*. Nevertheless, the biological activity of garlic compounds cannot be attributed only to ASH, as ASH is used as a comparison for allicin or sulfides in many biological studies, and it does not produce the same biological effects.

To summarise, not much is known about the biological fate of garlic compounds, neither are they detected in the blood after consumption, nor are new garlic derived organosulfur compounds.

The chemical mechanisms of the formation^(1, 13, 14) of different compound classes (ajoenes and dithiines) or specific bioactivities⁽¹⁵⁻¹⁷⁾ of those compounds will not be discussed in the introduction of this study and the reader is referred to other sources for further reading. The next section (1.2) exclusively focusses on the occurrence, formation, bioactivities and reactivity of DAS, as this is the class of compounds that was studied in this project in detail.

1.2 Diallyl polysulfides (DAS)

In addition to large amounts of allicin, other sulfinates (methyl and propenyl substituted) are also formed by the activity of alliinase, and, as a result, methyl and propenyl substituted polysulfides are formed as secondary products. All of the polysulfides have been tested for various biological activities, and the highest activity has usually been found for the diallyl polysulfides^(18, 19). Additionally, the diallyl substituted polysulfides have a more pleasant smell than the analogous dimethyl- and allyl-methyl compounds, which makes them a better candidate for applications in medicine or agriculture. Therefore this study and the following introductory sections focus on DAS.

1.2.1 Formation of DAS

A mechanism for the formation of DAS from allicin was suggested by Block⁽¹⁾ (Figure 1.5). The mechanism to form DAS3 was proposed to start with S-thiolation of allicin to form intermediate 1, which then hydrolyses to intermediate 2 under the liberation of allyl alcohol. Intermediate 2 is hydrolysed to intermediate 3 and liberates allyl perthiol (AS2H). Intermediate 3 is unstable and degrades to propene and sulfur dioxide (SO₂) and ASH can react with another molecule of allicin to form DAS3 in a reaction analogous to a thiol-disulfide exchange reaction. By direct analysis in real time mass spectrometry (DART MS) intermediate 2 and 3, allyl alcohol, SO₂ and propene have been detected upon cutting garlic⁽¹⁾. The ASH and AS2H molecules have not been detected.

Direct hydrolysis of allicin leads to liberation of ASH which reacts with another molecule of allicin to form DAS2. After the initial formation of DAS2 and DAS3 other DAS (S=1-6) are formed until a stable equilibrium is reached.

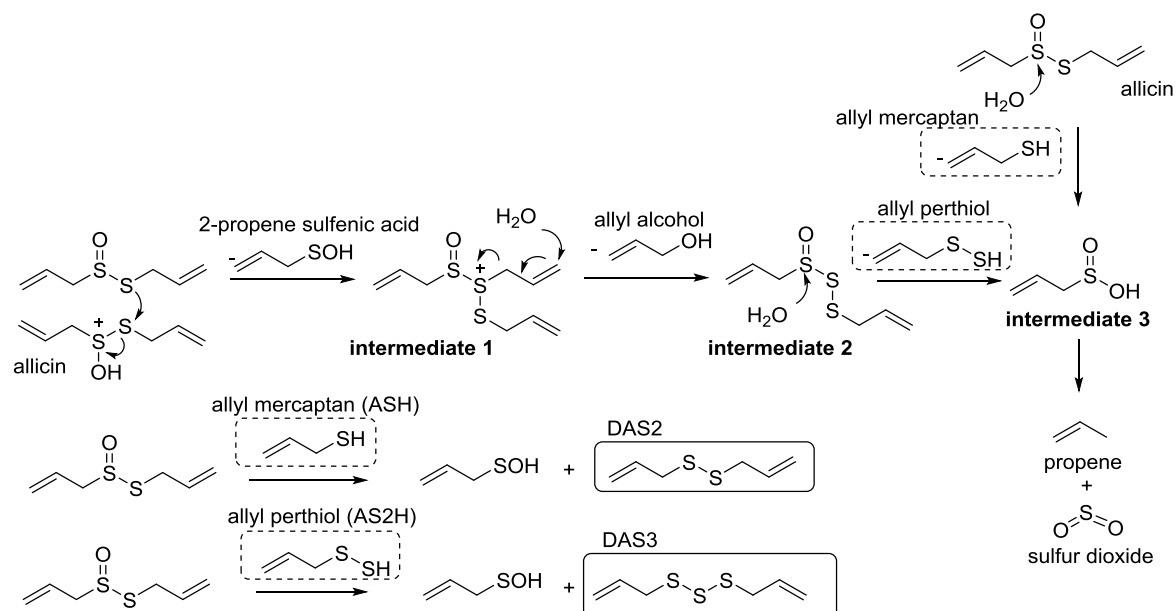


Figure 1.5: Suggested mechanism for the formation of DAS from allicin⁽¹⁾.

The hydrolysis is accelerated through heat, which leads to fast formation of DAS during cooking or during the production of steam distilled GO. Steam distilled GO typically consists of mainly DAS (26% DAS2, 19% DAS3, 8% DAS4, 4% DAS5, 1% DAS6) and smaller amounts of allyl

methyl sulfides (AMS2 8%, AMS3 15%, AMS4 6%)⁽⁴⁾. GO is often called 'garlic essential oil', which is not strictly true, as the GO is a product of steam distillation and the generated sulfides are not found in intact garlic cloves. Garlic cloves only contain tiny amounts of natural oil (0.2%), which does not contain any sulfur⁽⁴⁾.

1.2.2 Dietary uptake of DAS through garlic oil or cooked garlic

DAS are taken up by humans through consumption of cooked or fried garlic or steam distilled GO, but amounts of DAS taken up are difficult to estimate because of the different chemical transformations that allicin can undergo. Table 1.2 shows that allicin is formed on average in a concentration of about 3.7 mg/ g fresh weight of garlic. As one minute stir frying leads to disappearance of allicin and detection of 16% sulfides, we can estimate a concentration of 0.59 mg DAS/ g fresh weight of garlic. The average garlic clove weighs around 4 to 8 g, which corresponds to 2.4 to 4.7 mg DAS/ garlic clove. The physiological fate of DAS in the human body is largely unknown, as are potential benefits. DAS2 and DAS3 react *in vitro* with components of blood to form ASH⁽⁴⁾. Due to the limited knowledge of pathways or formed metabolites, estimations of beneficial health effects of DAS taken up in a normal diet or dose requirements cannot be made.

1.2.3 Bioactivity of DAS

DAS have demonstrated different biological activities, mainly studied through *in vitro* experiments (Figure 1.6). The most extensively studied areas are antimicrobial and anticarcinogenic properties of DAS. An example for the practical application of DAS is the DAS3-based medicine (allitridium) which is widely used in the People's Republic of China for the treatment of fungal diseases⁽²⁰⁾.

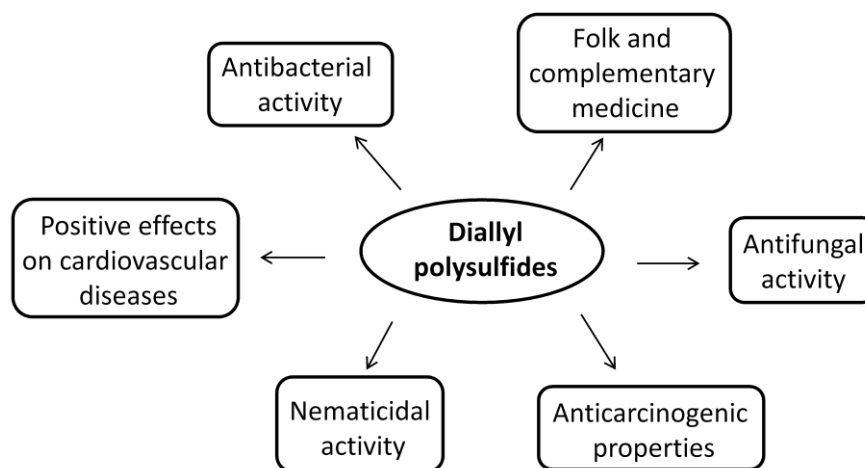


Figure 1.6: Different biological activities of DAS from garlic.

1.2.3.1 Antimicrobial activity

Table 1.3 gives some examples of antibacterial and antifungal activity of DAS1 to DAS4 compared to allicin. The antimicrobial activity increases with increasing number of sulfur atoms and the activity of DAS3 and DAS4 are in the same range compared to allicin.

Table 1.3: Minimum Inhibitory concentrations (MIC) (mg/L) of DAS and allicin against some bacteria and fungi.

Organism	DAS1	DAS2	DAS3	DAS4	Allicin
<i>Klebsiella pneumonia</i> ⁽²¹⁾	96	72	40	20	8 ⁽³⁾
<i>Helicobacter pylori</i> ⁽²²⁾	>1000	100	13-25	3-6	6-30
<i>Pseudomonas aeruginosa</i> ⁽²¹⁾	80	64	32	12	15 ⁽³⁾
<i>Bacillus cereus</i> ⁽²³⁾	64	14	4	1	ND
<i>Staphylococcus aureus</i> ⁽²⁴⁾	20	4	2	0.5	12 ⁽³⁾
<i>Candida albicans</i> ⁽²⁴⁾	32	4	1	0.5	0.3 ⁽³⁾

Little is known about the mode of antimicrobial action of the DAS and their cellular targets. Most studies are limited to the determination on Minimum Inhibitory Concentrations (MICs) and do not go into depth to investigate cellular interactions of DAS. One exception is a study done by Lemar *et al.* where the effects of 500 μ M DAS2 on *C. albicans* were investigated and DAS2 was found to induce cell death (necrosis and apoptosis) by inducing oxidative stress. Furthermore, GSH levels were determined and glutathione-S-transferase (GST) was identified as a cellular target for DAS2 ⁽²⁵⁾.

1.2.3.2 Selective activity against cancer cells

DAS3 and DAS4 both showed anticarcinogenic properties in a variety of studies using different cancer cell lines. The underlying mechanisms are not yet fully understood, but some progress has been made concerning the mode of action of DAS3 that leads to selective activity towards cancer cells: G₂-M Cell cycle arrest was repeatedly observed in different cancer cell lines ^(15, 26, 27) and the ability of DAS3 (20-40 μ M), but not DAS1 or DAS2 at the same concentrations to induce G₂-M phase cell cycle arrest in cultured PC-3 human prostate cancer cells was demonstrated. This event seemed to be related to a DAS3-induced increase in intracellular levels of reactive oxygen species (ROS). Interestingly, cultured normal prostate epithelial cells were not affected by DAS3 even at 40 to 80 μ M concentrations ⁽²⁷⁾. These findings point towards a selective toxicity of DAS3 in cancer cells, but not in the corresponding normal cells. In another study the growth of HCT-15 and DLD-1 human colon cancer cell lines was inhibited by DAS3 with IC₅₀s (half maximal inhibitory concentrations) of 11.5 μ M and 13.3 μ M respectively and a G₂-M cell cycle arrest was observed which led to apoptosis. In an *in vitro* system the disruption of the microtubule network due to S-allyl modifications on two cysteine residues of β -tubulin were observed ⁽²⁸⁾. Different stress pathways have been shown to be influenced through DAS3 mediated increased levels of ROS ^(26, 27, 29, 30).

In some studies the anticarcinogenic properties of DAS4 were investigated, determining slightly lower effective doses for DAS4 compared to DAS3 and similar results concerning the MOA of the two compounds (affected stress pathways, ROS induction and cell cycle arrest) ⁽³¹⁻³³⁾.

These are just some examples of biological activities of DAS and the list could be expanded much further and the nematocidal activities of DAS are reported in chapter 4. For a deeper understanding of the biological activity it is important to look at the underlying biochemical reactions of DAS within their target organisms/ cells. DAS show toxicity against a wide variety of different cell types and organisms, but the initiating biochemical reactions that lead to the toxicity might be very similar, and these will be discussed in the following sections.

1.2.4 Mode of action of DAS

1.2.4.1 Overview

Most of the suggested pathways are initiated through reaction of DAS with cellular thiols, either low molecular weight (LMW) thiols or protein thiols found in Cys residues of proteins (Figure 1.7). In case of DAS3 this reaction can lead to the formation of a mixed disulfide and AS2H. The AS2H itself is proposed to be a reactive molecule (section 1.2.4.3) that can undergo a variety of reactions, including superoxide radical ($O_2^{\cdot-}$) formation and reaction with another thiol (RSH), which can ultimately lead to hydrogen sulfide (H_2S) release. Other MOAs are summarised below.

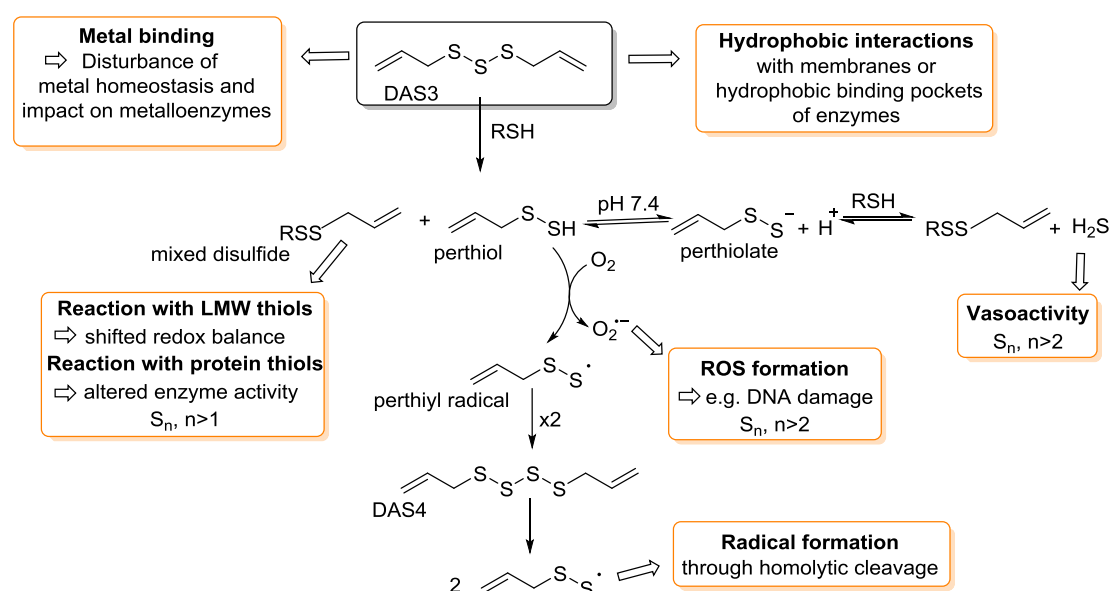


Figure 1.7: Possible reactions of DAS3 and their physiological consequences. The diagram shows an incomplete overview of possible reactions, cellular targets and pathways. All shown reactions are possible for DAS_n with $n>2$ and additional reaction products can be formed for longer chain DAS.

Metal binding

It is suggested that DAS can coordinate with metal ions which can lead to a disturbance in the metal ion homeostasis and can have an impact on metalloenzymes⁽¹⁹⁾. Dimethyl sulfides (DMS_n with $n=1-6$) were shown to coordinate with lithium displaying increased coordination strength for increasing number of sulfur atoms using *ab initio* methods⁽³⁴⁾. There are no data available yet about the *in vivo* ability of DAS to coordinate metal ions, but the metal coordination properties of sulfur strongly suggest such interactions.

Hydrophobic interactions

Hydrophobic interactions are associated with DAS which are more important for longer chain DAS because of their increased lipophilicity (logP values were shown to increase with increasing number of sulfur atoms from DAS1 (2.4) to DAS4 (3.1)⁽³⁵⁾). Hydrophobic interactions include interactions with cellular membranes as well as the binding to hydrophobic pockets of protein which leads to unfolding of the protein structure. Through comparison with their carbon analogues (1,6 heptadiene and 1,9 decadiene) it was found out that the sulfur containing DAS are by far more active than their carbon analogues⁽³²⁾. This shows that hydrophobic interactions alone are insufficient in explaining the activity of DAS. Nevertheless, part of the toxicity, especially when applied in higher concentrations may result from hydrophobic interactions as it was shown for DAS1 to DAS3 that they interact with membrane lipids to modify membrane fluidity⁽³⁶⁾.

Radical formation through homolytic cleavage

In the case of DAS4 homolytic cleavage, which leads to the formation of two perthiyl radicals is suggested. This process has been experimentally shown for dimethyl tetrasulfide (DMS4). The dissociation energy of DMS4 is lower (150 kJ) compared to the corresponding di- and trisulfide (293 kJ and 184 kJ respectively)⁽³⁷⁾. Furthermore, resonance interactions with adjacent sulfur atoms are thought to stabilise perthiyl radicals with $S > 1$ and the estimated bond energy (138 kJ) for the perthiyl radical is not much lower than that of DMS4⁽³⁷⁾, both leading to a stabilisation of the radicals. The homolytic cleavage has not been demonstrated for DAS4, but might possibly take place in a similar way.

S_x transfer reactions

The release of neutral S_x species ($x > 1$) from longer chain DAS is a topic of debate. The release of S₃ from the natural pentasulfide varacin was suggested by computational studies⁽³⁸⁾. Release of neutral sulfur species from DAS is theoretically possible, but has not been experimentally proven.

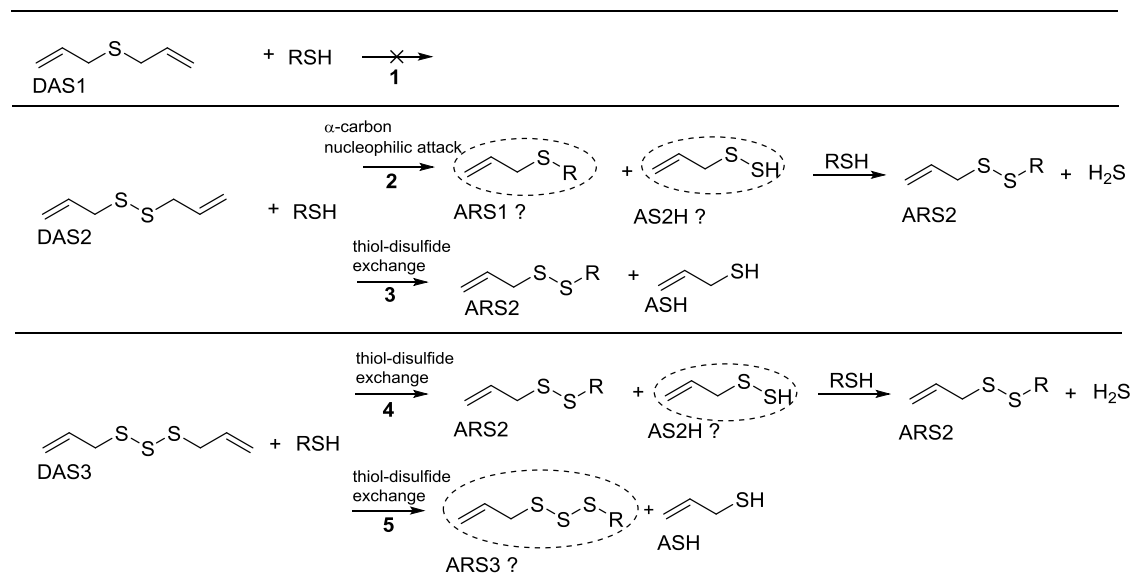
To summarise, very different MOA have been suggested for DAS, and most likely a combination of different mechanism and affected pathways leads to the extraordinary bioactivities of DAS. This study mainly focusses on the interaction of DAS with thiols, as this interaction can be seen as the central point of attack of DAS, which initiates the subsequent complex reaction cascades.

1.2.4.2 Modifications of LMW and protein thiols through DAS

1.2.4.2.1 Direct interactions between DAS and thiols

The most common explanation for the activity of DAS ($S > 1$) is their ability to react with LMW or protein thiols to form mixed di- or polysulfides (Figure 1.8 A, reaction 3 to 5) and therefore disturb the cellular redox balance and alter enzyme activities.

A



B

Reaction Number (as shown in A)	Starting materials (molar equivalents)			Half life (min)	Products (molar equivalents)		
	DAS2	DAS3	Cys/ GSH		ACS2	ASH	H ₂ S
3	1	-	2	45	1	1	NR
3	1	-	4	15	NR	NR	NR
4 or 5	-	1	2	<2	1	0.6	NR
4 or 5	-	1	8	NR	2	NR	NR
2	1	-	20	~ 0.5	NR	NR	0.4
4	-	1	20	~ 1	NR	NR	1

Figure 1.8: Reaction of DAS2 and DAS3 with thiols. A: (1) DAS1 cannot react with thiols in a thiol-disulfide exchange reaction. (2) DAS2 was suggested to react with thiols through an α -carbon nucleophilic-attack, because H₂S was observed as a reaction product⁽¹⁸⁾, but the primary products (ARS1 and AS2H) have not been detected. (3) DAS2 reacts with thiols in a thiol-disulfide exchange reaction leading to the formation of a mixed disulfide (ARS2) and allyl mercaptan (ASH). (4) and (5) DAS3 provides two positions for nucleophilic attack leading to different reaction products including a mixed trisulfide (ARS2) and a perthiol (AS2H), which have not been detected yet. B: Experimental results of DAS2 and DAS3 reacting with Cys (first four rows⁽⁴⁾) and GSH (last two rows⁽¹⁸⁾) to form mixed allyl-cysteine disulfide (ACS2), ASH and H₂S. NR: Not reported.

Thiol-disulfide exchange reactions are not possible for the monosulfide (DAS1, Figure 1.8, reaction 1), which may explain the inactivity of DAS1 in many experiments. In the case of DAS2, an additional reaction mechanism was suggested⁽¹⁸⁾, which involves an α - carbon nucleophilic attack and would lead to the formation of a mixed monosulfide (ARS1) and AS2H, which can then react with a thiol in a thiol-disulfide exchange reaction to liberate H₂S (Figure 1.8, reaction 2). The liberation of H₂S after incubation of DAS2 with a 20-fold excess of GSH was observed by Benavides *et al.*⁽¹⁸⁾. The primary reaction products have not been detected. More commonly DAS2 is thought to react with thiols (which have to be in their deprotonated thiolate form) in a thiol-disulfide exchange reaction (Figure 1.8, reaction 3) leading to the formation of a mixed allyl disulfide (ARS2) and ASH. The reaction between Cys and DAS2 has been shown to form ACS2 and ASH *in vitro*^(4, 39), supporting the thiol-disulfide exchange mechanism (Figure 1.8 B, reaction 3). DAS3 reacts with thiols in an analogous way in a thiol-polysulfide exchange reaction. As DAS3 has two chemically different sulfur atoms (the two terminal ones are chemically identical, but different from the central one) the thiolate can attack in two different positions. Attack on one of the outer sulfurs leads to formation of ARS2 and AS2H (Figure 1.8, reaction 4) and attack on the central sulfur leads to formation of a mixed trisulfide (ARS3) and ASH (Figure 1.8, reaction 5). Upon incubation of DAS3 with Cys, formation of ACS2 and ASH and an unknown product have been reported⁽⁴⁾ (Figure 1.8 B, reaction 4 or 5). The reaction between DAS3 and Cys was shown to be more than 20-fold faster compared to the one with DAS2. The identified products upon reaction of DAS3 with Cys (ACS2 and ASH) are missing one sulfur, which might get lost through release of H₂S⁽¹⁸⁾ (Figure 1.8 A, reaction 4). The unknown product after reaction of DAS3 with Cys has not been identified and therefore the full product distribution for this reaction is still unknown. Neither the AS₂H (or AS_nH, with n>2 for DAS4, DAS5 and DAS6) nor the ARS₃ (or ARS_n, with n>3 for DAS4, DAS5 or DAS6) have ever been reported in the literature. Chapter 2 of this study deals with the *in vitro* reactivity of DAS with different thiols and the characterisation of the reaction products.

1.2.4.2.2 Indirect thiol oxidation through ROS formation

In addition to the direct modification of LMW thiols and protein thiols through DAS, an indirect mechanism through formation of ROS is possible (Figure 1.9).

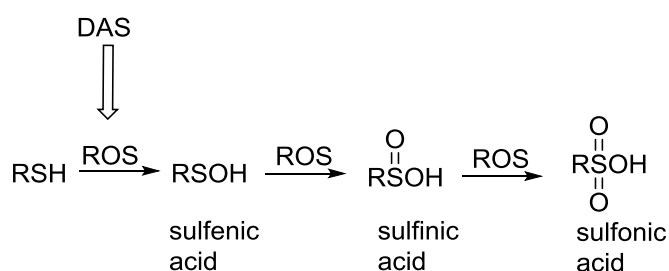


Figure 1.9: DAS induced reactive oxygen species (ROS) production indirectly leads to thiol oxidation.

DAS act as oxidants and subsequently formed ROS can oxidise thiols to sulfenic, sulfinic or sulfonic acid. The formation of sulfenic acid of protein thiols is a common reversible modification, but sulfinic acid formation is less common and sulfonic acid formation is irreversible. Formation of sulfenic acid can lead to increased disulfide concentrations as another thiol molecule can rapidly react with sulfenic acid to form a disulfide.

1.2.4.3 Role of allyl hydrosulfides (AS_nH)

Allyl hydrosulfides (AS_nH, n>1) are hypothesised to be formed as reaction products of DAS (S>2) reacting with thiols (Figure 1.10). The maximum theoretical number of sulfur atoms in AS_nH is always one smaller than the number of sulfur atoms in the DAS starting material. None of the AS_nH with n>1 has been detected and reported yet and therefore it is unknown if all of them are formed or which ones are preferably formed.

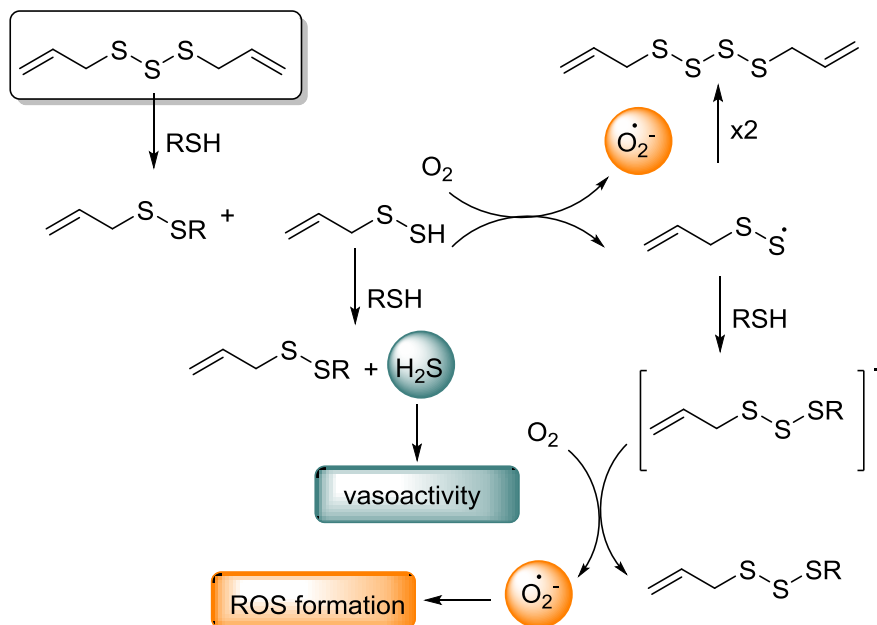


Figure 1.10: Superoxide radical formation and hydrogen sulfide liberation induced by allyl perthiol (AS₂H), a potential reaction product of the reaction between DAS₃ and a thiol.

Allyl hydrosulfides are sometimes regarded as the biologically active form of DAS. According to Munday⁽⁴⁰⁾ the thiol-polysulfide reaction can be regarded as the initial reaction releasing AS₂H which can convert O₂ to the superoxide radical (O₂^{•-}) in a pseudocatalytic cycle (Figure 1.10). In a first step DAS₃ reacts with RSH to form a mixed disulfide and AS₂H. In the next step AS₂H can reduce O₂ to O₂^{•-} and becomes oxidised itself to the perthiyl radical. The O₂^{•-} radical is the starting point for the generation of different ROS, like H₂O₂, or in the presence of metal ions hydroxyl (OH[•]) radicals. OH[•] radicals are highly reactive towards any carbon based biomolecule. They oxidise and hydroxylate DNA, RNA, proteins, enzymes and lipids which ultimately leads to cell death^(40, 41). The reaction cascade is called a pseudocatalytic cycle because two perthiyl radicals can reassemble to form a DAS₄ molecule, which is a DAS that could undergo a similar chain of reactions, but it contains one more sulfur atom than the starting compound (DAS₃)⁽⁴⁰⁾. Alternatively, the perthiyl radical may react with another thiol to form a highly reducing polysulfide anion. Using benzyl hydrodisulfide as an example Chatterji *et al.* showed that the perthiol reacts with molecular oxygen to form O₂^{•-} radicals under physiologically relevant conditions⁽⁴²⁾. This reaction cascade and the pseudocatalytic cycle have yet to be confirmed for AS_nH (n>1) but it would provide an explanation for the higher toxicity of DAS₃ and DAS₄ compared to DAS₂ and it would also explain the strong toxicity of DAS₃ and DAS₄ towards certain cell types even at very low concentrations.

Additionally, these reactions may provide an explanation for the selective toxicity towards cancer cells, which are often closer to a lethal ROS threshold than healthy cells.

Alternatively, the formed AS₂H can react with another thiol molecule to form a mixed disulfide (ARS₂) and liberate the vasoactive gas H₂S (Figure 1.10)⁽⁴⁰⁾. As mentioned before the liberation of H₂S upon incubation of DAS2 and DAS3 with a 20-fold excess of GSH was reported to lead to the formation of 0.4 and 1 molar equivalents of H₂S respectively (Figure 1.8 B, reaction 2 and 4). H₂S has been identified to be an important signalling molecule⁽⁴³⁾ and has shown cardioprotective functions⁽⁴⁴⁾. Pre-contracted aorta rings showed maximum relaxation after adding DAS3, followed by DAS2, matching the H₂S release profile of these compounds and demonstrating the H₂S mediated vasoactivity of DAS⁽¹⁸⁾.

1.2.4.4 Sulfur chain length dependent activity

There are two important observations when analysing the correlation between the sulfur chain length and the reactivity of DAS. Firstly, and more obvious, there is a clear increase in activity with the increasing number of sulfur atoms (shown for DAS1 to DAS4, no data available for DAS5 and DAS6). Secondly, the increase in activity is not linear, while DAS1 is inactive, DAS2 shows little activity and there is a big increase in activity from DAS2 to DAS3. There is a further increase in activity for DAS4, which is rather small. Finding out about the structure activity relationship is important, on the one hand for the use of the DAS (design of new drugs, application in agriculture) and on the other hand it can provide information about the biochemical interactions and cellular reactions of these molecules.

Chemically, the increase in activity from DAS1 to DAS2 can be explained by the ability of DAS2 to act as an oxidant and become reduced to a thiol. It can undergo thiol-disulfide exchange reactions which are responsible for biological activities and from which the DAS1 is excluded. The second big step in increasing activity can be explained by the ability of DAS3 to form AS₂H, which DAS2 is (possibly) excluded from. The importance of AS_nH (n>1) and the suggested function as oxidative stress initiator as well as H₂S release by this molecule was discussed in section 1.2.4.3. The rather small increase in activity for DAS4 could be due to its ability to form another species, the allyl hydrotrisulfide (AS₃H) when reacting with thiols. Another explanation may be the weaker bond strength of the central S-S bond of DAS4 which might result in homolytic cleavage of the molecule to form perthiyl radicals that trigger further reactions in the cell⁽¹⁹⁾. Additionally, it is likely that reactions with thiols (and other biomolecules) occur faster with increasing DAS sulfur chain length, which was shown for the reaction of DAS2 and DAS3 with Cys (Figure 1.8). Within this study it was investigated whether this increase in activity can be seen in different organism (a single-cell bacterium and a multicellular nematode are compared). Furthermore, DAS5 and DAS6 are included in these studies to elaborate whether there is a further increase in activity or if there is an optimum number of sulfur atoms.

1.3 Low molecular weight thiols and redox systems in different organism

To further understand the *in vivo* mode of action of DAS and the consequences of DAS reacting with LMW thiols, a closer look at the physiological functions of different LMW thiols in different organisms and their involvement in cellular pathways is necessary.

1.3.1 Overview

Non-protein LMW thiols (Figure 1.11) play an important role in the maintenance and regulation of a diverse array of cellular processes (Figure 1.12). For example, GSH is the major LMW thiol in eukaryotes and many Gram negative bacteria. However, not all organisms produce or utilise GSH. In particular, many Gram positive bacteria produce other LMW thiols such as mycothiol (MSH), bacillithiol (BSH), trypanothione [T(SH)₂] and γ -glutamylcysteine (γ -GC), which appear to serve as GSH surrogates. In addition to their major LMW thiol, many organisms also utilise additional thiol cofactors as redox buffers such as coenzyme-A (CoA), ovothiol (OSH) and ergothioneine (ESH) (Figure 1.11).

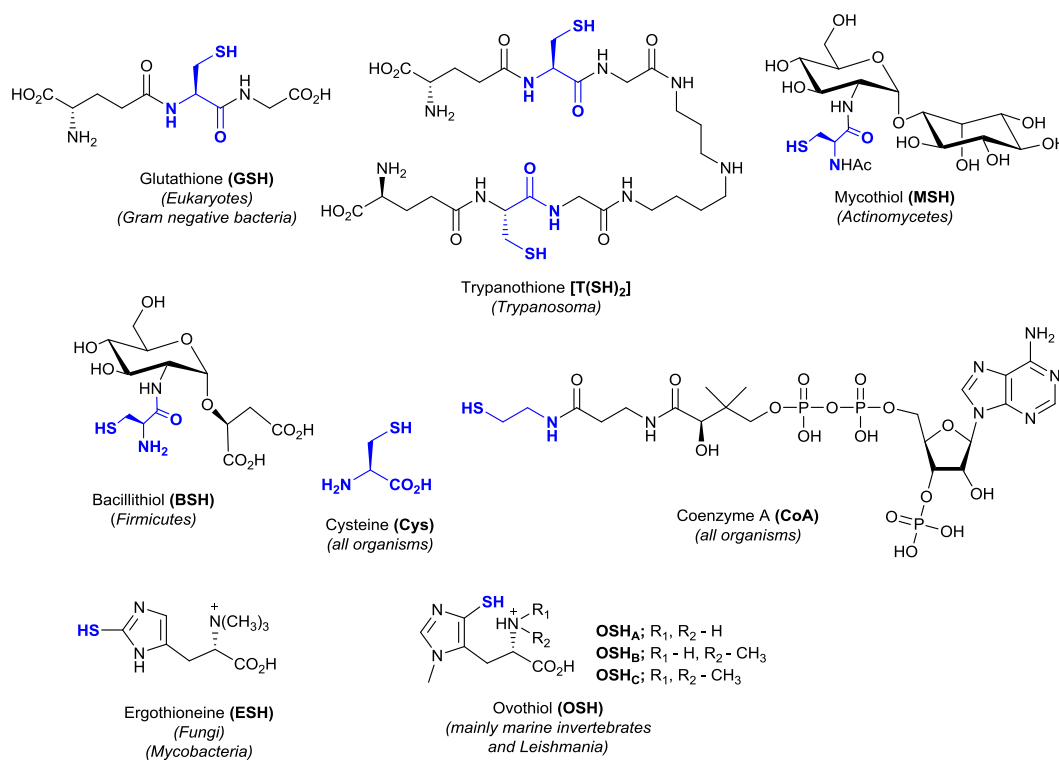


Figure 1.11: LMW thiols produced by different organisms.

LMW thiols play a critical role in maintaining an intracellular reducing environment via the reduction of toxic oxidants (e. g. H_2O_2 and NO). They also facilitate metal ion homeostasis and the detoxification of electrophilic xenobiotics/ metabolites. Reaction with protein thiols (formation of RS-S-protein mixed disulfides) is an important post-translational modification for redox regulation of many proteins as well as protecting exposed Cys residues from irreversible damage during oxidative stress ⁽⁴⁵⁾.

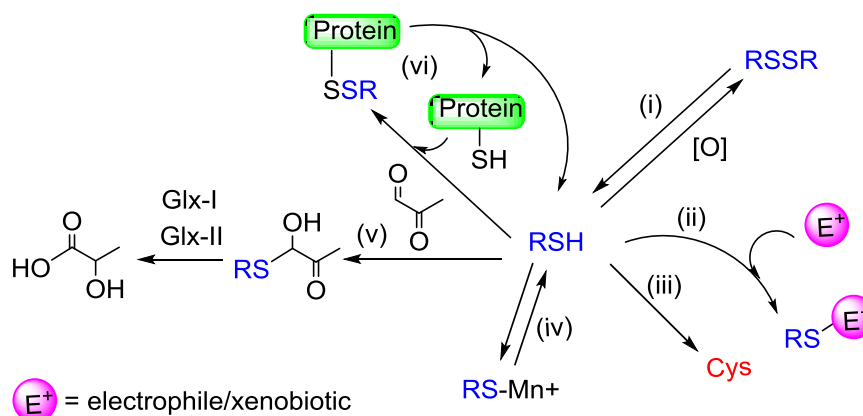


Figure 1.12: The main cellular functions of low molecular weight thiols: (i) As redox buffers; (ii) Xenobiotic detoxification; (iii) As an intracellular cysteine reservoir; (iv) Metal ion homeostasis; (v) Detoxification of reactive carbonyl electrophiles such as methylglyoxal; (vi) Redox regulation/protection of protein functions.

In the experimental part of this study the Gram positive bacterium *Bacillus subtilis* and the nematode *Steinernema feltiae* are used as model organisms. Therefore the focus on this introduction is on the LMW thiols produced by these organisms: BSH produced in *B. subtilis* and GSH produced in *S. feltiae* as well as the universally produced thiols Cys and CoA.

1.3.2 Glutathione

GSH is the most widely distributed LMW thiol, which is biosynthesised and utilised in all eukaryotes and most Gram negative bacteria and is present in millimolar concentrations ⁽⁴⁶⁾. Its metabolic functions include all of those summarised in Figure 1.12. The biosynthetic pathways for several other LMW thiols stem from that of GSH as it shares commonalities with those of γ -GC and $\text{T}(\text{SH})_2$. The first step in GSH biosynthesis involves the ATP-dependent amide bond formation between Cys and the carboxylate sidechain of glutamic acid to give γ -GC followed by another peptide synthetase which adds glycine onto the Cys carboxylate leading to GSH ⁽⁴⁷⁾.

For the purpose of this introduction the focus will be on the role of GSH as redox buffer and on GSH dependent redox active enzymes. There are several excellent reviews of GSH metabolism to which the reader is directed for further reading ⁽⁴⁸⁻⁵¹⁾.

1.3.2.1 GSH-dependent redox active enzymes

GSH is important for the maintenance of the cellular redox status and the GSH/GSSG ratio (between 30:1 and 100:1) is maintained by glutathione disulfide reductases (GR) (Figure 1.13). GR use the reducing power of nicotinamide adenine dinucleotide phosphate (NADPH) to reduce glutathione disulfide (GSSG) back to GSH ⁽⁴⁶⁾.

The relatively high pK_a of GSH (~ 9) helps to protect it from facile oxidation to sulfenic acid (GSOH), but it also means that the pK_a needs to be decreased for GSH to be deprotonated at physiological pH to perform a nucleophilic attack. GST decrease the pK_a of GSH (to ~ 6) and catalyse the conjugation of GSH with several compounds produced under oxidative stress⁽⁴⁶⁾. The expression of GST is regulated by the cellular redox status and represents a sensor which is able to transmit redox variations and induce apoptosis by modulating the stress kinase pathway. GST can also catalyse glutathionylation of Cys residues of proteins, which are oxidised to sulfenic acid through peroxide attack (Figure 1.13). The glutathionylation can either protect proteins from irreversible oxidation to sulfinic or sulfonic acid or regulate enzyme activity or transcription⁽⁵¹⁾. Glutathionylation is possible through an enzyme-independent thiol-disulfide exchange reaction between GSSG and a protein Cys thiolate, but the reaction is kinetically much less favoured⁽⁴⁶⁾.

The glutathionylation is reversed by another class of enzymes: Glutaredoxins (Grx) (Figure 1.13). Grx are small redox active enzymes of approximately one hundred amino-acid residues that use GSH as a cofactor. Grx are oxidized by their substrates, and reduced non-enzymatically by GSH, which is re-generated through GR⁽⁵²⁾.

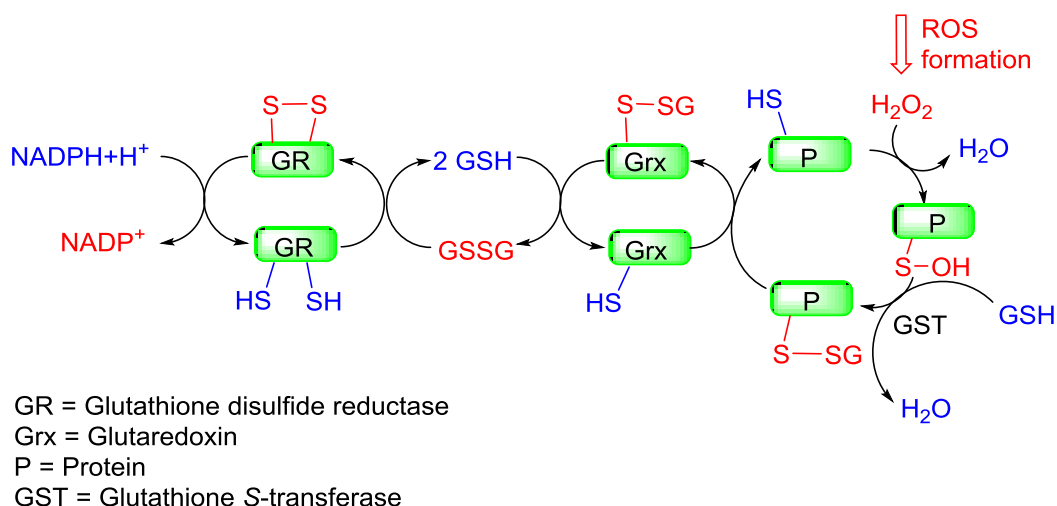


Figure 1.13: Oxidation of Cys residues of proteins to sulfenic acid by oxidants (e.g. H_2O_2) can have damaging or regulatory effects. Further oxidation to sulfinic or sulfonic acid is avoided through glutathionylation catalysed by glutathione-S-transferase (GST). Glutathionylation is reversed by Glutaredoxins (Grx). Ultimately reduced GSH is reconstituted by glutathione disulfide reductase (GR), which uses the reducing power of NADPH.

Other important redox active GSH dependent enzymes are glutathione peroxidases (Gpx), which reduce hydroperoxides to the corresponding alcohols through oxidation of GSH to GSSG. The enzymatic mechanism involves the oxidation of a selenocysteine residue to selenic acid, which reacts with GSH and is reduced back via reaction with another molecule of GSH⁽⁴⁶⁾. Another selenocysteine-independent class of GSH peroxidases are peroxiredoxins (Prx), which have a cysteine residue that is easily oxidised to sulfenic acid by peroxides. This oxidation process is reversed either by GSH or thioredoxins (Trx), another class of redox active enzymes, which are reduced by a specific Trx reductase that uses NADPH as a reductant⁽⁵³⁾.

These are just examples of pathways that GSH-utilising cells use to fight oxidative stress. The involvement of GSH in these pathways and redox cycles demonstrates the importance of GSH

in fighting oxidative stress and maintaining the redox status of the cell. Specific features of the GSH redox system in nematodes are discussed in chapter 4.

1.3.3 Bacillithiol

BSH has only been discovered recently in 2009⁽⁵⁴⁾ and was found to be the major LMW thiol in many Gram positive bacteria, which do not produce GSH. These include bacilli (*e.g. Bacillus anthracis*, *B. subtilis*, *B. cereus*, *B. megaterium*, *B. pumilis*) and some, but not all staphylococci (*e.g. Staphylococcus aureus*, *S. saprophyticus*) and streptococci (*Streptococcus agalactiae*)⁽⁵⁴⁾.

BSH biosynthesis is initiated by a glycosyltransferase (BshA) that catalyses the glycosylation of L-malic acid with uridine diphosphate-*N*-acetylglucosamine (UDP-GlcNAc) to afford *N*-acetylglucosamine-malate (D-GlcNAc-L-Mal) (Figure 1.14)^(55, 56). An *N*-acetyl hydrolase (BshB) then liberates the free amine glucosamine-malate (D-GlcN-L-Mal)⁽⁵⁵⁾. Gene knockout studies in *B. subtilis* have identified a bacillithiol synthase (BshC) which mediates the condensation of D-GlcN-L-Mal with L-cysteine to yield BSH. In the absence of this *bshC* gene, *B. subtilis* is unable to produce BSH, and the intracellular levels of its biosynthetic precursor (GlcNMal) have been shown to accumulate⁽⁵⁵⁾. This is very strong evidence that this BshC candidate mediates the final stage of BSH biosynthesis. Attempts to demonstrate the BSH synthase activity of BshC *in vitro*, however, have so far been unsuccessful. BshA and BshC are essential for BSH biosynthesis, but the activity of BshB is shared with another *N*-deacetylase⁽⁵⁵⁾. This redundancy is due to a candidate bacillithiol-*S*-conjugate amidase (Bca) that is able to *N*-deacetylate GlcNAc-Mal with comparable efficiency to that observed with BshB⁽⁵⁷⁾.

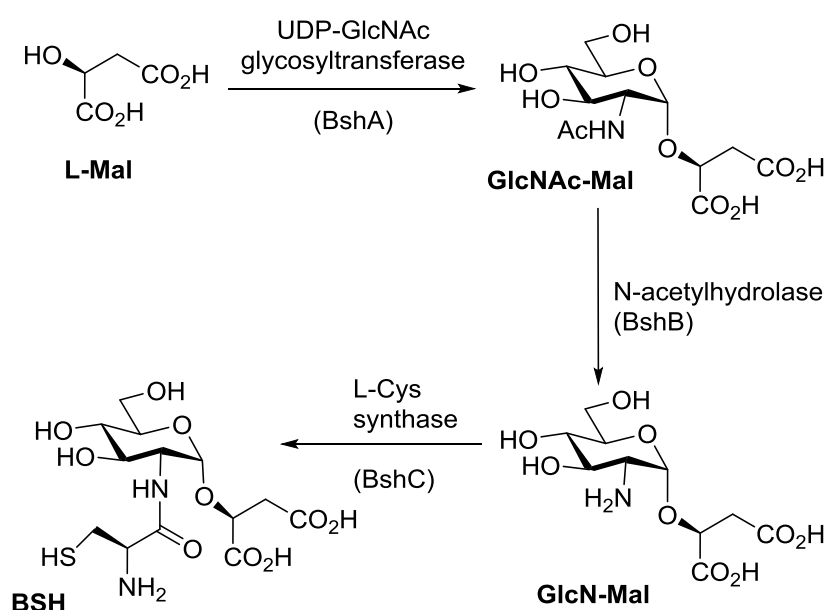


Figure 1.14: Biosynthesis of bacillithiol (BSH).

The main cellular functions of BSH are summarised in Figure 1.15. BSH deficient mutants of *B. subtilis* display increased sensitivity to oxidative, osmotic and acid stress as well as a 100-fold reduction in sporulation efficiency. The mutants also show increased sensitivity to some antibiotics (e.g. fosfomycin) ⁽⁵⁵⁾ and a bacillithiol-S-transferase (BST, FosB) was identified in *S. aureus*, that catalyses the inactivation of fosfomycin through S-conjugation of BSH to the epoxide motif of fosfomycin ⁽⁵⁸⁾.

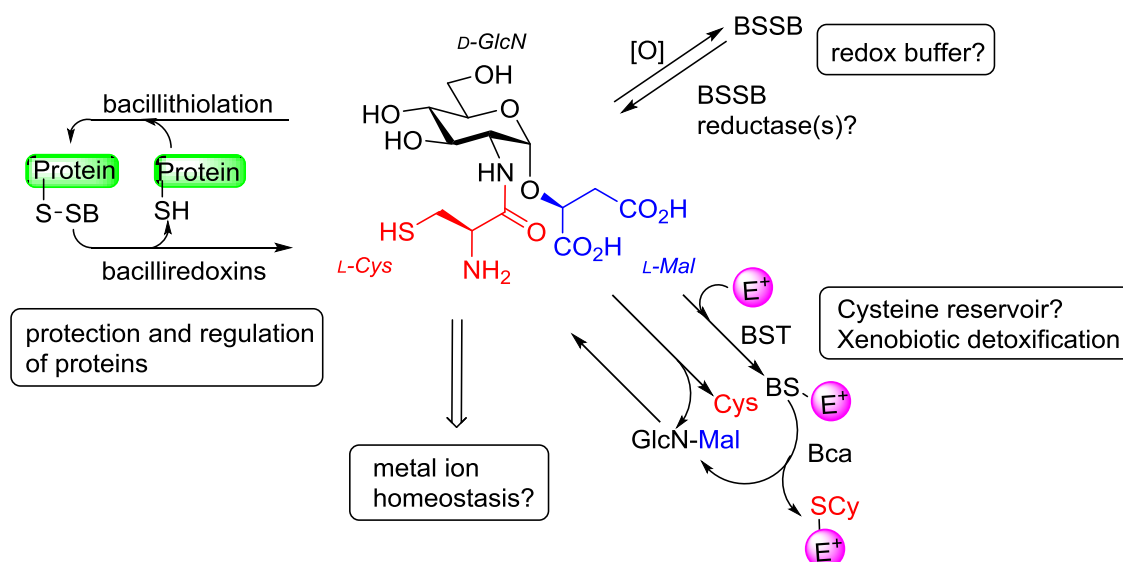


Figure 1.15: Overview of the functions of bacillithiol, some of which are still under investigation.

Intracellular BSH is predominantly present in its reduced form with BSH/ bacillithiol disulfide (BSSB) redox ratios ranging from 40:1 (in *B. anthracis*) ⁽⁵⁶⁾ to 400:1 (in *B. subtilis*) ^(54, 59). Reduced BSH is presumably maintained by an as yet unidentified BSSB reductase (BR). BSH also forms mixed disulfides with protein thiols (S-bacillithiolations) which can protect or regulate protein function. In *B. subtilis* a redox sensitive Prx transcription regulator (OhrR) is bacillithiolated during cumene hydroperoxide stress suggesting a function for BSH in redox sensing ^(60, 61). Several other proteins are also bacillithiolated when *Bacilli* are exposed to sodium hypochlorite (NaOCl) stress ^(62, 63). These include two methionine synthases (MetE and YxjG), a pyrophosphatase (PpaC) and a 3-D-phosphoglycerate dehydrogenase (SerA). Growth of both *ohrR* and BSH null mutants are severely impaired by NaOCl stress compared to the wild-type (WT). S-Bacillithiolation of OhrR leads to a 200-fold up-regulation of the OhrA Prx that confers protection against NaOCl ⁽⁶²⁾. S-Bacillithiolation of methionine synthases causes hypochlorite-induced methionine starvation/auxotrophy, which inhibits the initiation of protein translation ⁽⁶²⁾. This could serve to prevent the synthesis (and potential oxidative damage) of additional proteins whilst the cell detoxifies the oxidant and restores the thiol redox homeostasis.

Two bacilliredoxin (Brx) proteins have been identified recently (YphP (BrxA) and YqiW (BrxB)), which are widely conserved amongst BSH-producing Firmicutes and were found to mediate the de-bacillithiolation of BS-protein ^(55, 64). *In vitro* studies demonstrated that BrxB can restore DNA-binding activity to OhrR which is S-bacillithiolated, but not to OhrR that is S-cysteinylated and MetE was shown to be efficiently de-bacillithiolated by both BrxA and BrxB ⁽⁶⁴⁾.

In Gram negative bacteria, intracellular concentrations of Cys (~0.4 mM) are usually much lower than GSH (up to 10 mM) ⁽⁶⁵⁾. BSH levels in many Bacilli (eg. *S. aureus*, *B. anthracis*) are more comparable to those of Cys ⁽⁵⁴⁾. BSH levels in *B. subtilis* can increase from 0.5-5 mM as cell cultures progress from early-exponential growth to stationary phase (reported herein) ⁽⁵⁹⁾. It is not yet known how the catalytic efficiencies of BSH redox enzymes (i.e. Brx and BR) compare with their GSH counterparts.

The pK_a of BSH (~8) is lower compared to GSH (~9) which implies that it is more deprotonated at physiological pH and therefore more reactive, which can imply higher efficiency, but it could potentially also become oxidised to its disulfide or sulfenic acid more easily.

1.3.4 Cysteine

Cys is universally found in all cells. It is an amino acid which is frequently found at functionally and structurally important sites in many proteins where it takes part in a wide variety of biological functions, like catalysis, structure stabilisation or metal binding. Some enzymes contain Cys residues that can form intramolecular disulfide bonds depending on the oxidation status of their environment and the formation of disulfide bonds regulates the enzymatic activity. Thereby the redox environment can regulate certain enzymes that are important as oxidative stress responses.

In addition to Cys as an amino acid in proteins, free Cys is found in the cells. The Cys thiol is nucleophilic and easily oxidised and displays increased reactivity when deprotonated. It easily oxidises to its symmetric disulfide, cystine (CySS), especially in the presence of transition metal ions (such as Fe³⁺) ⁽⁴⁶⁾, and there are no enzymes characterised in prokaryotes which reverse the oxidation of CySS to recover reduced Cys ⁽⁴⁷⁾. Therefore most organisms use other, less reactive LMW thiols as their major redox buffer, where Cys forms part of (GSH, BSH, T(SH)₂ and MSH, where it is *N*-acetylated). Initially, it was believed, that Cys and BSH are present in similar concentrations in *B. subtilis* ⁽⁵⁴⁾, but recently (reported herein) it was discovered that BSH increases up to 5 mM during the exponential growth phase of *B. subtilis*, while Cys stays at lower concentrations, up to 0.3 mM ⁽⁵⁹⁾. This demonstrates the prominent role of BSH over Cys as the main redox buffer in *B. subtilis*.

1.3.5 Coenzyme-A

CoA is an essential thiol cofactor in all living organism and plays important roles in central metabolic pathways, like the Krebs cycle and fatty acid metabolism. NAD(P)H-dependent CoA disulfide reductases (CoADR) have been isolated and characterised in different BSH producing pathogenic bacteria (e.g. *S. aureus* ⁽⁶⁶⁻⁶⁸⁾ and *B. anthracis* ⁽⁶⁹⁾) indicating that CoA has intracellular redox functions. For bacteria, which utilise the CoADR/ CoA redox couple in addition to BSH, redundancy provided by these two thiol redox buffers may confer an advantage in virulence and/ or survival of such pathogens ⁽⁵⁶⁾. However, no CoADR is described in *B. subtilis* and a thiol pK_a of 9.83 ⁽⁷⁰⁾ means that CoA exists nearly exclusively in its unreactive thiol form at physiological pH. It is therefore reasonable to speculate that enzymes must be present to lower the pK_a of CoA (similar to GST for GSH), but no such enzymes have yet been discovered.

In dormant spores of *B. megaterium* about 45% of CoA are bound to proteins as mixed disulfides and more than 75% of these are cleaved during germination ⁽⁷¹⁾, which demonstrates

a thiol redox regulation or protection role of CoA similar to that of GSH. Enzymes that reverse the formation of mixed disulfides between CoA and proteins are not known.

1.3.6 Interaction between DAS and LMW and protein thiols

The interaction of DAS with LMW thiols and the resulting disturbance of the redox balance inside the cells were highlighted as possible MOA of DAS in section 1.2.4.2. In the next section the reactivity of different LMW thiols based on their physical constants will be discussed in more detail (section 1.3.6.1) before discussing the biological importance of the thiol-polysulfide exchange between DAS and thiols *in vivo* (section 1.3.6.2).

1.3.6.1 Thiol-disulfide exchange reactions

As mentioned before, the initial reaction between DAS and LMW thiols is a thiol-polysulfide exchange reaction analogous to a thiol-disulfide exchange reaction. The speed of the reaction is dependent on the pK_a of the thiol, because the attacking thiol needs to be deprotonated for the reaction to occur (see Figure 1.16), and the redox potential of the thiol.

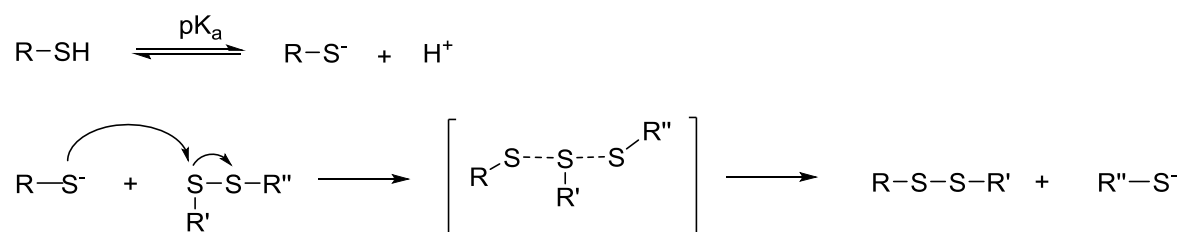


Figure 1.16: General mechanism for thiol disulfide exchange reactions. The thiolate attacks the sulfur atom of the disulfide in a nucleophilic substitution reaction and forms a linear SSS-type transition state complex, before the thiol is liberated as a leaving group⁽⁷²⁾.

The redox potential is a measurement of a chemical species to acquire electrons and thereby be reduced. The more negative the potential, the smaller the species' affinity for electrons and therefore the greater the tendency to become oxidised. GSH has a more negative redox potential than BSH and Cys (Table 1.4) and therefore gets more easily oxidised, which means that it is a stronger reductant.

Table 1.4: Thiol redox potentials and pK_a values⁽⁵⁹⁾.

	GSH	BSH	Cys
Standard redox potential	-240 mV	-221 mV	-223 mV
Microscopic thiol pK_a (when amino group is protonated)	8.93 ⁽⁷³⁾	7.97	8.38

The pK_a is the pH at which the proton is exactly half dissociated. The lower the pK_a value, the more deprotonated is the acid/ thiol group at a certain pH. BSH has the lowest pK_a value (7.97), followed by Cys (8.38) (Table 1.4), and therefore BSH is more deprotonated at a certain pH compared to Cys and GSH (8.93), which translates into higher reactivity in thiol-disulfide exchange reactions, where deprotonation of the thiol is required for the reaction to occur.

1.3.6.2 Biological importance of thiol-disulfide exchange between DAS and LMW thiols and protein thiols *in vivo*

In a biological context thiol-disulfide exchange reactions are too slow to be of metabolic importance, but certain enzymes accelerate the process up to seven orders of magnitude ⁽⁷²⁾. For example oxidoreductases, like Trx and Grx (which catalyse the reduction of Cys residues in proteins) contain a redox active CXXC motif at their active site, where the *N*-terminal Cys can act as a nucleophile and undergo a thiol-disulfide exchange reaction and form a mixed disulfide with its substrate. This is followed by an intramolecular attack of the *C*-terminal Cys on the *N*-terminal Cys to obtain the oxidised CXXC motif and release the reduced substrate thiol ⁽⁷²⁾.

The reactions between DAS and LMW thiols feature some important differences compared to normal thiol-disulfide exchange reactions: DAS contain more than two sulfur atoms in a chain and the reactivity increases with increasing number of sulfur atoms, shown for DAS2 and DAS3 (Figure 1.8 B). The nucleophilicity and acidity of the attacking thiolate is regarded as the main driver of the reaction, but the electrophilicity and stability of the attacked sulfur as well as the acidity of the leaving group play important roles as well ^(72, 74). These properties are considerably different for DAS. Lower pK_a of the leaving group increases the rate of reaction, which facilitates the reaction of DAS with LMW thiols, where allyl hydropolysulfides (AS_nH , $n>1$) can form leaving groups, which have been reported to have lower pK_a values than the corresponding thiols ⁽⁷⁵⁾. Additionally, the dissociation energy decreases with increasing sulfur chain length (shown for DMS2 to DMS4 ⁽³⁷⁾), which may make the longer chain DAS more prone to nucleophilic attack from a thiolate. Nevertheless, the reaction products of DAS with LMW thiols (mixed polysulfides and AS_nH with $n>1$) have never been detected *in vivo*. As a consequence of this reaction, the pool of reduced LMW thiols decreases, which has often been observed upon DAS treatment ^(18, 25, 40, 76), providing some evidence of the occurrence of this reaction *in vivo*.

Another important question is the stability of the mixed di- and polysulfides *in vivo*. As cells have strong enzymatic mechanism in place to keep the cellular environment reduced, the mixed di- and polysulfides might become rapidly reduced. This could happen through either a thiol-disulfide exchange reaction with another molecule of GSH, BSH or Cys acting as nucleophile or enzymatic reduction by GR. Mixed di- or polysulfides have not yet been shown to be a substrate for GR, but DAS3 was shown to be a substrate for the enzyme ⁽⁷⁷⁾ as well as glutathione trisulfide (GSSSG) ⁽⁷⁸⁾. The substrate kinetics for GSSSG and GSSG were shown to be comparable, whereas the reduction of DAS3 is less favoured and might not be relevant *in vivo*.

Cys residues in proteins are often found at structurally, regulatory or catalytically important sides as well as in binding sites. Therefore allyl-modifications or oxidations of Cys residues can have an impact on enzyme activity. Depending on the function of the modified enzyme, different cellular pathways can be disturbed. For example Cys-hydrolases, -dehydrogenases and phosphatases as well as various zinc-finger proteins lose activity upon the oxidation of their key Cys residues ⁽⁴¹⁾. The cation channel TRPA1, which signals acute pain and neurogenic inflammation, was found to be reversibly activated through interaction of DAS2 with key Cys residues. A triple mutant, where conserved Cys residues were replaced by alanine or serine residues did not show activation upon DAS2 treatment, but activation was sustained through other non-covalent binding inductors ⁽⁷⁹⁾. Although this study did not directly demonstrate covalent modifications and disulfide formation between DAS2 and Cys residues of the protein,

strong evidence for such interaction was provided. Another example involves the covalent *S*-allyl modification of two Cys residues of β -tubulin after incubation with DAS3, detected by mass spectrometry (MS). These modifications led to *in vitro* inhibition of β -tubulin which was suggested as a reason for the DAS3-induced G₂/M cell cycle arrest observed in human colon cancer cell lines in the same study⁽²⁸⁾.

1.4 Objectives and strategy of this project

Garlic has been used to cure diseases for centuries and modern research has been investigating the beneficial effects of garlic. Especially garlic derived DAS are under investigation because of their antibacterial and anticarcinogenic properties, which are of similar intensity to allicin, but DAS have the advantage of greater stability compared to allicin, which is an important factor for applications in medicine or agriculture. This study focusses on the application of DAS as a nematicide to combat the threat of these important plant pathogens. Due to toxicity issues of many synthetic pesticides, they have been banned⁽⁸⁰⁾ and there is a severe shortage of pesticides against certain pathogens (e.g. potato cyst nematodes (PCN) damaging potato crops). There is an urgent need for new, eco-friendly pesticides, which has led to an increased interest in the research of bioactive natural products. To further exploit the extraordinary chemistry provided by garlic and DAS in particular, it is important to understand their MOA and biochemical pathways induced and affected by DAS (Figure 1.17). The overarching hypothesis which will be tested in this study involves the reaction of DAS with LMW or protein thiols which leads to the formation of mixed di- or polysulfides (ARS2) and reactive hydro polysulfides (AS2H) which are hypothesised to lead to ROS formation. DAS derived ROS formation can then lead to further disulfide formation of LMW and protein thiols.

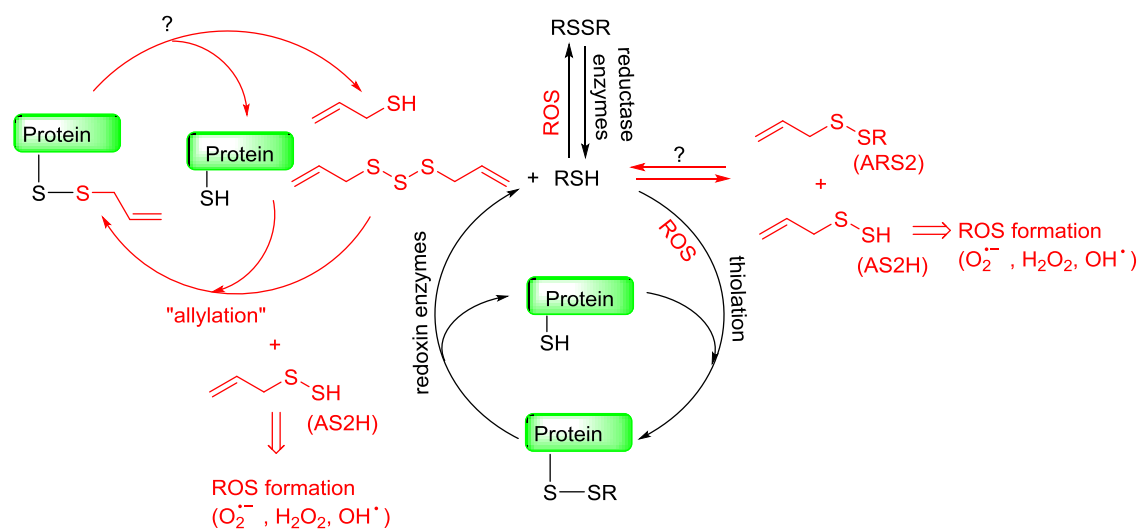


Figure 1.17: Hypothesised interaction of DAS with cellular LMW and protein thiols leading to ROS formation and a disturbance of the cellular redox status.

This study focusses on five main areas:

- a) Synthesis and purification of DAS3 to DAS6
- b) Elucidation of the structure-activity relationship of DAS1 to DAS6 in different test organism (*B. subtilis* and *S. feltiae*)
- c) *In vitro* reactivity of DAS with LMW thiols as one possible MOA of DAS and identification and characterisation of the reaction products
- d) *In vivo* MOA: Analysis of LMW thiols, disulfides and DAS metabolites in *B. subtilis* and *S. feltiae* and posttranslational protein modifications in *B. subtilis* after DAS treatment
- e) Applications of DAS formulations as a nematicide to combat plant pathogenic nematodes in field trials

Through an easy one pot synthesis followed by HPLC purification, DAS3 to DAS6 were gained in high purity and sufficient quantity for testing in different bioassays. This study is one of the first ones to include DAS5 and DAS6 in biological testings as these compounds are not commercially available and difficult to handle, because of stability issues⁽⁸¹⁾.

The structure-activity-relationship between different DAS compounds was established through determination of MICs against *B. subtilis* and dose-response curves show the activity against *S. feltiae*.

To investigate the *in vitro* reactivity of DAS with LMW thiols and to identify and characterise new reaction products, nuclear magnetic resonance spectroscopy (NMR), high performance liquid chromatography (HPLC) and MS methods were employed and differences in reaction speed and product composition for different DAS and different LMW thiols were elucidated.

LMW thiols and disulfides as well as DAS metabolites in cell extracts of *B. subtilis* and *S. feltiae* were fluorescently labelled and analysed by HPLC, allowing for high sensitivity and individual analysis of different metabolites within one particular sample. Posttranslational modifications in the *B. subtilis* proteome after DAS treatment were analysed by Western Blot and MS (Dr. Haike Antelmann, Institute for Microbiology, Ernst-Moritz-Arndt-University of Greifswald, Germany) methods identifying a wide range of modified proteins.

Finally, DAS formulations were used in field trials, performed with ECOSpray Ltd., to explore the nematicidal activity against PCN (*Globodera* spp.) and root-knot nematodes (RKN, *Meloidogyne* spp.) in a field setting. Some background information about the biology of these pathogens and their control is given in chapter 4, before presenting the experimental results.

In summary, the objective of this study is to investigate the interaction of DAS with thiols as one possible MOA, the structure-activity relationship of DAS in different test organism to elaborate the most active molecule(s) and their possible applications as a nematicide in agriculture. A wide range of techniques has been employed to evaluate the biological activity of DAS, ranging from chemical, biochemical and microbiological methods over nematological experiments up to commercial field trials and their statistical analysis.

2 Diallyl polysulfides and their reactivity with low molecular weight thiols

2.1 Synthesis, purification and characterisation of diallyl polysulfides

Diallyl polysulfides (DAS) are naturally found in aged garlic extracts and garlic oils (GOs), where they are present as mixtures with varying composition. In this study pure DAS as single molecule entities were used instead of mixtures, like GOs or extracts. Purified DAS (DAS1-DAS4) are commercially available, but commercial products are often not showing high purity. Therefore, for the purpose of this study, DAS molecules were chemically synthesised and purified.

2.1.1 Synthesis of DAS

One common method for the synthesis of alkyl and aryl polysulfides is the reaction of thiols with dichlorosulfanes⁽⁸²⁾ (Figure 2.1). Since only SCl_2 and S_2Cl_2 are commercially available, polysulfides prepared by these reactions are primarily tri- and tetrasulfides.

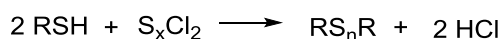
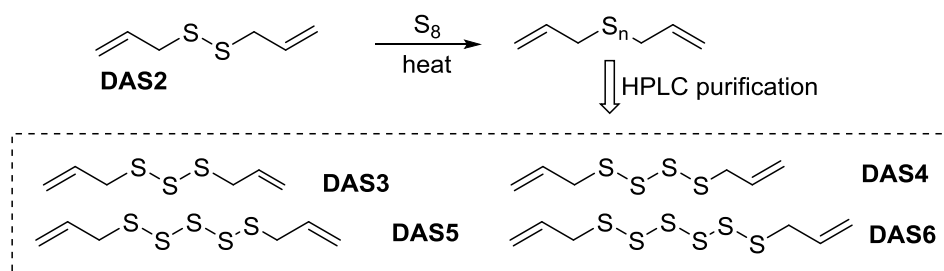


Figure 2.1: Synthesis of polysulfides through reaction of thiols with dichlorosulfanes⁽⁸²⁾.

Instead of individually synthesising DAS3 to DAS6, a mixture of DAS was synthesised using a published⁽⁸³⁾ and patented method (Figure 2.2).

A General reaction scheme



B Mechanism

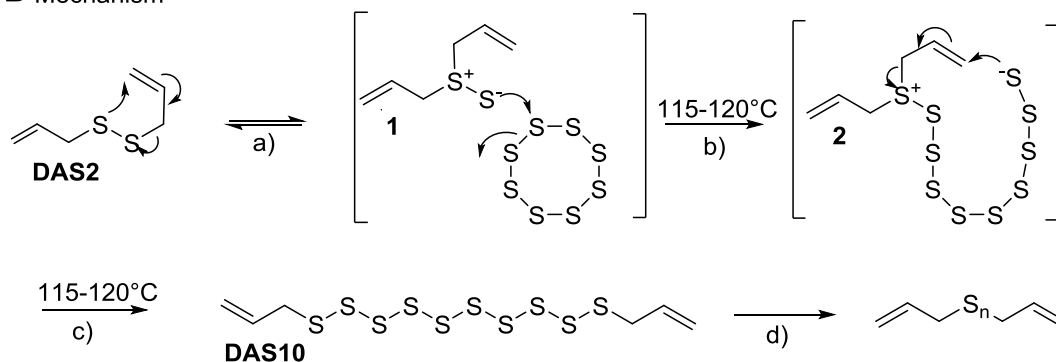


Figure 2.2: Synthesis of DAS mixture from DAS2 and elemental sulfur. A: General reaction scheme. B: Mechanism of the reaction.

DAS2 and elemental sulfur (1.5:1 molar equivalents, calculated for sulfur as S₈) are used as starting materials. The proposed mechanism⁽⁸³⁾ involves the following distinct steps (Figure 2.2 B) : (a) DAS2 exists in equilibrium with diallyl thiosulfoxide **1** when heated and (b) at a temperature of 115 - 120 °C the diallyl thiosulfoxide reacts with the molten sulfur to form a diallyl thiodecasulfoxide intermediate **2**. (c) This intermediate **2** rearranges to produce diallyl decasulfide (DAS10). (d) In the final step, DAS10 equilibrates to a mixture of DAS containing different numbers of sulfur atoms in a linear chain.

A colour change from yellow through orange to brown was observed and the reaction was stopped after one h. The product of the reaction is a brown, viscous oil, that can be analysed by High Performance Liquid Chromatography (HPLC) to determine the exact DAS composition.

Advantages of this synthesis are the quick reaction, the cheap and readily available starting materials, the simplicity of the performance and the high amount of higher DAS (DAS5 and DAS6) gained by this reaction. A disadvantage is that the product is a mixture of many different DAS, which requires a time-consuming purification (section 2.1.2). A second disadvantage is the lack of a well-defined end point of the reaction, which results in slight changes in the DAS composition in different reaction batches.

2.1.2 Purification and isolation of DAS3 to DAS6

To isolate the pure individual DAS, the reaction mixture was purified by reverse phase (RP) preparative HPLC and the detection was performed through ultraviolet (UV) absorption at 210 nm. The purity of the collected fractions was confirmed by analytical HPLC (section 2.1.3) before DAS were extracted in hexane and dried under vacuum ($\leq 30^\circ\text{C}$, because of heat instability of compounds). The purity was re-confirmed by analytical HPLC. DAS3 to DAS6 are slightly yellow to brown viscous oils with higher viscosity and darker colour with increasing number of sulfur atoms. They were obtained with purities between 90 and 99% and were stable at -20°C in the dark for several months when stored as pure, dry compounds. Higher DAS ($S > 6$) could not be isolated and purified because of their instability. Other purification methods (normal phase (NP) and RP flash chromatography and distillation) were attempted to speed up the purification process, but did not yield DAS with sufficient purity. Because of the similar chemical structures of DAS3 to DAS6 (they only differ by different numbers of sulfur atoms from one another) their chromatographic elution profiles are very similar and therefore the higher resolution provided by HPLC through smaller particle size of the solid matrix is necessary for clean separation of the molecules.

2.1.3 Characterisation of DAS

2.1.3.1 Characterisation by HPLC

HPLC analysis of the synthesised DAS was performed with slight alterations of a method previously described⁽⁸¹⁾. Isocratic elution at a flow-rate of 1.5 mL/ min using 90% (v/v) MeOH provided good separation of DAS1 to DAS6 through a C₁₈ column with additional phenyl functionality (250 x 4.6 mm) within 16 min (Figure 2.3). Detection was carried out through UV absorption at 210 nm.

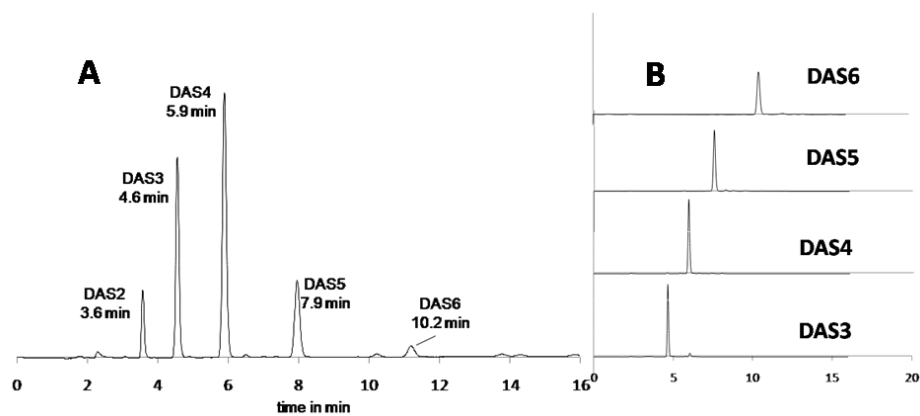


Figure 2.3: HPLC analysis of DAS. A: Standard mixture of DAS and B: Synthesised and purified DAS.

2.1.3.2 Characterisation by Nuclear Magnetic Resonance (NMR) spectroscopy

The purified DAS (Figure 2.4 A) were analysed by ^1H -NMR and ^{13}C -NMR spectroscopy (Figure 2.4 B and C). The ^1H -NMR spectrum shows three distinct signals (Figure 2.4 B) as the molecule is symmetric with $2 \times 3 \text{ CH}_n$ groups. Protons that are in an identical chemical environment in a symmetric molecule show identical signals. The CH_2S protons (1) form a doublet of doublets at 3.06-3.59 ppm and this peak is the most useful one for comparing and distinguishing between the DAS. The doublet of doublets of triplets (ddt) at 5.65 - 5.98 ppm represents the two $=\text{CH}$ protons (2) and the multiplet at 4.98 – 5.90 ppm represents the four terminal $=\text{CH}_2$ protons (3) (Figure 2.4 B). ^1H -NMR data for the different DAS shows that the differences in chemical shifts decrease with an increase in sulfur atoms in the chain (Figure 2.4 B). It is possible to distinguish between DAS1, DAS2, DAS3, DAS4 and maybe DAS5, but peaks for DAS5 and DAS6 are overlaying and it is not possible to distinguish between them only on the basis of ^1H -NMR data.

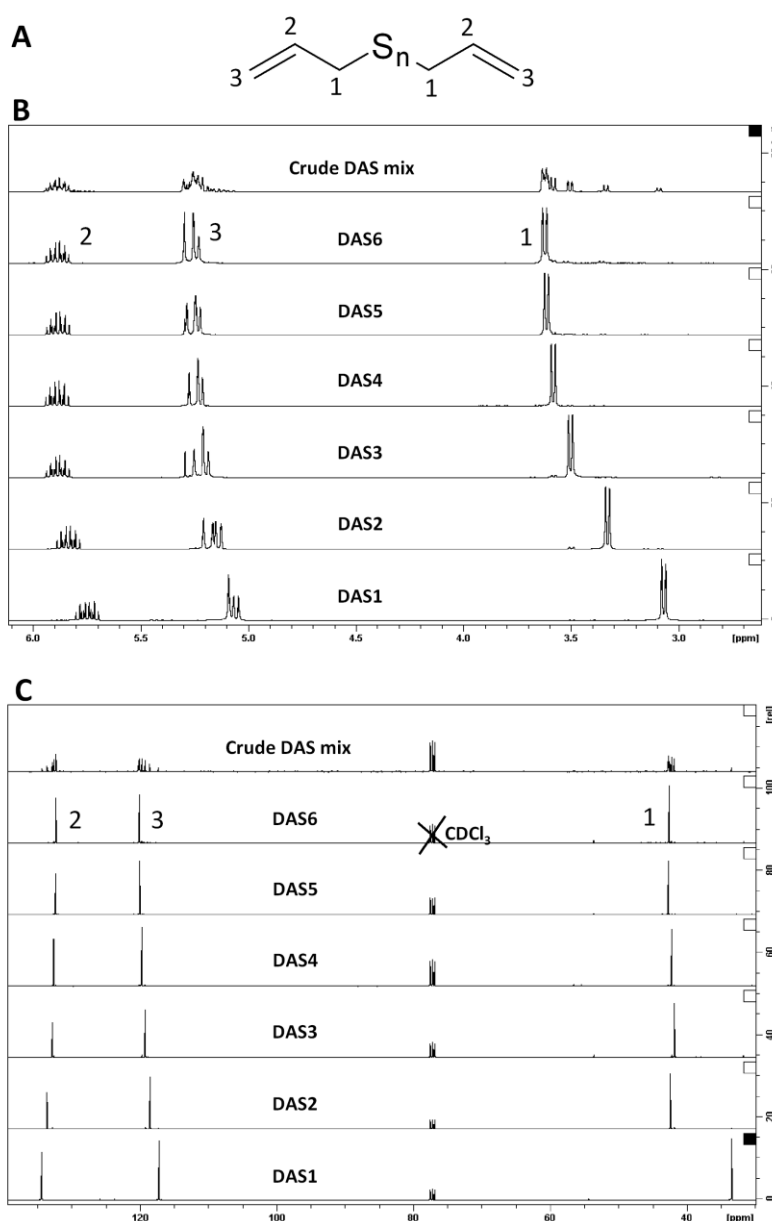


Figure 2.4: NMR characterisation of DAS. A: Chemical structure of DAS. B: ^1H -NMR spectra of pure DAS1 to DAS6 and a DAS mixture (crude). C: ^{13}C -NMR of pure DAS1 to DAS6 and a DAS mixture (crude).

In addition to $^1\text{H-NMR}$, $^{13}\text{C-NMR}$ can be used to characterise DAS (Figure 2.4 C). As observed in the $^1\text{H-NMR}$ spectra, there are three distinct signals for the six carbon atoms in the DAS molecule, due to the symmetry of the molecules. The signal representing the two CH_2S carbon atoms on each side of the sulfur (1) is different for DAS1 (33.50 ppm) compared to all other DAS (between 41.90 and 42.82 ppm). The signals of the $=\text{CH}$ carbon (2) and the terminal $=\text{CH}_2$ carbons (3) are very similar for all DAS (between 132.49 and 135.33 or 117.42 and 120.31 ppm respectively). Due to the small changes in peak shifts for different DAS, $^{13}\text{C-NMR}$ is not very useful for the differentiation between DAS.

It is plausible that peak shifts do not differ much for different DAS in $^1\text{H-}$ and $^{13}\text{C-NMR}$, since all corresponding protons and carbons experience similar chemical environments in the different DAS. Only the number of sulfur atoms between the two allyl groups changes, which has the biggest influence on the CH_2S groups next to the sulfur atom (1), but even this effect becomes smaller with increasing number of sulfur atoms.

2.1.3.3 Characterisation by Liquid Chromatography-Mass Spectrometry (LC-MS)

For the characterisation of DAS by LC-MS a Coordination Ion Spray Mass Spectrometry (CIS-MS) method was chosen ⁽¹⁾. Due to their non-polarity and poor ionisation properties, DAS could not be detected by LC-MS on their own. Instead, methanolic samples of pure DAS were mixed with silver tetrafluoroborate (AgBF_4) and analysed as their silver adducts $[\text{M}+\text{Ag}^+]$. Silver coordinates strongly to sulfur and therefore DAS can be detected as silver ions. As silver exists in two isotopes (107 and 109), with relatively equal distribution (silver 107 makes up 52%), two characteristic peaks of approximately the same intensity can be seen for each compound. DAS2 to DAS6 were detected as their silver adducts by direct injection using methanol (MeOH) as solvent and electrospray ionisation (ESI) with detection in positive mode. Figure 2.5 shows examples of the CIS-MS for DAS4 and DAS5.

For the DAS6 sample also $\text{DAS5}+\text{Ag}^+$, $\text{DAS4}+\text{Ag}^+$ and $\text{DAS3}+\text{Ag}^+$ were detected, which might be the result of instability of the DAS6 under the ionisation conditions or the sample initially contained some shorter chain DAS impurities formed through DAS6 rearrangements (section 2.2).

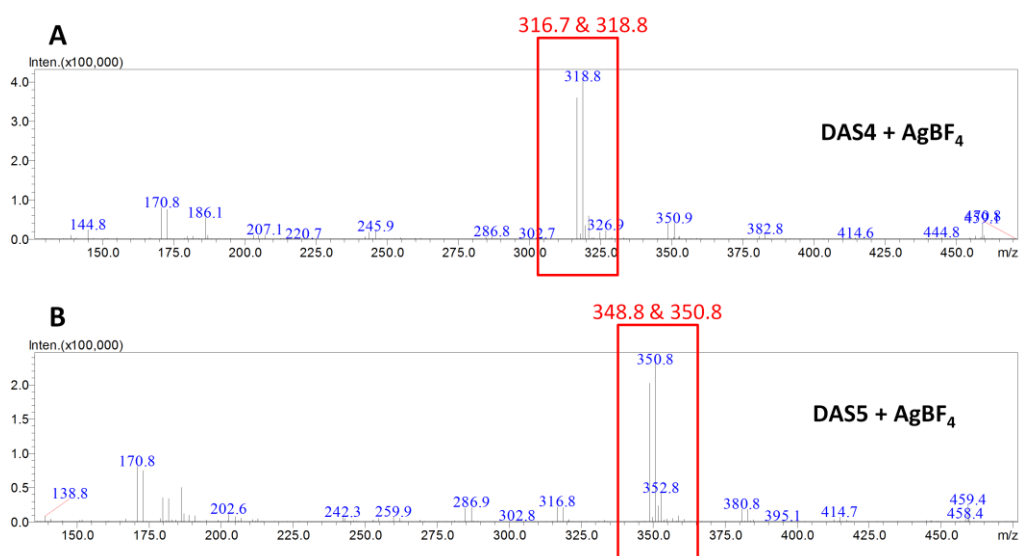


Figure 2.5: Mass spectra of DAS4 and DAS5 coordinated with silver $[\text{M}+\text{Ag}^+]$ detected after electrospray ionisation (ESI) in the positive mode. Two characteristic peaks of similar intensity are detected for each compound due to the two isotopes of silver (107/109). A: Silver-coordinated masses of DAS4 were calculated as 317.4 and 319.4 m/z and found as 316.7 and 318.8 m/z . B: Silver-coordinated masses of DAS5 were calculated as 349.5 and 351.5 m/z and found as 348.8 and 350.8 m/z .

2.2 Stability of DAS

The stability of all DAS up to DAS6 as pure oils stored at -20°C for several months was confirmed by repeated analysis of purified samples by HPLC and ¹H-NMR.

Especially the longer chain DAS (S>3), are not very stable at room temperature (RT). During the purification process a decrease in purity was observed when samples were left under vacuum for increased time durations. Formation of other chain length DAS from a pure (>95%) sample was detected. The following sections describe the stability of DAS4 to DAS6. DAS1 to DAS3 are stable at RT in MeOH: H₂O solutions for at least one week. All stability studies discussed in section 2.2 were conducted by Taris Macedo de Santana (School of Pharmacy, University of East Anglia, UK).

HPLC purified fractions in 80% MeOH and 20% H₂O were used without further processing. Samples were kept in amber HPLC vials at RT (20°C) and were repeatedly analysed by HPLC as described in section 2.1.3.1. The sum of all peak areas (DAS peaks and unknown peaks) was normalised to 100% and percentage peak areas were calculated for each of the DAS from DAS3 to DAS7. The identity of DAS7 was not confirmed, because no pure DAS7 has been obtained for full characterisation. The appearance of DAS7 is based on an additional HPLC peak eluting with longer retention time (rt) compared to DAS6.

Whilst DAS4 is quite stable at RT over eleven hours (from 96% to 90% purity), the purity of DAS5 decreases from 95% to 64% over seven hours while the purity of DAS6 decreases to 11% from originally 72% in five hours (Figure 2.6). Clearly, increasing sulfur chain length makes the molecule less stable.

Upon degradation of the original DAS, other DAS are formed and their concentration in the samples increases over time (Figure 2.6). Higher concentrations of other DAS are formed in the DAS6 sample as compared to the DAS5 and DAS4 samples. DAS4 and DAS5 are still the main species in their sample after five hours (Figure 2.6 A and B, respectively), whereas DAS6 has already decreased down to 12% in the same time and the main species in the sample are DAS4 and DAS5 (Figure 2.6 C). All of the analysed molecules (i.e. pure DAS4, DAS5 or DAS6) formed DAS3, DAS4, DAS5 and DAS6 over time. Additionally, DAS7 was detected in the DAS6 sample, highlighting that all DAS are forming lower and higher chain DAS upon formation of an equilibrium.

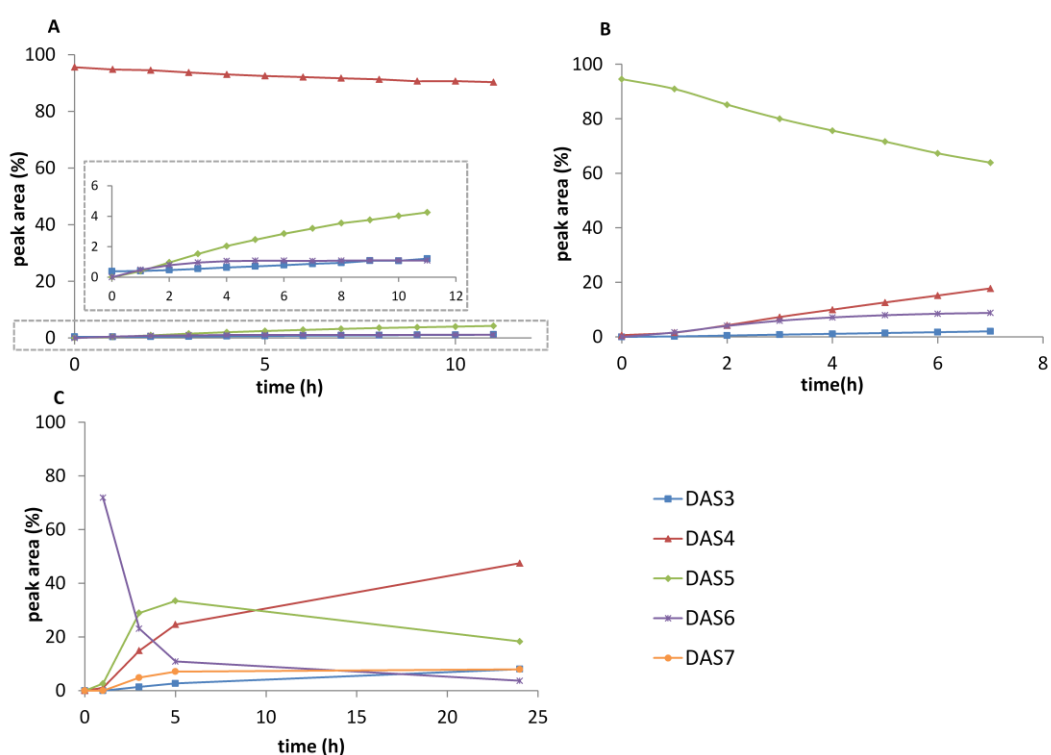


Figure 2.6: Formation of DAS mixtures from pure, single molecule samples in 80% MeOH, 20% H₂O at RT in amber vials (n=1). A: DAS4 forms small amounts of DAS3, DAS5 and DAS6 over 11 hours. B: Formation of DAS3, DAS4 and DAS6 in a pure sample of DAS5 within seven hours. C: Most of DAS6 forms other DAS (mainly DAS4 and DAS5) within five hours.

A “sulfur count” (sulfur atoms for all detected DAS at a certain time point were added up and sums were compared at different time points) revealed that the number of sulfur atoms in the population of DAS does not change in a particular sample of DAS4 or DAS5 over time. This observation excludes the drop out of elemental sulfur or release of hydrogen sulfide (H_2S) as a mechanism for formation of different chain length DAS from a pure sample. Instead, an intermolecular mechanism is suggested, where the DAS molecule is in equilibrium with its thiosulfoxide (Figure 2.7 a), which can attack a sulfur atom of another DAS molecule to form a longer sulfur chain (Figure 2.7 b). Attack of the resulting hydrodisulfide (AS_nH) on the allyl group leads to the formation of two DAS molecules where the overall number of sulfur atoms is equal to the starting one, but a disproportionation has taken place (Figure 2.7 c). Note the similarity with the mechanism of the synthesis of DAS mixtures through reaction of DAS2 with elemental sulfur (Figure 2.2 ⁽⁸³⁾). This mechanism is also based on the ability of DAS to form diallyl thiosulfoxides, which are able to react with another sulfur atom in a nucleophilic attack.

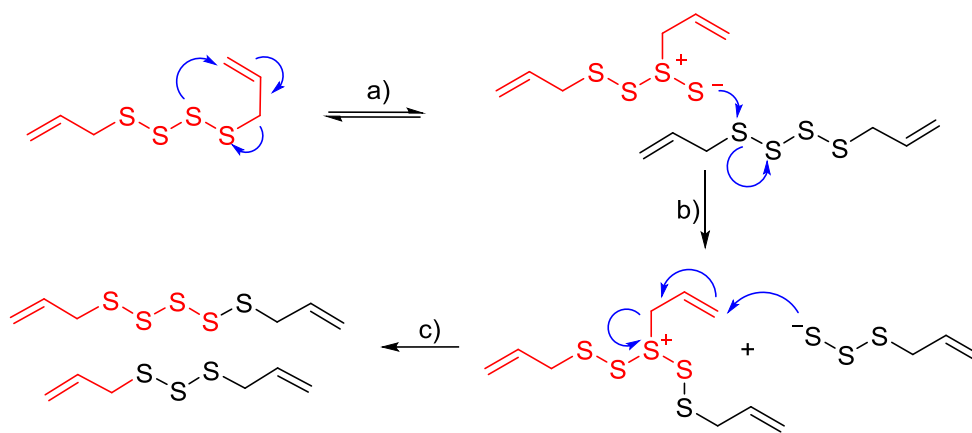


Figure 2.7: Suggested mechanism for the disproportionation of DAS and formation of DAS mixtures from a pure sample containing a single molecule.

To summarise, it is striking that all analysed DAS (DAS4-DAS6) form an equilibrium mixture of different chain length DAS. The speed of this formation depends on the number of sulfur atoms, and clearly the longer the sulfur chain, the less stable the compound and the faster the formation of other DAS. Therefore, it is reasonable to assume that DAS3 forms other DAS in a similar way, but much slower and is therefore stable for at least one week at RT. In other stability studies, it has been observed that lower temperature slows down this disproportionation reaction, and light increases the reaction speed, with temperature having a bigger influence. Principally the disproportionation of DAS takes place in a similar manner even at lower temperatures and is always faster for longer chain DAS.

2.3 Reactivity of DAS with low molecular weight thiols

One possible mode of action of DAS is the interaction of DAS with low molecular weight (LMW) thiols followed by the formation of a mixed polysulfide and AS_nH (section 1.2.4.3). The reaction between DAS and LMW thiols is of high biological importance as the main function of LMW thiols (which are present in most organisms in millimolar concentrations), like glutathione (GSH) or bacillithiol (BSH) is the maintenance of the cellular redox status (section 1.3).

For the purpose of this chapter the chemical reactions between DAS and LMW thiols were studied to gain insights into possible reaction products likely to be formed *in vivo*. The formation of mixed allyl-cysteine disulfide (ACS2) upon incubation of Cys and DAS2 or DAS3, as well as the liberation of allyl mercaptan (ASH) have been observed previously ⁽⁴⁾. No experimental evidence for the formation of mixed polysulfides ($S > 2$) between DAS and LMW thiols or the formation of AS_nH ($n > 1$) is given in the literature. This chapter aimed to characterise the reaction products of the thiol-polysulfide exchange reaction between DAS and LMW thiols in more detail, and especially to detect and prove the formation of the reduced form of DAS (AS_nH , $n > 1$).

In this chapter the reactivity of DAS with GSH, BSH and Cys is studied, because these are the main LMW thiols produced in the model organism that are used for *in vivo* studies in the following chapters (chapter 3: *B. subtilis* produces BSH and Cys, chapter 4: nematodes produce GSH and Cys amongst other thiols).

2.4 The reduced form of DAS

2.4.1 Formation of allyl perthiol (AS2H)

To evaluate whether DAS3 forms the allyl perthiol (AS2H) under reducing conditions, DAS3 was incubated with the reducing agent tris(2-carboxyethyl)phosphine (TCEP). DAS3 was added in 10-fold excess to allow the formation of AS2H (Figure 2.8), which can be further reduced to ASH in the presence of excess TCEP.

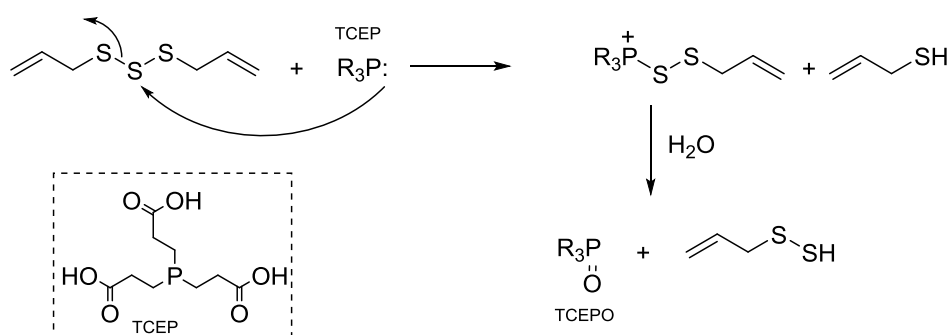


Figure 2.8: Reduction of DAS3 by TCEP leads to formation of allyl mercaptan (ASH) and allyl perthiol (AS2H).

At different time points aliquots of the reaction mixture were labelled with monobromobimane (mBBr), which forms fluorescent adducts with thiols (Figure 2.9 A). The reaction mixture was then analysed by fluorescence HPLC. Allyl mercaptan-monobimane (ASmB) was detected as the main product by comparison with a synthesised and characterised standard (Figure 2.9 B). Additionally, a peak with a longer *rt* compared to ASmB was detected (Figure 2.9 B).

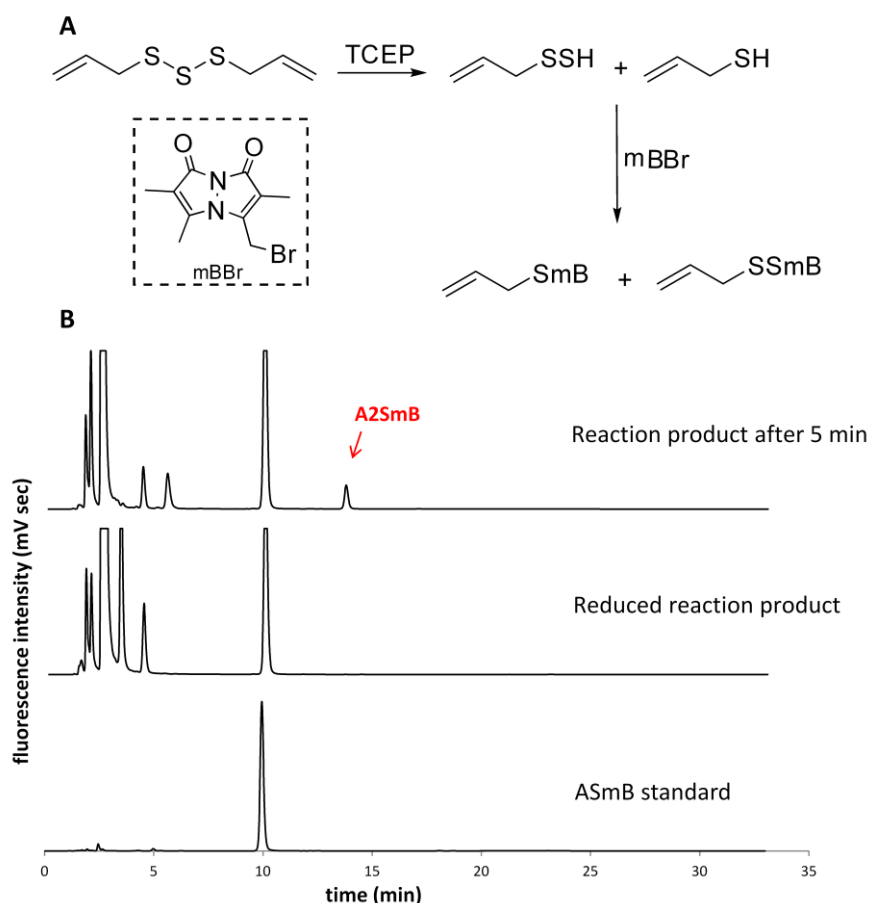


Figure 2.9 A: Reaction between 100 mM DAS3 and 10 mM TCEP in Heps buffer (pH8) and CH_3CN and subsequent thiol labelling with mBBr. B: HPLC analysis of the reaction mixture after five minutes, monitored by fluorescence detection (ex: 385 nm, em: 460 nm). Comparison of the reaction product (top) with the reduced reaction product (middle) and the characterised ASmB standard (bottom).

The unknown peak was purified by HPLC and repeated reduction with TCEP showed mBSH as major product (see Figure 2.10 A and B). Additional mBBR bimane labelling showed the presence of ASmB. Therefore the identity of the unknown peak was confirmed as allyl perthiol-monobimane (AS2mB).

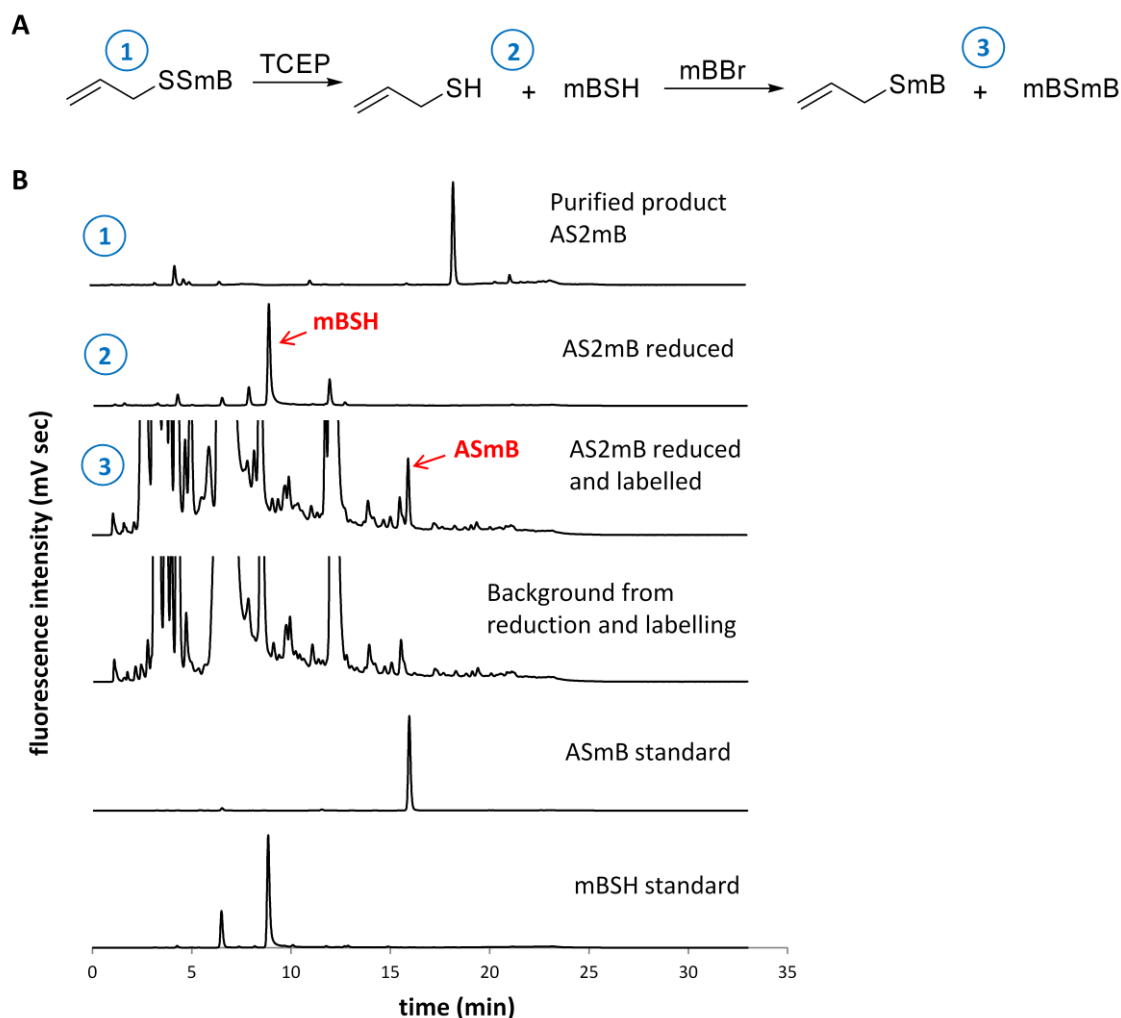


Figure 2.10: Confirmation of allyl perthiol (AS2H) formation. A: Reactions and B: Fluorescence HPLC analysis (ex: 385 nm, em: 460 nm).

To further confirm the identity of the AS2mB molecule, the collected fractions from HPLC containing the purified peaks were analysed by LC-MS. The mass was detected in positive mode as proton adduct ($296.9 m/z$, calculated $297.07 m/z$) at which there were also some impurity/background peaks at higher masses ($>500 m/z$).

As the reaction of DAS3 with TCEP forms higher amounts of the ASmB (ratio of about 10:1 detected by HPLC) compared to AS2mB, it could not be isolated in sufficient quantity for characterisation by NMR spectroscopy. Furthermore, the isolation of unlabelled AS2H was not possible as it is only a transient molecule that degrades very fast. At the endpoint of the reaction no AS2H was detected.

To evaluate whether the formation of AS₂mB is also likely in a biological context, GSH was used as a reducing agent. In a similar fashion to the reaction with TCEP, 10 molar equivalents of DAS₃ were reacted with GSH and the products of the reaction were labelled with mBBr at different time points (from ten seconds to two hours).

HPLC analysis showed the formation of AS₂mB upon reaction of DAS₃ with GSH. The major thiol product captured by mBBr labelling was ASH, which shows its highest concentration between 5 and 10 min (see Figure 2.11). The AS₂mB concentration is between 3 and 20-fold lower than the ASmB concentration and peaks between 1 and 20 minutes.

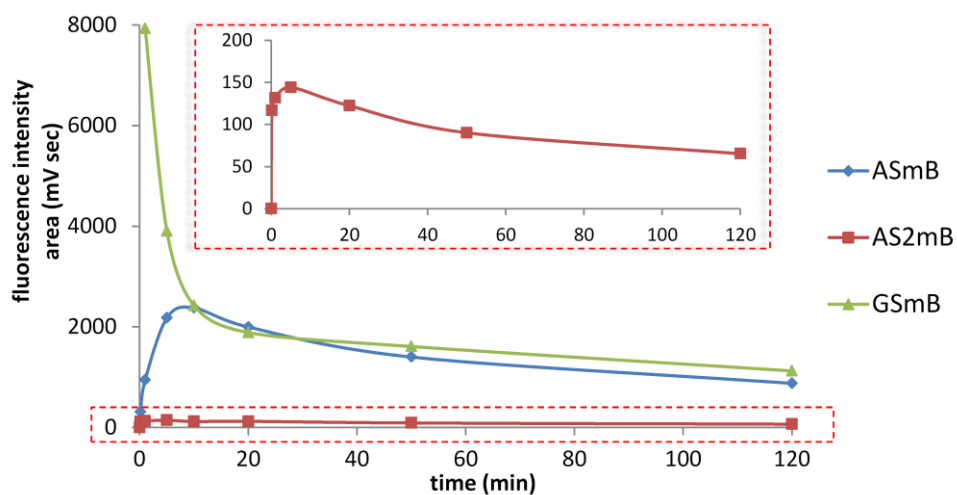


Figure 2.11: Analysis of product formation over time after reaction of 100 mM DAS₃ with 10 mM GSH in Hepes buffer (pH8) and CH₃CN (n=1). Peak areas from fluorescence HPLC analysis of mBBr labelled products (ex: 385nm, em: 460nm).

The confirmation of the formation of AS₂H from DAS₃ under reducing conditions is very important because the postulated mode of action of DAS is based on the existence of these molecules. However, AS_nH (n>1) have never been detected before and nothing is known about their stability and reactivity. Additionally, the bimeane adduct of AS₂H can serve as an HPLC standard to investigate the formation of AS₂H *in vivo* (see chapter 3).

2.4.2 Formation of allyl hydrotrisulfide (AS3H)

After confirming AS2H as a product of the reaction of DAS3 with GSH, the formation of AS3H through reaction of DAS4 and DAS5 with GSH was monitored. The reaction was performed as described previously for DAS3 and the mBBr labelled reaction products were analysed by HPLC using fluorescence detection (Figure 2.12).

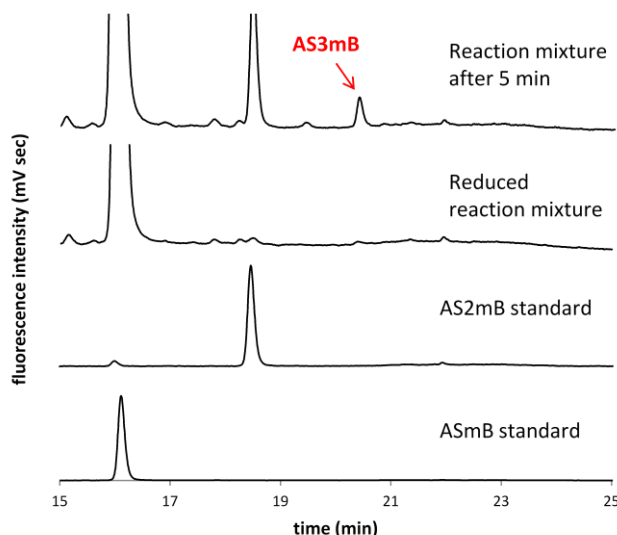


Figure 2.12: HPLC traces of reaction mixture after reacting 100 mM DAS4 with 10 mM GSH (pH8 Hepes buffer and CH₃CN). The reaction mixture labelled with mBBr after five min, the labelled and subsequently reduced reaction mixture and the purified AS2mB and ASmB standards (top to bottom). All analysed by fluorescence HPLC (ex: 385 nm, em: 460 nm).

The HPLC trace of the reaction mixture shows an additional peak at higher rt (20.6 min), which was suspected to be AS3mB. As described for the reaction with DAS3, the reaction mixture was reduced with TCEP which leads to the disappearance of the AS2mB peak and the unknown peak at 20.6 min. Therefore, it was confirmed that the unknown peak has at least one disulfide bond that was reduced by TCEP. More likely is the existence of AS3mB as AS2mB was confirmed to elute at 18.7 min.

For further confirmation, LC-MS analysis was performed. The unknown peak at 20.6 min was purified by collection from HPLC and analysed by LC-MS with a gradient of H₂O and MeOH containing 0.05% acetic acid. Using this method the mass of AS3mB was detected, but additionally the sample showed the masses for ASmB and AS2mB. Nevertheless, in the UV trace of the LC the different products were separated and by only analysing the masses of the peak eluting at 5.9 min and subtracting the background, the mass of AS3mB was confirmed as 328.9 *m/z* (calculated 329.04 *m/z*) for the proton adduct and 350.9 *m/z* (calculated 351.03 *m/z*) for the sodium adduct. Possibly the sample collected from HPLC and used for LC-MS still contained a mixture of ASmB, AS2mB and AS3mB as the amount of AS3mB was very small in comparison to the other components (50-fold less than ASmB). Small contamination of the other products can therefore make a big difference for the purity of the sample. Additionally, it is possible that AS3mB is not ionising as well as the other products.

The progression of the reaction of DAS4 and DAS5 with GSH (Figure 2.13 A and B, respectively) shows that ASmB is the most dominant thiol species detected (up to 30-fold greater than AS2mB and up to 50-fold greater than AS3mB). The concentrations of AS2mB and AS3mB are more similar, with AS2mB being up to two-fold more concentrated. The ASmB concentration in the reaction with DAS4 peaks at about five minutes whereas the ASmB concentration in the reaction with DAS5 already peaks at one minute. This may point towards a higher reactivity of DAS5 with GSH compared to DAS4.

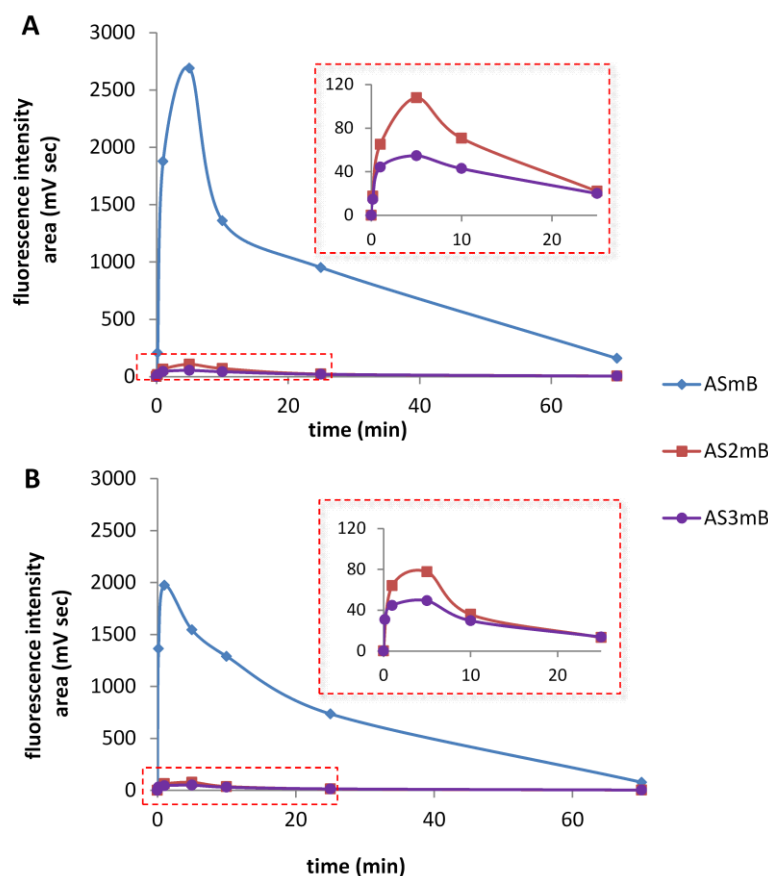


Figure 2.13: Formation of thiol (ASmB), perthiol (AS2mB) and hydro trisulfide (AS3mB) products after reaction of A: 100 mM DAS4+ 10 mM GSH in HEPES buffer pH8 and CH₃CN (n=1) and B: 100 mM DAS5+ 10 mM GSH in HEPES buffer pH8 and CH₃CN (n=1) analysed by fluorescence HPLC (ex: 385 nm, em: 460 nm).

Even though full characterisation of AS2mB and AS3mB was not possible, enough characterisation was done to prove the formation of these molecules, upon reaction of DAS with GSH. Therefore, it has been shown for the first time that upon reaction with GSH, DAS form AS2H and/ or AS3H (depending on the number of sulfur atoms of the starting material). Upon reaction of DAS5 with GSH, theoretically the formation of AS4H is possible, but it has not been detected in this study. This might be due to the very low stability of this product and therefore inability to “catch” and label the product with mBBr. Although AS4H has not been detected in this study, it does not imply that the compound is not formed.

2.5 Formation of mixed allyl-glutathione sulfides (AGS(2-5))

2.5.1 DAS2 and GSH form mixed disulfide

Having demonstrated the formation of AS2H and AS3H, formation of the allyl-glutathione mixed di- and polysulfides (AGS_n) within the same reaction mixtures was investigated. To start with, the least complex reaction using DAS2 and GSH, which should only lead to the formation of the mixed disulfide (AGS2), was performed (Figure 2.14).

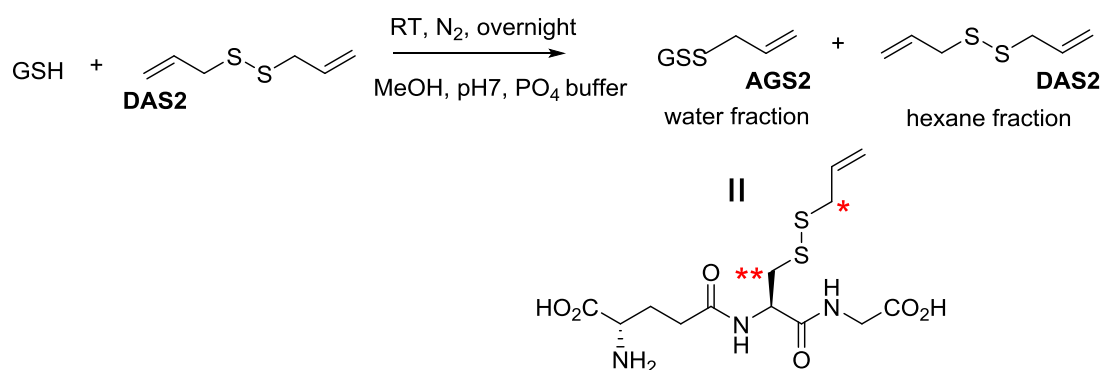


Figure 2.14: DAS2 and GSH form mixed allyl-glutathione disulfide (AGS2).

GSH was reacted with a 10-fold molar excess of DAS2 to ensure full conversion of GSH into mixed disulfide and avoid formation of glutathione disulfide (GSSG) (Figure 2.14).

After overnight incubation under nitrogen (N_2), the reaction was washed with hexane to remove excess of DAS2 and the water soluble fraction showed pure AGS2 by 1H -NMR (see Figure 2.15). The magnified two doublets of doublets representing the CH_2S protons of the Cys part (highlighted as position ** in Figure 2.15 B) do not shift significantly for AGS2 compared to GSSG, because the chemical environment for the protons of the molecule does not change significantly for a mixed compared to a symmetric disulfide. There is a small downfield shift for the doublet representing the CH_2S protons of the allyl group of AGS2 compared to DAS2 (highlighted as *). The singlet at 3.9 ppm in the GSSG spectrum represents the glycine CH_2 which shifted upfield for AGS2, where it overlaps with the multiplet representing the glutamic acid CH_2 at 3.7 ppm (highlighted as *** in Figure 2.15).

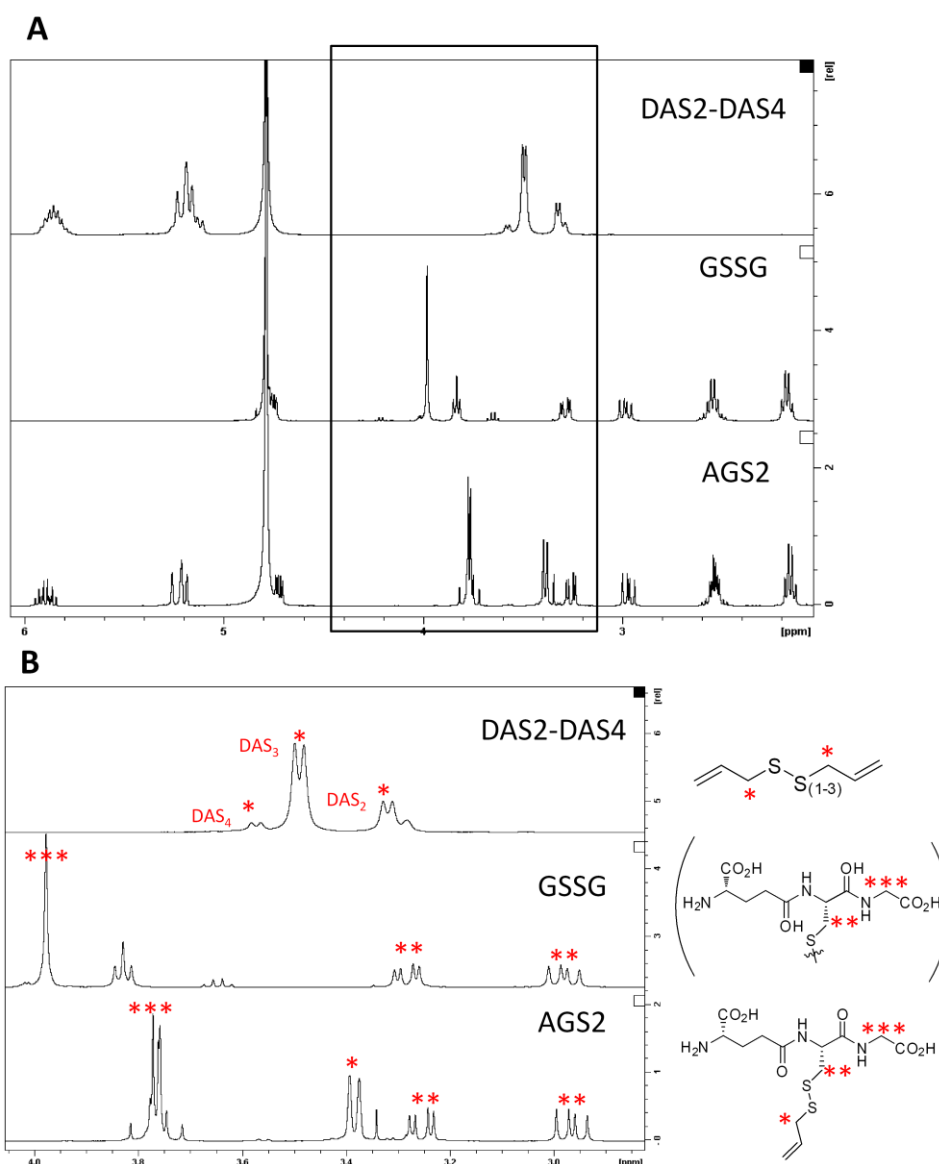


Figure 2.15: 1H -NMR of AGS2 compared to the symmetric disulfides DAS2 to DAS4 and GSSG. A: Full 1H -NMR spectra. B: Section of the 1H -NMR spectra covering peaks of main interest.

The molecule was analysed by ^{13}C -NMR and 2D NMR (data not shown) and the structures of the two halves of the molecule were confirmed. As the chemical shifts for the proton and carbon signals do not differ much for mixed and symmetric disulfides (see Figure 2.15 for ^1H -NMR), the connection between the two halves of the molecules was attempted to be confirmed by HMBC, NOESY and ROESY NMR experiments. HMBC experiments allow the correlation of nuclei over two to four chemical bonds and NOESY and ROESY allow the correlation of protons through space, not only through chemical bonds. Therefore, a correlation between the two CH_2S groups (position * and ** in Figure 2.14) may be visible by HMBC, NOESY or ROESY NMR spectroscopy, which would establish the connection of the molecule over the disulfide bond. This was not the case as probably the distance between those groups over the sulfur bridge is too far. Instead, the final confirmation of the structure of the molecule was achieved by LC-MS using ESI in positive and negative mode, showing masses of 380.1 m/z for $[\text{M}+\text{H}^+]$ (calculated 380.09 m/z), 378.1 m/z for $[\text{M}-\text{H}^+]$ (calculated 378.08 m/z) and 402.1 m/z for $[\text{M}+\text{Na}^+]$, calculated 402.08 m/z .

2.5.2 DAS3 and GSH form mixed di- and trisulfide and liberate AS2H

After characterising AGS2 originated from the reaction between DAS2 and GSH, the same reaction was performed substituting DAS2 with DAS3 (see Figure 2.16). A 10-fold molar excess of DAS3 was used and the reaction was stirred at RT overnight under N_2 . The reaction mixture was washed with hexane the next day to remove excess DAS3. The water and hexane fractions were analysed separately by NMR spectroscopy and HPLC (UV detection).

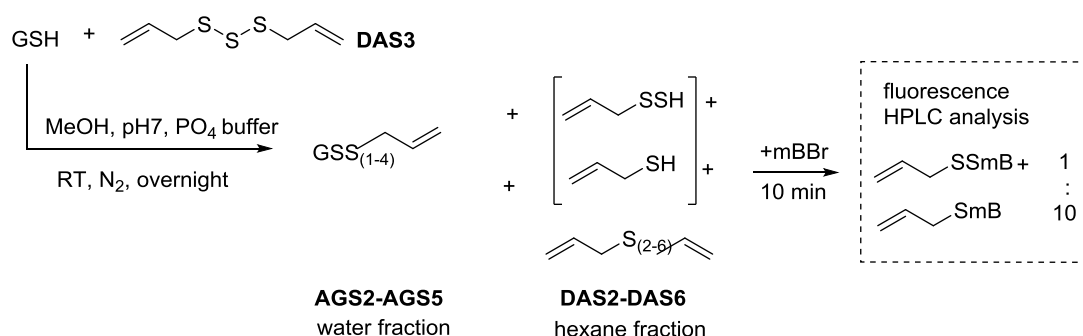


Figure 2.16: The reaction of a 10-fold excess of DAS3 with GSH forms a mixture of mixed di- to pentasulfide (AGS2-AGS5, water fraction) and a mixture of DAS2 to DAS6 (hexane fraction) after overnight incubation. MBBR labelling after 10 min and fluorescence HPLC analysis showed the formation of allyl mercaptan (ASH) and allyl perthiol (AS2H).

NMR and LC-MS analyses of the water fraction containing mixed disulfide (AGS2) and mixed trisulfide (AGS3)

The comparison of the $^1\text{H-NMR}$ spectrum of the aqueous fraction with pure AGS2 confirms that AGS2 is also the main product after the reaction between DAS3 and GSH (see Figure 2.17). However, there are additional peaks between 3 and 4 ppm which show the same pattern as the peaks representing the CH_2S protons (position * and ** in Figure 2.17).

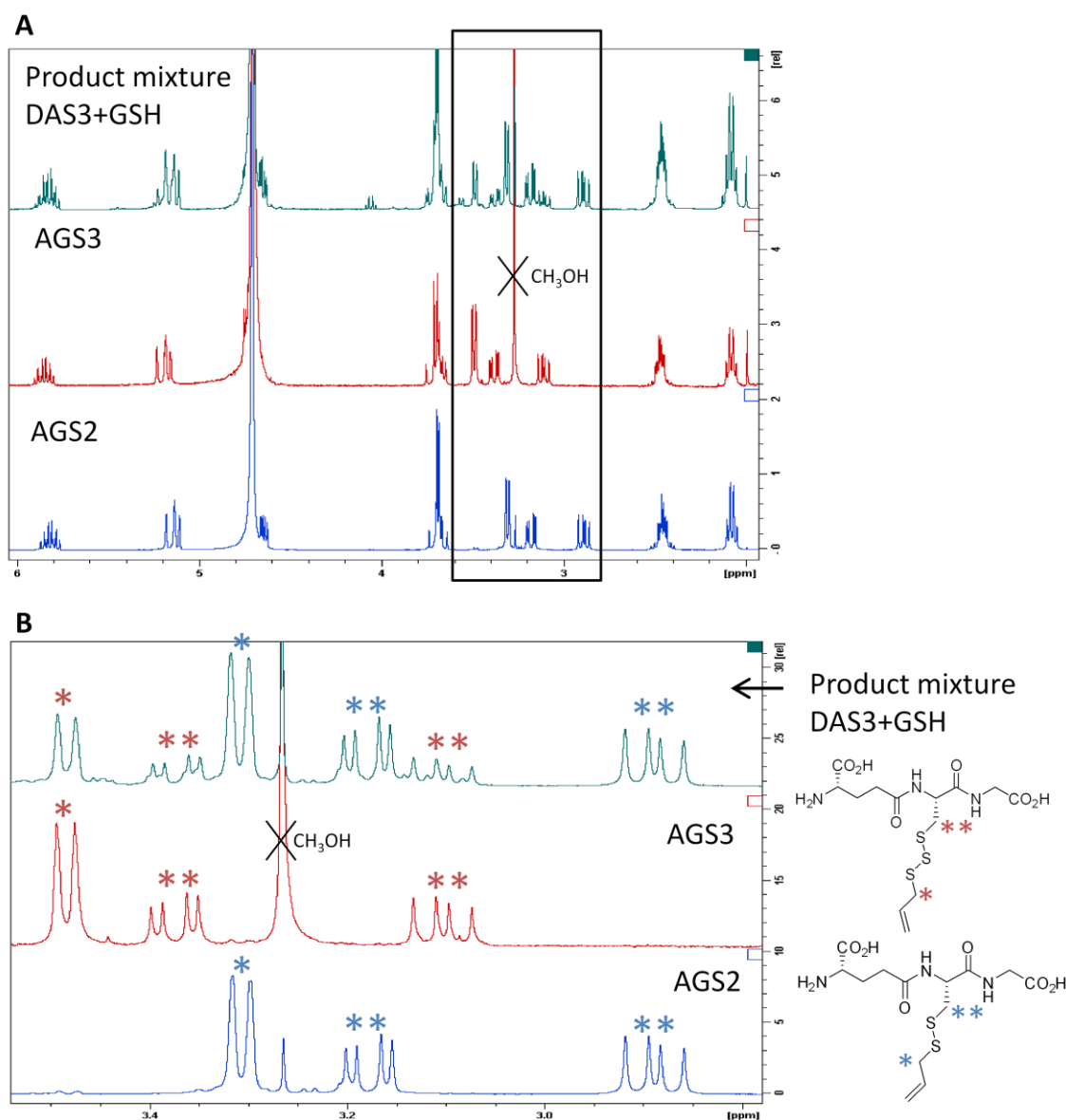


Figure 2.17: Comparison of $^1\text{H-NMR}$ spectra of AGS2 (bottom), AGS3 (middle) and product mixture from reaction of DAS3+GSH (top). A: Full NMR spectra. B: Expansion of $^1\text{H-NMR}$ spectra covering main peaks of interest.

These results suggest the formation of the AGS3, since only the peaks next to the sulfur bridge would shift, all the other protons are exposed to nearly identical chemical environments in the two analysed molecules. Integration of the allyl CH_2S protons (*) in Figure 2.17 for AGS2 and AGS3 shows a ratio of about 2:1 (AGS2:AGS3), indicating that double as much mixed disulfide is formed compared to mixed trisulfide. Additionally, the mixture was analysed by $^{13}\text{C-NMR}$ which showed two signals very close to each other for all carbons (data not shown), which also

hints towards the formation of AGS2 and AGS3. To gain final confirmation of the formed unknown compound the mixture was purified by HPLC using UV detection at 220nm and the purified product was characterised by NMR and LC-MS ($^1\text{H-NMR}$ of purified AGS3 is shown in Figure 2.17).

NMR and LC-MS analysis of pure AGS3

AGS3 was purified from the mixture by HPLC and full NMR spectroscopic characterisation was performed. Proton chemical shifts of AGS3 are comparable to AGS2, with just a few characteristic differences (Figure 2.17). The two doublets of doublets representing the CH_2S protons of the GSH part of the molecule (highlighted as **) shift downfields compared to the AGS2 molecule. The same downfield shift was observed for the doublet representing the CH_2S protons on the allyl part of the molecule (highlighted as *). This downfield shift with increasing number of sulfur atoms is a characteristic feature that is also observed in the $^1\text{H-NMR}$ analysis of the series of DAS molecules (Figure 2.4).

Characterisation by LC-MS was achieved by direct injection using 40% MeOH, 60% H_2O and ESI. The proton and sodium adduct were detected in positive mode (412.0 m/z , calculated 412.07 m/z and 434.0 m/z , calculated 434.05 m/z , respectively) and additionally, the mass was detected in ESI negative mode (410.1 m/z , calculated 410.05 m/z).

HPLC analysis of the water fraction

Interestingly, when the water fraction of the reaction was analysed by HPLC, not only the AGS2 (36%) and AGS3 (39%) were detected, but also AGS4 (6%) and AGS5 (<1%). This is unexpected as the reaction was done with DAS3 and GSH as starting materials and the expected products were AGS2 and AGS3. Nevertheless, the observation of the formation of AGS4 and AGS5 can be explained with the reaction cascade shown in Figure 2.18.

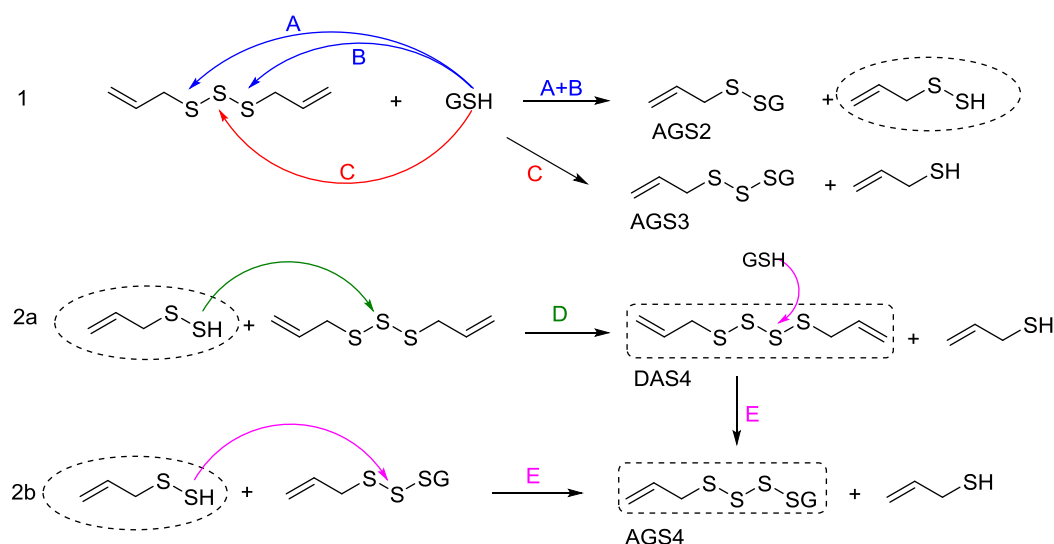


Figure 2.18: Formation of DAS4 and AGS4 after initial reaction of DAS3 with GSH. (1) The initial reaction of DAS3 with GSH can lead to formation of a perthiol (2a) which can react with DAS3 to form DAS4 (2b) or with AGS3 to form AGS4. Thiols and perthiols need to be deprotonated to perform a nucleophilic attack, but for uniformity all thiols and perthiols are shown in their protonated form.

In the initial reaction of DAS3 with GSH only mixed di- and trisulfide are formed (Figure 2.18, path A-C). The generated AS₂H molecule is very reactive and upon reaction with either DAS3 (which is in excess) (path D) or AGS3 (path E), the DAS4 and AGS4 can be formed. In a similar way the formation of AGS5 is possible via a reaction of AS₂H with AGS4.

Analysis of the hexane fraction

The hexane fraction contained all hydrophobic DAS molecules, which were used in excess in this reaction. DAS3 was used as starting material, but HPLC analysis revealed a mixture of DAS2 to DAS6 (DAS2: 30%, DAS3: 38%, DAS4: 20%, DAS5: 8%, DAS6: 3%) after overnight incubation of the reaction mixture. As the initial reaction of DAS3 with GSH forms a mixed di- or trisulfide, as by-product ASH or AS₂H are formed. These reactive thiols can in turn react with DAS3 to form other chain length DAS until all thiol is oxidised and an equilibrium mixture is established. Figure 2.18 shows the formation of DAS4 in the reaction mixture and in the same way (by reacting DAS4 with AS₂H) higher polysulfides can be formed until a stable equilibrium is reached.

In section 2.2, instability of DAS on their own was discussed. The DAS3 molecule on its own was confirmed to be stable under the reaction conditions when GSH was absent. Therefore, the formation of other DAS is clearly accelerated by the reaction with GSH.

2.5.3 DAS3 to DAS6 all form mainly mixed di- and trisulfide upon reaction with GSH

The same type of reaction was repeated with DAS4, DAS5 and DAS6, always using a 10-fold molar excess of DAS. HPLC analysis showed the formation of AGS2, AGS3, AGS4 and traces of AGS5 (<1%) for all reactions (Figure 2.19 A). The AGS4 and AGS5 peak were collected and analysed by MS using ESI positive and negative mode. The results for AGS4 [m/z ES⁺ (M+H)⁺: 444.0, calculated 444.04, (M+Na)⁺: 475.9 calculated 476.01; ES⁻ 442.1 calculated 442.02]; and AGS5 [m/z ES⁺ (M+H)⁺: 475.9, calculated 476.01, (M+Na)⁺: 497.9, calculated 497.99; ES⁻ 473.9 calculated 474.00] confirmed the identity of the two molecules.

HPLC analysis of DAS shows formation of DAS2 to DAS6 during the reactions, no matter which of the DAS was used as the starting material. As shown in Figure 2.19 B, the final distribution of products after overnight incubation is very similar for all the reactions. DAS and AGS_n seem to form a stable equilibrium which does not depend much on the number of sulfur atoms in the DAS starting material.

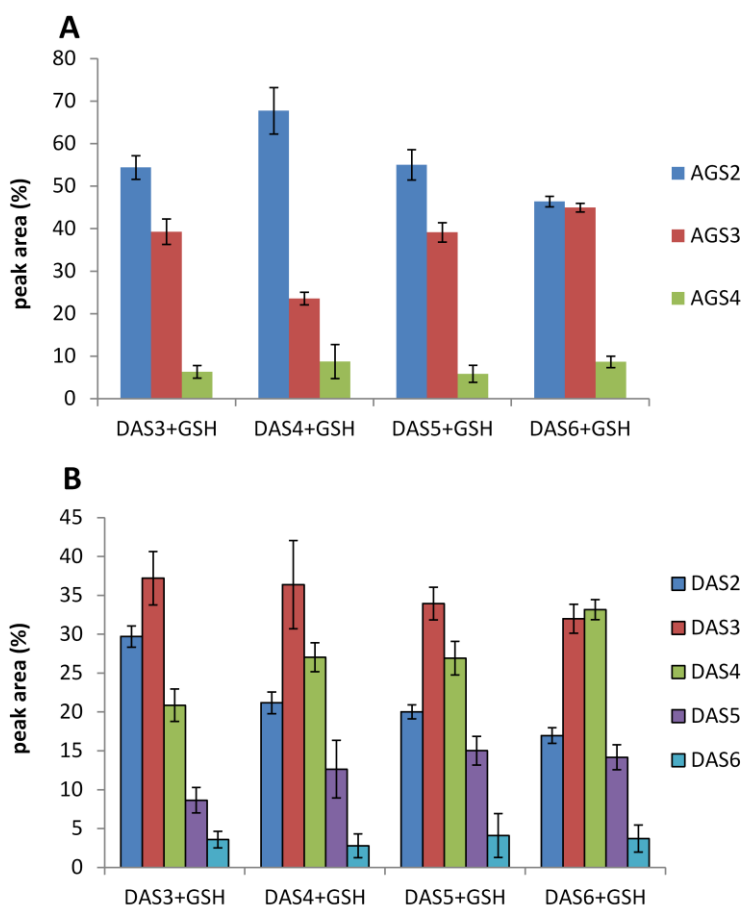


Figure 2.19 A: Distribution of different AGS_n and B: Distribution of different DAS after overnight incubation of 100 mM DAS with 10 mM GSH in Hepes buffer (25 mM, pH8, 50% CH₃CN, n=2, error bars show the range of the data). AGS_n and DAS have been analysed on two different HPLC methods and the sums of AGS_n and DAS were separately normalised to 100%.

2.6 Formation of mixed allyl-bacillithiol sulfides (ABS(2-4))

BSH was recently discovered as redox buffer produced in many Gram positive bacteria, e.g. Bacilli⁽⁵⁴⁾, like *Bacillus subtilis* which is used as a model organism in this study.

2.6.1 DAS2 and BSH form mixed disulfide

BSH was reacted with a 10-fold excess of DAS2 as previously described for GSH and the excess DAS2 was removed by hexane washes after overnight incubation of the reagents. Pure mixed allyl-bacillithiol disulfide (ABS2) was obtained (Figure 2.20). The reaction was done on a small scale and, therefore, only enough material was obtained for ¹H-NMR analysis and LC-MS analysis. ¹H NMR clearly showed the three indicative peaks for the allyl group (CH₂S (1): doublet at 3.43 ppm, =CH (2): ddt at 5.94 ppm and =CH₂ (3): multiplet at 5.20-5.40). The CH₂S protons of the BSH part of the molecule (4) showed the disulfide state of the molecule (two doublets of doublets at 3.09 and 3.23 ppm). There was no evidence for the formation of other di- or polysulfides or residual reduced BSH.

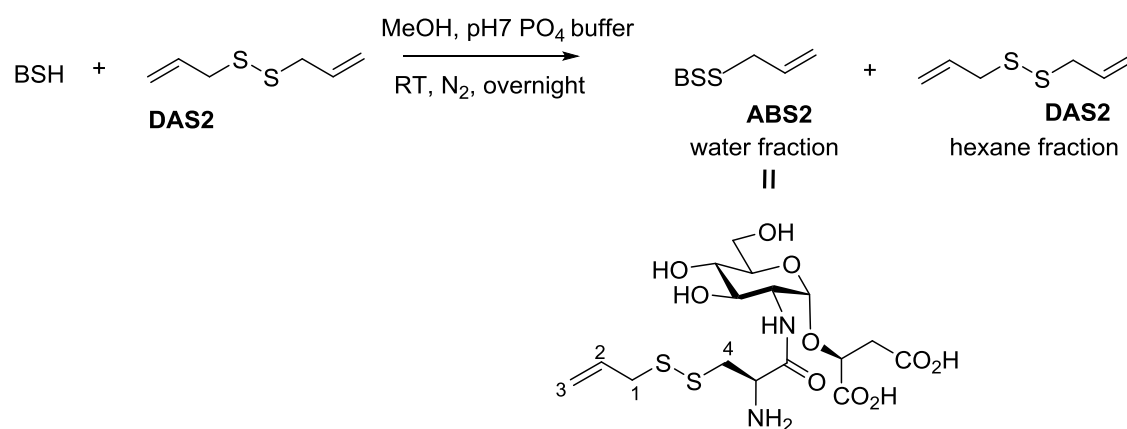


Figure 2.20: Reaction between BSH and a 10-fold excess of DAS2 forms pure mixed disulfide.

Additionally, HPLC analysis of the sample showed a single peak eluting at 3.1 min. The mass of the molecule was confirmed to be 471.1 *m/z* ([M+H]⁺ calculated 471.52 *m/z*) and 493.1 *m/z* ([M+Na]⁺ calculated 493.50 *m/z*) in positive mode and 469.0 *m/z* (calculated 469.50 *m/z*) in negative mode.

2.6.2 DAS5 and BSH form a mixture of mixed di- to tetrasulfide (ABS(2-4))

DAS5 was reacted with BSH using a 10-fold molar excess of DAS5 (Figure 2.21). The formation of different mixed allyl-bacillithiol di- and polysulfides (ABS_n) and their relative distribution was studied.

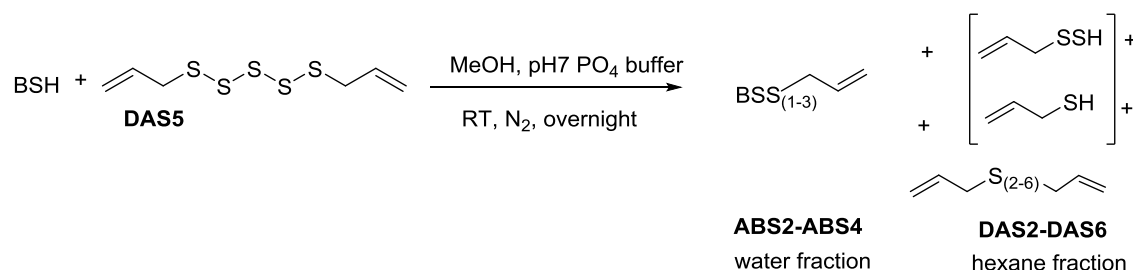


Figure 2.21: Reaction of BSH with a 10-fold excess of DAS5 forms mixed allyl-bacillithiol di- and polysulfides (ABS2-ABS4).

The reaction mixture was analysed by HPLC after overnight incubation before any work-up (Figure 2.22) and showed ABS2 and two other peaks (rt=4.8 min and 9.8 min). The unknown peaks were suspected to be ABS3 and ABS4, in analogy to the formation of higher mixed polysulfides from GSH and DAS5 and their longer retention times on RP HPLC. The sum of the integrated peak areas of the three peaks was normalised to 100% and the peak areas were 41%, 54% and 5% for ABS2, ABS3 and ABS4, respectively. After the work-up, which involved the concentration of the reaction mixture and hexane washing to remove excess DAS, repeated HPLC analysis showed a very different distribution of peak areas: 77% for ABS2, 33% for ABS3 and ABS4 was under the detection limit (Figure 2.22).

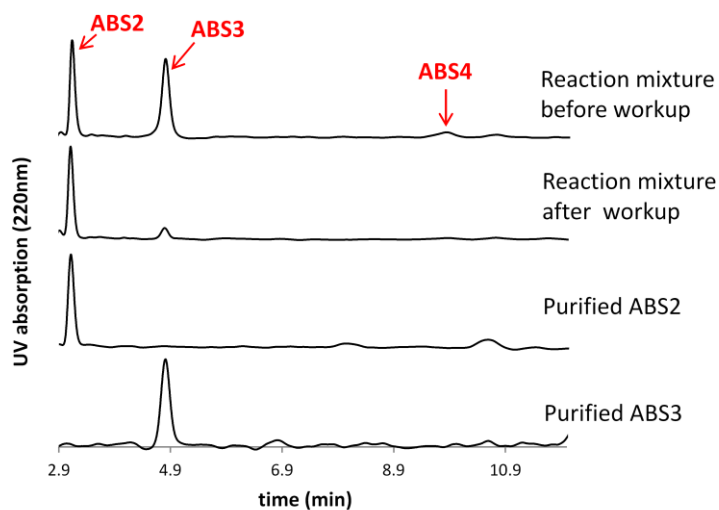


Figure 2.22: HPLC analysis of reaction mixtures before and after workup.

This observation highlights the instability of the longer chain ABS_n. Upon concentration of the sample, the equilibrium of the mixture shifts in favour of the mixed disulfide. This instability has not been observed with the AGS_n compounds. This instability might also be the reason why the masses of ABS3 and ABS4 have not been detected by LC-MS, even after HPLC purification of the mixture resulting in single pure compounds (confirmed by HPLC). Therefore no final confirmation of the identity of these compounds could be achieved. If this reaction could be

repeated on a larger scale (which was not possible in this study) the characterisation of the reaction products could be achieved.

After observing this instability and shift in equilibrium, the reaction was repeated and monitored over time to evaluate whether the equilibrium also shifts during overnight incubation. The reaction was analysed by HPLC hourly (first measurement 10 minutes after mixing the components), but only slight changes in the ABS_n distribution were observed (Figure 2.23).

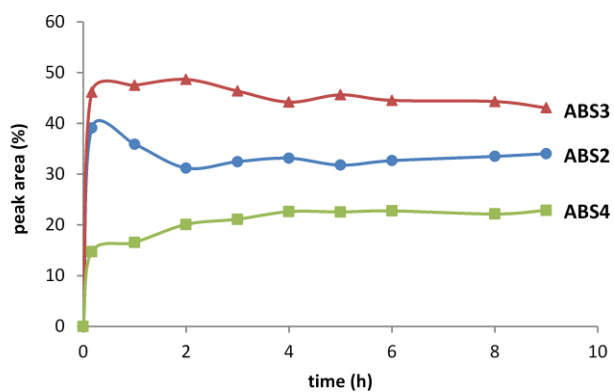


Figure 2.23: Product formation after reaction of 27 mM DAS5 with 2.7 mM BSH in PO₄ buffer (100 mM, pH7, n=1) and MeOH, monitored over time by HPLC (UV absorbance at 220 nm). The sum of the three main product peak areas was normalised to 100% for each time point.

In the first analysis (10 min after reaction start), the peak areas were 39%, 46% and 15% for ABS2, ABS3 and ABS4 respectively, changing after four hours to 33%, 44% and 23% respectively. Within the first four hours the ABS2 seems to decrease slightly while that of ABS4 increases and after this, the distribution of ABS_n seems to be stable (measured for additional five h). This experiment confirms that the formation of the mixed ABS_n is very quick at pH 7, since only 10 min are required to nearly reach the final equilibrium. The same pattern was observed for the formation of mixed AGS_n. Additionally, it has also been observed that upon concentration of a mixture of ABS_n, the equilibrium can shift in favour of the ABS2.

2.7 Formation of mixed allyl-cysteine sulfides (ACS(2-4))

Cys is present in cells as free thiol (and disulfide) and is also present as an amino acid in proteins, where it can form intra- or intermolecular disulfide bonds with other protein Cys residues. The oxidation state of Cys residues can have important regulatory functions (section 1.3.4). The formation of mixed allyl-cysteine disulfide (ACS2) upon incubation of Cys and DAS2 or DAS3, as well as the liberation of ASH have been observed previously⁽⁴⁾. Additionally, ACS2 has been chemically synthesised and characterised by a different method⁽⁸⁴⁾. The ability of DAS2 and DAS5 to form mixed di- and polysulfides with Cys is investigated in this section.

2.7.1 DAS2 and Cys form mixed disulfide (ACS2) and cystine (CySS)

A 10-fold excess of DAS2 was reacted with Cys overnight in a mixture of MeOH and phosphate buffer to form the mixed disulfide (Figure 2.24). After the work-up of the reaction (concentration and hexane washes to remove excess DAS2) the reaction mixture was not soluble in water or MeOH and was finally dissolved in 300 mM hydrochloric acid (HCl), after washing with water to remove the phosphate buffer.

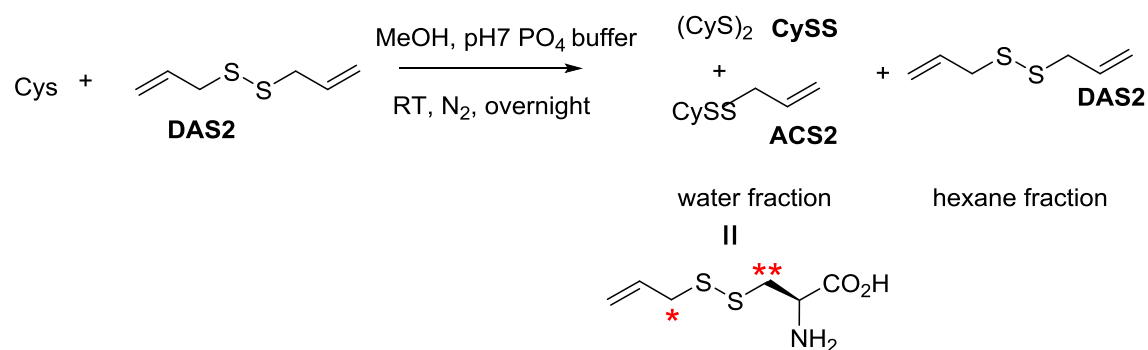


Figure 2.24: Cysteine and DAS2 form a mixture of mixed allyl-cysteine disulfide (ACS2) and cystine (CySS).

HPLC and NMR analysis showed that the reaction contains a mixture of different products (Figure 2.25). The two sets of two doublets of doublets are characteristic for the CH_2S of Cys (** Figure 2.25 B) in the disulfide form. Additionally, the three characteristic signals for the allyl group indicate that a mixture of CySS and ACS2 was obtained.

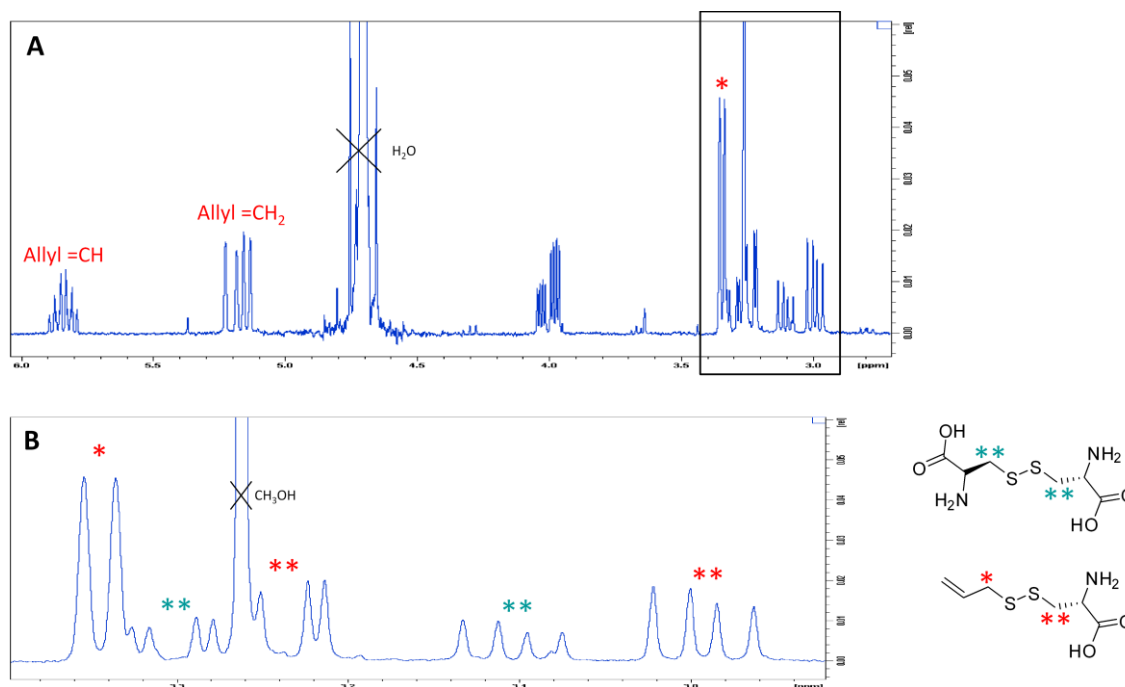


Figure 2.25: 1H -NMR spectrum of the reaction mixture after reacting a 10-fold excess of DAS2 with Cys. A: Full 1H -NMR spectrum and B: Section of 1H -NMR spectrum showing main peaks of interest. Highlighted region shows two sets of peaks for the CH_2S of cysteine (**), which indicates formation of cystine (CySS) and ACS2. The doublet at 3.35 ppm (*) represents the CH_2S group of the allyl part of the molecule.

Two main peaks were observed by HPLC, one was identified as CySS (RT=2.7 min, 37%) by comparison with a pure CySS standard (Figure 2.26). As the NMR analysis indicated formation of ACS2, it was assumed that the other HPLC peak was representative for ACS2 (RT=3.4 min, 63%). The reaction was repeated with a 20-fold excess of DAS2 to maximise formation of ACS2, but still led to formation of a mixture of CySS (33%) and ACS2 (67%) (analysed by HPLC, before work-up, Figure 2.26).

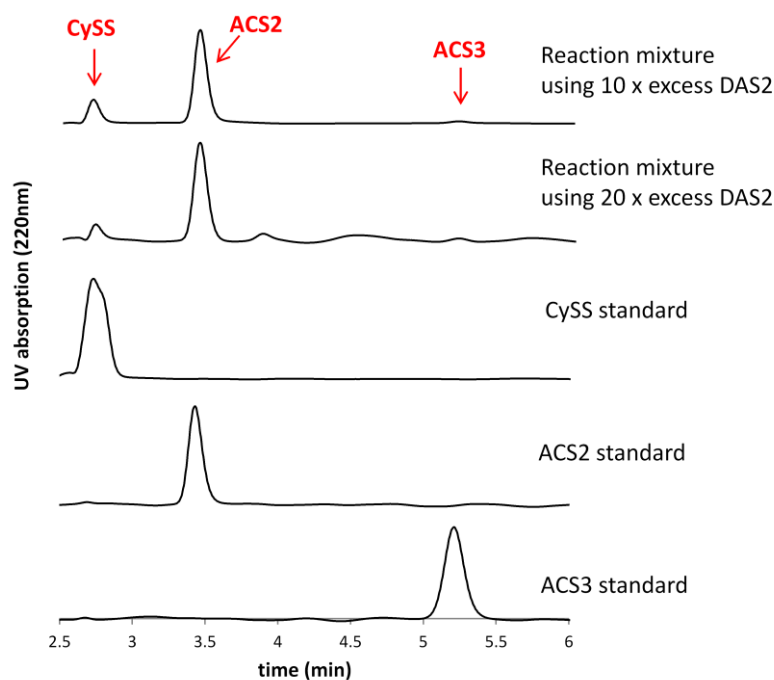


Figure 2.26: HPLC analysis of the reaction mixtures from cysteine reacted with DAS2.

These results indicate that Cys is not as reactive towards DAS2 as BSH or GSH, because it forms a significant amount of CySS, even when DAS2 is used in large excess (up to 20-fold). The physical properties of Cys and BSH are very similar (pK_a : 7.97 and 8.38 and redox potential -221 mV and -223 mV for BSH and Cys, respectively⁽⁵⁹⁾) and therefore a similar reactivity of both thiols towards DAS2 was expected.

ACS2 was not isolated in enough quantity for NMR analysis and the mass for ACS2 was not detected, even after purification of the compound by HPLC.

2.7.2 DAS5 and Cys form a mixture of CySS and mixed di- to tetrasulfide (ACS(2-4))

Cys and a five-fold molar excess of DAS5 were reacted to investigate whether mixed allyl-cysteine polysulfides (ACS_n) are formed (Figure 2.27), as observed for GSH and BSH.

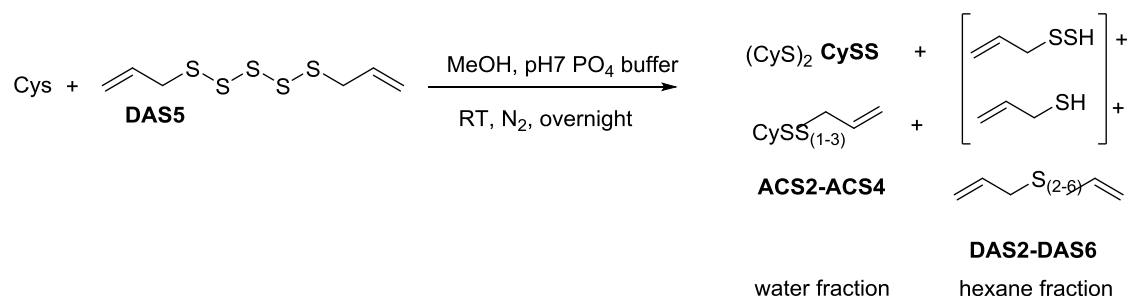


Figure 2.27: Reaction between Cys and a five-fold excess of DAS5 leads to formation of mixed di- and polysulfides (ACS₂-ACS₄), cystine (CySS) and DAS₂-DAS₆.

After overnight incubation, the reaction mixture was dried, washed with hexane and water and analysed by HPLC and NMR. HPLC analysis revealed a mixture of CySS, ACS₂, ACS₃ and ACS₄ (Figure 2.28 A and B). The distribution of mixed polysulfides in the mixture is similar to what was observed for GSH and BSH, but additionally CySS is formed as the major product even in the presence of a five-fold molar excess of DAS5, which was expected to favour the formation of mixed polysulfides.

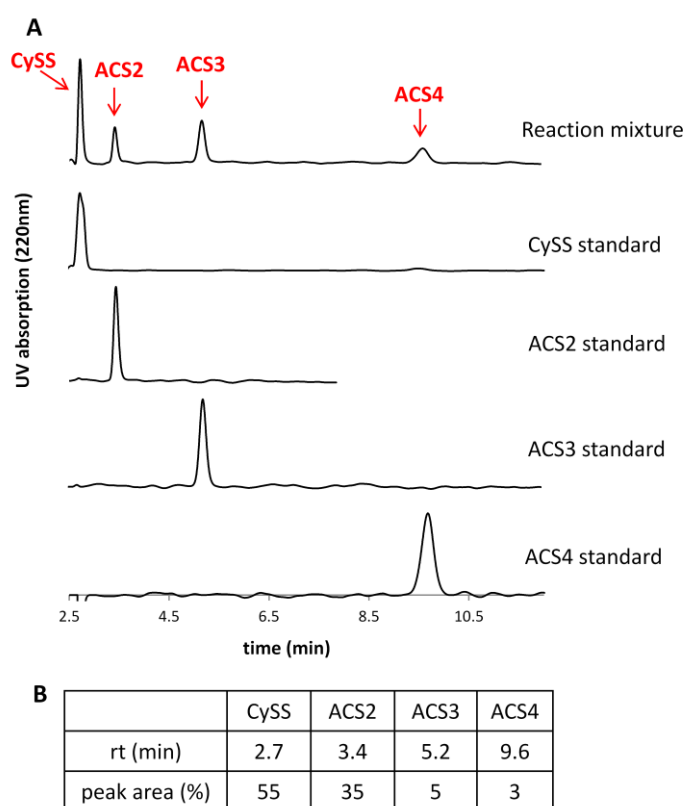


Figure 2.28: A: HPLC chromatograms of product mixture after reaction and work-up of DAS5 with Cys. B: Retention times (rt) and percentage peak areas of the formed products.

These results highlight again the lower reactivity of Cys towards DAS or the faster autoxidation of Cys to CySS compared to other thiols like BSH or GSH.

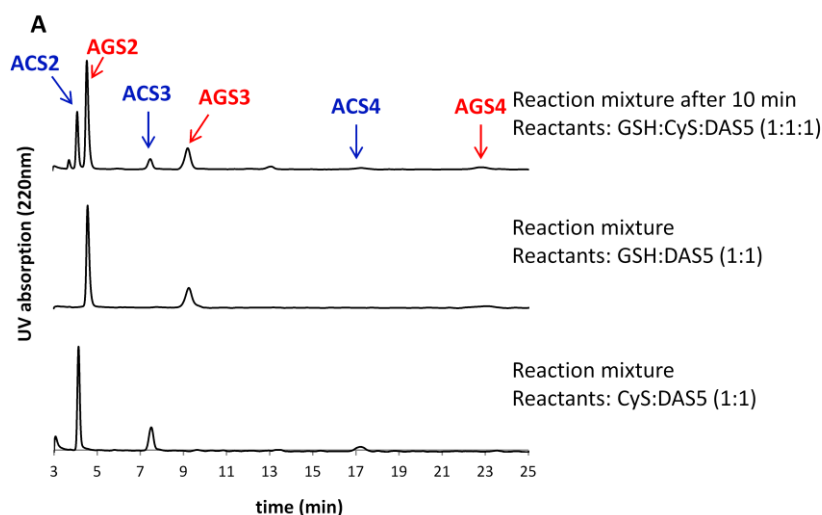
LC-MS analysis confirmed the identity of the ACS4 molecule as 303.1 m/z ($[M+2Na]^+$, calculated 303.38 m/z), but masses for ACS2 and ACS3 were not detected.

2.8 Reactivity of DAS5 towards different thiols

After analysing the formation of mixed polysulfides from individual biological thiols with DAS, the preferred reaction of DAS5 when more than one thiol is available was analysed. This situation can, in a limited fashion, represent the cellular environment where different thiols are present. For direct comparison of the favoured reaction partner of DAS5, equimolar concentrations of GSH, Cys and DAS5 (1 mM each) at pH 7.2 were used (section 2.8.1). This experiment simulates the cytosolic conditions in nematodes (*Steinernema feltiae* is used as a model organism in chapter 4). A similar experiment was performed to simulate the possible reactions of DAS5 in *B. subtilis*, which produces BSH and Cys. BSH, Cys and DAS5 were used in equimolar concentrations (1 mM each) and the reaction was performed in phosphate buffer at pH 7.7, the intracellular pH of *B. subtilis* ⁽⁸⁵⁾. This simple experiment can help to elucidate preferred reactivities of DAS with a certain biological thiol.

2.8.1 Comparison of the reactivity of DAS5 with GSH vs. Cys

GSH, Cys and DAS5 were mixed in phosphate buffer at pH 7.2 and the reaction mixture was degassed with N₂. The sum of the peak areas of the four main product peaks obtained by HPLC analysis was normalised to 100%. HPLC analysis 10 minutes after mixing showed a mixture of mainly AGS2, ACS2, AGS3, ACS3 and possibly traces of AGS4 and ACS4 (Figure 2.29 A and B).



B

	AGS2	ACS2	AGS3	ACS3	AGS4	ACS4
rt (min)	4.6	4.1	9.2	7.5	22.9	17.1
peak area (%)	50.5	21.8	20.0	7.7	<1	<1

Figure 2.29: A: Chromatograms of competition reaction between GSH, Cys and DAS5 compared to control reactions where only one thiol (GSH or Cys) was reacted with DAS5. All reactants were used at 1 mM concentration in PO₄ buffer at pH 7.2. B: Retention times (rt) and percentage peak areas of formed products.

The reaction was re-analysed after 2, 6 and 20 h, but the distribution of products did not change in that time period. This suggests that DAS5 preferably reacts with GSH compared to Cys (total AGS_n are about 2.5-fold higher compared to total ACS_n, assuming that all products show similar UV absorptions at 220 nm), but both thiols are reaction partners of DAS5. Similar to previous experiments, where DAS5 was reacted individually with GSH or Cys, the main reaction products are mixed disulfides followed by trisulfides and only traces of higher polysulfides ($S > 3$). The reaction proceeds very fast, because at 10 min, a stable mixture of reaction products is formed. Disregarding other parameters in a cellular environment of the nematode *S. feltiae* the reaction of DAS5 with GSH would be even more favoured compared with Cys, because of the more than two-fold higher intracellular concentration of GSH compared to Cys (see chapter 4).

2.8.2 Comparison of the reactivity of DAS5 with BSH vs. Cys

The same reaction was repeated, replacing GSH with BSH and adjusting the pH to 7.7, to simulate the intracellular thiols in *B. subtilis*. HPLC analysis after 10 min revealed mixed polysulfides to be ABS2, ACS2, ABS3, ACS3 and possibly traces of ABS4 and ACS4 (Figure 2.30 A and B). The formation of mixed polysulfides from different thiols (BSH and Cys) is similar, as 55% total ABS2 and ABS3 are formed compared to 45% total ACS2 and ACS3.

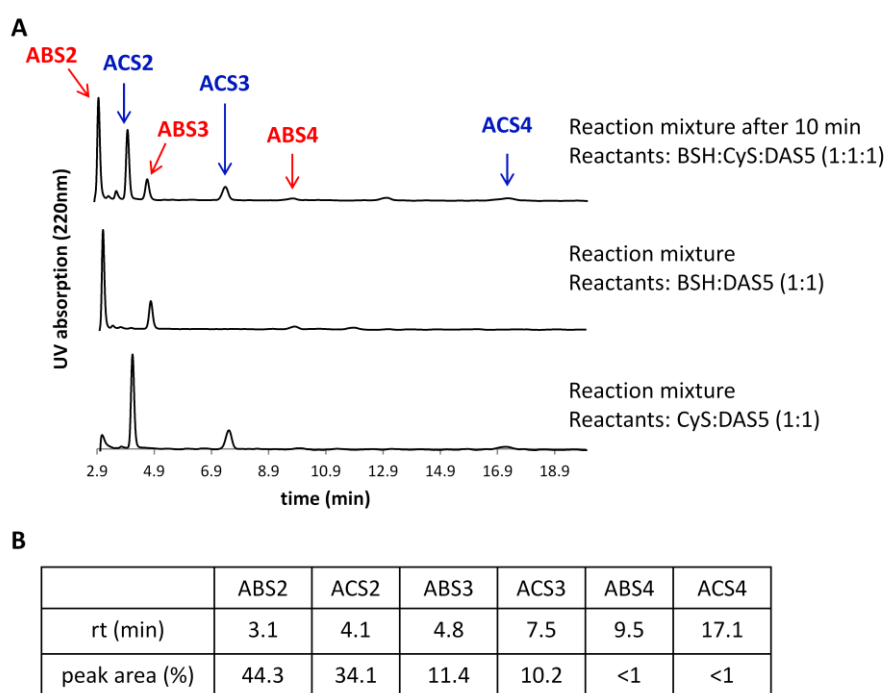


Figure 2.30: A: Chromatograms of competition reaction between BSH, Cys and DAS5 compared to control reactions where only one thiol (BSH or Cys) was reacted with DAS5. All reactants were used at 1 mM concentration in PO₄ buffer at pH 7.7. B: Retention times (rt) and percentage peak areas of formed products.

The small difference in reactivity of BSH and Cys might be due to their pK_a values (7.97 for BSH and 8.38 for Cys), which implicates that more BSH is in the deprotonated reactive form at pH 7.7. The small difference in reactivity might have a big impact in the cellular environment of *B. subtilis* as BSH concentrations are up to 17-fold higher than Cys concentrations in *B. subtilis* (see chapter 3). The mixed disulfides are found in the highest concentrations in the mixture,

followed by trisulfides and only traces of tetrasulfides can be detected, which is in accordance with previous observations in similar reactions.

2.9 Initial product formation upon DAS reacting with GSH

2.9.1 Experimental methods to measure product formation over time

These experiments aimed to elucidate the relative reactivity of DAS compared to each other, but also, to compare the reactivity of the different sulfur atoms in one molecule. In the initial reaction of the thiol (GSH) with DAS, the thiol has multiple points of attack to form a mixed di- or polysulfide. By monitoring the product formation over time, it was possible to elucidate which of the sulfur atoms in a specific DAS molecule is most reactive. Previously the reactivity for nucleophilic attack of different sulfur atoms in trisulfides were compared and several reasons for the higher reactivity of the terminal sulfurs were elaborated in an *ab initio* study⁽⁸⁶⁾. In all tested trisulfides a kinetic preference (8-21 kJ/mol) was found for the terminal sulfur atom. The attack of the terminal sulfur leads to formation of a disulfide and a perthiol, with the perthiol being a better leaving group than the thiol and therefore favouring this reaction thermodynamically. Additionally, steric hindrance of the central sulfur atom was found to be a reason for preferred nucleophilic attack on the terminal ones. Furthermore, charges were calculated for terminal and central sulfur atoms in methyl- and dimethyl substituted trisulfide and the terminal sulfur with the methyl substituent was found to be slightly positively charged while the central sulfur carries a negative charge. Therefore, the central atom was predicted to be less susceptible to nucleophilic attack⁽⁸⁶⁾. For tetrasulfides the central S-S bond has been observed to be weaker than the terminal S-S bonds⁽⁸⁷⁾, which may favour nucleophilic attack on one of the central sulfur atoms. The preferred position of nucleophilic attack in DAS3, DAS4 and DAS5 was investigated in the following sections.

Instead of just analysing the endpoint of the reaction, the reactions were adjusted to enable the monitoring of the rate of formation of different products over time. A second adjustment in this set of experiments is the ratio of DAS to GSH. Two different ratios of DAS to GSH were used (1:1 and 1:5). The latter ratio with GSH in excess is likely to be more relevant to what can be expected under physiological conditions (at least when cells are initially exposed to DAS and they start to penetrate the cell). The reactions were done in NMR tubes and ¹H-NMR spectra were recorded periodically over time. The pH was adjusted for reactions with different DAS to ensure the reaction proceeds slow enough to be monitored. At low pH, the amount of GSH found in the deprotonated form (reactive form) is low thus the reaction is slower at lower pH.

To analyse the data for this set of experiments the GSH peak at 2.5 ppm (representing the $\text{CH}_2\text{-C=O}$ protons of the glutamic acid part of GSH), which did not change much for all GSH containing molecules, was normalised to the total initial GSH concentration (see Figure 2.31 A). All peaks were integrated accordingly, for symmetric DAS integrals were divided by two because the integrals taken represent four protons and the reference GSH peak represents only two protons. As a result, approximate molar concentrations were determined for all molecule species formed over time. Integrals for DAS and AGS_n were taken for the doublet representing the CH_2S of the allyl group, because only the chemical shift for these protons was different for the different molecules (Figure 2.31 B).

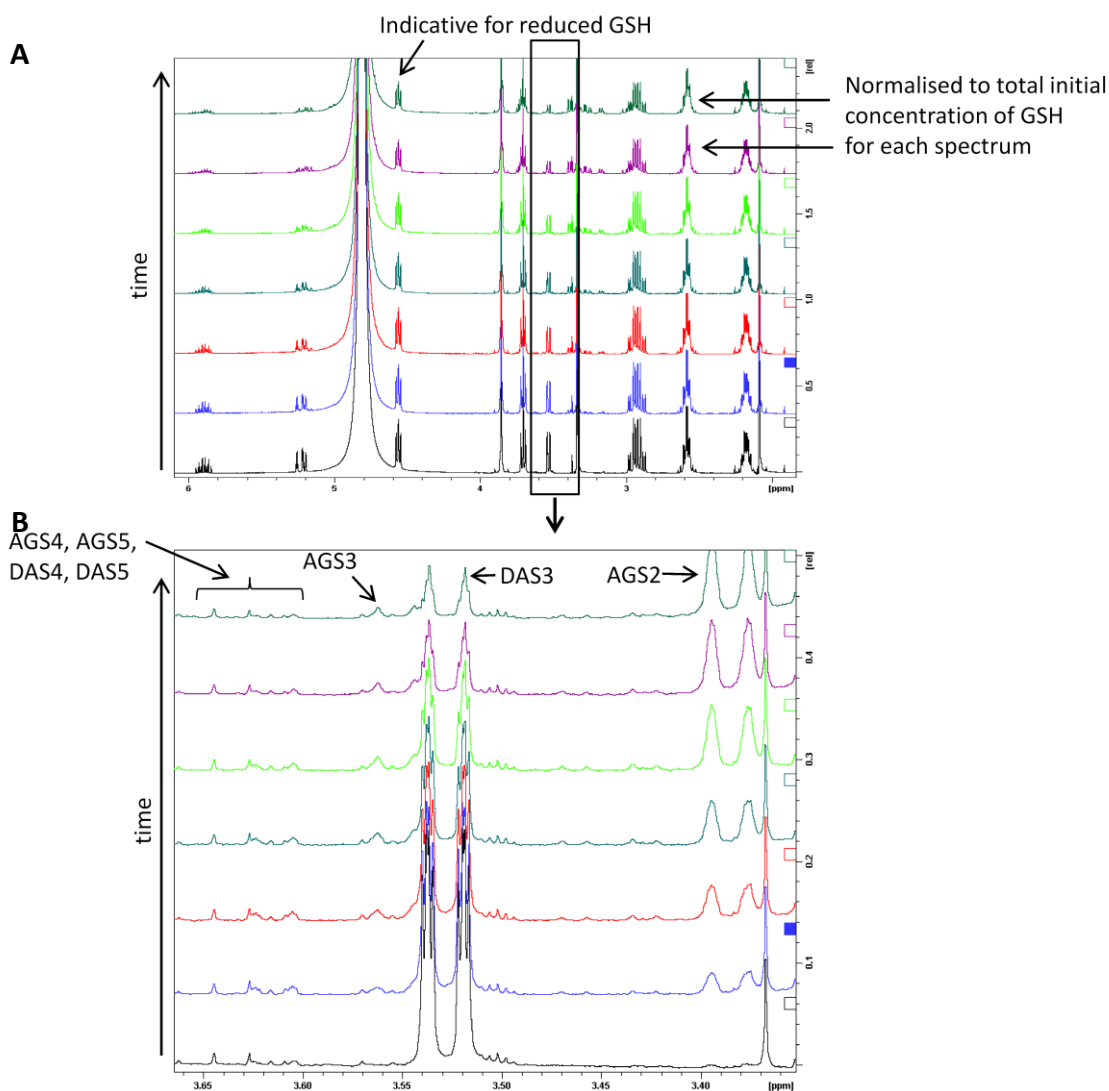


Figure 2.31: Example of $^1\text{H-NMR}$ time course (bottom to top), done for the reaction with DAS3 and GSH. A: The overview spectrum shows the GSH peak (representing the $\text{CH}_2\text{-C=O}$ of the glutamic acid part of GSH) that was used to normalise the integrals and the peak indicative for reduced GSH (representing the $\alpha\text{-CH}_2$ protons of Cys in reduced GSH). B: The magnified region shows the doublets representing the CH_2S protons of the allyl group. This doublet (or half the doublet multiplied by two for AGS3) was integrated to get concentrations of the molecules in solution. The region for AGS4, AGS5, DAS4 and DAS5 does not show clear doublets, because of low concentrations and overlapping peaks. DAS2 (doublet around 3.3 ppm) is overlain by the CD_3OD peak.

Each of these CH_2S groups is represented through a doublet for the different molecules, but some of the doublets are partly overlaying. In this case integrals of one half of the doublet were integrated and multiplied by two. The more sulfur atoms in the chain, the smaller is the difference in the chemical shift for the CH_2S protons. Therefore, it was not possible to clearly identify and differentiate DAS4, AGS4 and DAS5 (see Figure 2.32). The characteristic doublets for DAS4 and DAS5 were compared using a standard spectrum of DAS. The peak for the AGS4 doublet was assumed to overlay with one half of the doublet for DAS4 and DAS5 (peak number 2 and 3 respectively in Figure 2.32), because of the asymmetric pattern of the doublets for DAS4 (peak number 1 and 2) and DAS5 (peak number 3 and 4). Therefore, the peak area for AGS4 was estimated as described in Figure 2.32.

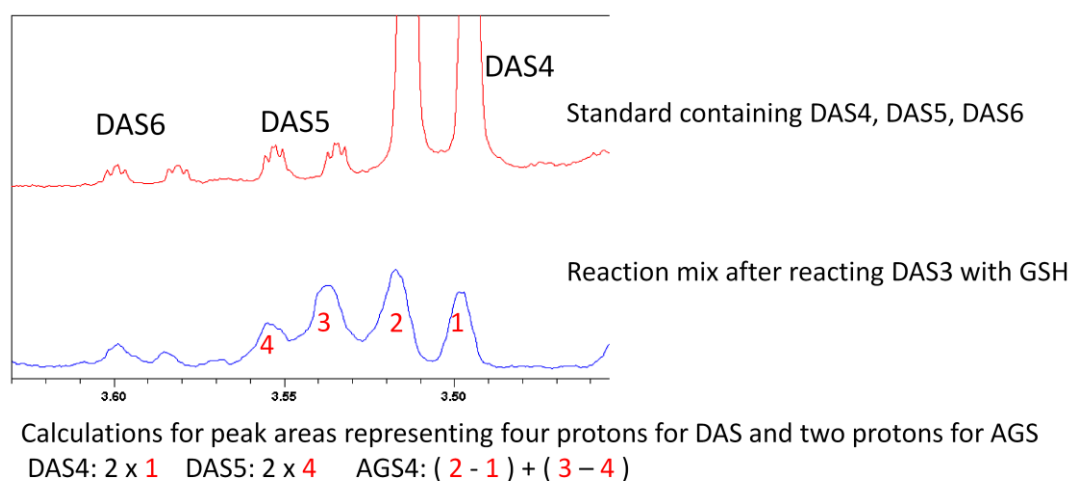


Figure 2.32: 1H -NMR of a standard mixture of DAS (top) and a reaction mixture of DAS3+GSH, magnified into the region of interest displaying the characteristic doublet for DAS4, DAS5, DAS6 and AGS4. Below: Method to calculate peak areas for overlaying peaks.

Another complicating factor was, that the higher polysulfides (DAS and mixed polysulfides with $S > 3$) are formed in very low concentrations and pure NMR reference standards are not available for AGS4 and AGS5. Whenever numbers are presented for DAS4, AGS4 or DAS5 it is important to notice that final confirmation about the identity of these peaks was not achieved, as they were overlaying. Nevertheless, it was possible to monitor formation of AGS2 and AGS3 over time after reaction of DAS3, DAS4 and DAS5 with GSH. Depending on the quality of the spectra, numbers for higher DAS and AGS_n are recorded, but it should be kept in mind that the method for taking these integrals does not provide good accuracy. Therefore, these numbers can only give an indication about relative reactivity and formation of reaction products.

For each reaction a control reaction without GSH was performed and the stability of the DAS under reaction conditions was confirmed for the time duration of the experiment.

2.9.2 Initial product formation upon reaction of DAS3 with GSH

To monitor the initial reaction of DAS3 with GSH, the two components were mixed and transferred into an NMR tube using a MeOD/ D_2O solvent mix to ensure solubility of both components. Before and after mixing, the solutions and the NMR tube were degassed with N_2 to minimise O_2 in the reaction. The first reaction was conducted at near physiological pH (7.4),

but the reaction progressed too fast. Already in the first NMR spectrum (about 10 min after mixing the reactants) the equilibrium had been reached. This highlights the high reactivity of DAS3 towards GSH and the need to lower the pH to monitor the progress of the reaction. At a lower pH less GSH is in the deprotonated form and therefore, the reaction proceeds slower. Different pHs were tested and when adjusting the pH to 6.4 (for 1:1 molar ratio) or 5.3 (for 1:5 molar ratio) the progression of the reaction was monitored periodically until an equilibrium had been reached. Figure 2.33 A and C show the decrease in DAS3 which is reacting to form other mixed and symmetrical polysulfides in a reaction using 1:1 and 1:5 molar ratios of DAS3 and GSH respectively.

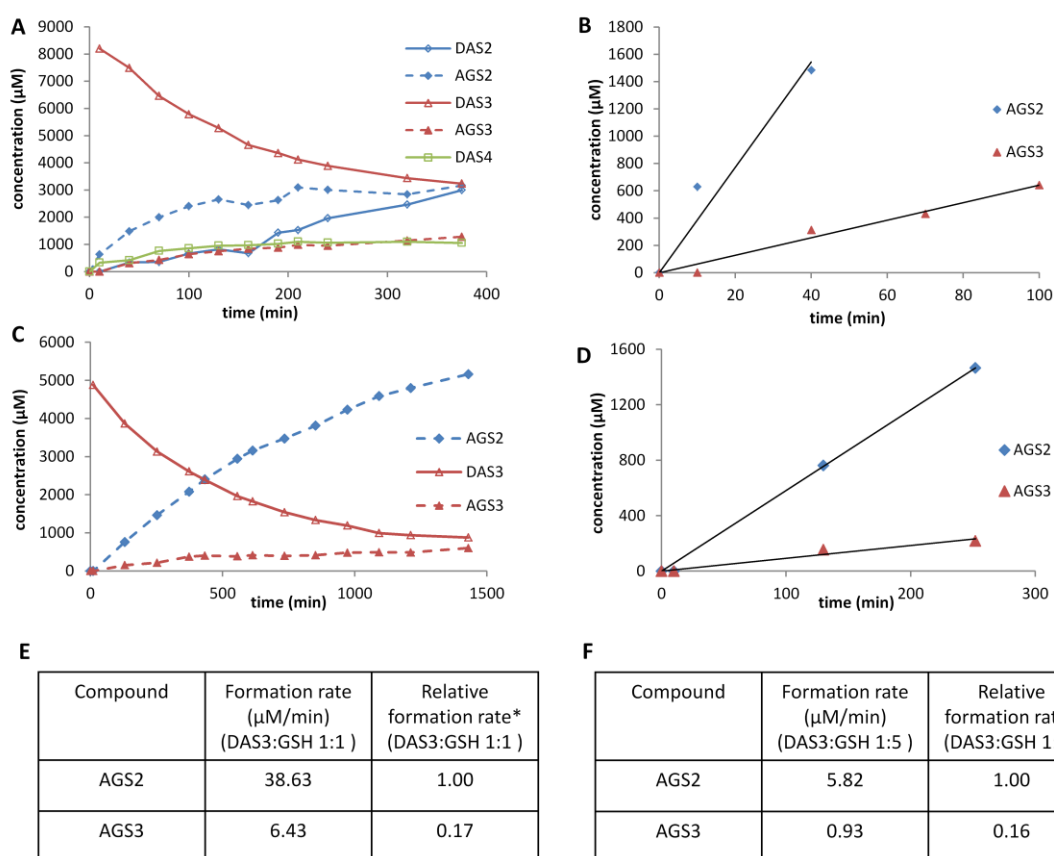


Figure 2.33: Initial reaction of DAS3 with GSH. **A:** Overview of the formation of different molecules over time (6.4 mM of DAS3 and GSH each, pH 6.4, $n=1$). **B:** Initial formation of AGS2 and AGS3 (conditions as described for A). The slope of the linear fit shows the rate of product formation. **C:** Overview of formation of different molecules over time until an equilibrium is reached [DAS3 (6.4 mM) and GSH (32 mM), pH 5.3, $n=1$]. **D:** Initial formation of AGS2 and AGS3 (conditions as described for C). The slope of the linear fit shows the rate of product formation. **E:** Formation rates of AGS2 and AGS3 using a 1:1 molar ratio of DAS3 to GSH. **F:** Formation rates of AGS2 and AGS3 using a 1:5 molar ratio of DAS3 to GSH.*For the relative reaction rate, the formation rate of AGS2 was individually normalised to 1 for each experiment.

The speed of formation of AGS2 and AGS3 was compared by estimating a linear relationship (product formation over time) for the start of the reaction (0 to 40 min for AGS2 and 0 to 100 min for AGS3). The slope of the linear fit for the formation of AGS2 and AGS3 (see Figure 2.33 B and D) represents the rate of product formation over time. The ratio of both slopes (AGS2:AGS3 6:1) shows that AGS2 is formed about 6 times faster than AGS3 for both reactant ratios. Considering that the attack of GSH on the two terminal sulfur atoms leads to the formation of AGS2 (the two terminal sulfur atoms are chemically identical) and only the attack

on the central sulfur atom leads to the formation of AGS3 (see Figure 2.18), the ratio of reactivity for the different sulfur atoms seems to be about 3:1 (terminal: central sulfur in DAS3) with the terminal ones being more reactive independent of the ratio of the reactants. This result is consistent with previous observations and can be explained by a number of calculated factors that lead to preferential nucleophilic attack on the terminal sulfur atom⁽⁸⁶⁾, like kinetic preference, less steric hindrance, and the lower pK_a of the AS2H leaving group⁽⁷⁵⁾⁽⁷²⁾. Furthermore, the terminal atoms of the dimethyl substituted trisulfide were calculated to carry a positive charge and thus be more prone to nucleophilic attack than the central, negatively charged one, which might be similar in the case of DAS3⁽⁸⁶⁾.

It is important to note that the formation of AGS2 and AGS3 might be affected by several different reactions happening very fast. The formed AS2H is a highly reducing molecule and might therefore attack mixed- or diallyl polysulfides and rearrange them rapidly (see Figure 2.18).

2.9.3 Initial product formation upon reaction of DAS4 with GSH

In the reaction with GSH and DAS4, GSH can attack two chemically different sulfur atoms: The two terminal atoms (path A and B in Figure 2.34) or the two central atoms (path C and D in Figure 2.34). Attack on position A and B results in a mixed disulfide and attack in position C and D can either result in mixed tri- or tetrasulfide.

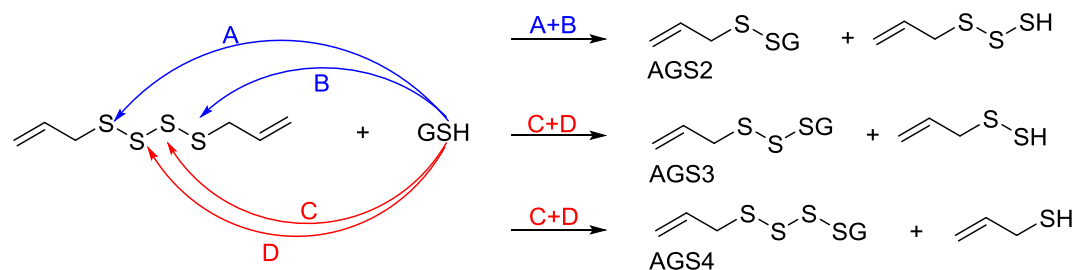


Figure 2.34: Different pathways and products for the reaction of DAS4 with GSH.

Figure 2.35 A gives an overview of formation of different products upon reaction of a 1:1 ratio of DAS4 to GSH.

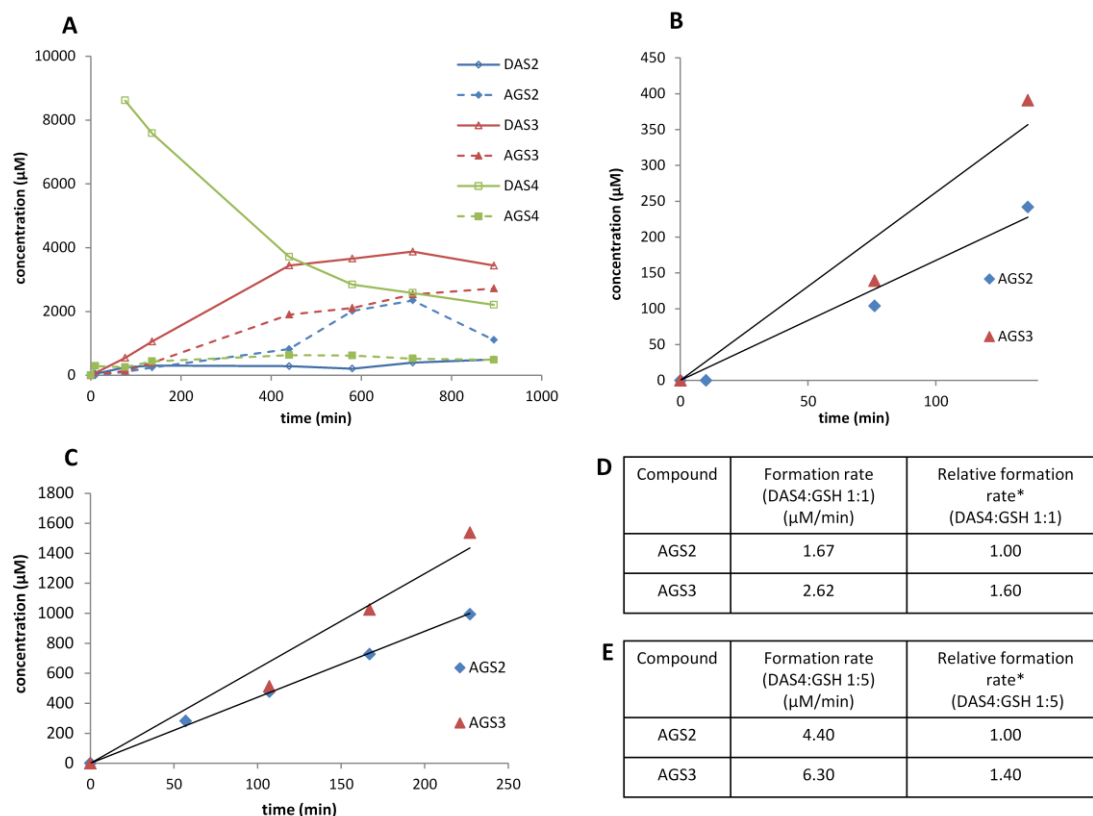


Figure 2.35: Initial reaction of DAS4 with GSH. A: Overview of formation of different molecules over time until an equilibrium is reached (6.4 mM of DAS4 and GSH each, pH 4.2, $n=1$). B and C: Initial formation of AGS2 and AGS3 [B: conditions as described for A and C: DAS4 (6.4 mM) :GSH (32 mM) pH 3.9, $n=1$]. The slope of the linear fit shows the rate of product formation. D: Formation rates of AGS2 and AGS3 using a 1:1 molar ratio of DAS4 to GSH. E: Formation rates of AGS2 and AGS3 using a 1:5 molar ratio of DAS4 to GSH. *The relative reaction rate is compared to the rate of AGS2 formation, which was individually normalised to 1 for each experiment.

Initially AGS3 is formed preferably over AGS2 (Figure 2.35 B and C). AGS4 seems to be formed as well, but cannot be fitted in a linear model starting with a concentration of zero at time zero. The concentration of AGS4 (at least when using equimolar concentrations of DAS4 and GSH) is much higher than the concentrations of AGS2 and AGS3 at the first measurement after 10 min (280 μM for AGS4 versus no AGS2 or AGS3). This, and the fact that AGS3 is formed preferably over AGS2 (~1.5: 1 Figure 2.35 B and C) suggests, that the two central atoms of the DAS4 molecule are more likely to be attacked by GSH. These results highlight, similar to what has been seen for the reaction between DAS3 and GSH that the ratio of reactants does not influence which products (mixed di- or trisulfides) are formed. It also emphasises, that the central sulfur atoms of the DAS4 molecule are more reactive for nucleophilic attack of the GSH nucleophile, compared to the terminal ones (the reaction occurs more through path C and D in Figure 2.34 than path A and B). This is different to the observations that have been made for the reaction between DAS3 and GSH, where mainly mixed disulfide was formed and therefore the nucleophilic attack mainly occurs on the terminal sulfur atoms of the DAS3 molecule. The central S-S bond in DAS4 has been shown to be weaker than the terminal S-S bonds⁽⁸⁷⁾, which seems to make the central sulfur atoms more prone to nucleophilic attack. The initial formation of mainly tri- (and tetra-)sulfides compared to disulfides might be an important difference for the *in vivo* activity of DAS4, which was observed to be much higher compared to DAS3.

Until an equilibrium is reached, more complex reaction cascades are involved where reaction products of the initial reaction keep reacting with other di-/ polysulfides leading to a change in the distribution of molecules (Figure 2.35 A).

To monitor the progression of the reaction between DAS4 and GSH, the pH was decreased (pH 4.2 for 1:1 and pH 3.9 for 1:5 molar ratio), compared to the reaction of DAS3 with GSH (pH 6.4 for 1:1 and pH 5.3 for 1:5 molar ratio). When DAS4 was reacted with GSH at the same pH as that used for DAS3, the equilibrium was already reached at the first measurement after 10 min. This is an interesting result in itself as it highlights the higher reactivity of GSH towards DAS4 compared to DAS3 and may, at least partly, explain the higher biological activity of DAS4 compared to DAS3.

2.9.4 Initial product formation upon reaction of DAS5 with GSH

Similarly as just described for DAS4, the pH had to be decreased further to monitor the reaction between DAS5 and GSH (pH 2.9 for 1:5 molar ratio). This highlights a further enhancement in the reactivity of GSH towards DAS5 compared to DAS4. The increase in reactivity might be one of the reasons for the higher biological activity of DAS5 compared to DAS4.

As shown in Figure 2.36, there are three chemically different sulfur atoms in the DAS5 molecule, which can be attacked by GSH. The attack in position A or B leads to the formation of AGS2, the attack in position C or D leads either to formation of AGS3 or AGS5; and the attack in position E results in formation of AGS4.

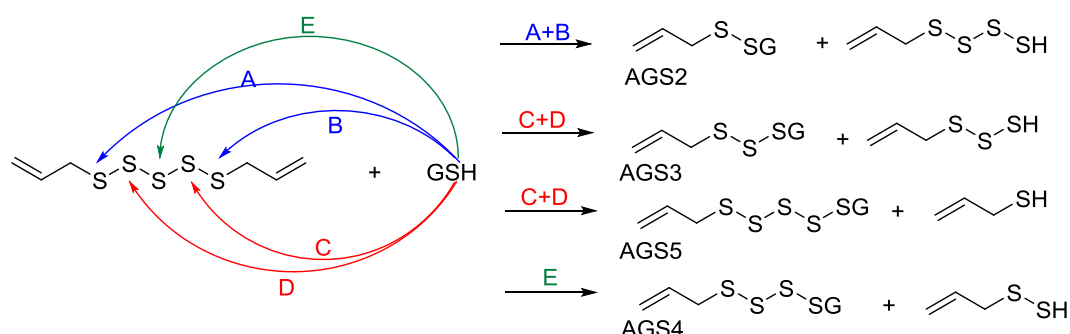


Figure 2.36: Different pathways and products for the reaction of DAS5 with GSH.

At the first time point (10 min) the concentration of AGS3 is higher than AGS2 and AGS4 (Figure 2.37 A and B, AGS5 could not be measured), which suggests the highest reactivity of the sulfur atoms in position C and D. However, as the reaction progresses the concentration of AGS2 increases over AGS3 over AGS4 (rate of formation approximately 3:2:1, Figure 2.37 C).

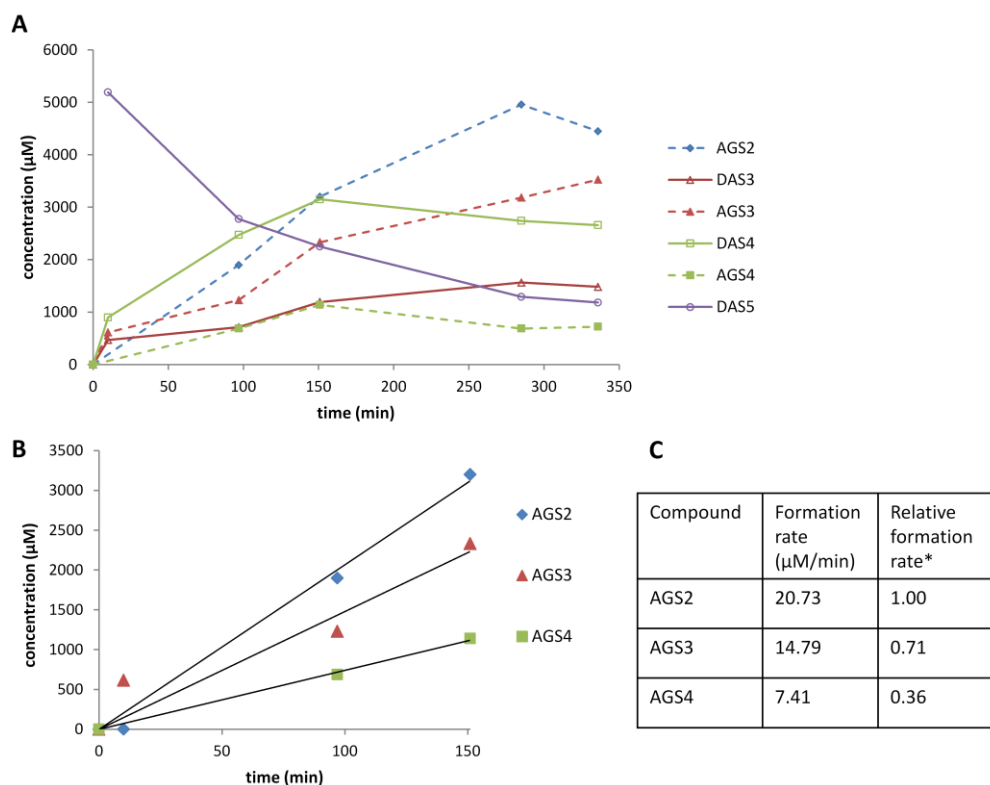


Figure 2.37: Initial reaction of DAS5 (6.4 mM) with GSH (32 mM), pH 2.9, n=1. A: Overview of formation of different molecules over time until an equilibrium is reached. B: Initial formation of AGS2, AGS3, AGS4. The slope of the linear fit shows the rate of product formation. C: Formation rates of AGS2, AGS3 and AGS4. *The relative reaction rate is compared to the rate of AGS2 formation, which was normalised to 1.

As there are two possible sulfur atoms in the molecule that can be attacked to form AGS2 (two terminal sulfurs) or AGS3 (two sulfurs adjacent to the central one), but only one (the central

one) leads to the formation of AGS4, the reactivity of the sulfur atoms is about 3:2:2 (terminal: middle: central). It is important to keep in mind that in this experiment AGS5 could not be quantified because of overlapping peaks in the corresponding NMR spectrum.

As soon as DAS5 reacts with GSH, regardless of the position of attack, another reactive sulfur species (AS(1-4)H) is formed, which may quickly reduce symmetric or mixed disulfides. Therefore it cannot be assumed that the products obtained in this experiment all result from the initial reaction of GSH with DAS5. The follow-on reactions may be faster and drive the reaction to the equilibrium and not the initial attack of GSH. With increasing number of sulfur atoms in the DAS starting material, the reactions become more complex and therefore it cannot be finally confirmed which sulfur atom in the DAS5 molecule is more prone to nucleophilic attack.

2.9.5 Reaction rates of different DAS with GSH

From the formation rates of AGS2 and AGS3, the pH independent formation rates were calculated to account for the different GS⁻ concentrations present in the different reactions performed at different pH (Table 2.1). For all shown reactions the starting concentrations of DAS were 6.4 mM and a five-fold excess of GSH (32 mM) was used. As the reaction with DAS4 and DAS5 with GSH progressed much faster than the reaction of DAS3 with GSH, the pH was decreased to allow the measurement of the initial reaction rates. The pH independent formation rates of AGS2 and AGS3 were obtained by dividing the formation rates of AGS2 and AGS3 by the GS⁻ concentration (Table 2.1).

The pH independent formation rates of AGS2 and AGS3 show that upon reaction of GS⁻ with DAS4, AGS2 is formed nearly 20-fold faster and AGS3 is formed 160-fold faster compared to the reaction of DAS3 with GS⁻. Even greater is the difference in reaction speed of DAS5 with GS⁻ compared to DAS3 with GS⁻: AGS2 is formed more than 800-fold faster (45-fold faster compared to the reaction between GS⁻ and DAS4) and AGS3 is formed 3800-fold faster (23-fold faster compared to the reaction between GSH and DAS4). These huge differences in the reaction speed may be an explanation of the higher biological activities of longer sulfur chain DAS. A reason for the increased reactivity of longer chain DAS may be the lower dissociation energies with increasing number of sulfur atoms, which were reported to decrease from 293 kJ to 150 kJ for the dimethyl substituted DAS2 to DAS4⁽³⁷⁾.

Table 2.1: Reaction speed of DAS3, DAS4 and DAS5 with GSH. Starting concentrations of DAS3, DAS4 and DAS5 were 6.4 mM and starting concentration of GSH was 32 mM in all reactions.

DAS	pH	GS ⁻ ^a (%)	GS ⁻ ^b (μ M)	AGS2 ^c (μ M min ⁻¹)	AGS3 ^c (μ M min ⁻¹)	AGS2 ^d (min ⁻¹)	AGS3 ^d (min ⁻¹)	AGS2 ^e normalised	AGS3 ^e normalised
DAS3	5.3	0.023	7.36	5.82	0.93	0.79	0.13	1	1
DAS4	3.9	9.33×10^{-4}	0.30	4.40	6.32	14.67	21.07	18.57	162.08
DAS5	2.9	9.33×10^{-5}	0.03	20.73	14.79	691.00	493.00	874.68	3792.31

^aPercentage of GS⁻ thiolate at the pH of the reaction, calculated based on a thiol pK_a of 8.93 for GSH.

^bConcentration of GS⁻ at the start of the reaction (depending on GSH concentration and pH of the reaction).

^cFormation of AGS2 and AGS3 (μ M) measured at the start of the reaction and plotted over time (min⁻¹). The slope of the linear fit gives the formation rate (μ M min⁻¹). ^dFormation rate (previous columns, μ M min⁻¹) divided by the GS⁻ concentration (μ M) gives the pH independent formation rate (min⁻¹). ^epH independent formation rates of AGS2 and AGS3 through reaction of DAS3 with GS⁻ were normalised to 1.

To summarise, these experiments suggested that the terminal sulfur atoms of DAS3 are more reactive compared to the central one leading to mainly AGS2 formation, which is the opposite for DAS4, where the two central sulfur atoms seem to be more prone to nucleophilic attack leading to mainly AGS3 formation. No clear result was obtained for comparable reactivities of the sulfur atoms in the DAS5 molecule. The product distribution seems to be independent of the reactant ratios, at least for the two different tested ratios (DAS:GSH 1:1 and 1:5). Through the initial thiol-polysulfide exchange between DAS and GSH a reduced AS_nH molecule is liberated and it is likely that further reactions are driven by the reactivity and reducing power of this molecule species. The final product distribution is likely to be governed by the thermodynamic stability of the different products. Importantly, a great increase in reaction speed from DAS3 over DAS4 to DAS5 with GSH was observed, which highlights the increased reactivity of longer chain DAS (Figure 2.38). In a different study, the reaction rate of a cyclic pentasulfide ring system (7-methylbenzopentathiepin) with GSH has been found to be at least 34-fold faster (at least $60 \text{ M}^{-1} \text{ s}^{-1}$) compared to the reactivity of a benzyltrisulfide with GSH ($1.77 \text{ M}^{-1} \text{ s}^{-1}$)⁽⁸⁸⁾. The exact reaction rate for the pentasulfide was not determined, but the increase in reaction rate with longer sulfur chain is in accordance with the results obtained in the present study. Therefore, thiol-polysulfide exchange reactions are likely to be, unlike normal thiol-disulfide exchange reactions, of metabolic importance *in vivo*.

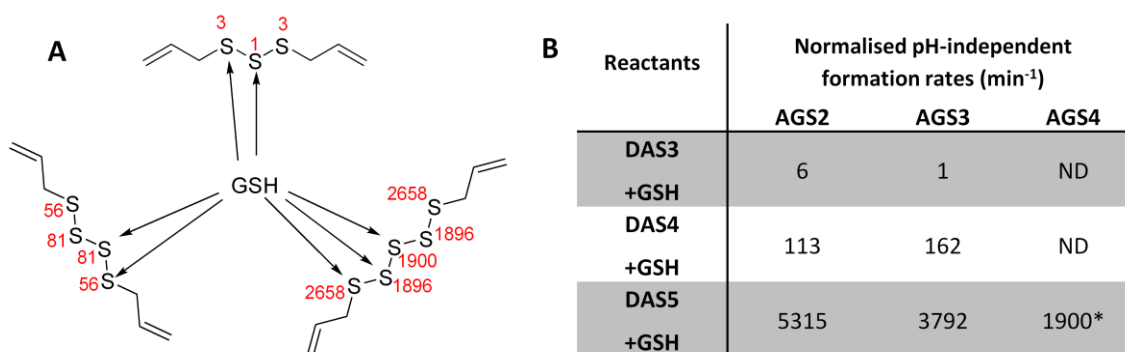


Figure 2.38: A: Relative reactivity of different sulfur atoms in DAS3, DAS4 and DAS5 for nucleophilic attack from GSH. B: Relative pH independent formation rates of AGS2, AGS3 and AGS4 upon reaction of GSH (32 mM) with DAS3 (6.4 mM, pH 5.3), DAS4 (6.4 mM, pH 3.9) and DAS5 (6.4 mM, pH 2.9). The pH independent formation rate of AGS3 was normalised to one. *Formation rate of AGS4 was determined as $7.41 \mu\text{M min}^{-1}$, resulting in a pH independent formation rate of 247 min^{-1} .

2.10 Summary and Conclusions

Due to the importance of the reaction of DAS with LMW thiols for the MOA of DAS, and the complexity of *in vivo* studies, the chemical reactivity of DAS with LMW thiols was investigated on a chemical level. Using this simplified method the formation of AS2H and AS3H, the reduced species of DAS after reaction with GSH, was proven for the first time. The reduced form of DAS is proposed to be the active form of DAS⁽¹⁹⁾ and AS_nH are hypothesised to have strong reducing properties^(41, 89) which contribute to their biological activity. AS2H and AS3H are suggested to be able to reduce O₂ to the superoxide radical⁽⁴²⁾, which in a cellular environment can be the first step towards an oxidative burst. Additionally, the pK_a of perthiols is found to be lower than the pK_a of the corresponding thiols⁽⁷⁵⁾, which indicates that the perthiols are more deprotonated at physiological pH than their corresponding thiols, and therefore more reactive. For example, the thiol of 2- [(3- aminopropyl) amino] - methanesulfenothioic acid has a pK_a value of 7.6 whereas the pK_a for the corresponding perthiol was measured as 6.2, showing a difference of 1.4 pK_a units between the thiol and the corresponding perthiol⁽⁷⁵⁾. Transferring this trend to ASH (pK_a measured as 9.96⁽⁹⁰⁾) and AS2H, it would suggest a pK_a of ~8.6 for AS2H. It can be speculated that this trend (decreased pK_a values) continues for the reduced forms of DAS4, DAS5 and DAS6 (AS3H, AS4H and AS5H), which would explain their increased reactivity. In fact AS4H and AS5H have not been detected and their formation depends on the point of the nucleophilic attack by the thiol. Additionally, the suggested mechanism for the DAS induced release of the vasoactive gas H₂S, is dependent on formation of AS_nH (n>1)⁽¹⁸⁾. AS_nH (n>1) are proposed to react with a thiol molecule to form a mixed disulfide and liberate H₂S. H₂S liberation was observed after reaction of a 20-fold excess of GSH with DAS2 or DAS3⁽¹⁸⁾, suggesting that the excess of thiol triggers this pathway.

To summarise, the reduced forms of the DAS are important for their MOA and different studies suggest their extraordinary chemical reactivity to be responsible for the activity of DAS^(18, 40, 42, 89). Therefore, the detection and proof of the existence of these molecules, which is reported in this study for the first time, closes an important gap in the study of the DAS molecules. Additionally, it provides useful standards for HPLC analysis of mBBR derivatised cell samples of *B. subtilis* where the formation of these DAS metabolites will be investigated *in vivo* (chapter 3).

Furthermore, the formation of mixed polysulfides (with up to five sulfur atoms in a linear chain) upon reaction of DAS with GSH, BSH and Cys was proven. The suggested reaction mechanism is a thiol-polysulfide exchange reaction where the thiol attacks one of the sulfur atoms of the DAS molecules. This is the first step in a cascade of reactions and further reactions can lead to the liberation of the vasoactive gas H₂S or formation of ROS (Figure 1.10), the exploration of which is beyond the scope of this study. Nevertheless, it is important to notice that these reactions are likely to contribute to the bioactivity of DAS.

The presented *in vitro* investigations also highlight the complexity of the reaction of DAS with LMW thiols. No matter which of the DAS (S>2) is used as the starting material in a reaction with LMW thiols, as reaction products DAS2 to DAS6, their reduced counterparts (AS_nH) and allyl-mixed polysulfides were observed. Therefore, in an *in vivo* context cellular changes are not necessarily the result of reactions undertaken by the originally added DAS molecule, but possibly reactions undertaken by a mixture of metabolites derived from the added molecule.

Comparison of the reactivity of DAS5 towards GSH and Cys or BSH and Cys revealed that more mixed di- and polysulfides are formed with GSH and BSH compared to Cys. In a cellular context this observation is likely to be amplified because BSH is up to 17-fold more concentrated than Cys in *B. subtilis* (chapter 3) and the GSH concentration in *S. feltiae* is more than double than the Cys concentration (chapter 4). It is important to note, that the cellular environment is more complex and reactions are enzymatically catalysed rather than purely chemical reactions determined by thermodynamic equilibria. Furthermore, there are other cellular thiols, which were not taken into account in these experiments (e.g. CoA and Cys residues of proteins). It is possible that DAS preferably react with Cys residues of proteins compared to free LMW thiols, which was not investigated in this section. Furthermore, the stability of the mixed polysulfides in a cellular environment is unknown. The cellular environment is highly reducing and strong enzymatic mechanisms are in place to defend the cells against oxidative stress (section 1.3.6.2), which may lead to rapid reduction of mixed polysulfides.

Some important differences between the different chain length DAS were observed: With increasing number of sulfur atoms in DAS, the reaction with GSH progressed faster: AGS2 and AGS3 formation was nearly 40 times faster for DAS4 compared to DAS3 and another 30-fold increase in reaction speed was observed for DAS5 compared to DAS4. Secondly, the reaction of DAS4 with GSH initially led to the formation of higher concentrations of mixed tri- (and possibly tetra-) sulfide, whereas DAS3 and GSH mainly formed mixed disulfide. Both observations may be important for the different *in vivo* potencies of the different DAS molecules.

- **Identification of novel DAS metabolites after reaction with LMW thiols:** The reduced form of DAS (AS2H and AS3H) is often suggested to convey the biological activity of DAS and these molecules have been detected in this study for the first time. Additionally new mixed polysulfides with up to 5 sulfur atoms have been shown to be formed upon DAS reaction with LMW thiols.
- **Increased rate of reaction of DAS with GSH with increased number of sulfur atoms:** The formation of mixed polysulfides upon reaction of DAS with GSH was 40-fold faster for DAS4 compared to DAS3 and another 30-fold faster for DAS5. This strongly increased reaction rate is likely to contribute to the higher biological activity of longer chain DAS, which is often observed, but cannot be fully explained to date.
- **Differences in product formation upon DAS reacting with GSH:** The reaction of DAS3 with GSH initially mainly leads to formation of mixed disulfides, whereas the reaction of DAS4 with GSH initially leads to similar concentrations of mixed di- (AGS2) and trisulfide (AGS3). These findings demonstrate that the terminal sulfur atoms in the DAS3 molecule are more prone to nucleophilic attack than the central ones, whereas the reactivity of all sulfur atoms in DAS4 is similar. In a biological setting these differences in product formation may have an impact on further reactions and signalling events and may contribute to the higher biological activity of DAS4 compared to DAS3.

3 Structure-activity relationship and mode of action of diallyl polysulfides – investigated on the model organism *Bacillus subtilis*

3.1 Introduction

3.1.1 Aims and overview of this chapter

One of the key questions, addressed in this chapter, is whether the activity of diallyl polysulfides (DAS) increases with increasing number of sulfur atoms. An increasing toxicity of longer chain DAS, up to DAS4 against various microorganisms (Table 1.3) is reported in the literature⁽¹⁹⁾. No biological data has been published for pure DAS5 or DAS6 and, therefore, it was investigated whether this trend (increasing activity with increasing number of sulfur atoms) continues for DAS5 and DAS6. To this end, growth experiments with *B. subtilis* under DAS stress were conducted and the effects of DAS on growth and vitality of *B. subtilis* cultures were monitored (section 3.2.).

Furthermore, the alteration of the cellular thiol redox status as one possible mode of action of DAS was investigated, which is hypothesised in literature⁽⁴⁰⁾ and also through our results in chapter 2. The effect on the cellular redox balance is thought to occur by the interaction of DAS with low molecular weight (LMW) and protein thiols, which were investigated in this chapter using *B. subtilis* as a model organism. The method development for LMW thiol and disulfide quantification is discussed in Appendix 1.

3.1.2 Model organism: *Bacillus subtilis*

B. subtilis, which is used as a model organism in this study, is a non-pathogenic Gram positive bacterium. *B. subtilis* has the ability to form endospores, and, therefore it can tolerate extreme environmental conditions. It is commonly found in the soil, but recently it has been debated whether the human gastrointestinal tract is the true habitat of this species⁽⁹¹⁾. *B. subtilis* is the best-characterised member of the Gram positive bacteria and its complete genome sequence is published⁽⁹²⁾. *B. subtilis* produces bacillithiol (BSH), cysteine (Cys) and coenzyme A (CoA) as LMW thiols (Figure 1.11).

3.2 Structure-activity relationship of DAS determined through *B. subtilis* growth experiments

For the experiments in this chapter the *B. subtilis* wild-type (WT) strain CU1065 and a BSH deficient mutant (disrupted in *bshA*, encoding a glycosyltransferase that mediates the first step in BSH biosynthesis) were used. The WT and mutant strains were a generous gift from Prof. J. D. Helmann (Cornell University, USA). The comparison of DAS susceptibility between the WT and the *bshA*⁻ mutant helped to examine the importance of BSH as a target for DAS.

3.2.1 Methodology

To evaluate and compare the toxicity of different DAS towards *B. subtilis*, three different methods were used (Figure 3.1).

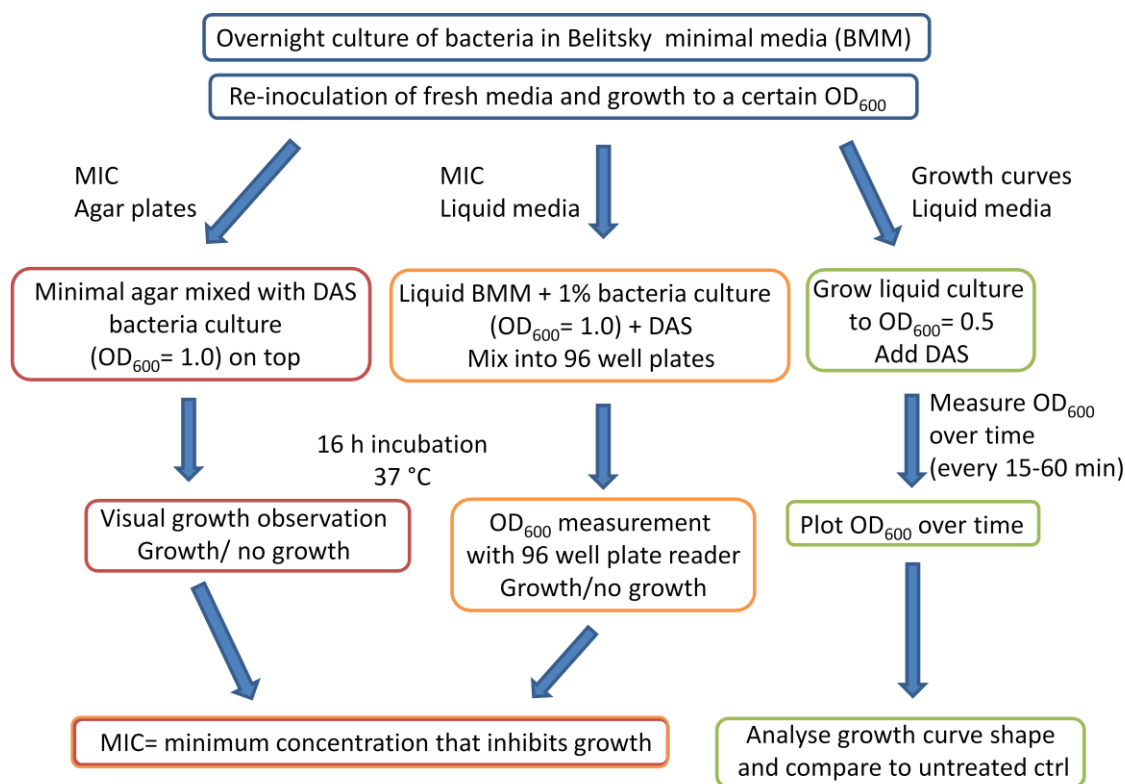


Figure 3.1: Overview of different methods to investigate the influence of DAS towards the growth of *B. subtilis*. MIC=Minimum Inhibitory concentration. OD=Optical Density. Ctrl=control.

3.2.1.1 Determination of Minimum Inhibitory Concentrations (MIC)

The Minimum Inhibitory Concentration (MIC) of a compound can either be determined by inoculating bacteria on agar plates, with the compound distributed evenly in the agar, or in liquid media. In both experiments the cultures are inoculated overnight at 37°C. After 16 hours bacterial growth is categorised as grown or not grown for each concentration. For the MIC experiment on agar plates this decision is based on visual examination of the plates (magnified, if needed). The analysis of cultures in liquid media was done by measuring the optical density at 600 nm (OD_{600}) of the overnight cultures and comparing them with a blank that does not contain bacteria.

Problems

Both these methods are extremely sensitive to variations in certain experimental parameters: The density of bacterial culture used as inoculum, incubation time and temperature, incubation media, and criteria for analysis of growth. Therefore, it is important to keep these parameters consistent within all experiments performed. For both MIC determination methods, the incubation time was critical, since after several days, growth was observed on plates that did not show initial growth after 16 hours of incubation. This result might be due to

the nature of the DAS compounds (volatile, unstable) or confounding growth of the bacteria (bacteria metabolising the compound and/or becoming resistant).

Another problem for the MIC determination on agar plates is the agar temperature when mixing with the DAS compounds and pouring the plates. If the agar is too hot there is the risk of degradation of heat sensitive compounds (like DAS) and if the temperature is too low, the agar solidifies too quickly and prevents proper mixing of the agar with the compounds.

In liquid culture, DAS formed milky suspensions, which affects the OD₆₀₀ reading. Therefore, for each DAS concentration a blank without bacteria was prepared. Another problem arose because of the high volatility of DAS. When using 96 well plates for the determination of MICs in liquid media, DAS diffused into adjacent wells and affected the results. To address this problem, wells in between treatments were inoculated without DAS, which served as a positive control for the growth of the bacteria.

Advantages

Both the MIC methods are fast and easy for testing a range of compounds in different concentrations. It is, therefore, a useful method to screen large numbers of compounds and find effective concentrations of new compounds. Another advantage of the MIC method is the numerical output and the ability to compare the results with those reported in the literature. When doing so, some standardised experimental parameters, should be considered such as the type of growth medium, inoculum density and incubation conditions⁽⁹³⁾. In this study the MICs of DAS1 to DAS6 against the *B. subtilis* WT and the *bshA*⁻ mutant were determined using the two different methods.

3.2.1.2 Growth curves

The typical pattern of a bacterial growth curve consists of an initial lag phase, an exponential growth phase (log phase) and a stationary phase, which can be observed by measuring OD₆₀₀. When adding a drug at early exponential phase (OD₆₀₀ between 0.3 and 0.5 for *B. subtilis*) the response of the culture can be observed. Depending on the toxicity and concentration of the compound there can be a decrease in the OD₆₀₀, which corresponds to bacterial lysis, due to bacteriocidal effects of the added drug. Alternatively, an inhibited or slowed growth of the bacterial population can be observed by constant or slowly increasing OD₆₀₀ readings compared to the control culture. This bacteriostatic effect is often reversible. After metabolising the drug, the bacterial culture continues dividing normally and the population starts growing exponentially again.

By monitoring the growth response of a population after the addition of a certain compound, important information can be gained: Speed of the bacterial response towards the compound, differentiation between bacteriocidal and bacteriostatic compounds and the recovery time of the culture from the compound. Growth curve experiments were performed for all DAS at different concentrations to gain detailed information about their influence on the growth of *B. subtilis* populations.

3.2.2 MIC determinations of DAS towards the *B. subtilis* WT and the *bshA*⁻ mutant

The susceptibility of the WT and the *bshA*⁻ mutant of *B. subtilis* towards DAS1 to DAS6 was investigated on agar plates (Figure 3.2 A and B) and in liquid media (Figure 3.2 C).

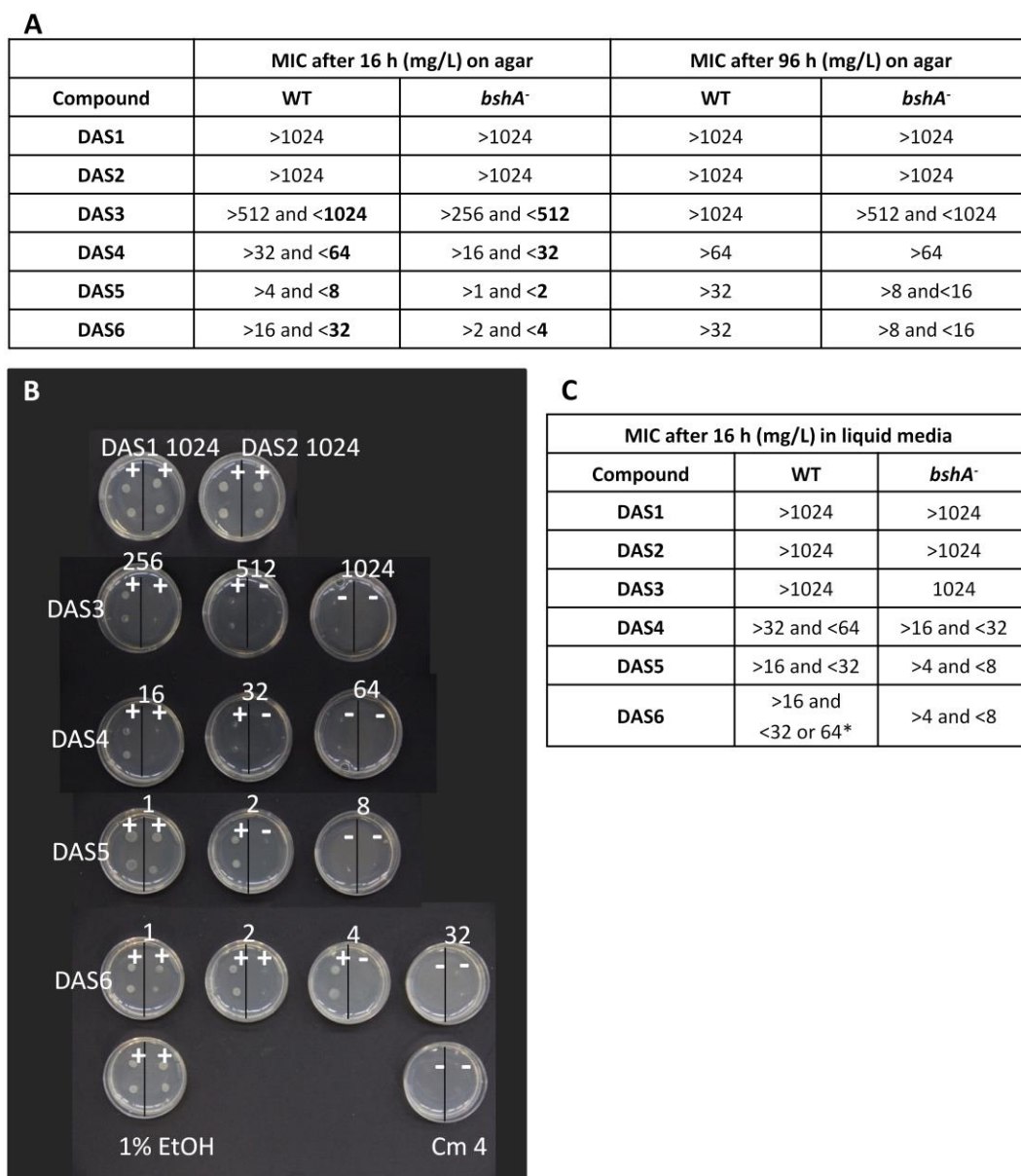


Figure 3.2: A: Summary of the results of MIC determination on agar plates for DAS1 to DAS6 (mg/L) against the *B. subtilis* WT and the *bshA*⁻ mutant after 16 hours and 96 hours of incubation at 37°C. All concentrations were tested in triplicates and the experiment was performed twice. B: Agar plates for MIC determination after 16 hours of incubation. Numbers indicate concentration in mg/L. The *B. subtilis* WT culture was spotted on the left hand side of each agar plate and the *bshA*⁻ culture was spotted on the right hand side. Growth is indicated by +, while no growth is indicated by -. In some cases faint dots on the agar appear even though no colonies were growing, because the agar was punctured with the pipette tip when applying the bacteria. Growth on 1% EtOH is shown as a DAS vehicle control. No growth on chloramphenicol 4 mg/L (Cm 4) is shown as positive control for growth inhibition of an antibiotic known to inhibit *B. subtilis* growth. C: MIC (mg/L) of DAS against *B. subtilis* WT and *bshA*⁻ mutant in liquid media in 96 well plates after 16 hours of incubation at 37 °C. Each concentration was tested in triplicates and the experiment was performed twice. *different results were obtained from different experiments.

There are two important observations elucidated by the MIC values determined on agar plates after 16 hours of incubation: Firstly, the MIC values for both strains (WT and *bshA*⁻ mutant) decrease with increasing number of sulfur atoms in the chain, up to DAS5, with the 8 to 32-fold difference between MIC values of DAS3 and DAS4 being particularly notable. The trend continues with the MIC of DAS5 against *B. subtilis* WT being 4 to 16-fold lower than that of DAS4. DAS6 shows less potency than DAS5 against the WT, with a 2 to 8-fold higher MIC than that of DAS5. DAS3 is more potent than DAS1 and DAS2, but the magnitude of this observation remains unknown, because MICs for DAS1 and DAS2 exceeded the maximum tested concentrations due to restrictions in solubility. Secondly, for each of the DAS the MIC for the *bshA*⁻ mutant is lower compared to the MIC of the WT. This difference in susceptibility highlights a role for BSH in protection against DAS stress/toxicity, and may suggest that either 1) the mode of action of DAS involves an interaction with BSH and/ or 2) BSH might provide protection against oxidative stress induced by the DAS molecules. Nevertheless, there is only a modest increase in susceptibility of the mutant to DAS3 to DAS6 which suggests that there may be other modes of dealing with DAS stress in the mutant strain.

To confirm the MIC results that were obtained with the agar plate method, the MIC was also determined in liquid media in 96 well plates (Figure 3.2 C). The trend of the results, showing increasing potency for increasing numbers of sulfur atoms and higher susceptibility of the *bshA*⁻ mutant, is the same as observed using the agar plate method.

There are no literature values for the MIC of DAS towards *B. subtilis*, but compared to the MIC for ajoene (another organosulfur compound produced in garlic) towards *B. subtilis* (5 mg/L⁽⁹⁴⁾ or 14 mg/L⁽⁹⁵⁾) the obtained MICs are in a similar order of magnitude. Compared to the MIC of DAS towards another *Bacillus* strain *B. cereus* (64, 14, 4 and 1 mg/L for DAS1 to DAS4 respectively⁽²³⁾) the MIC values for DAS towards *B. subtilis* are higher, which corresponds to higher resistance of *B. subtilis* towards the DAS.

3.2.3 DAS induced dose dependent growth inhibition of *B. subtilis*

Growth curves were used to examine the rate of toxicity of different sublethal DAS concentrations towards *B. subtilis* (Figure 3.3). The time of growth inhibition increased with increasing DAS concentrations. To achieve the same growth inhibition, lower concentrations of longer chain DAS are required, which highlights the higher potency of longer chain DAS against *B. subtilis* (DAS6>DAS5>DAS4>DAS3>DAS2). For example, to achieve a two hour growth inhibition, approximately 500 μM DAS2, 150 μM DAS3, 50 μM DAS4, 25 μM DAS5 or DAS6 were required.

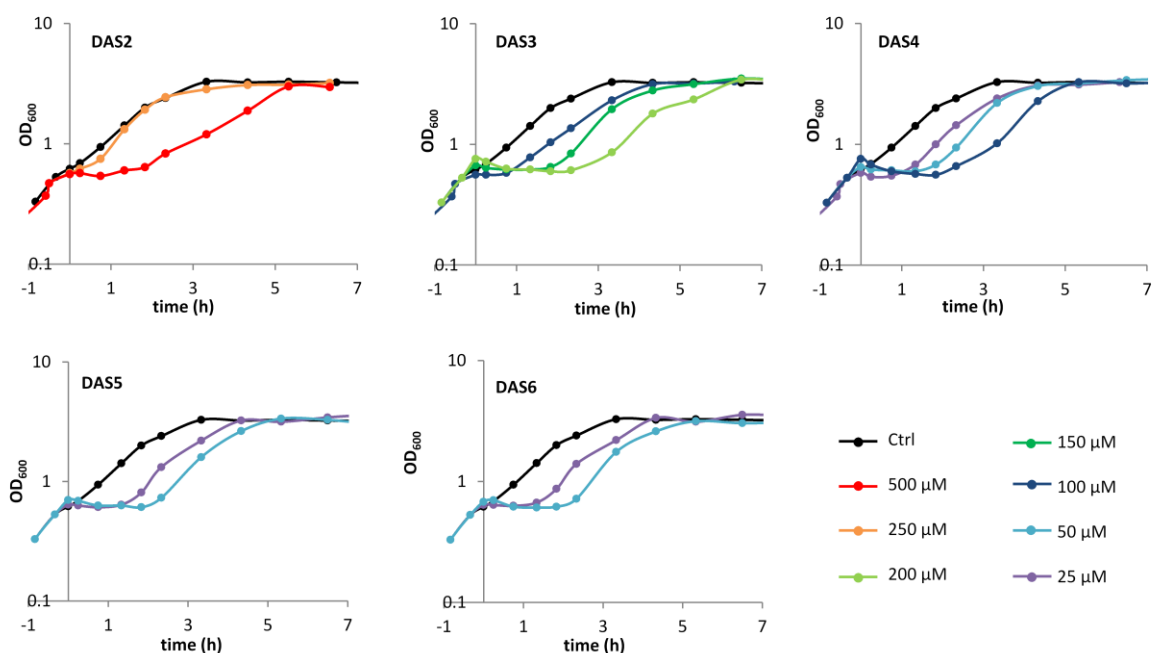


Figure 3.3: Influence of different concentrations of DAS2 to DAS6 on the growth of *B. subtilis* WT ($n=1$). DAS were added at $\text{OD}_{600}=0.5$ (normalised to time zero for all graphs). All cultures contained 1% final concentration of EtOH and were grown in Belitsky Minimal Media.

3.2.4 BSH helps *B. subtilis* to recover from DAS stress

After confirming that the BSH null mutant grows at a similar rate compared to the WT, growth curves were recorded for both strains after DAS stress (Figure 3.4). The *bshA*⁻ mutant took longer to recover from DAS stress compared to the WT for all tested DAS in all tested concentrations. The recovery time for the *bshA*⁻ mutant was about one to three hours longer for a certain DAS concentration and no recovery of the *bshA*⁻ mutant was observed for DAS2 at 500 μ M and DAS3 at 200 μ M even after seven hours, although the WT recovered after two or three hours, respectively. These results are in good agreement with the determined DAS3 to DAS6 MIC values, which were lower for the *bshA*⁻ mutant compared to the WT.

These findings again highlight the importance of BSH when dealing with DAS stress and a possible role of BSH in detoxification or metabolising of DAS.

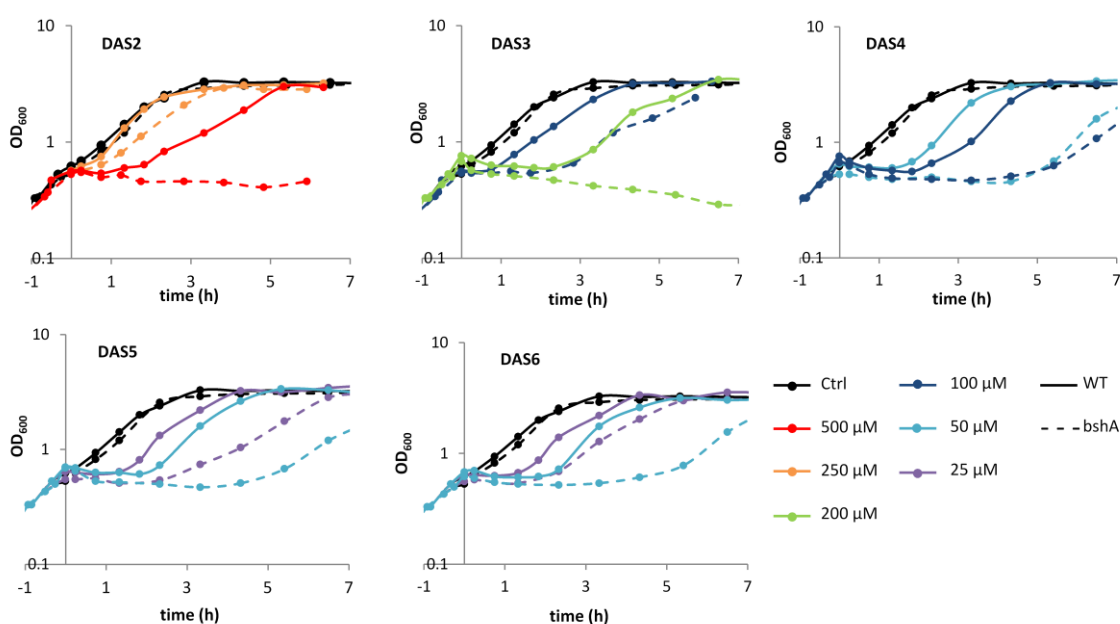


Figure 3.4: Growth comparison of *B. subtilis* WT and *bshA*⁻ mutant after DAS treatment (n=1). DAS were added at OD₆₀₀=0.5 (normalised to time = 0 for all graphs). All cultures contained 1% final concentration of ethanol and were grown in Belitsky Minimal Media.

3.3 Hypothesis for the interaction of DAS with cellular thiols

Figure 1.15 shows the cellular reactions that BSH is involved in, to protect the cells from oxidative stress. We hypothesise that DAS can interfere with these normal functions of BSH, and these pathways are highlighted in red in Figure 3.5.

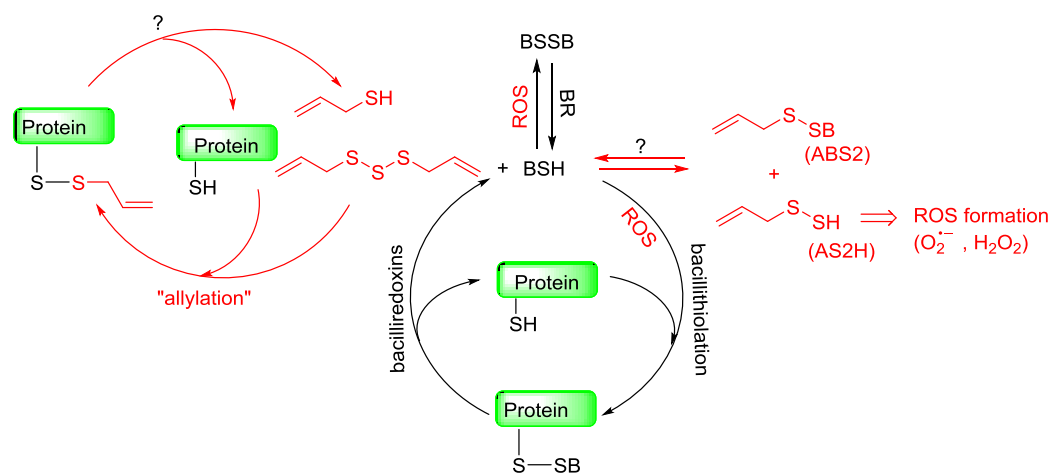


Figure 3.5: BSH redox system (shown in black) and hypothesised DAS interference in these reactions (shown in red). BR: Bacillithiol disulfide reductase. ROS: reactive oxygen species.

One possible mode of action is the (reversible) formation of mixed allyl-bacillithiol disulfide (ABS2) and the liberation of allyl perthiol (AS2H), analogous to the chemical reactions described for DAS + BSH in chapter 2. This would lower the pool of reduced intracellular BSH and therefore change the redox status of the cell. The ABS2 formation may be reversible by enzymatic reduction through bacillithiol disulfide reductases (BR), analogous to glutathione disulfide reductases (GR), which are not yet identified for the BSH redox system, or through chemical reduction by another molecule of BSH to form bacillithiol disulfide (BSSB) and allyl mercaptan (ASH). The reaction of BSH with DAS may act as an initial buffer for DAS toxicity, which would explain higher susceptibility of the BSH null mutant observed in growth experiments (section 3.2.2 and 3.2.4). Other possible points of DAS attack are Cys and CoA (not shown in Figure 3.5) and Cys residues in proteins, which are all present in the *bshA*⁻ mutant. The formation of mixed allyl di- or polysulfides with Cys residues of proteins would alter cellular functions, as the redox state of protein Cys residues often acts as a regulatory switch for protein function⁽⁷²⁾.

There are two possible mechanisms for the formation of mixed disulfides from cellular thiols and DAS. A direct thiol-polysulfide exchange reaction might take place, where BSH, Cys, CoA or protein thiols react with a DAS molecule, which leads to the formation of a mixed di-/polysulfide and a thiol/perthiol/hydro trisulfide (as shown for reaction with GSH in chapter 2, Figure 2.18). Thiol-disulfide exchange reactions between “normal” cellular thiols and disulfides are too slow to be of biological relevance^(70, 72), but this might be different for DAS molecules (chapter 2).

DAS have also been shown to induce the formation of reactive oxygen species (ROS)⁽⁴⁰⁾ through formation of AS2H and AS3H that may reduce water to the superoxide radical⁽⁴²⁾, which can further react to form hydrogen peroxide or hydroxyl radicals. Therefore, DAS stress

may indirectly lead to the (reversible) formation of BSSB and bacillithiolation of proteins via ROS. Both, BSSB formation and protein bacillithiolation are protection mechanism against oxidative stress, by minimising the irreversible overoxidation of free BSH and protein Cys residues to sulfinic or sulfonic acid.

Although these hypotheses are supported by the growth studies in section 3.2 and chemical reactivity studies with DAS and LMW thiols (chapter 2), further work is required to confirm the mechanism of DAS toxicity *in vivo*. Therefore in the next section we discuss the *in vivo* quantification of key metabolites for the suggested pathways (Figure 3.5).

3.4 LMW thiol and disulfide levels in *B. subtilis*

3.4.1 Methodology

LMW thiol levels were determined through fluorescent labeling of cell extracts with the thiol-selective reagent monobromobimane (mBBr) and subsequent HPLC analysis. Disulfides were reduced to their corresponding thiols and subsequently labelled and analysed by HPLC. Cellular thiol and disulfide content is determined as $\mu\text{mol/g}$ residual dry cell weight (rdw), which can be converted into mM concentrations ⁽⁹⁶⁾. Quantification of disulfides through the corresponding thiols leads to the lack of distinction between symmetric (e.g. BSSB) and mixed (e.g. ABS2) disulfides. Therefore, all BSH-derived disulfides will be abbreviated BSSR, to indicate that the other half of the molecule is unknown. Furthermore, the differentiation between di- and polysulfides is impossible with the method used. The method development and optimisation is described in detail in Appendix 1. Especially the disulfide analysis from cell extracts required optimisation, which led to the development of different methods through which different results were obtained leading to inconsistencies within the presented data for disulfides. For further details, the reader is referred to section 1.4 in Appendix 1.

3.4.2 LMW thiol and disulfide levels in *B. subtilis* under non-stress conditions

LMW thiol and disulfide levels of *B. subtilis* WT under non-stress conditions were initially analysed during a complete growth curve of the bacteria, to determine the variations in the BSH, Cys and CoA concentrations during different growth phases. Figure 3.6 A shows that BSH is present in higher concentrations than Cys and CoA, and BSH increases during the exponential growth phase. There is a decrease in BSH concentration around $\text{OD}_{600}=3$ which interrupts the steady increase from the beginning of the exponential phase (0.3 mM) to the stationary phase (5.2 mM).

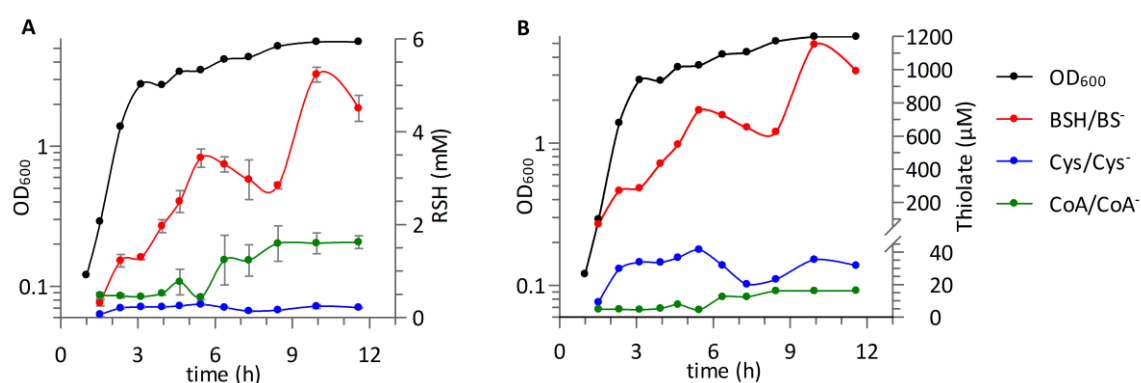


Figure 3.6: A: Thiol levels and B: Thiolate levels in *B. subtilis*.

CoA concentrations are consistently lower than BSH, but they also increase four-fold during the growth curve (0.4 to 1.6 mM). Cys concentrations are the lowest (0.1-0.3 mM) and stay relatively constant during the whole growth curve. At the maximum BSH level, its concentration is 17-fold and 3.5-fold higher than those of Cys and CoA, respectively. However, the thiol group of BSH is more acidic than that of Cys, CoA and GSH, and, therefore, at physiological pH (*i.e.* pH 7.7 in *B. subtilis* ⁽⁸⁵⁾), the percentage thiolate for BSH, Cys and CoA is 22%, 15% and 1%, respectively ⁽⁵⁹⁾. The significance of this becomes evident when the cellular

LMW thiol concentrations in *B. subtilis* are converted into the respective thiolate concentrations at physiological pH (Figure 3.6 B). This shows that at its highest concentration the bacillithiolate level is 30-fold and 70-fold greater than the thiolate anion concentrations of Cys and CoA, respectively.

The comparison of thiol levels of *B. subtilis* grown in two different media (Figure 3.7) reveals that BSH levels increase during the growth phase to reach a maximum of 5.2 mM in luria broth (LB) media and 4.3 mM in Belitsky minimal media (BMM). Both experiments show a characteristic decrease in BSH concentration at the beginning of the stationary phase. In BMM Cys concentrations are slightly higher (up to 1.2 mM) and CoA values are similar to the ones measured in LB media (up to 1.5 mM).

Thiol levels in different media

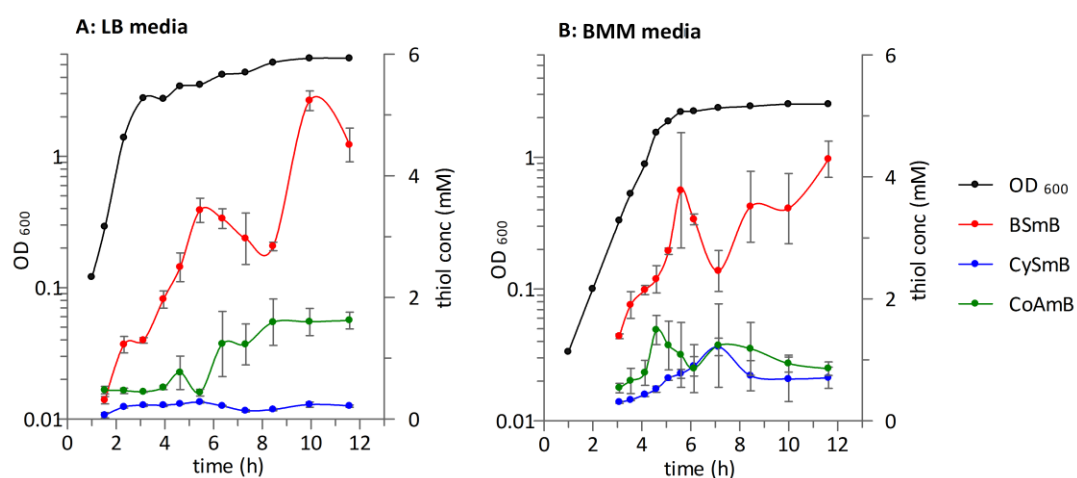


Figure 3.7: Comparison on thiol levels in *B. subtilis* grown in different media. **A:** Luria Broth (LB) media and **B:** Belitsky minimal media (BMM).

Previous thiol analyses of *B. subtilis* reported much lower levels of BSH, often equivalent to, or no more than five-fold greater than, those of Cys (Table 3.1) ^(54, 55). These reported measurements were only taken from cell cultures at a single time-point, usually during mid-exponential growth ($OD_{600}=0.8$ to 1.4). The original analyses of BSH content in *B. subtilis* reported BSH levels of 0.6-1.9 $\mu\text{mol/g rdw}$.

Table 3.1: Thiol concentrations ($\mu\text{mol/g rdw}$) in *B. subtilis* WT CU1065. Error margins are given as standard deviation. *error<25%

BSH	Cys	CoA	OD_{600}	Culture conditions
1.0 ± 0.1	0.58 ± 0.14	1.1 ± 0.1	0.8 – 1.2	Trypticase soy broth, triplicates from single culture ^{(55) (54)}
1.9 ± 0.3	0.38 ± 0.05	0.24 ± 0.03	0.8 – 1.2	
0.6*	0.6*	0.6*	1.4	
1.2 ± 0.13	0.2 ± 0.02	0.5 ± 0.04	1.4	LB, triplicates from three different cultures (this study) ⁽⁵⁹⁾
2.1 ± 0.07	0.4 ± 0.03	0.8 ± 0.2	0.9	BMM, triplicates from three different cultures (this study)

The intracellular concentrations of BSH were then estimated based on the global assumption that all of the bacteria analysed contained $\sim 3 \mu\text{L}$ of intracellular water per mg of dry weight⁽⁵⁴⁾. For $0.6 \mu\text{mol/g rdw}$, this equates to an intracellular BSH concentration of approximately 0.2 mM . However, the rdw to intracellular water ratios are not the same in all bacteria. Calculations for *B. subtilis* suggest that $\sim 50\%$ of cell mass comprises intracellular water⁽⁹⁶⁾. Therefore, a BSH measurement of $0.6 \mu\text{mol/g rdw}$ in *B. subtilis* equates to an intracellular concentration of 0.6 mM (*i.e.* 3-fold higher than previously reported).

In a separate set of experiments, BSSB and cystine (CySS) concentrations were determined (Figure 3.8 A). CoA disulfide (CoASS) cannot be measured with the method used, because the reducing agent dithiothreitol (DTT) leads to hydrolysis of Acetyl-CoA (CoASAc) and subsequent mBBR labelling leads to an overestimation of CoA-disulfide. BSSB and CySS concentrations are maintained between $7\text{--}17 \mu\text{M}$, and are at their lowest level as the cells approach stationary phase when a reduction in BSH (by $\sim 1 \text{ mM}$) is also observed. Some of this BSH might be used in the bacillithiolation of proteins⁽⁶³⁾ to help regulate function during the transition from exponential to stationary phase.

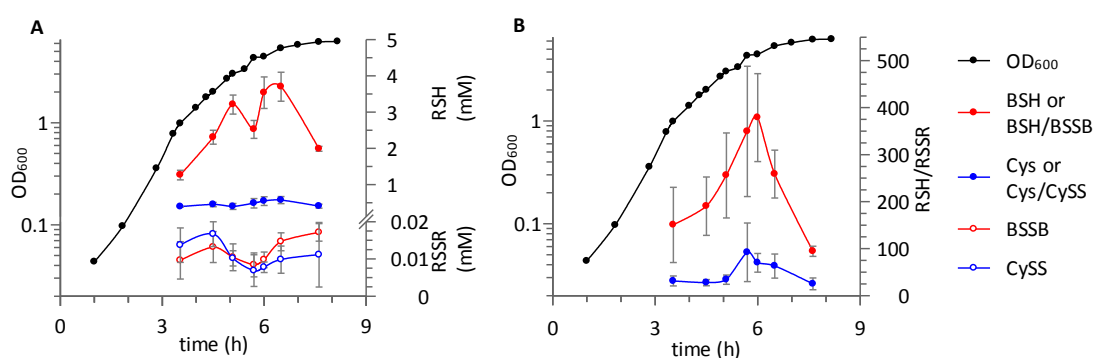


Figure 3.8: A: Comparison of thiol and disulfide levels and B: Redox ratios in *B. subtilis*.

Throughout the growth curve, the thiol-disulfide ratio for BSH (ranging from 100:1 to 400:1) is consistently higher than that of Cys (25:1 to 90:1) (Figure 3.8 B). For both thiols, these redox ratios peak during early stationary phase growth.

In summary these experiments have demonstrated that BSH is present in *B. subtilis* in much higher concentrations (up to 5.2 mM) than previously reported and are comparable to levels reported for GSH in some Gram negative bacteria⁽⁶⁵⁾. BSH levels are increasing during the exponential growth phase of *B. subtilis* and reach their maximum in stationary phase. This is a very important observation, and establishes the baseline levels to allow the examination of the effects of DAS on the LMW thiol levels. Additionally we confirmed that BSH and Cys are mainly found in their reduced state (redox ratios of up to 400:1 and 90:1 for BSH and Cys, respectively), which permits comparisons with the thiol redox status upon DAS treatment. Thiol levels of *B. subtilis* grown in different media (LB media vs. BMM) were found to be similar. But as LB media can contain Cys, which may react with DAS in the media, further experiments, to investigate changes in thiol levels upon DAS stress, were performed in BMM.

3.4.3 Influence of DAS3 on thiol and disulfide levels in the *B. subtilis* WT and the *bshA*⁻ mutant

3.4.3.1 Thiol and disulfide levels after DAS3 treatment

Thiol and disulfide levels after DAS3 treatment in *B. subtilis* WT

B. subtilis WT was grown to an $OD_{600}=0.5$ and 100 μM DAS3 was added. A decrease in BSH, Cys and CoA thiol levels was observed immediately after DAS treatment (sample was taken two minutes after adding DAS3, Figure 3.9). The decrease is most prominent for BSH, which declined by approx. 90% compared to a 50% decrease observed for Cys and CoA. After 30 min the thiol levels recovered to the initial concentrations before DAS3 addition.

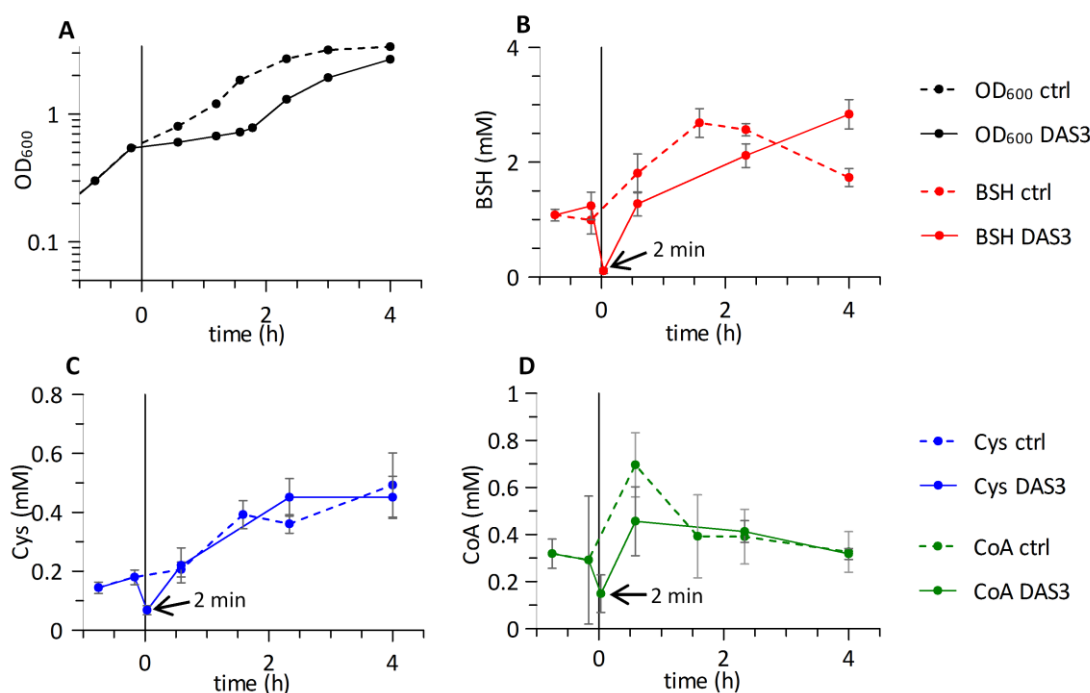


Figure 3.9: Thiol levels in *B. subtilis* WT after treatment with 100 μM DAS3. Triplicate cultures were split in two and DAS3 was added to half the cultures at $OD_{600}=0.5$ (normalised to time zero). The mean is plotted and error bars show standard deviation. A: Growth curves of the treated and untreated cultures. B: BSH levels, C: Cys levels and D: CoA levels in an untreated and treated culture of *B. subtilis*.

In the same experiment BSSR and CySSR concentrations were determined (using disulfide Method 2, Appendix section 1.4.2) and 30 minutes after DAS3 addition a decrease in disulfide levels for BSSR and CySSR was observed (Figure 3.10 A and B). After 2.5 hours BSSR and CySSR levels of the DAS treated cultures increase four-fold while the levels of the control cultures are relatively constant.

The changes in thiol and disulfide levels are also reflected in the redox ratio (Figure 3.11 C and D). The BSH/BSSR and Cys/CySSR ratios decrease immediately after DAS3 is added. The redox ratios recover after 30 min, but decrease again at 2.5 hours.

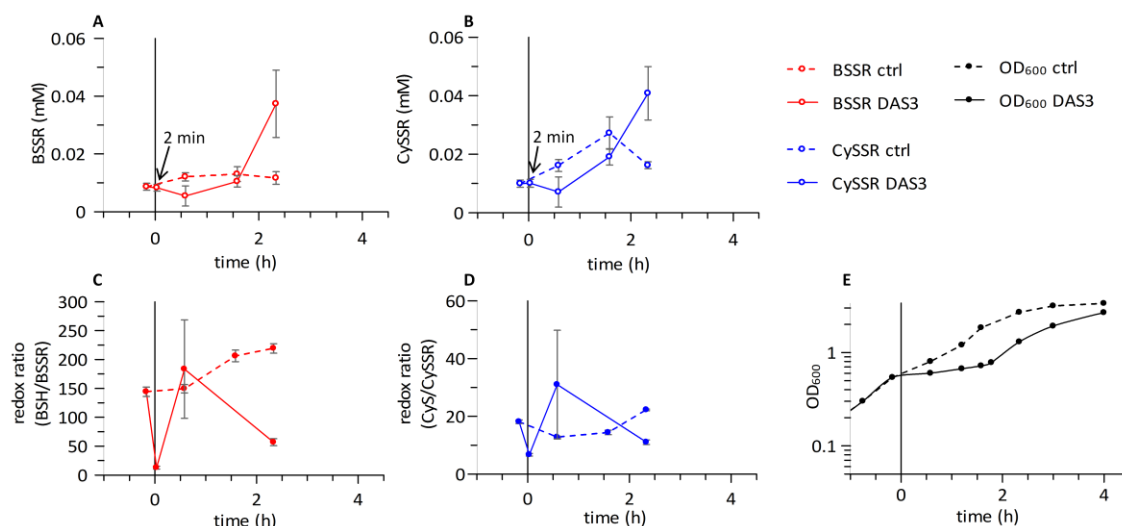


Figure 3.10: Disulfide levels (A+B) and redox ratios (C+D) in *B. subtilis* after treatment with 100 μM DAS3. Triplicate cultures were split in two and DAS3 was added to half the cultures at OD₆₀₀=0.5 (normalised to time zero). The mean is plotted and error bars show the standard deviation. E: Growth curves of treated (100 μM DAS3) and untreated cultures.

To summarise, it is striking, that BSH, Cys and CoA thiol levels dramatically drop, immediately after adding DAS3. The strongest decrease is observed for BSH which can be explained by its higher cellular concentrations and lower pK_a, which leads to higher reactivity at physiological pH. Reasons for the rapid thiol decrease may be the oxidation of thiols to either mixed or symmetric disulfides or overoxidation to sulfinic or sulfonic acids due to DAS induced ROS formation. Alternatively, thiols may react with protein thiols (e.g. bacillithiolation) to protect them from DAS induced oxidative stress. Disulfide (BSSR, CySSR) levels also decrease slightly upon treatment with DAS, although the response is delayed. This concomitant decrease in disulfides does not support the hypothesis of formation of mixed or symmetric disulfides. Either these molecules are not formed or they are not detected due to efficient reduction by an enzymatic mechanism (e.g. BR), or they are unstable under our assay conditions. Through *in vitro* experiments that were performed to validate disulfide analysis Method 2 for mixed disulfides (Appendix section 1.4.2) it became evident that the method can lead to underestimation of disulfides and, therefore, possibly does not represent the ‘true’ disulfide levels in *B. subtilis* after DAS3 treatment. Clearly, the changes in the overall thiol/disulfide ratios of BSH and Cys after DAS3 treatment reveal that there is a strong influence of DAS3 on the redox status of *B. subtilis*, however, the mechanism for recovery is not yet fully understood.

Thiol and disulfide levels in a *B. subtilis* BSH null mutant after DAS3 treatment

The influence of the same concentration of DAS3 (100 μ M) on a *B. subtilis* *bshA*⁻ mutant was also investigated (Figure 3.11). The growth curves of the DAS3 treated *B. subtilis* *bshA*⁻ mutant showed longer growth inhibition (about three hours, Figure 3.11 A) compared to the WT (about two hours). It was investigated whether this longer growth inhibition correlates with sustained decreased thiol levels.

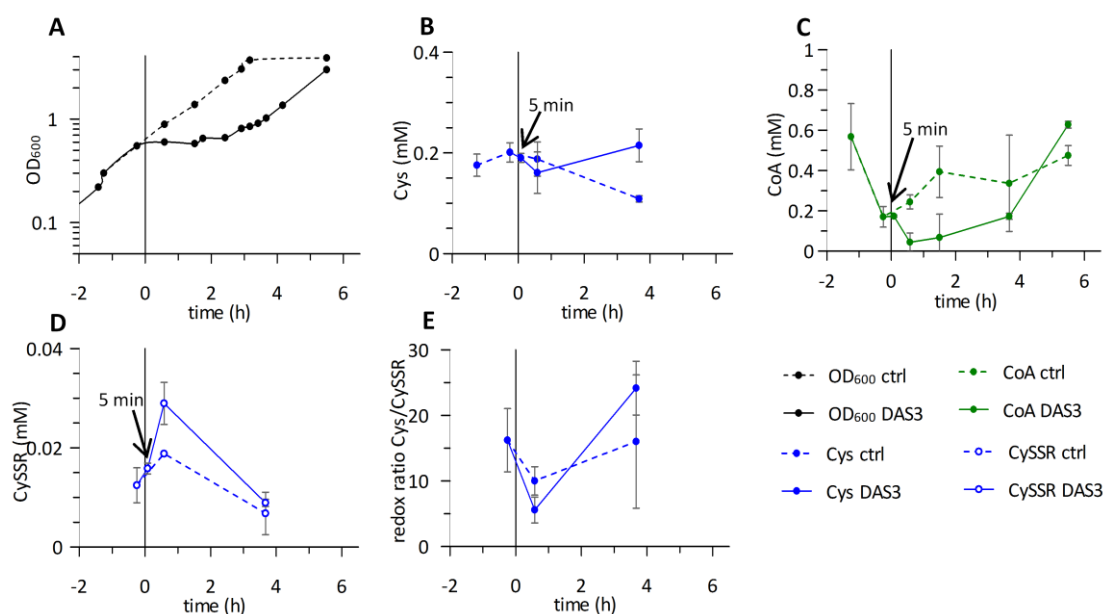


Figure 3.11: Thiol and disulfide levels in *B. subtilis* *bshA*⁻ after treatment with 100 μ M DAS3 at $OD_{600}=0.5$. **A:** Growth curves of treated and untreated culture (time point of adding DAS3 was normalised to time zero). **B:** cysteine levels **C:** CoA levels **D:** cystine levels and **E:** redox ratio of cysteine (Cys/CySS).

We hypothesised a stronger influence of DAS3 on Cys and CoA in the *bshA*⁻ mutant as there is no BSH present to act as redox buffer. However, no difference in Cys levels in the *bshA*⁻ mutant after DAS3 treatment was observed (Figure 3.11 B). In contrast, there was a four-fold decrease in CoA 30 min after DAS3 treatment (Figure 3.11 C). The recovery in CoA levels corresponds to the resumption of growth after about 4 h. The CySS levels increased 30 min after DAS3 treatment and both the CySS levels in the control and treated culture, decreased after 3.5 hours (Figure 3.11 D). The Cys/CySS redox ratio after DAS3 treatment does not differ greatly from the redox ratio measured in the untreated control culture (Figure 3.11 E).

In summary, the mutant strain takes longer to recover, which suggests that in the WT, BSH helps to deal with DAS stress. The BSH null mutant is still able to deal with DAS, although less efficiently, which suggests that the cells use different mechanisms to deal with DAS stress. Free Cys does not seem to play a major role in these mechanisms, although CoA may be involved in the absence of BSH.

3.4.3.2 DAS3 metabolites in the *B. subtilis* WT and the *bshA*⁻ mutant

To determine cellular DAS3 metabolites the cells were separated from the growth medium by centrifugation. Therefore, the measured DAS3 metabolite concentrations may possibly be not truly intracellular, but reflect DAS3 metabolites adsorbed to the membranes through hydrophobic interactions. Concentrations of allyl di- and polysulfides and their reduced ASH counterpart were analysed after treatment of *B. subtilis* with 100 μ M DAS3. Control experiments proved the stability of DAS3 in the media in the absence of the cells within the time frame of the experiment. Therefore, all observed changes are due to interactions between DAS3 and the bacteria cells. The allyl di- and polysulfides were indirectly analysed through reduction (which yields ASH) and subsequent labelling with mBBR. Therefore, this method does not differentiate between mixed (e.g. allyl-bacillithiol) and symmetric (diallyl) di- and polysulfides.

Analysis of the WT immediately after DAS3 treatment shows that 66% of the polysulfide exists in its reduced form (ASH) in the WT cells and the highest concentrations of the reduced and oxidised species are measured after only two min (0.3 and 0.58 mM, respectively, Figure 3.12 A). There is a decrease of both species over time and within two hours and four hours, respectively, allyl di- and polysulfides and ASH levels were no longer detectable, which correlates with the recovery of bacterial growth. These results suggest that DAS3 is either taken up into the cells rapidly, where it gets reduced through chemical or enzymatic reactions, or, DAS3 may get reduced extracellularly in the media through redox active enzymes found in the membrane of *B. subtilis* ^(97, 98).

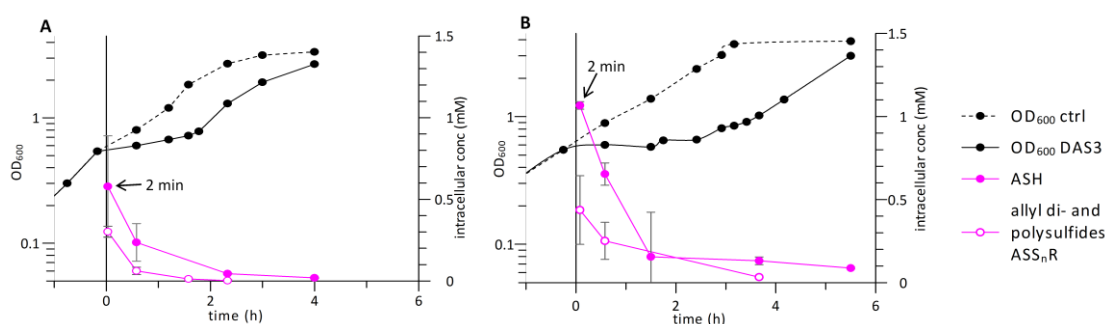


Figure 3.12: Cellular concentrations of allyl di- and polysulfides (ASS_nR) and allyl mercaptan (ASH) after treatment of A) *B. subtilis* WT B) a BSH knockout mutant with 100 μ M of DAS3.

The initial allyl di- and polysulfides concentrations are similar for the WT and the mutant (Figure 3.12 B). However, the initial ASH concentration in the *bshA*⁻ mutant (1.1 mM) is nearly double compared to the WT, suggesting that DAS3 is quickly reduced in the *bshA*⁻ mutant, e.g. through reaction with protein thiols (section 3.5.2). Furthermore, it suggests that BSH may react with ASH upon DAS treatment in the WT, leading to lower ASH levels in the WT compared to the BSH null mutant. The intracellular decrease of allyl di- and polysulfides and ASH in the BSH null mutant is slower compared to the WT. No allyl di- and polysulfides and very low concentrations of ASH were detected after four or six hours, respectively. This time delay also correlates with the longer growth inhibition in the BSH null mutant compared to the WT and suggests a role of BSH in the detoxification of these metabolites.

3.4.4 Influence of DAS4 on LMW thiol and disulfide levels in the *B. subtilis* WT

The effect of DAS4 on LMW thiol and disulfide levels in the *B. subtilis* WT was examined by the addition of 92 μM DAS4 at $\text{OD}_{600}=0.4$. A decrease in BSH, Cys and CoA levels was observed immediately after DAS4 treatment (Figure 3.13). BSH and Cys decreased by about 80% and CoA about 60% two min after exposure. BSH and CoA recover to pre-treatment levels after 30 minutes, whereas Cys levels are restored after 90 min. These results are similar to what was observed after DAS3 treatment, where thiol levels decreased immediately, with the strongest effect observed for BSH.

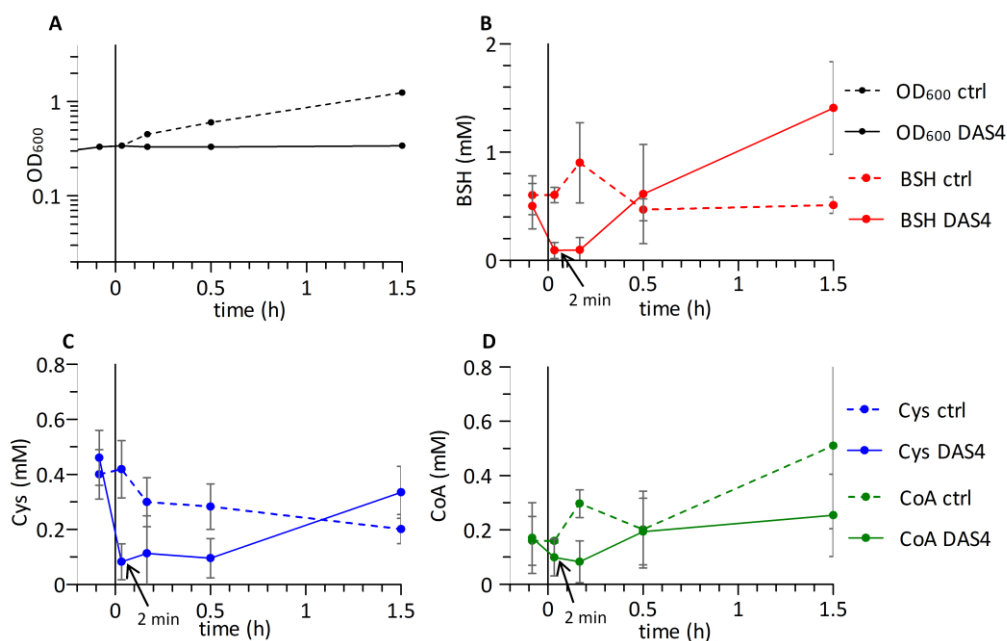


Figure 3.13: Thiol levels in *B. subtilis* after DAS4 (92 μM) treatment. DAS4 was added to the culture at $\text{OD}_{600} = 0.4$ and cultures were grown in triplicates for DAS4 treated and control cultures. Error bars show the standard deviation of triplicate samples. A: Growth curves, B: BSH levels, C: Cys levels and D: CoA levels up to 1.5 hours after DAS4 treatment.

Figure 3.14 gives an overview of the recovery of thiol levels up to six hours after adding DAS4.

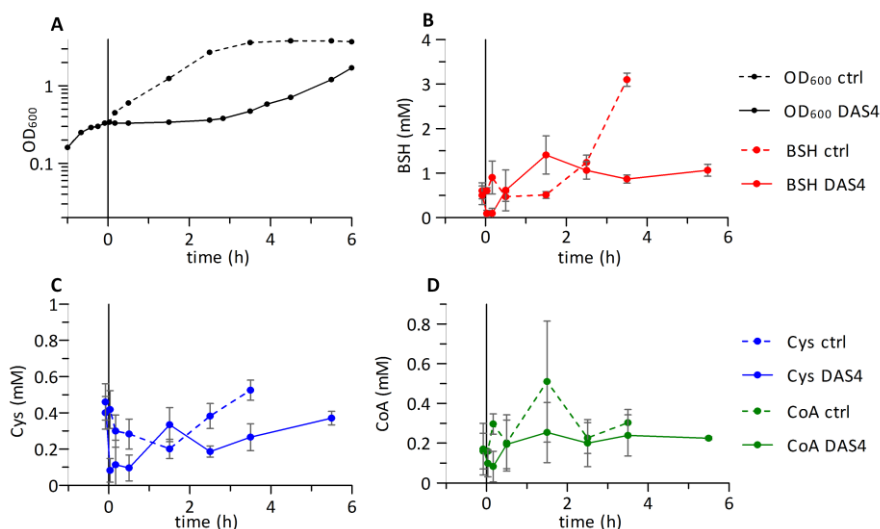


Figure 3.14: Thiol levels in *B. subtilis* after DAS4 (92 μM) treatment. DAS4 was added to the culture at $\text{OD}_{600} = 0.4$ and cultures were grown in triplicates for DAS4 treated and control cultures. Error bars show the standard deviation of triplicate samples. A: Growth curves, B: BSH levels, C: Cys levels and D: CoA levels.

In the same experiment disulfide levels were determined. BSSR and CySSR levels were analysed and additionally cellular concentrations for the sum of CoA disulfide (CoASSR) and CoASAc were determined. As mentioned previously, the current disulfide analysis method cannot differentiate between these two molecules. Interestingly, BSSR levels decreased after DAS4 treatment (Figure 3.15 B), whereas CySSR and CoASSR + CoASAc levels increased after DAS4 treatment (Figure 3.15 C and D).

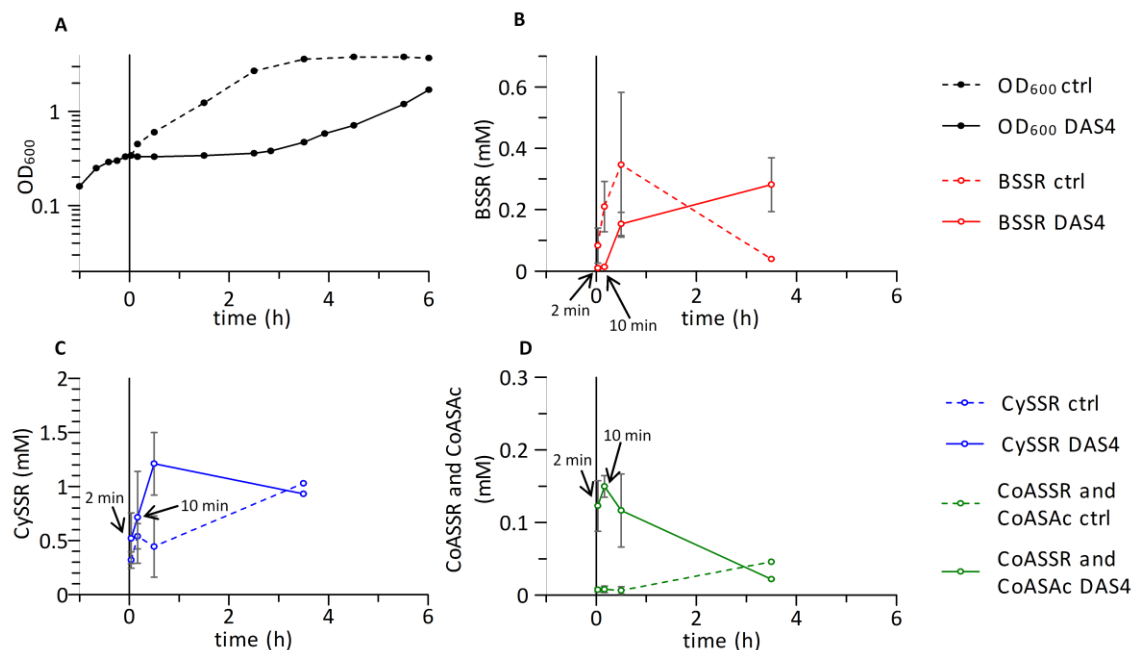


Figure 3.15: Disulfide levels in *B. subtilis* after DAS4 (92 μ M) treatment. DAS4 was added to the culture at OD₆₀₀ = 0.4 and cultures were grown in triplicates for DAS4 treated and control culture. Error bars show standard deviation of triplicate samples. A: Growth curves, B: BSSR levels, C: CySSR levels and D: CoASSR and CoASAc levels.

The increased CySSR and CoASSR + CoASAc levels may originate from the formation of mixed disulfides through reaction of a thiol (Cys or CoA) with DAS4 or can account for symmetric disulfides (CySS or CoASS) or CoASAc.

Interestingly, however, the disulfide levels in the control culture were much higher compared to previous observations. BSSR levels reached 0.3 mM and CySSR concentrations even exceeded 1 mM. This might either reflect the modified disulfide analysis Method 3 (Appendix section 1.4.3) used in this experiment compared to Method 2 used for analysis of DAS3-treated *B. subtilis* cultures. Increased disulfide levels may also be due to artificial oxidation during cell storage or derivatisation, as the cells were stored at -20°C for a couple of weeks prior to derivatisation and the derivatisation protocol was altered compared to previous analyses (Appendix section 1.4.3).

3.4.4.1 DAS4 metabolites in *B. subtilis*

Reduced cellular metabolites derived from DAS4 (AS_nH) were analysed as described for DAS3-treated *B. subtilis* (section 3.4.3.2). Immediately after adding DAS4, 1.3 mM ASH and 0.5 mM AS₂H were detected (Figure 3.16). Both reduced species were still at high levels after 10 min and then started to decrease and AS₂H and ASH nearly approached zero after 1.5 hours and 5.5 hours, respectively.

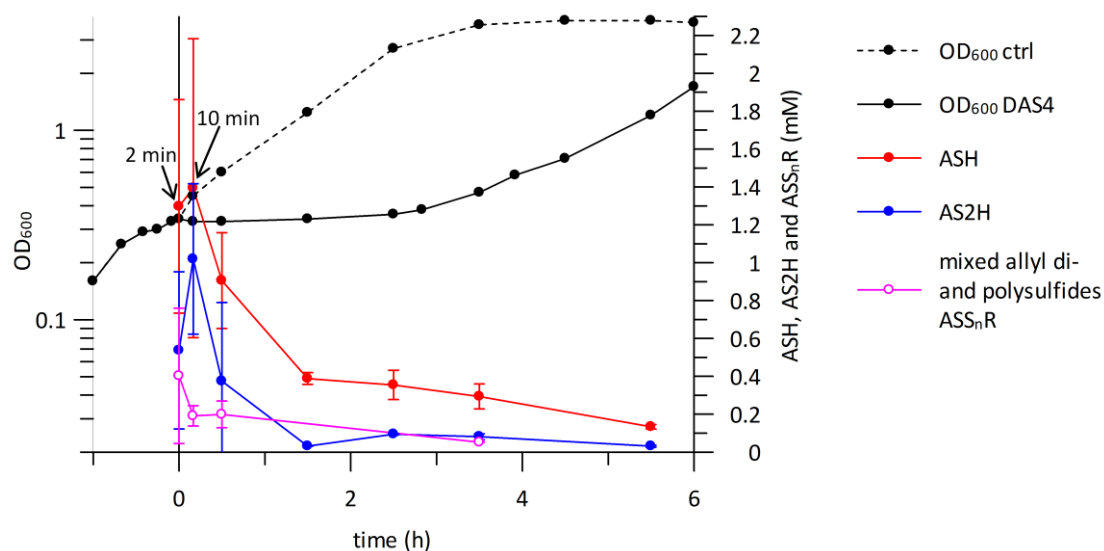


Figure 3.16: Diallyl polysulfide metabolites detected in *B. subtilis* after DAS4 (92 μ M) treatment.

Additionally, mixed polysulfides, formed by the reaction of DAS with cellular thiols, were detected. Specific mixed di- or polysulfides cannot be differentiated, but extraction of the sample with Et₂O before reduction of disulfides removed all DAS and, therefore, all detected AS_mB must be derived from a mixed di- or polysulfide. Immediately after DAS4 treatment, 0.4 mM of mixed polysulfides are formed, which coincides with a drop in BSH, Cys and CoA levels and an increase of CySSR and CoASSR+CoASAc levels. These observations suggest the rapid cell penetration and reaction of DAS with cellular thiols. The decrease to relatively low levels of DAS metabolites detected after about three hours coincides with the recovery of the culture from DAS4 stress.

These results support our hypothesis of mixed di- or polysulfide formation between Cys and CoA and DAS4 (Figure 3.17), as there is a simultaneous decrease of Cys, and CoA levels with an increase of disulfides (CySSR, CoASSR+CoASAc and ASS_nR) and an increase in allyl (per)thiol (ASH and AS₂H). However, the fate of BSH after DAS4 treatment remains unknown, as we see a decrease in both thiol and disulfide levels for BSH. In previous *in vitro* experiments formation of mixed di- and polysulfides of BSH with DAS was observed (chapter 2) and the resulting molecules are very reactive. Mixed ABS_n may be formed, but can possibly react further with other thiols, like protein thiols to form bacillithiolated or “allylated” proteins (Figure 3.17). The formation of thiolated proteins may be an explanation for the decrease in BSH and BSSR observed in our experiments. In the next section (3.5) we examine whether DAS4, BSH or mixed polysulfides may react with protein Cys residues to cause protein bacillithiolation or allylation.

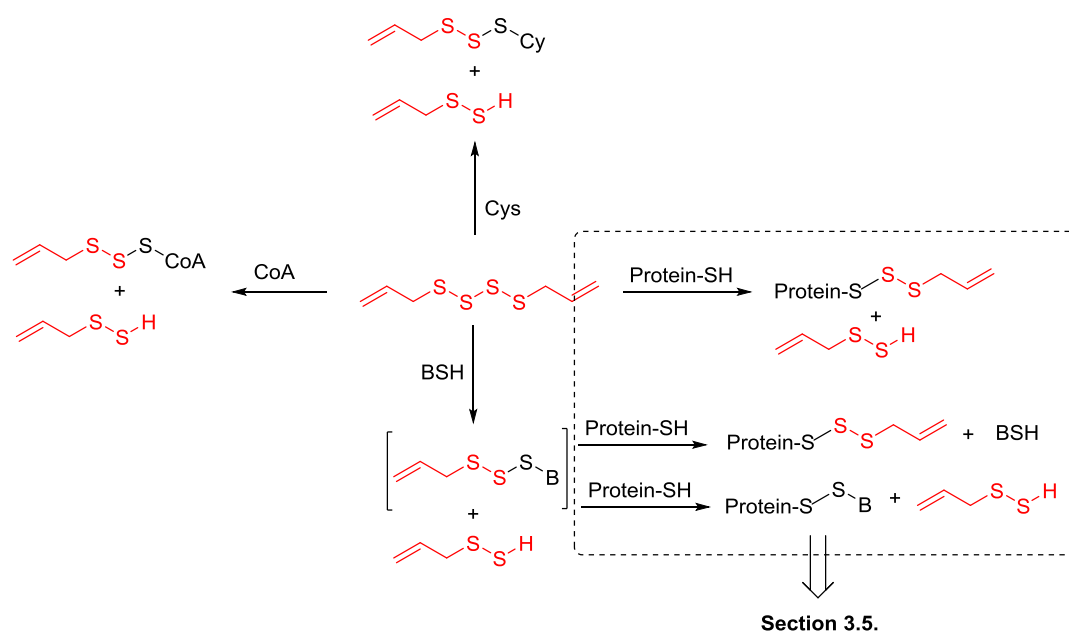


Figure 3.17: Proposed reactions of DAS4 with LMW and protein thiols, which would explain the measured changes in cellular thiol and disulfide concentrations. This is not a complete overview of reactions that may occur.

3.5 Posttranslational modification of protein thiols as a consequence of DAS treatment

3.5.1 Bacillithiolation of proteins

BSH can posttranslationally modify proteins by formation of a mixed disulfide with protein Cys residues (Figure 3.18 A). This modification can have regulatory functions and can act as a protective measurement against irreversible over-oxidation of protein thiols to sulfinic or sulfonic acids (Figure 3.18 B). Upon ROS attack, it is thought that Cys residues can be oxidised to sulfenic acids, which can quickly react with cellular BSH to form a mixed disulfide. The reverse process (de-bacillithiolation) was recently discovered to be catalysed by a group of enzymes called bacilliredoxins⁽⁶⁴⁾.

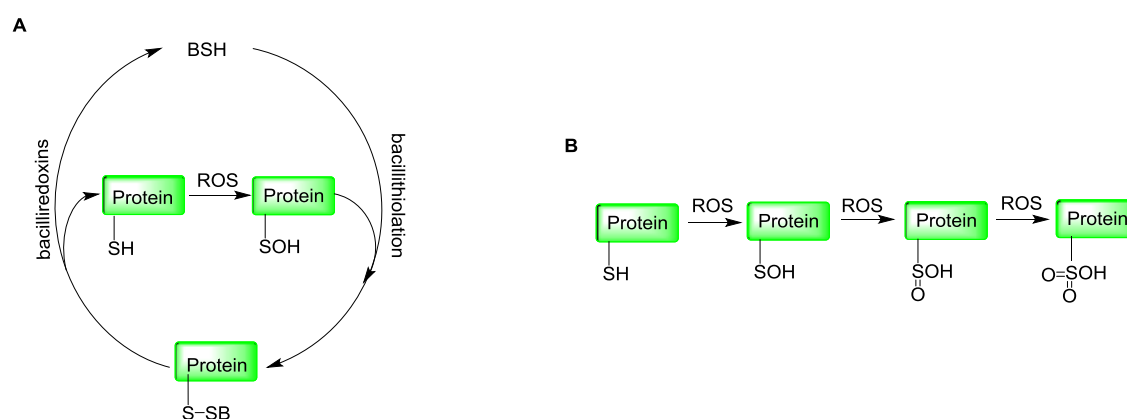


Figure 3.18: A: Bacillithiolation of proteins. B: Overoxidation of proteins.

Examples of bacillithiolated proteins in *B. subtilis* after different stress treatments are given in the introduction (section 1.3.3). In this section we investigate protein bacillithiolation in *B. subtilis* after DAS treatment.

3.5.1.1 Bacillithiolation of proteins in *B. subtilis* after DAS treatment analysed by Western Blot

B. subtilis was grown in BMM and treated with 200 μ M DAS3 or 400 or 800 μ M DAS2 once the cells had reached an OD₆₀₀ of 0.5. Proteins were sampled at various time points for analysis by Western Blot. Bacillithiolated proteins were detected via primary BSH-specific antibodies⁽⁶³⁾, followed by secondary anti-IgG antibodies fused to alkaline phosphatase. Purified methionine synthase (MetE) and purified bacillithiolated MetE⁽⁶⁴⁾ were used as negative and positive controls, respectively.

In the Western Blot, differences of treated cells compared to the untreated control, would indicate altered bacillithiolation of proteins. The control in Figure 3.19 A reveals that there is a high background for the untreated cells, which might be due to either high basal levels of protein bacillithiolation or due to unspecific binding of the primary or secondary antibody. The anti-BSH antibody (isolated from rabbits after injection of BSH conjugated to the keyhole limpet haemocyanin carrier) is polyclonal and might bind to different parts of the BSH molecule (Cys, malic acid or glucosamine). Therefore, there might be cross-reactivity with cysteinylated or glycosylated proteins.

Nevertheless, the Western Blot of the untreated control was compared with the DAS3 treated Blots. Some bands with higher molecular weight are less intense for the DAS3 treated samples (especially 30 and 60 min samples, Figure 3.19 A, see red box), but the corresponding protein gel, reveals that this is due to lower protein concentration of these proteins in the samples and not due to less bacillithiolation of these proteins (Figure 3.19 B). The bacillithiolated and the native MetE show that the antibody binds specifically to bacillithiolated proteins as there is a strong band for bacillithiolated MetE and only cross-reactivity with contaminating proteins in the native MetE lane (see blue box in Figure 3.19 A).

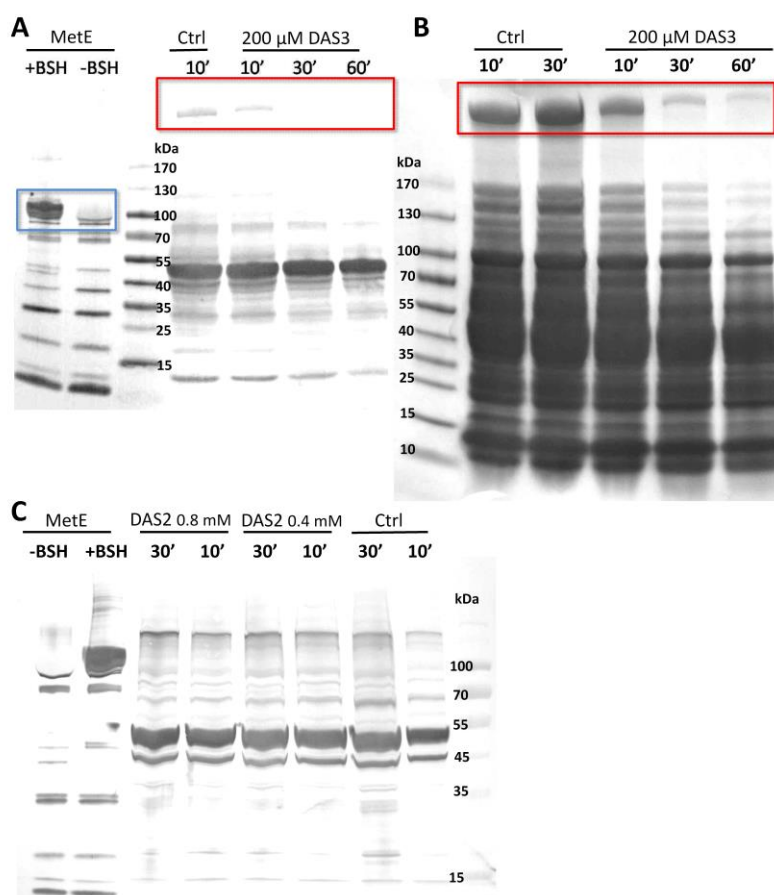


Figure 3.19: Western Blot analysis and protein gel of DAS2 and DAS3 treated *B. subtilis* WT. **A:** Western Blot of untreated cells and DAS3 treated cells taken 10, 30 and 60 min after 200 μ M DAS3 exposure (DAS3 added at $OD_{600}=0.5$) and bacillithiolated MetE as positive control and native MetE as negative control. **B:** Corresponding protein gel of DAS3 treated cells showing aliquots taken 10, 30 and 60 min after exposure. **C:** Western Blot analysis of DAS2 treated cells (0.4 or 0.8 mM DAS2 added at $OD_{600}=0.5$) and untreated controls. Native MetE and bacillithiolated MetE were used as positive and negative control, respectively.

As no increase in bacillithiolation could be identified by Western Blot after DAS3 treatment, the experiment was repeated using DAS2. The results are shown in Figure 3.19 C, which do not reveal any differences between the DAS2 treated cells and untreated cells. Again, there is a high background on the Western Blot, which is due to bacillithiolation of proteins under non-stress conditions or unspecific binding of the antibody.

To summarise, unlike the reports for cumene hydroperoxide^(60, 61) and NaOCl^(62, 63), there is no increased bacillithiolation of proteins upon DAS2 or DAS3 treatment detectable by Western Blot. Further confirmation was gained by Dr. Haike Antelmann (Ernst Moritz Arndt Greifswald University, Germany) who did not detect increased bacillithiolation of *B. subtilis* proteins after DAS2 or DAS4 treatment analysed by mass spectrometry (MS) methods.

3.5.2 S-Allylation of proteins after DAS4 treatment

As there is no increased bacillithiolation of *B. subtilis* proteins after DAS treatment, the possibility of S-allyl or SS-allyl modifications of Cys residues of proteins was investigated (Figure 3.17). In collaboration with Dr. Haike Antelmann, Cys residue modifications in *B. subtilis* after DAS4 treatment using MS were analysed. More than 80 proteins were identified with S-allyl and SS-allyl modifications (Table 3.2). The detected allylated proteins cover a wide range of functions, from enzymes important for amino acid synthesis, carbohydrate and energy metabolism to enzymes involved in sporulation or the stress response.

Eleven proteins were identified where the allylated Cys is placed in either the active site or the binding site of the enzyme (based on similarity, extracted from the Uniprot database, www.uniprot.org). These modifications can impair enzyme function and therefore alter the cellular metabolism. For example, two proteins involved in the oxidative stress response (alkyl hydroperoxide reductase and thioredoxin-like protein YdbP) were found to be allylated in the Cys residue, which is predicted to act as a redox switch and is involved in disulfide bond formation. This redox active mechanism may be disturbed by the allyl-modification of the active Cys residue and may impair the enzyme's role in DAS4 protection. Other proteins show allylation in the predicted active site Cys residue, like the methionine sulfoxide reductase MsrB, which is important for the repair of oxidatively damaged proteins. Similarly, the glutamyl-tRNA synthetase is allylated in two of its predicted zinc binding sites after DAS4 treatment.

The extent of protein allylation after DAS4 treatment highlights the diversity of cellular targets and pathways that are influenced by DAS. The DAS molecules have a clear influence on LMW thiols, but they also affect enzymes which are involved in cellular metabolism and the oxidative stress response. It is not clear whether S-allylation of Cys residues that are neither in the active site nor in a binding site have influences on protein function. Cys residues are often found in structurally or functionally important regions and therefore S-allyl modifications can have an extensive impact on enzyme function and corresponding cellular pathways. Further work, in collaboration with Dr. Haike Antelmann, will enable a detailed analysis of the functional effect of S-allylation on *B. subtilis* proteins.

Table 3.2: Overview of allylated proteins found in *B. subtilis* after DAS4 (92 µM) treatment categorised according to their functions. The proteins were digested and peptide fragments were analysed by mass spectrometry. Experiments were performed by Dr. Haike Antelmann (Greifswald University, Germany). Proteins that are allylated in a functionally important Cys residue (based on similarity extracted from the Uniprot database, except for one protein where a reference is given) are written in red.

Amino acid biosynthesis (18)	AN ^b	Isocitrate dehydrogenase [NADP]	P39126
D-3-phosphoglycerate dehydrogenase	P35136	6-phosphogluconate dehydrogenase, decarboxylating 2	P80859
5-methyltetrahydropteroyltriglutamate-homocysteine methyltransferase	P80877	Putative sugar phosphate isomerase	P39156
Bifunctional homocysteine S-methyltransferase/5,10-methylenetetrahydrofolate reductase	O06745	Dihydrolipoyl dehydrogenase^e	O34324
Aspartate aminotransferase	P53001	Protein biosynthesis (8)	
Argininosuccinate synthase^a	O34347	Elongation factor Tu^f	P33166
Cystathionine gamma-synthase/O-acetylhomoserine (thiol)-lyase	O31631	Ribosome maturation factor RimP	P32726
Arginine biosynthesis bifunctional protein	P36843	Elongation factor G	P80868
Glutamine synthetase	P12425	Elongation factor Ts	P80700
Branched-chain-amino-acid aminotransferase 2	P39576	Aspartyl-tRNA synthetase	O32038
Sulfite reductase [NADPH] flavoprotein alpha-component	O32214	50S ribosomal protein L14	P12875
Methylthioribose kinase	O31663	Aspartyl/glutamyl-tRNA(Asn/Gln) amidotransferase subunit B	O30509
Threonine synthase	P04990	Glutamyl-tRNA synthetase^g	P22250
Carbamoyl-phosphate synthase arginine-specific large chain	P18185	Stress response (7)	
Methylthioribose-1-phosphate isomerase^{(99) b}	O31662	Alkyl hydroperoxide reductase subunit C^e	P80239
2-isopropylmalate synthase	P94565	Universal stress protein YxiE	P42297
ATP phosphoribosyltransferase	O34520	4-diphosphocytidyl-2-C-methyl-D-erythritol kinase	P37550
Lactate utilisation protein	O07020	Thioredoxin-like protein YdbP^e	P96611
Homoserine kinase	P04948	General stress protein 14	P80871
DNA & RNA metabolic processes and purin biosynthesis (10)		ATP-dependent zinc metalloprotease FtsH	P37476
UPF0477 protein	O31629	Peptide methionine sulfoxide reductase MsrB^c	P54155
Ribonuclease J 2	O31760	Vitamin biosynthesis (3)	
Carbamoyl-phosphate synthase pyrimidine-specific large chain	P25994	Thiaminase-2	P25052
Adenylosuccinate lyase	P12047	6,7-dimethyl-8-ribityllumazine synthase	P11998
Inosine-5'-monophosphate dehydrogenase^c	P21879	Aspartate 1-decarboxylase	P52999
NADPH-dependent 7-cyano-7-deazaguanine reductase	O31678	Miscellaneous (9)	
Adenine phosphoribosyltransferase	O34443	Putative nitrogen fixation protein YutI	O32119
Phosphoribosylaminoimidazole-succinocarboxamide synthase	P12046	Sporulation-control protein Spo0M	P71088
Purine nucleoside phosphorylase DeoD-type	O34925	Surfactin synthetase	Q45675
Transcription-repair-coupling factor^d	P37474	Chemotaxis protein CheW	P39802
Carbohydrate and energy metabolism (9)		Phosphate acetyltransferase	P39646
Dihydrolipoyl dehydrogenase	P21880	Enoyl-[acyl-carrier-protein] reductase [NADPH] FabL	P71079
Succinyl-CoA ligase [ADP-forming] subunit alpha	P80865	Putative 2-hydroxyacid dehydrogenase yoaD	O34815
(R,R)-butanediol dehydrogenase	O34788	Response regulator aspartate phosphatase F	P71002
Phosphoenolpyruvate-protein phosphotransferase	P08838	Succinate-semialdehyde dehydrogenase [NADP+]^c	P94428
2,3-bisphosphoglycerate-independent phosphoglycerate mutase	P80865	Uncharacterised (15)	

^abinding sites on each site adjacent to allylated Cys, ^ballylated Cys is transition state stabiliser ^callylated Cys in active site, ^dnucleotide binding site adjacent to allylated Cys, ^eallylated Cys involved in redox active disulfide bond formation, ^fallylated Cys in nucleotide binding site, ^gallylated Cys is metal binding site, ^hAN=accession number.

3.6 Summary and Conclusions

Using *B. subtilis* as a model organism, a structure-activity relationship for DAS molecules was established, showing increasing activity of DAS with an increasing number of sulfur atoms from DAS1 to DAS5. No further increase in activity was observed for DAS6. From DAS3 to DAS4 the most dramatic difference in activity was observed. DAS4 and DAS5 may possess the optimum balance between stability and a long enough sulfur chain to promote chemical reactivity. The increased susceptibility of a BSH null mutant towards all DAS gave initial insights into the role of BSH for the DAS stress response.

Treatment of *B. subtilis* with sublethal concentrations of DAS3 or DAS4 led to a rapid, reversible decrease in BSH, Cys and CoA levels. A simultaneous increase in CySSR and CoASSR+CoASAc concentrations was only observed after DAS4 treatment. Final confirmation of disulfide levels and mixed disulfide formation was not achieved, because of the complexity and inconsistency of the disulfide quantification method. Nevertheless, *in vitro* studies (chapter 2) showed, that DAS readily reacted with LMW thiols to form mixed di- and polysulfides and, therefore, it is evident that DAS react with LMW thiols and thereby disturb the intracellular redox status.

Importantly, DAS3 and DAS4 derived metabolites were detected in *B. subtilis*. The intracellular concentration of the reduced form of DAS3 (ASH) was higher than the DAS3 concentration itself, which shows that DAS are rapidly reduced upon entering the cell. Furthermore, an important difference between the metabolites of DAS3 and DAS4 was elucidated: After DAS3 treatment only ASH was detected, whereas AS₂H concentrations were nearly as high as ASH concentrations after DAS4 treatment. This highlights an important difference between the two DAS molecules and due to the extraordinary chemical properties of AS₂H (ROS formation, H₂S release, section 1.2.4.3), the increased AS₂H liberation is likely to contribute to the higher biological activity of DAS4 compared to DAS3.

In addition to the reaction of DAS with LMW thiols, proteomic studies revealed more than 80 proteins that are S-allylated or SS-allylated after DAS4 treatment, including those involved in protein biosynthesis or carbohydrate and energy metabolism. Some of the S-allyl-modifications were found on Cys residues predicted to be involved in regulatory, active or binding sites, which can have implications for the catalytic functioning of the enzyme. Interestingly, two enzymes involved in the oxidative stress response were found to be allylated in their predicted redox active center, which might impair their functioning and their response to DAS4 stress. Unlike modern drugs, which are designed to inactivate a single molecular target (e.g. a certain enzyme) or interaction, we have shown that DAS react with a wide range of cellular targets and initiate a variety of complex cellular chain reactions.

In summary, we were able to shed some light on the *in vivo* interactions of DAS with LMW and protein thiols. This study identified important DAS metabolites which have not been previously detected.

One open question is the fate of BSH, as BSH and BSSR levels both decreased after DAS3 and DAS4 treatment and no bacillithiolation of proteins was detected. As DAS are known to induce ROS formation, one possible explanation may be the ROS induced over-oxidation of BSH to the corresponding sulfenic (BSOH), sulfinic (BSO₂H) or sulfonic (BSO₃H) acid. ROS induced protein oxidations to sulfenic and sulfinic acids were recently found to inherit important regulatory functions^(100, 101) and new chemical probes were developed for *in vivo* analysis of the sulfenic

⁽¹⁰²⁾ and sulfonic ⁽¹⁰³⁾ acid modifications of protein Cys residues. The application of these probes for the analysis of the oxidation status of BSH may shed some light on the fate of BSH.

Other future experiments could focus on developing more direct methodologies for the detailed analysis of DAS, DAS-derived metabolites and mixed polysulfides. A promising strategy for the direct detection of DAS includes the fluorescent labelling of allyl groups via a photoclick reaction with tetrazoles to form fluorescent pyrazoles ⁽¹⁰⁴⁻¹⁰⁶⁾. This strategy was used *in vivo* to visualise translationally incorporated or genetically encoded alkene-containing proteins ^(107, 108) and might be applicable for *in vivo* detection of fluorescently labelled DAS. Recently a method was published, that allows the selective visualisation of perthiols and polysulfides, but not thiols ⁽¹⁰⁹⁾. This is the first polysulfide-selective bioorthogonal reaction and was shown to be applicable for perthiol and polysulfide detection *in vivo*.

Due to time limitations, these methods could not be developed and applied for DAS detection, but provide scope for further *in vivo* analysis of DAS and DAS-derived metabolites.

- **The potency of DAS against *B. subtilis* increases with increasing number of sulfur atoms up to DAS5 with no further increase for DAS6.**
- **A *B. subtilis* BSH null mutant shows increased susceptibility to DAS stress compared to the WT indicating a role of BSH in DAS detoxification. Other ways of dealing with DAS stress must be present in the BSH null mutant.**
- **DAS treatment leads to rapid reversible depletion of reduced LMW thiol concentrations in *B. subtilis* and thereby leads to a disturbance of the redox balance.**
- **The reduced form of DAS (ASH and AS2H), which has not been detected before, but is often suggested to be the biologically active form of DAS, was detected *in vivo* in *B. subtilis*. Differences in DAS metabolite concentrations after DAS3 and DAS4 treatment may explain the higher biological activity of DAS4.**
- **Proteomic studies revealed more than 80 proteins that are S-allylated or SS-allylated after DAS4 treatment showing the diversity of cellular DAS targets.**

4 Influence of diallyl polysulfides on (plant pathogenic) nematodes and applications in crop protection

This chapter deals with the nematicidal activity of diallyl polysulfides (DAS) in bioassays and attempts to elucidate a possible nematicidal mode of action of DAS. Furthermore, field trial data gathered on carrot and potato crops is presented demonstrating the nematicidal activity of DAS granule formulations in a field setting. Before presenting the experimental work, an introduction about plant-parasitic nematodes is given, mainly concentrating on the species relevant for this study and current practices for control of plant pathogenic nematodes in the UK.

4.1 Plant pathogenic nematodes

Nematodes are worm-like, non-segmented and bilaterally symmetric invertebrates that contain a body cavity. They possess a complete digestive system but lack a respiratory or circulatory system. The body wall consists of a multi-layered cuticle, a hypodermis and internal musculature ⁽¹¹⁰⁾ (Figure 4.1.).

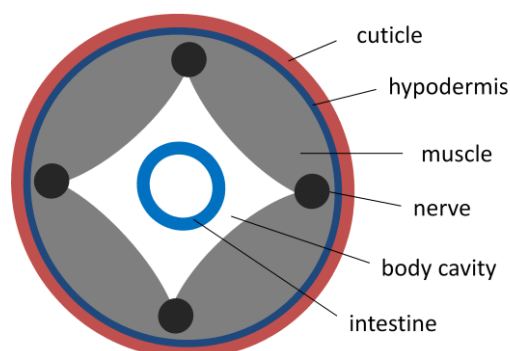


Figure 4.1: Schematic cross section of a nematode.

Most nematode species are free-living, they feed on microorganisms in water and soil and inhabit the topsoil at levels in excess of two billion per hectare ⁽¹⁾. Some nematodes are parasites of animals or plants and this chapter focusses on plant pathogenic nematodes.

Plant parasitic nematodes can be classified into four different groups according to their parasitic habits. Ectoparasites, also called free living nematodes, remain on the surface of the plant tissues and feed by inserting their stylet (feeding apparatus) into cells that are within reach. Migratory endoparasites can penetrate the plant tissue and move freely in all stages of their life cycle. Sedentary endoparasites enter the plant roots as juveniles and develop to an adult inside the root where they establish a permanent feeding site. The root-knot nematode (RKN) *Meloidogyne* spp. and the potato cyst nematode (PCN) *Globodera* spp. belong to the sedentary endoparasites and will be discussed more detailed in sections 4.1.1 and 4.1.2. The last group of parasitic nematodes (semi-endoparasites) only partially penetrates the roots, leaving two-thirds of the posterior half projecting into the soil ⁽¹¹¹⁾.

Through intensification of agriculture and worldwide trade of agricultural products, plant pathogenic nematodes were able to spread and increase in numbers on cultivated land leading

to yield losses of important agricultural products in all parts of the world. Shorter reproduction cycles of nematodes at higher temperatures lead to higher nematode stress in tropic or sub-tropic regions, but here we will concentrate on plant parasitic nematodes in temperate agriculture. General yield losses and therefore economic losses through plant parasitic nematodes are difficult to estimate, because of great variations (depending on type of crop, parasite, soil, climatic conditions etc. and secondary effects, like transmission of viruses and attraction of other parasites through plant wounds induced by nematodes). Important staple root-crops, like potato or sugar beet as well as cereals suffer from damage through plant pathogenic nematodes. Evans *et al.* compile comprehensive information about plant parasitic nematodes in temperate agriculture ⁽¹¹²⁾. The experimental field work which is presented in this chapter, was done on potato crops, infested by *Globodera* species, and carrot crops, infested by *Meloidogyne* spp., and therefore the introduction concentrates on the biology and plant parasitic habits of these nematode families.

4.1.1 Root-knot nematodes (*Meloidogyne* spp.)

Meloidogyne spp. belong to the family of *Heteroderidae*, are sexually dimorphic and mature females are between 0.4 and 1.3 mm long. On a global scale *Meloidogyne* spp. are the most destructive of all nematode parasites of agricultural and horticultural crops. They are most prevalent in tropics and sub-tropics, but important temperate crops (e.g. sugar beet or carrots) are also hosts of some species and they can be responsible for substantial yield losses. *Meloidogyne* spp. have a very broad host range, infecting nearly all cultivated vegetables, herbs and even weeds. There are a number of important *Meloidogyne* spp., each one adapted to slightly different climatic conditions and different hosts (with tomato being a universal host for all *Meloidogyne* species). *M. hapla* is especially adapted to cooler climates with a temperature optimum of 15-25 °C and is, unlike most other *Meloidogyne* spp., able to maintain itself in the soil over the winter in cooler climates. *M. hapla* infects a wide variety of root vegetables, cucurbits, cruciferae and lots of other vegetables ⁽¹¹²⁾. A new species of *Meloidogyne* was described in the Netherlands in 2004: *Meloidogyne minor* ⁽¹¹³⁾. It has since been identified in different countries in North West Europe, especially evoking yellow patch disease on golf turfs ⁽¹¹³⁻¹¹⁵⁾. *M. minor* was also found to be a parasite on potato and its host plant range and distribution across Europe is under investigation ⁽¹¹⁶⁻¹¹⁸⁾. Above-ground symptoms of *Meloidogyne* spp. infested plants are chlorosis and stunting and roots show galling or forking and formation of many side roots (Figure 4.2 B-D).

Meloidogyne spp. are sedentary endoparasites, they spend part of their life cycle sedentary, feeding within the host plant root (see Figure 4.2 A). The duration of the life cycle is strongly influenced by soil temperature. In northern Europe there is usually only one life cycle per growing season, in milder climates four or five generations may be completed within one growing season.

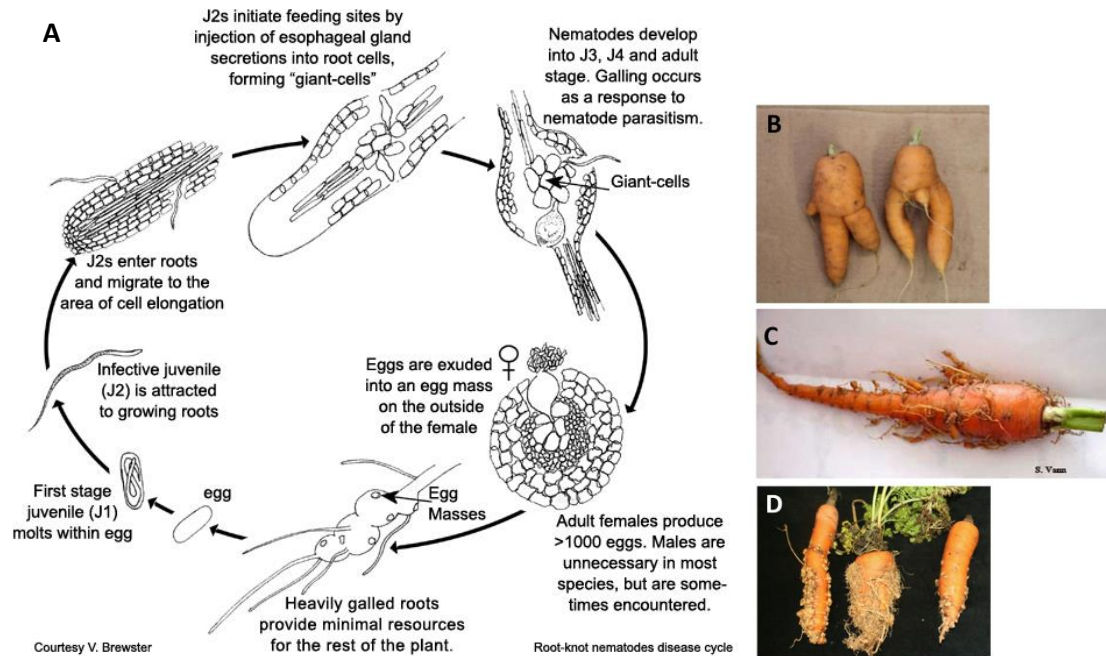


Figure 4.2: A: Life cycle of root-knot nematodes (*Meloidogyne* spp.)⁽¹¹⁹⁾ Stage 2 juveniles (J2) hatch from eggs and invade root tips, migrate to their feeding site where they become sedentary and induce formation of multinuclear giant cells. Gall formation occurs and development to J3 and J4 takes place within the plant root. Adult females develop to pear shape and excrete a gelatinous matrix through the rectum as a globule into which several hundred eggs are deposited. The egg production is usually parthenogenetic, but vermiform males are produced by all species. The production of male increases with adverse conditions (e.g. overcrowding in the root). B-D: Symptoms of carrots induced RKN. B: Root forking, C: Formation of many side roots, D: Formation of root galls.

Meloidogyne spp. attack the root system of the host and lead to formation of abnormal roots (see Figure 4.2 B-D), therefore root vegetables, like carrots have zero tolerance towards *Meloidogyne* spp. If nematode juveniles are in the soil at the beginning of the crop season, the potential for serious damages exists and must be controlled as carrots showing root galls or root forking lose their commercial value.

As most other nematodes, *Meloidogyne* spp. are predominantly found in coarse textured sandy soils, as opposed to fine textured clay mineral soils, because they rely on air-filled pores in the soil for locomotion.

4.1.2 Potato cyst nematodes (*Globodera* spp.)

Globodera spp., like *Meloidogyne* spp., belong to the family of *Heteroderidae*. *Globodera* spp. are also called round cyst nematodes and the two major potato pathogens are the white potato cyst nematode *G. pallida* (wPCN) and the yellow potato cyst nematode *G. rostochiensis* (yPCN). The cultivated potato (*Solanum tuberosum*) originates from the Andes in South America, where PCN coevolved with its host. Today potatoes are a major global crop and PCN

are found in at least 58 countries. Economically, PCN are the most critical nematode species on potatoes and strict regulations and quarantines are conducted in many countries to limit PCN populations⁽¹¹²⁾. 17 % of the UK's arable land is used to cultivate potatoes⁽¹²⁰⁾ and PCN induces the greatest nematode damages across the UK. *Globodera* spp. have a very narrow host range: Potato, tomato and eggplant are the only commercially important hosts of *Globodera* spp.. To compensate for the narrow host range they developed a mechanism to endure in the soil for more than a decade in absence of a host: The body wall of the mature female tans (formation of a cyst) to protect up to 500 eggs, which hatch upon detection of a diffusate from the host plant (so called egg hatching factor, which is not identified yet⁽¹²¹⁾). In absence of a host, about 1/3 of juveniles hatch, but some can remain viable as long as 20 years and upon presence of a host, the life cycle starts again (see Figure 4.3 A for full life cycle). PCN complete one life cycle per growing season, but the long-standing endurance of cysts in the soil for more than a decade illustrates a major problem for PCN control.

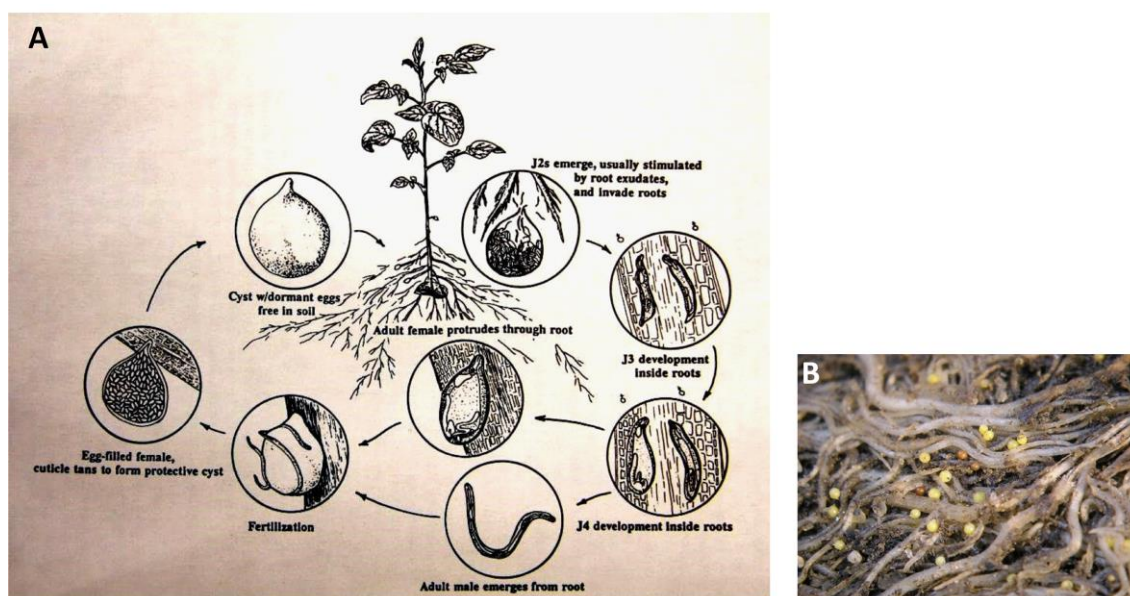


Figure 4.3: A: Life cycle of potato cyst nematodes (*Globodera* spp.)⁽¹¹²⁾. Stage 2 juveniles (J2) emerge from the egg upon detection of the egg hatch factor and enter the root tip of the host plant. In the root they become sedentary and feed on the host plant and develop into J3 and J4. Vermiform males emerge from the root, females increase in size, erupt through the root surface, but are still connected to the root. They start to produce eggs, release a male attractant, followed by fertilisation, after which the female dies and the cuticle hardens to form a protective cyst containing 200-500 eggs. Cysts can endure in the soil for more than a decade and the life cycle starts again upon registration of the host. B: Adult PCN females (pale) and tanned cysts (dark brown) on potato roots.

Above-ground symptoms of PCN infected potato plants are poor growth of plants in small patches, water and mineral deficiency and premature death. Potato roots infected with PCN show white females around flowering time turning into dark brown cysts (Figure 4.3 B), which are left behind in the soil at harvest. Potato tubers may also be infected, and cysts are found on their surface, but this is less common. Therefore, the damage of PCN to potato is more indirect compared to RKN on carrot, where the edible part of the plant is attacked directly. PCN feed from the root system of potato plants, resulting in underdeveloped roots, which causes poor plant growth through water and nutrient deficiency of the plant and ultimately reduce yields.

4.1.3 Crop protection against pathogenic nematodes in the UK –practices and challenges

Traditionally, parasitic nematode populations were kept low through crop rotation and other cultivating practices. Through intensification of agriculture, additional control measures were required. Methods to control nematodes, such as the development and use of resistant cultivars, traditional agricultural practices like crop rotation, adaptations of planting and harvest times or flooding of soil are still important and supporting efforts regarding the development of biological control are pursued. The first report of chemical control of nematodes dates back to the end of the 19th century where a fumigant, that penetrates the air space of the soil and kills nematodes and eggs, was introduced. Typical fumigants that have been used since then can be divided into two classes: Halogenated carbons and methyl isothiocyanate liberators. Both classes of fumigants are phytotoxic and need to be applied long before planting. The other class of control chemicals are non-fumigants, which can be subdivided into organophosphates and carbamates. Both of which dissolve in soil water and do not kill nematodes directly, but alter nematode behaviour through inhibition of acetylcholine esterase and prevention of the breakdown of the neurotransmitter acetylcholine. This results in a constant firing of electrical signals and can therefore cause a breakdown of the nervous system. Organophosphates inhibit acetylcholine esterase irreversibly, whereas inhibition induced by carbamates is reversible. Both classes of non-fumigant nematicides are not phytotoxic and can therefore be applied as granule or liquid material at the time of initiating the crop. All of the described nematocides cause environmental and health concerns. A widely used fumigant, methyl bromide (whose usage was banned) has been shown to damage stratospheric ozone ^(122, 123) and especially organophosphate pesticides evoked health concerns for people who are in direct contact (e.g. farm workers), due to the irreversible inhibition of acetylcholine esterase ⁽¹²⁴⁻¹²⁷⁾. Carbamates and Organophosphate are water soluble and have been detected in groundwater ⁽¹²⁶⁾ and residues occasionally exceed the maximum residue level in the crop ⁽¹²⁸⁾. Due to these environmental and health concerns, many synthetic pesticides have been banned or are under re-evaluation by responsible authorities ⁽⁸⁰⁾. In this review process approximately 500 of 900 active substances were not approved for future use within the EU. For some horticultural crops, the number of approved bioactives to combat certain pests is severely limited. Oxamyl (trade name Vydate[®]) was the most used nematicide in the UK in 2012 ⁽¹²⁰⁾. Other important nematicides used in the UK are fosthiazate (trade name Nemathorin[®]) and ethoprophos (trade name Mocap[®]) (both belonging to organophosphates) (Figure 4.4), but continued future licensing of these actives is uncertain, because of increasing health concerns.

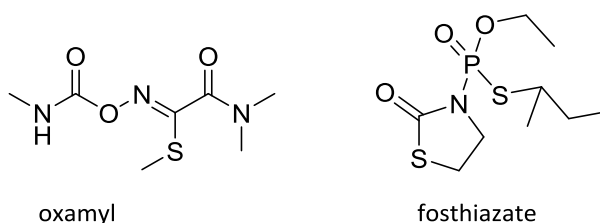


Figure 4.4: Chemical structures of nematicides used in the UK in 2012. Oxamyl (Vydate[®]) belongs to the carbamate pesticides whereas fosthiazate (Nemathorin[®]) is an organophosphate.

There is clearly an increasing urgency for new and alternative pest control products and methods, and many plant derived natural products show nematicidal activity^(129, 130). The presented study concentrates on the nematicidal activity of the DAS molecules and the potential of DAS formulations as nematicides.

4.1.4 Nematicidal effects of garlic

Studies concerning the nematicidal effects of garlic often use aqueous or ethanolic garlic extracts, which are toxic to different plant pathogenic nematodes in bioassays⁽¹³¹⁻¹³³⁾. Results gained from pot experiments or field trials are inconsistent: Phytotoxic effects of aqueous and ethanolic garlic extracts on tomato plants are described⁽¹³³⁾, as are reductions of root galling, egg masses and infective juveniles of *M. incognita* and increases in yield upon treatment with aqueous garlic extract⁽¹³⁴⁾. Additionally, aqueous garlic extract was shown to have a repellent effect towards the nematode *Caenorhabditis elegans*⁽¹³⁵⁾. Unfortunately, all mentioned studies did not determine the specific constituents of garlic extracts. Fresh, aqueous garlic extracts does not contain DAS in high concentrations, and it is more likely that other, more water soluble compounds found in freshly cut garlic, like allicin, are responsible for the nematicidal activity (section 1.1). However, aged garlic extracts or ethanolic garlic extracts contain DAS as active principles. Nematicidal activities of DAS2 and DAS3 are described against the pine wood nematode (*Bursaphelenchus xylophilus*) with DAS3 having a more than 10-fold lower LC₅₀ (half lethal concentration) compared to DAS2⁽¹³²⁾. Activities of higher DAS have not yet been tested. Distilled garlic oil (GO) was found to significantly reduce root galling after inoculation of tomato roots with RKN (*M. incognita*)⁽¹³⁶⁾, but the exact constituents of the GO were not identified. Generally GO mainly consists of DAS in varying distribution, as the steam distillation of garlic homogenate leads to formation of mainly DAS3, which then equilibrates to a mixture of DAS2-DAS6 (section 1.2.1⁽⁴⁾).

As there are no reports of the nematicidal activity of longer chain DAS (S>3), the nematicidal activity of DAS3 to DAS6 was investigated in this study in simple mortality bioassays. Additionally, the nematicidal mode of action of DAS was investigated. As the previous chapter showed that DAS react with low molecular weight (LMW) thiols and therefore alter the cellular redox status in *B. subtilis*, investigations focussing on this interaction (DAS reacting with LMW thiols) in nematodes were conducted.

4.1.5 Glutathione redox system in nematodes

Like all eukaryotes, nematodes produce glutathione (GSH) as their main LMW thiol, which is responsible for maintaining a reduced cellular environment. GSH synthesis and the GSH redox system are well characterised in mammalian cells and a similar system exists in nematodes (shown through bioinformatic analyses of the genome of *C. elegans*), which is less well characterised. GSH, Cysteine (Cys), γ -glutamylcysteine (γ -GC) and cysteinylglycine (CysGly) were detected in *C. elegans*⁽¹³⁷⁾ and a γ -GC synthetase (catalysing the rate limiting step in GSH biosynthesis) was found and characterised in *Onchocerca volvulus*⁽¹³⁸⁾. A GSH synthetase (catalysing the second step in GSH biosynthesis) was found in *C. elegans*⁽¹³⁹⁾. Characteristic enzymes involved in redox cycling of GSH, like glutathione-S-transferases (GST), glutathione disulfide reductase (GR) and glutaredoxins (Grx) have been identified and characterised in various nematode species. Nematode specific GSTs have been proposed as drug targets for parasitic nematodes^(140, 141), but GSTs with high similarity to mammalian GSTs were found as

well⁽¹⁴²⁾. Grx from *G. rostochiensis*⁽¹⁴³⁾ and *Brugia Pahangi*⁽¹⁴⁴⁾ have been characterised and a GR was identified in *C. elegans*⁽¹⁴⁵⁾. Detailed characterisation or importance of the GSH redox system for the parasitism of individual species is largely unknown. An exception is a study showing alteration of GSH metabolism in roots infected by RKN, where GSH depletion in the host plant impaired egg formation and modified the sex ratio of RKN. Thus GSH was shown to have a key role in the parasitic life stages of RKN⁽¹⁴⁶⁾.

4.2 *In vitro* nematicidal activity of DAS

4.2.1 Nematicidal activity of DAS against *Steinernema feltiae*

To investigate the nematicidal activity of DAS, determine active concentrations and establish a structure relationship for different chain length DAS, we used the entomopathogenic soil nematode *Steinernema feltiae* as a model organism. *S. feltiae* is used as a soil inoculum by gardeners on a domestic scale, because it is an obligate insect-parasite in nature, feeding from a wide range of insects and other arthropods, which are unwanted in a garden environment (e.g. vine weevil or larvae of crane flies). *S. feltiae* exists in a mutual relationship with the bacterium *Xenorhabdus bovienii*, which is required for the nematode to infect and kill a suitable insect host from which it can feed. *S. feltiae* are readily available to purchase from gardening shops and they are provided partly desiccated, which ensures that they last for several weeks at 4°C and once suspended in water they become mobile. The entomopathogenic living of *S. feltiae* was not investigated in this study and *S. feltiae* was not brought in contact with any possible host. To determine the toxicity of different DAS against *S. feltiae* a nematode suspension was prepared in water and aliquots were incubated with different DAS in various concentrations (250-1000 µM). At different time points, the viability of the nematodes was checked by observation of the nematode suspensions under a binocular and live and dead nematodes were counted. The experiment was set up as a blind experiments to avoid biased analysis of the samples. Live and dead nematodes are easily differentiated as dead nematodes are immobile and shaped straight and live nematodes move undulating (Figure 4.5).

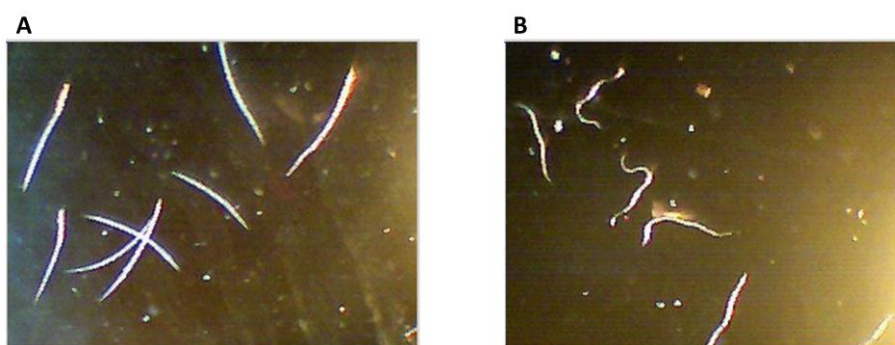


Figure 4.5: *S. feltiae* observed using a binocular at 45x magnification A: Dead nematodes are straight. B: Live nematodes move undulating.

After 24 hours of incubation in DAS containing solution the nematodes were transferred in DAS free solution (water) to ensure that they are dead and not just paralysed.

The percentages of dead nematodes were plotted against the different DAS concentrations at different times (Figure 4.6 A) and clearly after two hours of incubation DAS3 induces the highest mortality (about 80% mortality at 750 μM and 100% mortality at 1000 μM) whereas the other DAS induce 10% to 30% mortality at the same concentrations. After four hours DAS4 is nearly as effective as DAS3 whereas DAS5 and DAS6 are largely ineffective after four hours. After six hours mortality induced by DAS5 and DAS6 slightly increases and after 24 hours 750 μM concentrations of all DAS lead to 100% mortality. 500 μM concentrations lead to 35% to 70% mortality with DAS4 showing the highest activity, followed by DAS5, followed by equal mortality induced by DAS3 and DAS6. Repeated count of live and dead nematodes after 24 hours in water did not show recovery of nematodes.

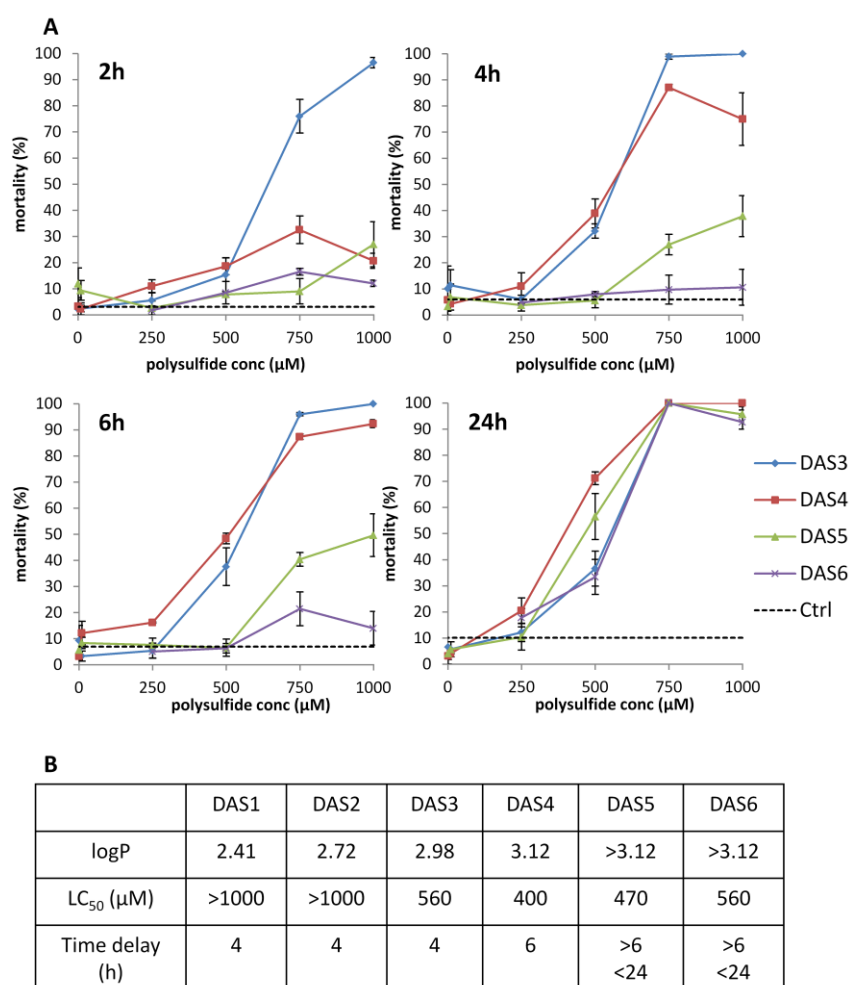


Figure 4.6: A: *In vitro* nematicidal activity of DAS towards *Steinernema feltiae*. For each concentration of DAS3, DAS4, DAS5 and DAS6 (250 μM , 500 μM , 750 μM and 1000 μM) nematodes were incubated in H_2O containing 1% EtOH. The control only contains nematodes in 1% EtOH in H_2O . At each time point dead and live nematodes were counted (approximately 30 nematodes in each sample aliquot) using a binocular at 45x magnification and percentage mortality was plotted against DAS concentration for different time points. Each concentration and the untreated control were analysed in triplicates and error bars represent the standard error of the mean. B: Drug uptake characteristics of DAS1 to DAS6. logP values were determined for DAS1 to DAS4⁽³⁵⁾ and estimated to be greater for DAS5 and DAS6, because of increasing sulfur chain length. The LC₅₀ describes the dose of the drug that kills half of the nematode population and was determined through dose response curves after 24 hours for DAS3 to DAS6. 1000 μM of DAS1 and DAS2 induce <10% mortality after 24 hours, higher concentrations were not tested and therefore no accurate LC₅₀ was determined for DAS1 and DAS2. The time delay describes the time difference between adding the drug to the nematodes and the time point when the maximum toxicity was observed.

Interestingly, this data shows that the speed of activity correlates to the number of sulfur atoms in the chain and the final toxicity after 24 hours is relatively similar for DAS3 to DAS6 (LC₅₀ in Figure 4.6 B). The time delay of activity for the longer chain DAS can be explained by their increased hydrophobicity with increasing number of sulfur atoms. The logP value is a measure for hydrophobicity and was determined for DAS1 to DAS4⁽³⁵⁾ (Figure 4.6 B). LogP values for DAS5 and DAS6 were not determined, but it can be assumed that they further increase with increasing number of sulfur atoms. According to Ho *et al.*⁽¹⁴⁷⁾ the main route of drug uptake in nematodes is through the cuticle and the rate determining barriers are the porous cuticle matrix and the hypodermal membrane. The logP is the best single predictor for drug absorption over the cuticle and the hypodermal layer and drug absorption increases with increasing lipophilicity, reaching a plateau around a logP value of 2.5⁽¹⁴⁷⁾. The effectiveness of a drug is determined through a combination of drug uptake and efficacy of the drug, once it has passed the cuticle and hypodermal barrier. In our experiment the speed of activity (see time delay in Figure 4.6 B) decreased with increased lipophilicity, which can be explained by slower uptake over the cuticle. Although the logP of DAS1 and DAS2 would predict a faster uptake than for DAS3, they show less potency (higher LC₅₀). This can be explained by the limited chemical reactions they undergo (compared to longer chain DAS) and therefore they are less effective once they are absorbed by the nematode. Additionally, drug accumulation by the parasite tissues to levels that may by far exceed those in the surrounding medium peaks around a drug logP of 2.0⁽¹⁴⁷⁾ and may explain the final LC₅₀ values after 24 h: DAS4 < DAS5 < DAS3 = DAS6 (Figure 4.6 B). The balance between drug accumulation and intracellular drug efficacy seems to be most adequate in the case of DAS4, followed by DAS5, followed by nearly equal potency of DAS3 and DAS6. Possibly, DAS3 is taken up faster and accumulated better in the cells, but is not as effective, whereas DAS6 penetrates the cuticle much slower, but shows higher activity once the cuticle and hypodermal barrier is passed.

The bigger size of the longer chain DAS is less likely to be responsible for the slower uptake, as a size restriction was only found to be important for molecules with a molecular weight of more than 2000 Dalton⁽¹⁴⁷⁾ and all the tested DAS molecules have molecular weights of less than 300 Dalton.

In addition to crossing the cuticle and hypodermal barrier, the drug has to get distributed within the organism by crossing membranes, which may also be faster for DAS3 compared to longer chain DAS.

4.2.2 Nematicidal activity of DAS against *Meloidogyne minor*

M. minor nematodes were provided by Dr. Colin C. Fleming (Agri-Food and Biosciences Institute, Belfast, Northern Ireland) and mortality bioassays were performed to investigate the *in vitro* activity of DAS against the plant parasitic nematode *M. minor*. DAS3 (800 µM) and DAS4 to DAS6 (all <500 µM) induced more than 95% mortality after 24 h. Even when used in much lower concentrations (<100 µM) all DAS3 to DAS6 induced >80% mortality after 24 h. This suggests a higher toxicity of DAS against *M. minor* compared to *S. feltiae*. Because of the lack of sufficient numbers of *M. minor*, detailed analysis about dose-responses for different DAS concentrations, as described for *S. feltiae*, could not be performed for *M. minor*.

4.3 Mode of action of nematicidal activity of DAS

Experimental results in *B. subtilis* have shown a disturbance of the redox balance induced by DAS, and therefore, in the next sections LMW thiol and disulfide levels in *S.feltiae* after DAS3 treatment were determined to elucidate if there is a similar correlation as seen for *B. subtilis*.

LMW thiol and disulfide concentrations were determined as described for *B. subtilis* (section 3.2.1 and Appendix 1) with some adjustments specifically for the thiol and disulfide analysis in cell extracts from nematodes (Appendix section 1.5).

4.3.1 LMW thiol concentrations in *S. feltiae* under non-stress conditions

Up to now, LMW thiol levels have only been published for the nematode *C. elegans* ⁽¹³⁷⁾, which is often used as a model organism. To validate the labelling method used, thiol levels in *S. feltiae* were compared with published thiol levels of *C. elegans* (Table 4.1). Cys, CysGly and γ -GC concentrations are similar in *S. feltiae* and *C. elegans* and the determined GSH levels in *S. feltiae* are about $\frac{1}{2}$ to $\frac{1}{4}$ compared to the published concentrations for *C. elegans*. As typical for eukaryotes, the most abundant LMW thiol in *S. feltiae* is GSH (10.1 nmol/mg total protein) and Cys concentrations are relatively high as well (4.1 nmol/mg total protein). The biosynthetic precursor of GSH, γ -GC, and a degradation product of GSH, CysGly, were also detected. These experiments elucidate the distribution and concentrations of LMW thiols in *S. feltiae* under non-stress conditions.

The disulfide levels in Table 4.1 were reproducible in independent experiments and resulting redox ratios for Cys, GSH and CysGly are about 25 to 30, which means that about 25 to 30-fold more thiol is present than disulfide. Glutathione disulfide (GSSG) concentrations in *C.elegans* were similar ⁽¹⁴⁵⁾ compared to the ones determined in *S. feltiae* and the resulting redox ratio in *C. elegans* (70:1) is higher compared to *S. feltiae* (25:1), because of higher reduced GSH levels in *C. elegans*. The disulfide concentration and therefore the redox ratio for γ -GC could not be determined, because of overlapping peaks in the HPLC chromatogram of the disulfide analysis.

Table 4.1: Thiol and disulfide levels in nematodes. Comparison between *S. feltiae* (own data) and *C. elegans* ^(137, 145). Own experiments were done in triplicates and errors are given as standard deviation.

	Cys or CySS	CysGly or CysGlySS	γ -GC	GSH or GSSG
Thiol levels in <i>S. feltiae</i> (nmol/mg total protein)	4.1 (\pm 0.53)	1.26 (\pm 0.11)	2.03 (\pm 0.25)	10.11 (\pm 0.68)
Thiol levels in <i>C. elegans</i> ⁽¹³⁷⁾ (nmol/mg total protein)	6.63	1.51	2.21 2.3 ⁽¹⁴⁵⁾	20.9 40 ⁽¹⁴⁵⁾
Disulfide levels in <i>S. feltiae</i> (nmol/mg total protein)	0.20 (\pm 0.029)	0.04 (\pm 0.006)	ND	0.41 (\pm 0.13)
Disulfide levels in <i>C. elegans</i> ⁽¹⁴⁵⁾ (nmol/mg total protein)	ND	ND	ND	0.57
Redox ratio in <i>S. feltiae</i> (thiol/disulfide)	20.86 (\pm 4.11)	31.28 (\pm 5.59)	ND	24.53 (\pm 8.13)
Redox ratio in <i>C. elegans</i> ⁽¹⁴⁵⁾ (thiol/disulfide)	ND	ND	ND	70

4.3.2 Influence of DAS3 on LMW thiol and disulfide levels in *S. feltiae*

S. feltiae was incubated with 750 μM DAS3 and LMW thiol and disulfide levels were analysed before and after the treatment (Figure 4.7). After 40 min of incubation with DAS3 a 50% reduction in the GSH concentration and a 40% reduction in the Cys concentration were observed (Figure 4.7 A). $\gamma\text{-GC}$ and CysGly concentrations did not change significantly upon DAS3 treatment. From 40 to 195 minutes, none of the thiol concentrations changed. Interestingly, the concentration of ASH was very high (nearly 10-fold higher than GSH) at both time points measured.

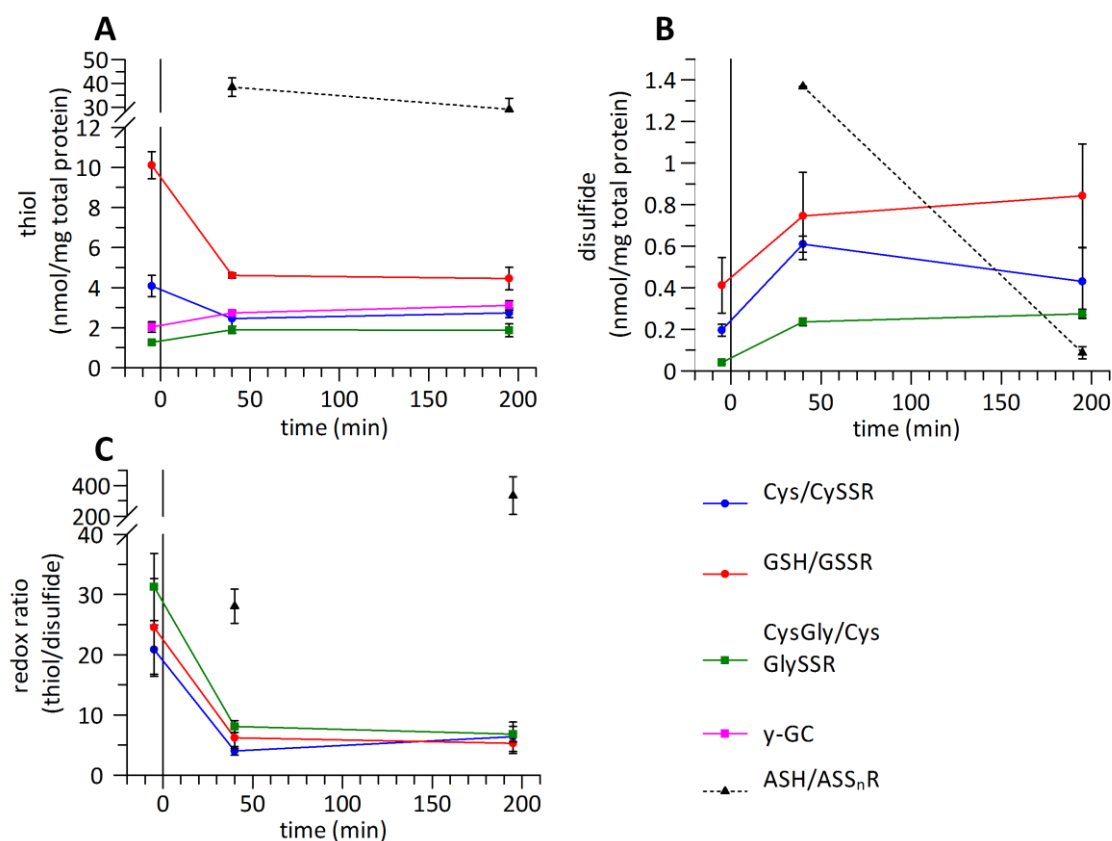


Figure 4.7: A) Thiol levels, B) Disulfide levels and C) Redox ratios measured in *S. feltiae* 5 min before and 40 and 195 min after treatment with 750 μM DAS3.

All analysed disulfides (CySSR, GSSR and CysGlySSR) showed low levels before treatment, which more than doubled for CySSR and CysGlySSR and nearly doubled for GSSR after treatment with DAS3 (Figure 4.7 B). These concentrations did not change at the next time point after 195 min. Additionally, mixed or symmetric allyl di- or polysulfides (ASS_nR, derived from DAS3 or DAS3 itself) were detected at concentrations nearly 30-fold lower compared to its reduced equivalent (ASH) after 40 min of incubation with DAS3. It nearly disappeared after 195 min of incubation with DAS3.

The thiol-disulfide redox ratios for all analysed molecules decreased after DAS3 treatment and stayed low (Figure 4.7 C). Only the redox ratio of the allyl species was very high (about 300:1) after 195 min, which points out that nearly all intracellular DAS3 derived molecules were reduced at this point in time.

These results support the hypothesis, which was already discussed in chapter 2 and 3, suggesting the reaction of DAS3 with LMW thiols to form mixed disulfides. Thiol levels (GSH and Cys) decrease after DAS3 treatment, whereas disulfide levels (GSSR, CySSR, CysGlySSR) increase. Nevertheless, the changes in the redox ratios are not instant, as seen in *in vitro* experiments in chapter 2 and in *B. subtilis* in chapter 3. Thiol levels were still as high as in the control after 10 min of incubation (Figure 4.8), but after 40 min thiol levels decreased (Figure 4.7).

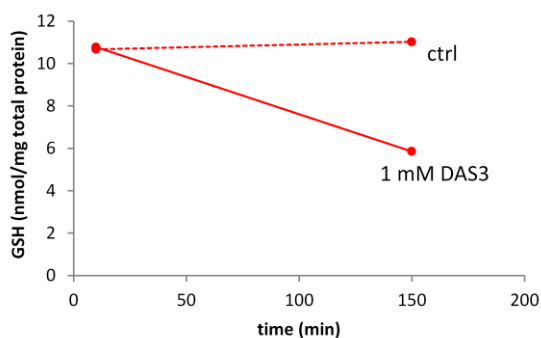


Figure 4.8: Comparison of GSH levels in nematodes treated with 1 mM DAS3 and an untreated control. Measurements were done 10 and 150 min after adding DAS3.

The time-delay in the experiment with *S. feltiae* may be generated through a time-delay in DAS3 uptake (i.e. through the cuticle and hypodermal barrier) or distribution within the organism. Between 40 and 195 min of incubation, thiol and disulfide levels do not change significantly. The concentration of DAS3, which was used to lower the GSH concentration to 50%, was quite high (750 μ M). These observations suggest that the cellular uptake of DAS3 is rather slow and continuous over a long period of time (see section 4.2.1). This would explain the delayed decrease of thiol levels as well as the high concentration of DAS3 which is required to observe a 50% decrease in GSH levels. A potential problem for the thiol and disulfide concentration determinations can be a mixed population of live and dead nematodes. Figure 4.6 shows, that incubation with 750 μ M DAS3 leads to about 80% mortality in *S. feltiae* after two hours, which is likely to be the reason for non-recovery of the thiol levels.

4.3.3 Intra- and extracellular DAS levels detected in *S. feltiae*

The extracellular medium, containing DAS3, in which nematodes were incubated, was analysed for DAS3 and DAS3 metabolites (ASH and ASS_nR). *S. feltiae* were incubated in solution containing 750 µM DAS3 and the nematodes were separated from the supernatant after 40 min. The supernatant was kept and the nematodes were washed twice with Hepes buffer (pH 7.5) and once with the same buffer containing 10% CH₃CN. All washes were mBBr derivatised for thiol and disulfide analysis. As shown in Table 4.2 no reduced ASH was found in the extracellular medium, and the concentration of ASS_nR was very low in both the medium (20 µM) and the two buffer washes (6-8 µM), considering that 750 µM DAS3 were added to the medium. However, washing with slightly more hydrophobic solvent (10% CH₃CN) substantially increased the detected ASS_nR concentration (520 µM). These observations suggest that DAS3 became embedded in the outer cuticle of the nematodes through hydrophobic interactions. These interactions were disturbed through washing with more hydrophobic solvent and DAS3 was released and detected in the surrounding solution.

Table 4.2: Intra- and extracellular reduced (ASH) and oxidised (ASS_nR) DAS3 metabolites in *S. feltiae*. *S. feltiae* were suspended in water containing 750 µM DAS3 and 1% EtOH. After 40 min the supernatant was separated from the nematodes, the nematodes were washed twice with Hepes buffer and subsequently washed with 10% CH₃CN in Hepes buffer, pH 7.5. The supernatant and all washes were analysed for thiols (ASH) through mBBr labelling and di- and polysulfides derived from DAS3 (ASS_nR) through DTT reduction and mBBr labelling followed by fluorescence HPLC analysis (ex: 385 nm, em: 460 nm). Intracellular concentrations are quoted from a previous experiment (see section 4.3.2) and extracellular concentrations of reduced (ASH) and oxidised (ASS_nR) allyl species were calculated.

	ASS _n R	ASH
intracellular	1.4 (nmol/mg total protein)	35 (nmol/mg total protein)
extracellular	20 µM	0
buffer wash	6-8 µM	0
10% CH ₃ CN wash	520 µM	0

4.3.4 Summary and proposed mode of action

Upon incubation of *S. feltiae* with DAS3, DAS3 seems to become embedded in the outer cuticle of the nematode (Figure 4.9), as the main portion of DAS3 is not free in the solution around the nematodes, neither inside the nematodes (Table 4.2). The attachment of DAS on the nematode cuticle may damage the cuticle and contribute to the nematicidal activity of DAS, but these interactions were not investigated in more detail in this study.

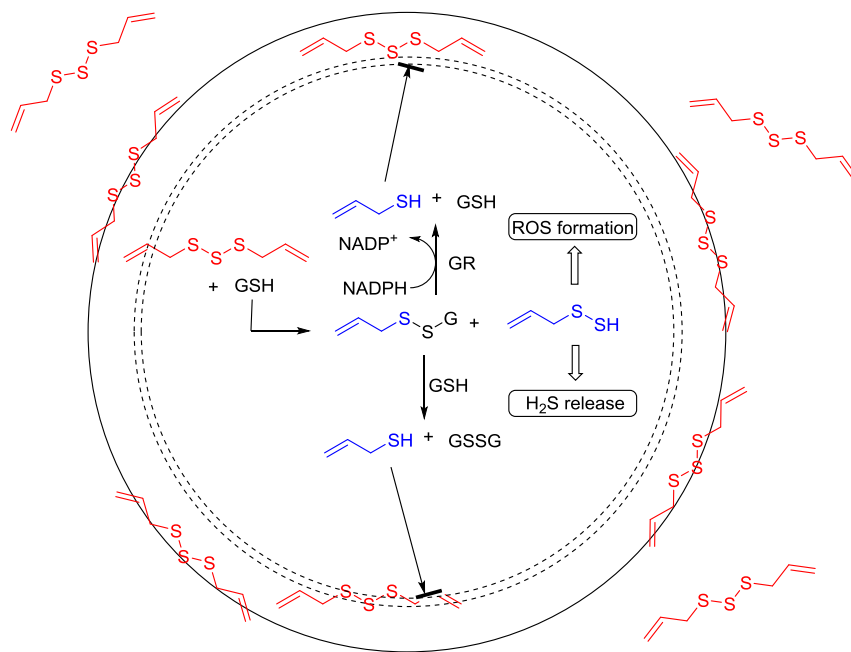


Figure 4.9: Proposed mode of action for the interaction of DAS3 with a nematode: Hydrophobic interactions with the nematode cuticle and intracellular reaction with GSH. DAS3 can react with GSH to form a mixed disulfide (AGS2) and an allyl perthiol (AS2H) or mixed trisulfide (AGS3) and allyl mercaptan (ASH) (the latter pathway is not shown). In a second step AGS2 or AGS3 can react with another molecule of GSH or possibly become reduced through glutathione disulphide reductase (GR) to liberate GSH and ASH.

Once inside the cell, DAS3 seems to react with LMW thiols (GSH and Cys levels decrease) to form mixed allyl-di- or polysulfides with GSH and Cys (GSSR and CySSR levels increase and intracellular ASS_nR are also detected). As the intracellular ASH concentration is much higher than ASS_nR concentration, it is likely that DAS3 and ASS_nR are quickly reduced to liberate ASH. This might happen through either a thiol-disulfide exchange reaction with another molecule of GSH or Cys acting as nucleophile or enzymatic reduction through GR. Mixed allyl-glutathione di- and polysulfides (AGS_n) have not yet been shown to be a substrate for GR, but DAS3 was shown to be a substrate for the enzyme⁽⁷⁷⁾ as well as glutathione trisulfide (GSSSG)⁽⁷⁸⁾ (Table 4.3), which is reduced via a two step mechanism. In the first step GSSSG is reduced to form GSH and glutathione perthiol (GSSH) and in a second step GSSH is reduced to GSH and H₂S.

The substrate kinetics for GSSG and GSSSG were shown to be comparable, whereas the reduction of DAS3 is less favoured and may not be relevant *in vivo* (Table 4.3).

Table 4.3: Enzyme kinetics for different substrates of glutathione disulfide reductase (GR). The Michaelis constant (K_m) is the substrate concentration at which the reaction rate is half of V_{max} (maximum rate at saturating substrate concentrations). k_{cat} is the turnover number and gives the maximum number of substrate molecules converted to product per enzyme molecule per second. k_{cat}/K_m is a measure of the efficiency of the enzyme to convert a certain substrate with higher numbers indicating better efficiency.

	K_m (μM)	k_{cat} (s^{-1})	k_{cat}/K_m ($\text{s}^{-1}\text{M}^{-1}$)
GSSG ⁽⁷⁸⁾	68	201.67	2.95×10^6
GSSSG ⁽⁷⁸⁾	62	177.67	2.87×10^6
DAS3 ⁽⁷⁷⁾	160	0.16	1×10^3

Nevertheless, the enzymatic reduction of mixed AGS_n have not yet been determined and the reduction may occur at a similar rate compared to GSSG and GSSSG. The catalytic mechanism involves a nucleophilic attack of a Cys residue of the enzyme on GSSG, leading to formation of a mixed disulfide between the enzyme and GSH and the liberation of a GSH molecule. Analogous the GSH part of AGS_n may be recognised and attacked by the enzyme and mixed disulfide formation between GSH and the enzyme can lead to liberation of AS_nH and in a second step to the liberation of GSH.

Similar to the observed changes in the thiol-disulfide redox status in this study, an increase in GSSG levels and therefore a change in the GSH/GSSG redox ratio was observed in *C. elegans* upon treatment with the allelopathic naphthoquinone juglone, which is known to induce reactive oxygen species (ROS) production and directly interact with GSH. The effect of juglone was even more pronounced in a GR knockout mutant and overexpression of the GR gene led to increased stress tolerance of *C. elegans* towards juglone ⁽¹⁴⁵⁾. This highlights the importance of the reduced GSH pool in dealing with oxidative stress, as enzymatic detoxification systems in the cell (e.g. Grx, Gpx, section 1.3.2.1) are highly dependent on reduced GSH.

4.4 Field trials

All determinations of nematode numbers in soil samples presented in this chapter were conducted by Dr. Colin C. Fleming (Agri-Food and Biosciences Institute, Belfast, Northern Ireland).

All obtained field trial results were statistically analysed using Microsoft Excel 2010 and a one tailed, type 2 (unpaired and independent, equal variances) t-test was performed.

4.4.1 From *in vitro* nematicidal activity in bioassays to an effective nematicide

In addition to the display of nematicidal activity in bioassays, chemical agents for nematode control need to be able to get to their receptor or target molecule in a field setting (Figure 4.10).

Degradation and uptake through non-target organisms (e.g. beneficial soil bacteria or non-pathogenic nematodes) and water solubility are important factors. Fast degradation or too much water solubility can lead to very quick disappearance of the nematicide. Too little water solubility can limit the distribution of the nematicide in the soil and delivery of the active to the nematode.

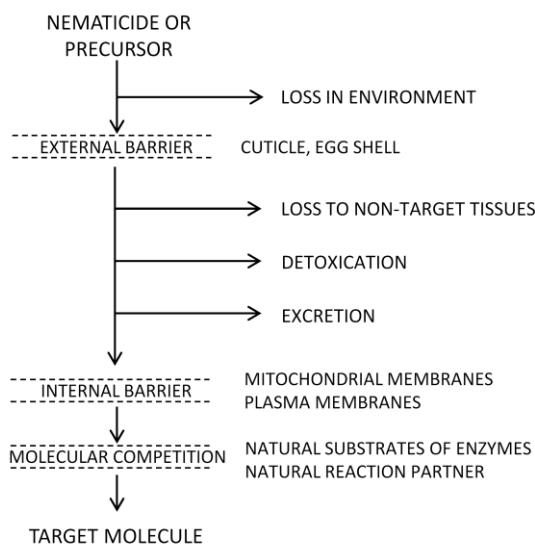


Figure 4.10: Penetration of a nematicide to a target molecule. Changed after Evans *et al.*⁽¹⁴⁸⁾.

Furthermore, the coincidence of high nematicide concentration in the soil with the emergence of nematode populations is critical and can be achieved through application of nematicides at the time of planting, as the reproduction of parasitic nematodes is triggered by the appearance of a suitable host. Application at the time of planting requires non-phytotoxicity of the nematicide. Moreover, limited toxicity towards non-target organism (insects, mammals, especially humans) is desirable. To summarise, the development of new nematicides is a great challenge as reliable performance under different weather and climatic conditions and different soil types has to be taken into consideration. Different characteristics of crops and

nematode parasites further complicate the development of generic nematicides, which meet all the above criteria.

The development of a nematicide from a natural product needs consideration of some other important aspects: From a plant extract, that shows nematicidal activity, the active compound(s) need to be identified and efficacy and dose requirements need to be tested. The concentration of active(s) in the final product needs to be constant to ensure maximum efficacy of the product. Therefore, quality control is essential as naturally actives in plants vary. Secondly, it needs to be ensured that the formulated product is stable under storage conditions for extended time periods and that concentration of actives does not vary over time.

4.4.2 Garlic formulations from ECOspray Ltd.

ECOspray Ltd. (Hilborough, Norfolk, UK) has taken up the challenge and developed a granule nematicide (NEMguard®), which is registered and approved in the UK to use on carrot and parsnip crops since 2011 and is also approved as a nematicide in Ireland, Turkey and Italy. Additionally a liquid formulation (Eagle Green Care®) is approved as nematicide for use on sports turfs (e.g. golf, football and rugby pitches). NEMguard® and Eagle Green Care® contain food grade garlic extract as active material, which is formulated with wood flour into a granule in the case of NEMguard®. The garlic extract contains a well defined and controlled mixture of DAS1 to DAS6, which shows high nematicidal activity and good stability. As the pure DAS molecules re-equilibrate to form mixtures of different chain length DAS (section 2.2), for agricultural purposes it is preferable to use a stable mixture, which does not transform. Another advantage of the mixture is sufficient water solubility through DAS1 and DAS2, but at the same time, high biological activity and efficacy through DAS3, DAS4, DAS5 and DAS6. Additionally, the mixture can help to provide actives for a longer time span, as we have seen different uptake kinetics for the different DAS molecules in bioassays with *S. feltiae* (section 4.2.1). The formulation into a granule also supports the controlled release of actives.

Besides NEMguard® and Eagle Green Care®, another formulation (TDE5), which is still under development, was used in the field trials described in this study. TDE5 contains the same garlic extract actives, additionally enriched with GO, and formulated with an emulsifier into a diatomaceous earth carrier matrix. The two different formulations, NEMguard® and TDE5, were compared with commonly used synthetic nematicides concerning their efficacy against RKN in carrot field trials and PCN in potato field trials.

4.4.3 Carrot Field Trials – Control of Root-knot nematodes

The carrot trials were performed on fields in Goole, Yorkshire (M.H. Poskitt Ltd, Kellington, UK) on sandy loam. The carrots (variety Nairobi) were drilled in early April 2012 and all applied nematicides (granule formulations) were applied at a single time point at the time of drilling.

4.4.3.1 Trial design

The trial was designed as a paired trial, applying each treatment adjacent to an untreated control (Figure 4.11). Two different rates of TDE5 were included in the trial, because the product is still under development and the rate for optimum efficacy needs to be determined.

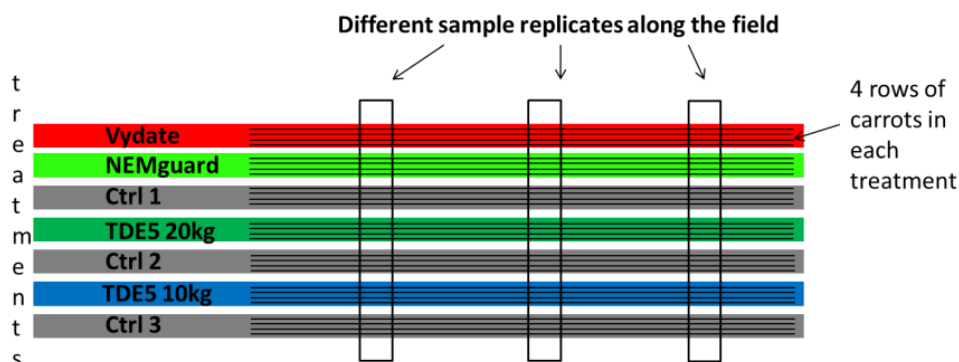


Figure 4.11: Paired trial design. Each treatment is paired with an untreated bed adjacent to it to minimise positional effects within the field.

Sample replicates were harvested adjacent to each other across the rows. This trial design has the advantage of minimising positional effects within the field. Nematodes are not evenly distributed within the field, but populations often appear in “hot spots” where they are accumulated. Therefore, having the treatment immediately next to an untreated plot gives a good chance of similar nematode populations in the treated and untreated beds.

4.4.3.2 Nematode populations in the field

Soil samples were analysed to determine populations of plant pathogenic nematodes seven weeks after drilling (Table 4.4).

Table 4.4: Plant pathogenic nematode species in the soil of the trial site seven weeks after carrot drilling.

Nematode	Common name	Threshold (number/litre soil)	Trial site (number/litre soil)
<i>Paratrichodorus</i> spp.	Stubby root	200-1000	250
<i>Longidorus</i> spp.	Needle	50	18
<i>Pratylenchus</i> spp.	Root lesion	2500	360

All plant pathogenic nematode species populations were below the threshold were treatment is advised. RKN were not found on this trial site although the field has a history of RKN damage and sandy loams offer a good soil for nematode movement because of their coarse structure.

Paratrichodorus spp. and *Longidorus* spp. are free living nematodes (migratory ectoparasites), which move freely in the soil and feed from a suitable host at all life stages by inserting their stylet into the plant tissue. *Paratrichodorus* spp. feed from the carrot root tip and therefore stops the normal growth of the root tip. *Longidorus* spp. are among the largest plant

pathogenic nematode and several nematodes often feed on a single root tip which results in enlarged multinucleate host cells. *Pratylenchus* spp. are migratory endoparasites, that invade roots in all juvenile stages and feed from the plant tissue, which causes necrotic lesions⁽¹¹¹⁾.

Although no RKN were found in the soil samples, the trial was continued, as damage introduced by other nematodes was analysed. The absence of RKN highlights a difficulty of field trials: RKN reproduce quickly upon appearance of a host, which makes it difficult to detect them before planting the crop. Therefore a trial site and a location have to be chosen by consideration of the history and general conditions of the field to estimate the likelihood of RKN presence.

4.4.3.3 Carrot assessments

Two carrot assessments were conducted: One early assessment, 17 weeks after drilling, and one assessment 23 weeks after drilling, which coincided with the time of carrot harvest.

4.4.3.3.1 Early vigour assessment after 17 weeks of seed drilling

The early vigour assessment was conducted to compare the vigour and early development of carrots as a consequence of different treatments (Figure 4.12). The carrot yields and percentage of root damage (root forking, root galling, root lesions, stubby roots) were analysed as a measure of nematode attack.

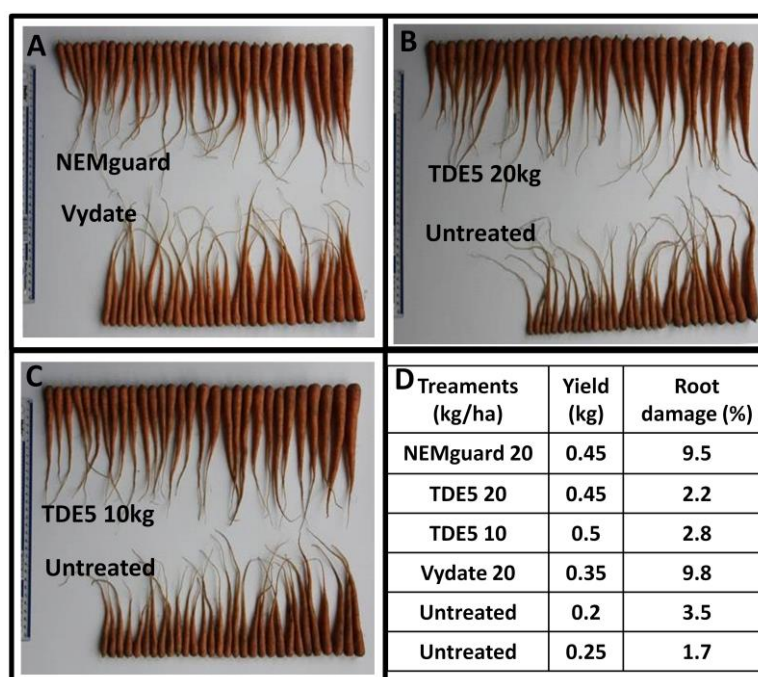


Figure 4.12: A-C: Visual comparison between different treatments: Root yields and uniformity after 17 weeks. Two rows of one m length were harvested for each treatment and the 30 biggest carrots are shown in the photographs. D: The yields and root damage in the table relate to the complete sample.

The early assessment of the young plants shows better developed carrots for all treatments compared to the untreated controls (Figure 4.12 D). The pictures in Figure 4.12 A-C give a visual impression of the paired samples, showing similar development for NEMguard® and Vydate® treated carrots (Figure 4.12 A) and better developed carrots for both TDE5 treatments

compared to the untreated controls (Figure 4.12 B and C). This can be an indication for higher root damage on untreated plant roots through nematode attack, which leads to decreased water and nutrient uptake through the roots and therefore decreased biomass accumulation. Surprisingly, the visual formation of abnormal roots, e.g. root forking, which is symptomatic of nematode attack, is highest for NEMguard® and Vydate® and no explanation for this observation can be given.

4.4.3.3.2 Assessment of carrots after 23 weeks

The carrot yields and root damage was analysed again at the time of carrot harvest (Table 4.5). NEMguard® and TDE5 (10 kg/ha) treated carrots show lower root damage and less variance than the untreated and Vydate® treated ones (Table 4.5) with none of these effects being statistically significant.

Table 4.5: Root damage by carrot weight and premium yield (crown diameter of 25-40 mm and minimum length of 14 cm) of carrots 23 weeks after planting (kg/ha), mean of five replicates, for each replicate two carrot rows of one m length were harvested. ^a the mean of plants m⁻¹ was between 49 and 53 for all treatments and untreated controls, except for control 1, where the mean of plants m⁻¹ was 46. Two of the replicates of control 1 showed <40 plants m⁻¹ which was not the case for any other treatment.

	Vydate® 20 kg/ha	NEMguard® 20 kg/ha	Ctrl 1	TDE5 20 kg/ha	Ctrl 2	TDE5 10 kg/ha	Ctrl 3
Root damage (%)	6.7 (± 3.4)	2.5 (± 1.9)	3.9 (± 4.5)	4.4 (± 4.0)	6.9 (± 6.9)	2.6 (± 2.1)	3.3 (± 3.3)
Premium Yield (kg/ha)	63.7 (±45.9)	60.3 (±40.8)	86.7 ^a (±37.3)	65.9 (±32.7)	41.6 (±27.7)	44.5 (±24.6)	49.3 (±27.9)

The premium yield comparison reveals the highest yield for one of the untreated controls, followed by very similar yields for TDE5 20 kg/ha, Vydate® and NEMguard®. The remaining two untreated controls and TDE5 10 kg/ha show lower yields. None of these differences is statistically significant. The untreated control 1 showed lower carrot numbers per area than all other treatments which may provide an explanation for higher premium yields, as fewer plants had more space to develop. The garlic derived nematicides (NEMguard® and TDE5 20 kg/ha) performed as well as Vydate®.

The nematode stress on this trial site was very low and therefore effects of the applied nematicides on yield and root damage is not obvious. Even the untreated controls show only <7% root damage, which indicates low nematode damage. This highlights a common problem of field trials under commercial conditions: There are many variables, which are difficult to foresee, which can influence the results. The conditions are not controlled and constant as in laboratory or greenhouse experiments, but the experiment takes place under the normal environmental fluctuations of climate, weather, population densities of soil organism etc. Therefore, the design, analysis and achievement of statistically significant data through field trials are very challenging. Often, results of field trials from different years and different trial sites have to be analysed together to obtain more significant results. Due to time limitations these field trials could not be repeated in this study, but ECOspray Ltd. keeps developing and testing different garlic formulations in field trials within the UK and also other European

countries. Their combined trial results clearly show activity of NEMguard® against RKN. Field trials conducted in warmer climates in Southern Europe often show more significant yield improvements through NEMguard® treatment, as the RKN damage of the untreated plants is usually higher. In a carrot field trial conducted in Summer 2008 in North Eastern Italy a convincing nematicidal effect of NEMguard was reasoned: “At harvest time, in the untreated control 60% of roots were damaged by *Meloidogyne* spp.. With this pest incidence, all treated plots resulted statistically different from the untreated control plots, but not among them. NEMguard® (15, 20 and 25 kg/ha) gave an efficacy from 66 to 75% and NemaCur® (300 kg/ha) gave an efficacy of 69%.”⁽¹⁴⁹⁾ The efficacy describes the differences in *Meloidogyne* spp. populations between treated and untreated plots calculated using Abbott’s formula and NemaCur® (containing phenamiphos as active ingredient, belonging to organophosphate pesticides, Bayer) was used as a comparison. The application rate of NemaCur® is higher because of a different application/ distribution technique.

From a farmer’s perspective the use of a nematicide can be advantageous even at low nematode levels, because it is very difficult to foresee nematode damages. Therefore it can be more economical to treat crops in every growing season than losing big parts of the crop in one particular year.

4.4.4 Potato field trial - Control of potato cyst nematodes

Control of PCN is particularly challenging and was not successful in the past in the UK. Due to some γ PCN resistant potato cultivars (52% of grown potatoes in 2001 were resistant against γ PCN⁽¹⁵⁰⁾) populations of γ PCN have decreased, but populations of wPCN, which are more difficult to control, have increased. Common control measures (five to seven year rotations between potato cultivation, application of carbamate nematicides and cultivation of γ PCN resistant cultivars) are not sufficient to decrease PCN populations, because a small number of cysts can outlast in the soil until a suitable host is sensed.

4.4.4.1 PCN distribution – an example

The photograph in Figure 4.13 illustrates the heterogenous distribution of PCN in a potato field (different trial site, photograph was provided by Dr. Roy Neilsen, James Hutton Institute, Dundee). Patches of beige colour show died off potato plants and therefore indicate areas of very high nematode population. The heterogenous distribution is a typical phenomena of nematode populations and highlights the difficulty in estimating nematode populations in a field by taking soil samples and also difficulties in the performance of field trials.



Figure 4.13: Aerial photograph of PCN damaged field during the summer. **A:** Heterogenous PCN distribution in the field, with beige patches indicating completely destroyed areas of the field. **B:** Two different trial positions within the same field are suggested. Number 1 covers an area of high nematode damage and number 2 covers an unaffected area. Photograph was taken and provided by Dr. Roy Neilsen.

There are at least seven plots in the indicated trial boundary (Figure 4.13 B (1)) where major pressure against any treated or untreated plot would have occurred. Allowing for randomisation across blocks, it is possible that two to three untreated plots could be in severely challenged areas and equally the converse could apply with a high dose treatment being in a severely challenged area. This statistical fact would introduce massive variances in data sets generated from a nematicide trial laid out in this area, with the clear potential for highly irregular outcomes with respect to the general indications of efficacy and dose related data structures. It is also noteworthy that a second trial in the same field (2) run adjacent to the first one would have produced a completely different outcome in terms of product efficacy, because of much lower nematode populations.

This example illustrates the difficulty of field trial performance and the generation of statistically significant data.

4.4.4.2 Trial design

The potato trial was conducted at Stowbridge Farm, Stretham (Adam Palmer, East of England) on organic soil using Maris Piper potatoes, a commercially successful potato cultivar with resistance against yPCN ⁽¹⁵¹⁾. All applied nematicides are granule formulations and were applied at a single time point at the time of drilling (26/04/13).

A paired trial was set up to compare TDE5 with Nemathorin® (fosthiazate) and an untreated control (Figure 4.14 A). Six sample replicates along the field, each one including four plants were harvested for yield analysis. From the same spots soil samples were taken before planting and at harvest time to compare initial (P_i) and final (P_f) PCN egg numbers in the soil.

Additionally, a completely randomised trial including five replicates of six different treatments was set up (Figure 4.14 B). Each block consists of three to four rows of potato at four m length and was completely harvested for the final analysis. Four different rates of TDE5 were applied, to compare efficacy of different doses. Soil samples were taken from each plot before planting and after the harvest.

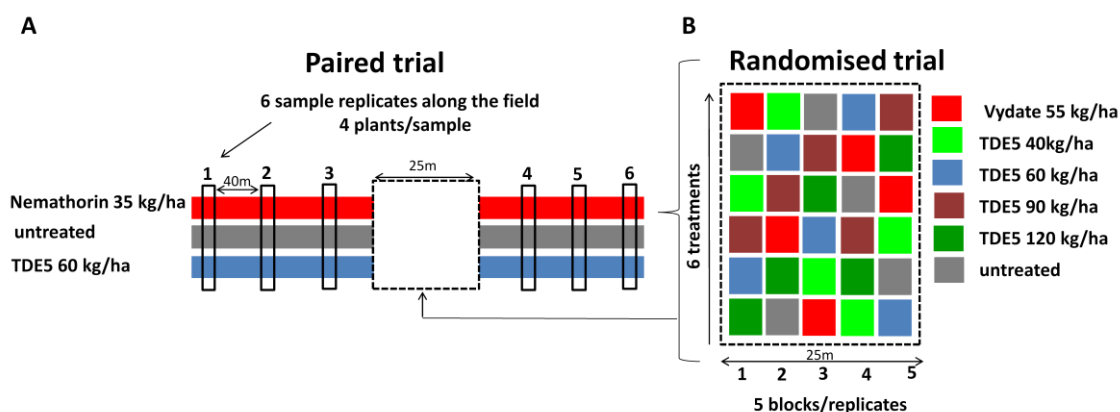


Figure 4.14: Potato trial designs. A: The paired trial design included TDE5, Nemathorin and an untreated control. B: The randomised trial was positioned in the middle of the paired trial and included four rates of TDE5, Vydate and an untreated control in five replicates.

4.4.4.3 Paired trial

4.4.4.3.1 PCN numbers and distribution

The PCN egg numbers determined before drilling showed a very inconsistent distribution within the potato field at the different plots (Table 4.6).

Table 4.6: Initial PCN distribution (P_i , eggs/g soil) in the potato field at the different sampling positions of the paired trial just before drilling and application of the nematicides.

Plot	TDE5	Control	Nemathorin®
1	65.64	59.75	61.97
2	12.14	44.33	8.22
3	7.72	4.13	12.83
4	13.2	5.5	6.78
5	6.22	2.31	3.84
6	1.32	1.61	8.8

High populations were found at plot one, significant populations at plot two and a general diminution of populations through to plot six, which had the lowest collective initial

populations. This is a good example of a typical distribution pattern of PCN nematodes, which are not evenly distributed within a field, but instead appear accumulated in “hot spots”, as shown in Figure 4.13. It also implies for our trial, that the replicates one to six experience very different PCN pressure. An advantage of the paired trial is that different treatments at the same position experience similar PCN populations and should therefore be comparable. The randomised trial was positioned between plot three and four (Figure 4.14), to ensure it experiences a medium PCN pressure.

PCN egg populations were repeatedly analysed at the six different plots after the potato harvest and the P_f/P_i value was calculated (Table 4.7).

Table 4.7: P_f/P_i values in the potato field at different sampling positions. P_i (initial PCN populations) were measured before drilling and P_f (final PCN populations) were measured at the time of harvest. Highest number at each plot is shown bold. ^a The lowest and highest value from each treatment were disregarded, because of the big variety in the dataset.

Plot	TDE5	Control	Nemathorin
1	1.7	1.3	4.4
2	23.3	3.8	19.6
3	22	24.1	11
4	19.8	42	33.7
5	31.6	38.3	42
6	116.6	89.5	16.7
Mean of 4 plots^a	24.2	27.4	20.3

The data in Table 4.7 clearly shows very different natural PCN population dynamics from plot one to plot six. The low P_f/P_i indices in plots one and two suggest a degree of natural suppression when the initial level of egg/g of soil is around 50 (Table 4.6). In contrast, when initial PCN populations are low, around five eggs/g of soil or less (plot five and six, Table 4.6) populations naturally increase very substantially by as much as two orders of magnitude. This inverse relationship (decrease in P_i leads to an increase in P_f/P_i) has been observed in other studies before ^(150, 152). Possible reasons for this phenomena are wounding of potato roots and/or stress on the plant through nematode invasion may infect the quantity and/or quality of the egg hatch factor produced by the potato root ⁽¹⁵²⁾. Furthermore, increased competition can lead to a higher proportion of males which limits the reproduction of the population ⁽¹⁵⁰⁾. Consequently, after application of a nematicide sufficient eggs are likely to survive to enable large populations of PCN to ‘rebound’ in the following growing season.

The inverse relationship between the initial population and the P_f/P_i is clearly evident in the paired trial data and highlights the complexity of the population dynamics of PCN and the limitations of P_f/P_i values in revealing nematicidal efficacy of a treatment. The P_f/P_i numbers are heavily dependent on a strongly fluctuating initial population.

The mean of four plots (because of the large variance the smallest and largest number of each treatment were not considered) show a slightly lower P_f/P_i ratio for TDE5 compared to the control and an even slightly lower ratio for Nemathorin® (none of the differences is statistically significant). None of the values gets close or even below five, which is regarded as a threshold value that indicates a nematicidal effect ⁽¹¹²⁾.

The limitations of P_f/P_i values for the determination of nematicidal effects against PCN became apparent and possibly yield comparisons can provide a better indication of PCN damage.

4.4.4.3.2 Yield comparison

Samples of the paired trial were harvested six months after drilling and total yields were significantly higher for TDE5 (58% yield increase) and Nemathorin® (23% yield increase) treated beds compared to the untreated control (Figure 4.15).

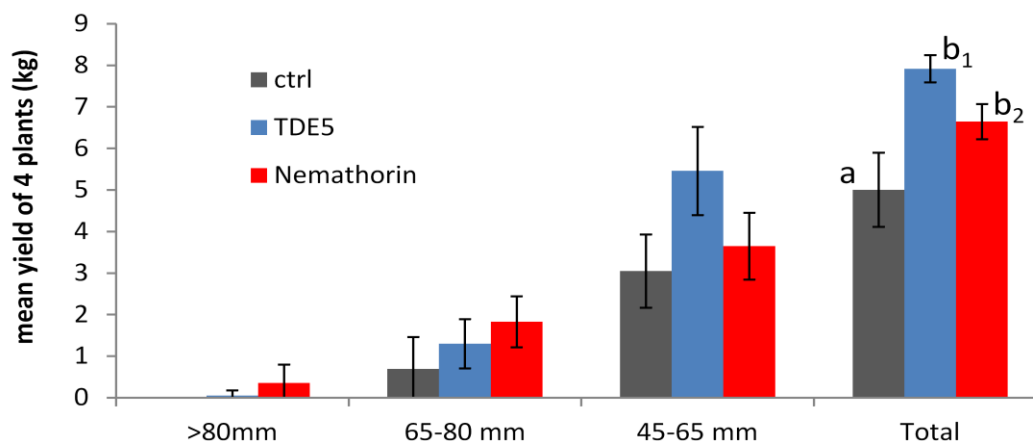


Figure 4.15: Potato yields of the paired trial. Mean yields of four harvested plants in six replicates for each treatment. Error bars represent standard deviation and different letters represent significantly different yields with a significance level of $\alpha=0.1$ (b_1 vs a : $P=0.006$, b_2 vs a : $P=0.052$).

TDE5 shows a higher total yield than Nemathorin®, which is not statistically significant. The size grade distribution shows that Nemathorin® treated beds yield slightly bigger potatoes (> 65 mm), while TDE5 produces more yield of medium sized potatoes (45-65 mm). As the sampling was done two weeks before the actual harvest, the size grade distribution may have changed until the time of harvest.

4.4.4.4 Randomised trial

4.4.4.4.1 PCN numbers and distribution

The initial egg numbers in the randomised trial indicated a reasonably even distribution of PCN across the blocks, the means ranging from 3.12-7.17 eggs/g soil (Table 4.8). PCN distribution within the plots was quite variable, with eight plots having less than 2.0 eggs/g soil (shown bold) and based on observations from the split plot comparison, these are prone to naturally regulated excessive PCN reproduction.

Table 4.8: Initial egg numbers (P_i , eggs/g soil) in different plots of the randomised trial before drilling and application of nematicides. Egg numbers < 2.0 eggs/g soil are shown bold.

Treatment	Block 1	Block 2	Block 3	Block 4	Block 5
Control	1.97	15.74	5.55	4.03	6.55
Vydate	0.7	6.68	6.41	10.41	4.24
40 TDE	4.54	1.42	0.09	0.33	11.65
60 TDE	1.2	4.45	4.78	4.86	0.73
90 TDE	6.91	5.82	15.77	1.58	15.46
120 TDE	3.38	2.3	4.12	7.76	4.36
Mean	3.12	6.07	6.12	4.83	7.17

The mean P_f/P_i values are >5 for all treatments and the untreated control (Table 4.9). The lowest reproduction can be seen for the TDE5 90 kg treatment ($P_f/P_i = 6.15$, shown bold), followed by TDE5 120 kg and Vydate (both $P_f/P_i \approx 13$). The other treatments show higher P_f/P_i values than the control. The lowest final egg numbers were counted in the TDE 60, 90 and 120 kg treatments (all under 60 eggs/g soil, shown bold). Because of the great variances within the datasets none of the treatments are significantly different from the untreated.

Table 4.9: Initial (P_i) and final (P_f) mean PCN egg numbers in eggs/g and calculated P_f/P_i values disregarding the replicates that were showing a $P_i < 2$. Lowest final egg number and lowest P_f/P_i among the treatments are shown bold. All P_f/P_i values < 5 are shown.

Treatment (kg/ha)	P_i (eggs/g)	P_f (eggs/g)	P_f/P_i	P_f/P_i values < 5	
Control	6.7	95.91	14.31493	0.79	
TDE5 40	3.6	70.34	19.53889		
TDE5 60	3.2	51	15.9375	3.6	
TDE5 90	9.1	56	6.153846	4.41	2.71 3.56
TDE5 120	4.4	56	12.72727	3.84	
Vydate	5.7	74	12.98246	0.47	

4.4.4.4.2 Yield comparison

The randomised trial was harvested 6.5 months after drilling and did not show significant yield differences for any of the treatments (Figure 4.16). The size grade distributions were also very similar for all treatments (data not shown). The mean plot yields are slightly lower for TDE5 in higher concentrations (90 and 120 kg/ha), which might be an effect of phytotoxicity. Yields for the two lower rates of TDE5, the untreated and Vydate® treated plots are all between 54 and 56 kg/plot. None of the nematicide applications resulted in increased potato yields. The observation, that Vydate® does not lead to a yield increase compared to the untreated control, shows that there is no specific problem with the efficacy of TDE5, but under the given conditions even the approved and commonly used nematicide Vydate® (oxamyl) does not increase yields.

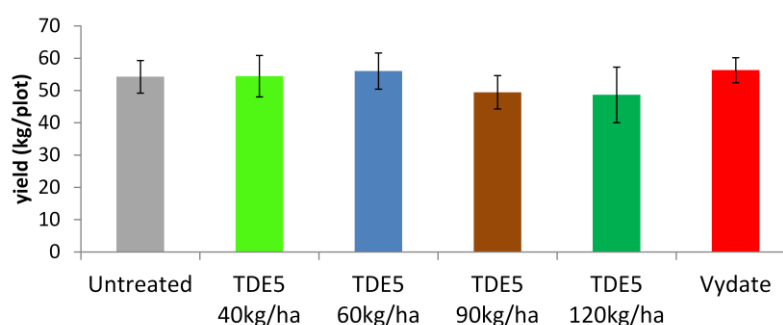


Figure 4.16: Yield comparison of different treatments from randomised trial. Error bars represent the standard deviation of five replicates and none of the yields is significantly different.

Importantly, there are a number of studies where even oxamyl (which is the most commonly used nematicide in the UK) did not control PCN satisfactory. In a study conducted by Whitehead *et al.* different nematicides (fumigants and non-fumigants) were tested in different soils in field trials all over the UK ⁽¹⁵³⁾. No clear outcome was achieved, with the efficacy depending on the potato cultivar and yield increases which were independent from egg numbers in the soil. This shows the complexity of controlling PCN and even widely used nematicides often do not show satisfactory results.

Taken together the yield results from the paired and randomised trial, suggests that there is a yield increase through TDE5 and Nemathorin® treatments (paired trial), which did not emerge from the randomised trial, because of the variable initial populations of PCN in the different plots. The paired trial minimises these positional effects as the different treatments are applied adjacent to one another. Nevertheless, the results are not clear-cut and further factorially consistent field trials in different years and/or at different locations would be important to elaborate the efficacy of TDE5 against PCN. This would create more data and allow much stronger statistical data analysis, which would provide better chances to obtain statistically significant results.

4.5 Summary and Conclusions

For the first time the nematicidal activity of pure DAS molecules was tested and the mortality bioassays demonstrated the sulfur chain length dependent speed of activity of different DAS against *S. feltiae*. Longer chain DAS require more time to display toxicity against nematodes. This observation was attributed to the higher hydrophobicity of longer chain DAS which was shown to be disadvantageous for crossing the cuticle and hypodermal membrane⁽¹⁴⁷⁾. The efficacy of a nematicide is dependent on a combination of its ability to cross the cuticle and hypodermal membrane barrier and its activity once this barrier has been crossed. DAS3 enters the nematode faster whereas DAS4 and DAS5 display a higher final toxicity. Therefore a mixture of different chain length DAS seems to provide a good combination to fulfil both desired parameters.

The mode of action of DAS was studied using *S. feltiae* as a model organism. LMW thiol levels were measured in *S. feltiae* for the first time and concentrations are similar compared to the LMW thiol levels measured in the model nematode *C. elegans*^(137, 145). Upon DAS3 treatment a decrease in GSH and Cys levels and a disturbance of the cellular redox balance was observed. In analogy to the interactions with BSH, which was observed in *B. subtilis* (chapter 3), the interaction with LMW thiols was confirmed to be one of the mechanisms of the nematicidal activity of DAS. Additionally, indications for hydrophobic interactions of DAS3 with the nematode cuticle were observed. No studies were performed to elucidate these interactions in detail or determine cuticle damage induced by DAS. Nevertheless, it is reasonable to speculate that there are other important modes of action for the nematicidal activity of DAS, like hydrophobic interactions with membranes, in addition to the reactivity of DAS with LMW thiols.

To investigate possible applications of DAS in crop protection, field trials were performed, where the efficacy of two garlic derived nematicides, NEMguard® and TDE5 (both containing mixtures of DAS1 to DAS6 formulated into a granule) were compared to synthetic nematicides on carrot and potato crops. One of the performed potato trials where the control of potato cyst nematodes was desired, showed significantly increased yields for the TDE5 and Nemathorin® (fosthiazate) treated beds. The other potato and carrot trials did not show significantly reduced symptoms or significantly increased yields by any of the used nematicides (garlic derived or synthetic). This was due to low RKN pressure in the soil of the carrot trial which led to healthy crops, even in the untreated beds. Concerning the performed potato trials, control of PCN is generally very difficult as indicated by inconsistent results for different nematicides⁽¹⁵³⁾. Nevertheless, the performed trials clearly showed that the garlic derived nematicides form an equally effective alternative compared to synthetic nematicides at a much lower environmental and health risk.

- DAS3 to DAS6 show similar levels of final nematicidal activity (>DAS1 and DAS2) against *S.feltiae* with longer chain DAS requiring more time to display toxicity against nematodes.
- For the first time LMW thiol and disulfide levels were measured in *S. feltiae* and DAS3 treatment leads to decreased GSH and Cys levels and therefore disturbs the intracellular redox balance.
- Hydrophobic interactions between DAS and the nematode cuticle were identified as an additional mode of nematicidal action of DAS.
- Two different garlic formulations containing DAS as active ingredients significantly increased potato yields in one potato trial and generally performed equally well compared to commonly used synthetic nematicides.

5 Conclusions and Outlook

In summary, the *in vitro* and *in vivo* analysis of diallyl sulfides (DAS), DAS metabolites and low molecular weight (LMW) and protein thiols have provided further insights into the complex reaction pathways initiated by the DAS molecules. Activity increase of DAS with increasing number of sulfur atoms up to DAS4 has often been observed. Inclusion of DAS5 and DAS6 in this study provides evidence of even higher antimicrobial activity of DAS5 compared to DAS4, but with no further increase for DAS6. From DAS3 to DAS4 the most dramatic difference in activity was observed and DAS4 and DAS5 may possess the optimum balance between stability and a long enough sulfur chain to promote high chemical reactivity.

Formation of the reduced counterparts of DAS, allyl perthiol (AS2H) and allyl hydrotrisulfide (AS3H) were detected for the first time. These molecules most likely drive the biological activity of DAS through formation of reactive oxygen species (ROS)⁽⁴²⁾ and H₂S release⁽¹⁸⁾ and, therefore, their detection upon reaction with LMW thiols closes an important gap in the elucidation of the mode of action of DAS. Importantly, DAS3 and DAS4 derived metabolites were also detected in *Bacillus subtilis*. The intracellular concentration of the reduced form of DAS (allyl mercaptan=ASH) was higher than the DAS3 concentration itself, which shows that DAS are rapidly reduced upon entering the cell. Furthermore, an important difference between the metabolites of DAS3 and DAS4 was elucidated: After DAS3 treatment only ASH was detected, whereas AS2H concentrations were nearly as high as ASH concentrations after DAS4 treatment. This may be one reason for the increased activity of DAS4. Other important differences between the different chain length DAS were observed *in vitro*: With increasing number of sulfur atoms in DAS, the reaction with glutathione (GSH) progressed faster: mixed allyl-glutathione di- and trisulfide (AGS2 and AGS3) formation was nearly 40-fold faster for DAS4 compared to DAS3 and another 30-fold increase in reaction rate was observed for DAS5 compared to DAS4 (Table 5.1).

Table 5.1: pH-independent formation rate of mixed polysulfides (AGS2, AGS3 and AGS4) after reaction of diallyl polysulfides (DAS3, DAS4 and DAS5) with GSH. Additionally reduced DAS (ASH, AS2H and AS3H) were identified as novel reaction products.

Starting material (mM)				pH independent product formation rate (min ⁻¹)			Additional identified products		
DAS3	DAS4	DAS5	GSH	AGS2	AGS3	AGS4	ASH	AS2H	AS3H
6.4	-	-	6.4	2.1	0.3	ND	+	+	-
6.4	-	-	32	0.8	0.1	ND	+	+	-
-	6.4	-	6.4	14.0	22.0	ND	+	+	+
-	6.4	-	32	14.7	21.1	ND	+	+	+
-	-	6.4	32	691	493	247	+	+	+

The presented *in vitro* investigations also highlight the complexity of the reaction of DAS with LMW thiols. No matter which of the DAS ($S > 2$) is used as the starting material in a reaction with LMW thiols, as reaction products DAS2 to DAS6, their reduced counterparts (AS_nH) and mixed allyl polysulfides were formed. The above observations suggest that, in an *in vivo* context the phenotypic effects observed in the presence of DAS molecules, may be attributed to the metabolites produced following reaction(s) with intracellular LMW thiols.

Treatment of *B. subtilis* with sublethal concentrations of DAS3 or DAS4 led to a rapid, reversible decrease in bacillithiol (BSH), cysteine (Cys) and coenzyme-A (CoA) levels. Final quantification of disulfide levels and confirmation of mixed disulfide formation as one possible mode of action was not achieved, because of the complexity and inconsistency of the disulfide quantification method. Nevertheless, *in vitro* studies showed, that DAS readily react with LMW thiols to form mixed di- and polysulfides, which had not been shown before.

Additionally, proteomic studies in *B. subtilis* have revealed *S*-allylation and *SS*-allylations of a wide range of proteins upon exposure to DAS4, which further highlights the complexity of DAS bioactivity and its impact upon a wide range of cellular targets. The full physiological and biochemical significance of these modifications is still under investigation.

One open question is the fate of BSH, as BSH and bacillithiol disulfide (BSSB) levels both decreased after DAS3 and DAS4 treatment and no bacillithiolation of proteins was detected. As DAS are known to induce ROS formation, one possible explanation may be the ROS induced over-oxidation of BSH to the corresponding sulfenic (BSOH), sulfinic (BSO_2H) or sulfonic (BSO_3H) acid. ROS induced protein oxidations to sulfenic and sulfinic acids were recently found to inherit important regulatory functions^(100, 101) and new chemical probes were developed for *in vivo* analysis of the sulfenic⁽¹⁰²⁾ and sulfinic⁽¹⁰³⁾ acid modifications of protein Cys residues. The application of these probes for the analysis of the oxidation status of BSH might shed some light on the fate of BSH.

Importantly, in the more complex, multicellular organism, the nematode *Steinernema feltiae*, the activity profile of DAS was very different compared to *B. subtilis*, with a similar activity for all DAS (DAS3 to DAS6), but faster activity of the DAS with shorter sulfur chain (DAS3 > DAS4 > DAS5 = DAS6). This observation was attributed to the increased hydrophobicity of longer chain DAS which was shown to be disadvantageous for crossing the cuticle and hypodermal membrane of the nematode⁽¹⁴⁷⁾. The efficacy of a nematicide depends on a combination of its ability to cross the cuticle and hypodermal membrane barrier and its activity once this barrier has been crossed. Consequently, DAS3 exerts its nematicidal activity faster than DAS4 and DAS5, but the latter two display higher final toxicities. Additionally, indications for hydrophobic interactions of DAS3 with the nematode cuticle were observed. Microscopic observations of the cuticle, through electron microscopy in particular, could possibly provide a visual impression of possible cuticle damage induced by DAS.

Similar to what was observed in *B. subtilis*, a decrease in GSH, the main redox buffer in *S. feltiae*, was observed. The disturbance of the intracellular redox balance through lowering the pool of reduced GSH or BSH was established as one important comprehensive mode of action (MOA) of DAS in two different organisms.

The observed differences dependent of the type of organism are very important if applications of DAS are considered, as the higher biological activity of longer chain length DAS observed in cell cultures or single cell organism do not necessarily translate into higher biological activity

within a multicellular organism. The use of DAS mixtures compared to single DAS molecules can be advantageous to ensure sufficient solubility and availability as well as high and prolonged activity against a range of target organisms. This also simplifies production and storage of DAS as DAS mixtures can be produced more easily compared to the pure molecules (section 2.1). Upon storage pure DAS molecules tend to equilibrate to mixtures of DAS, which are stable once the equilibrium has formed (section 2.2).

To investigate agricultural applications of DAS, field trials were performed, where the efficacy of two garlic derived nematicides (NEMguard® and TDE5, containing mixtures of DAS1 to DAS6 formulated into a granule) were compared to synthetic nematicides (Vydate® and Nemathorin®) on carrot and potato crops. The DAS derived nematicides were found to be an equally effective alternative compared to synthetic nematicides at a much lower environmental and health risk. Hazards to the food chain or agricultural workers (a feature of synthetic pesticides) can be excluded as garlic-derived nematicides decompose and get metabolised by plants or animals. Exploration of a nematode repellent effect of DAS in addition to the nematicidal effect could lead to further refinements of DAS derived nematicides⁽¹³⁵⁾. Unlike many other synthetic pesticides that have one specific MOA (e.g. the inhibition of acetylcholinesterase) DAS have multiple MOA, and hence the development of resistance in target organisms is minimised. In times of increasingly strict regulations for synthetic pesticides⁽⁸⁰⁾, further applications against plant pathogens (e.g. *Delia radicum*, cabbage root fly) show great potential to overcome potential pesticide shortages⁽⁸⁰⁾. Due to their non-hazardous nature DAS mixtures show great potential for applications in organic agriculture and their low-tech characteristics favour applications for crop protection in less developed countries.

To further investigate the MOA of DAS, future experiments should focus on developing more direct methods for the detailed analysis of DAS, DAS-derived metabolites and mixed polysulfides. A promising strategy for the direct detection of DAS includes the fluorescent labelling of allyl groups via a photoclick reaction with tetrazoles to form fluorescent pyrazoles⁽¹⁰⁴⁻¹⁰⁶⁾. This strategy was used *in vivo* to visualise translationally incorporated or genetically encoded alkene-containing proteins^(107, 108) and might be applicable for *in vivo* detection of fluorescently labelled DAS. Recently a method was published, that allows the selective visualisation of perthiols and polysulfides, but not thiols⁽¹⁰⁹⁾. This is the first polysulfide-selective bioorthogonal reaction and was shown to be applicable for perthiol and polysulfide detection *in vivo*.

Although it was not investigated in this study, the great potential of DAS for human therapeutic purposes should briefly be mentioned. DAS have been shown to kill a wide range of organisms harmful to humans, but do not cause too much harm to humans. They have also been shown to selectively kill cancer cells and DAS2, DAS3 and a GO have been shown to be toxic against *Culex pipiens quinquefasciatus*, an important vector of human pathogens⁽¹⁵⁴⁾. The DAS toxicity against disease transmitting mosquitos (e.g. malaria or dengue) is largely unexplored and future work should be done to investigate activity of longer chain DAS against different mosquito species known to transmit human diseases. Again, the different modes of action of DAS are an advantage to prevent resistance of pathogens and the lipophilicity and cell membrane permeability makes them promising drug candidates.

6 Materials and Methods

6.1 Materials and general experimental methods

Chemical reagents were purchased from Sigma-Aldrich, Acros, Fluka, Avocado, Merck and Novabiochem. Deuterated Nuclear Magnetic Resonance (NMR) solvents were purchased from Apollo Scientific Limited or Cambridge Isotope Laboratories.

Analytical High Performance Liquid Chromatography (HPLC) was conducted on a Jasco HPLC system equipped with two Jasco PU 1580 pumps, a MX-2080-32 dynamic mixer, a DG-1580-53 3-line degasser, a JASCO AS-2055 autoinjector, a JASCO FP-2020 fluorescence detector and a Jasco UV-1575 UV-VIS detector.

Automated normal phase (NP) and reverse phase (RP) flash chromatography was performed on a Biotage Isolera four system using Biotage SNAP (KP-SIL, 10g, for NP and 12 g, KP-C18-HS for RP) cartridges.

NMR spectra were recorded on Bruker 400 MHz or a Varian 300 MHz Gemini 2000 spectrometer. Chemical shifts for ^1H NMR are quoted in parts per million (δ) downfield from tetramethylsilane as an internal standard or to the residual solvent peak referenced as follows: D_2O to 4.80 ppm, MeOD to 3.31 ppm, CDCl_3 to 7.26 ppm. Chemical shifts for ^{13}C NMR are quoted in parts per million relative to the triplet from CDCl_3 referenced to 77.23 ppm, the septet from MeOD referenced to 49.15 ppm or spiked with MeOH or CH_3CN (49.50 or 1.47 ppm respectively) for D_2O . Coupling constants (J) are quoted in hertz (Hz). The following abbreviations are used: s = singlet, d = doublet, t = triplet, q = quartet, m = multiplet, dd = doublet of doublets, ddd = doublet of doublet of doublets, ddt = doublet of doublet of triplets.

Low-resolution electrospray mass spectrometry (MS) was performed on a Shimadzu LC 20AB prominence Liquid Chromatograph, an LCMS 210A Liquid Chromatograph Mass Spectrometer, a SPD M20A prominence DAD detector, DGU-20A3 prominence degasser and a SIL-20AC prominence autosampler.

Ultraviolet (UV) absorbance measurements were recorded on a PerkinElmer UV Lambda 25 UV/VIS spectrophotometer using disposable plastic cuvettes. Optical density (OD_{600}) measurements were performed on an Ultraspec 10 Cell Densitymeter (Amersham Biosciences) or on a Fluostar Omega microplate reader (Labtech).

For concentration of cell extracts and biochemical assays a refrigerated centrifuge (Hermle Z326K) and a Heraeus Pico 16 centrifuge (Thermo Scientific) were used.

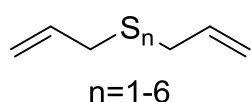
Ultrapure H_2O and HPLC-grade solvents were used for all HPLC, Liquid chromatography (LC)-MS and biochemical experiments.

6.2 Synthesis, purification and characterisation

6.2.1 Synthesis, purification and characterisation of diallyl polysulfides (DAS) (83)

Sulfur (S₈) (3.2 g, 12.5 mmol) was mixed with DAS2 (2.7 g, 18.5 mmol) and the reaction mixture was heated under vigorous stirring. At a temperature of 115-120°C the sulfur melted and the solution became homogenous. The reaction was stirred for 1 hour at 115-120 °C and a colour change from bright yellow to orange to brown was observed. Diluting an aliquot of the reaction mixture into EtOH, there was no sulfur precipitation indicating completion of the reaction. The reaction mixture was allowed to cool to room temperature (RT) affording the crude product as a brown viscous oil, which was purified by preparative RP HPLC. The reaction mixture was loaded on a C₁₈ handpacked column (2.5x 30 cm, 50-100 μm particle size) and eluted isocratic using 82% methanol and 18% H₂O and an increasing flow-rate from 5 to 10 mL/min during the run time (starting with 5 mL/min, increased to 7 mL/min after elution of DAS4, increased to 9 mL/min after elution of DAS5). UV detection was carried out at 240 or 210 nm.

The collected fractions were extracted with hexane (3 x 1/4 volume). The combined extract was concentrated on a rotary evaporator, resuspended in small volumes of dichloromethane and dried with a slow flow-through of air. Purified compounds were analysed by analytic HPLC to confirm purity (95-99%) and stored in the dark at -20°C.



DAS1 and DAS2 were obtained through vacuum distillation from a crude DAS mixture, performed and provided by Awais Anwar (ECOspray Ltd, Hilborough, UK).

Table 6.1: Coordination Ion Spray Mass Spectrometry (CIS-MS) of DAS.

	Formula	m/z calculated [M+Ag] ⁺	m/z found [M+Ag] ⁺
DAS2	C ₆ H ₁₀ AgS ₂ ⁺	253.17/255.17	252.8/254.8
DAS3	C ₆ H ₁₀ AgS ₃ ⁺	285.24/287.24	284.8/286.8
DAS4	C ₆ H ₁₀ AgS ₄ ⁺	317.30/319.30	316.7/318.8
DAS5	C ₆ H ₁₀ AgS ₅ ⁺	349.37/351.37	348.8/350.8
DAS6	C ₆ H ₁₀ AgS ₆ ⁺	381.43/383.43	380.7/382.7

Table 6.2: $^1\text{H-NMR}$ and $^{13}\text{C-NMR}$ characterisation of DAS in CDCl_3 .

	δ_{H} 400 MHz			δ_{C} 100 MHz ^a		
	CH_2S	$=\text{CH}$	$=\text{CH}_2$	CH_2S	$=\text{CH}$	$=\text{CH}_2$
DAS1	3.07 ddd 7.1 1.3 1.0	5.75 ddt 16.7 10.3 7.1	5.10-5.04 m	33.36	134.32	117.20
DAS2	3.33 ddd 7.4 1.2 0.8	5.83 ddt 16.9 10.0 7.4	5.12-5.21 m	42.35	133.56	118.50
DAS3	3.50 ddd 7.3 1.2 0.9	5.88 ddt 16.8 10.1 7.4	5.18-5.29 m	41.77	132.81	119.20
DAS4	3.58 ddd 7.3 1.2 0.8	5.89 ddt 16.9 10.0 7.4	5.20-5.28 m	42.18	132.60	119.70
DAS5	3.61 ddd 7.3 1.2 0.8	5.88 ddt 16.8 10.1 7.4	5.22-5.30 m	42.66	132.33	119.96
DAS6	3.62 ddd 7.3 1.2 0.8	5.88 ddt 16.8 10.1 7.4	5.22-5.30 m	42.54	132.30	120.05

^a ^{13}C shifts were assigned according to their HSQC and HMBC correlations.

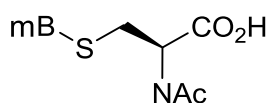
6.2.2 Synthesis and purification of thiol-monobimane (thiol-mB) standards

All thiols were commercially available and used without purification, except for bacillithiol (BSH), which was prepared by Dr. Sunil V. Sharma as previously described⁽¹⁵⁵⁾.

6.2.2.1 Synthesis, purification and characterisation of qualitative thiol-mB HPLC standards

For qualitative standards different thiols were reacted with monobromobimane (mBBr) to gain the fluorescent thiol-mB adducts and purified from unreacted starting materials and by-products.

N-Acetyl-L- (S)-cysteinyl-bimane (CysNAcmB)



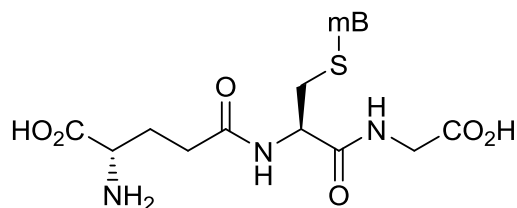
To a solution of CysNAc (11.2 mg, 0.074 mmol) and sodium bicarbonate (NaHCO_3) (15.1 mg, 0.18 mmol) in 2 mL H_2O , mBBr (14.8 mg, 0.055 mmol) in 1 mL CH_3CN was added. The reaction mixture was stirred in dark for 1 h. The product of the reaction was a bright yellow-green clear solution. CH_3CN was removed under vacuum and the product was freeze dried overnight. The freeze dried product was re-dissolved in a small amount of H_2O and

purification using automated RP chromatography (Biotage Isolera) eluting with 100% H₂O followed by increasing CH₃CN to 10% gave the pure product (14 mg, 72%).

¹H-NMR (400 MHz, D₂O) δ 4.34 (dd, 1H, J=4.40, 7.80 Hz), 3.84 (q, 2H, J=14.64 Hz), 3.06 (dd, 1H, J=4.43, 13.80 Hz), 2.96 (dd, 1H, J=7.82, 13.76 Hz), 2.41 (s, 3H), 1.97 (s, 3H), 1.82 (s, 3H), 1.75 (s, 3H)

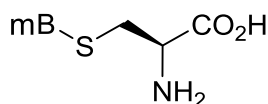
¹³C-NMR (75 MHz, D₂O) δ 175.90, 173.08, 162.60, 161.97, 149.38, 147.90, 112.93, 111.00, 53.54, 33.74, 24.18, 21.20, 10.44, 5.40, 4.96

Glutathione-bimane (GSmB)



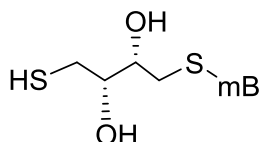
To a solution of GSH (26.1 mg, 0.085 mmol) and NaHCO₃ (20.3mg, 0.242 mmol) in 6 mL of H₂O, mBBr (21.7 mg, 0.08mmol) dissolved in 1.5 mL of CH₃CN were added. The reaction was stirred for 1.25 h and purification done as described for CySNAcmB gave pure GSmB (29 mg, 73%).

L-cysteinyl-bimane (CysmB)



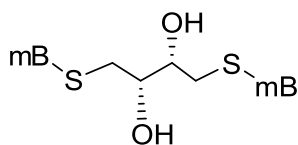
To a solution of L-Cys (8.4 mg, 0.07 mmol) and NaHCO₃ (14.2 mg, 0.17 mmol) in 2 mL of H₂O, mBBr (14.9 mg, 0.06 mmol) in 1 mL CH₃CN was added. The reaction mixture was stirred in dark for 1 h and purification done as described for CySNAcmB gave pure CysmB (14.7 mg, 68 %).

Dithiothreitol-bimane (DTTmB)

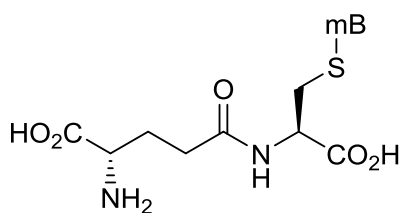


To a solution of dithiothreitol (DTT) (8.7 mg, 0.06 mmol) and NaHCO₃ (14.4 mg, 0.17 mmol) in 2 mL of H₂O, mBBr (14.9 mg, 0.06 mmol) in 1 mL CH₃CN was added. The reaction mixture was stirred in dark for 1 h and RP purification with a gradient of H₂O going up to 90% CH₃CN gave pure DTTmB (10.8 mg, 57%).

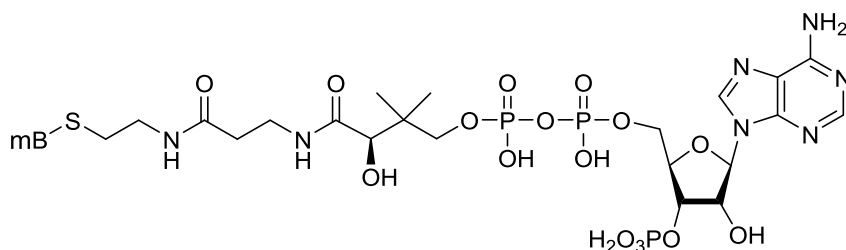
Dithiothreitol-dibimane (DTTmB₂)



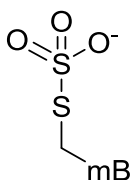
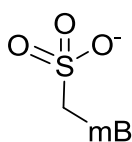
To a solution of DTT (3.5 mg, 0.02 mmol) and NaHCO₃ (8.6 mg, 0.10 mmol) in 2 mL of H₂O, mBBr (13.6 mg, 0.05 mmol) in 1 mL CH₃CN was added. The reaction mixture was stirred in dark for 1 h. The following purification was done as described for DTTmB and DTTmB₂ was obtained (10.7 mg, 73%).

γ -glutamylcysteine-bimane (γ -GCmB)

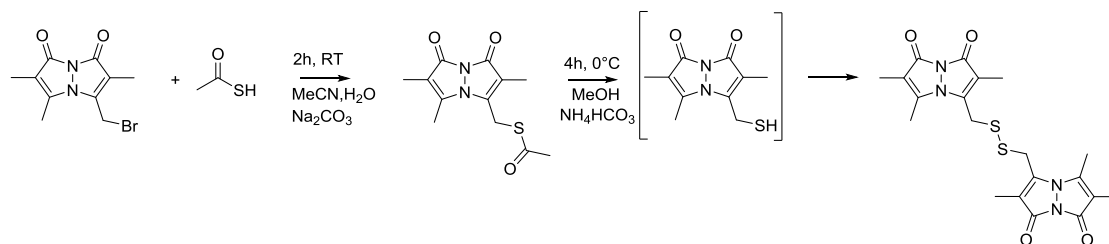
To a solution of γ -GC (8.9 mg, 0.035 mmol) and NaHCO_3 (7.6 mg, 0.09 mmol) in 2 mL of H_2O , mBBr (8 mg, 0.03 mmol) in 1 mL CH_3CN was added. The reaction mixture was stirred in dark for 1 h and purification done as described for CySNAcmB gave pure γ -GCmB (11.8 mg, 89 %).

Coenzyme A-bimane (CoAmB)

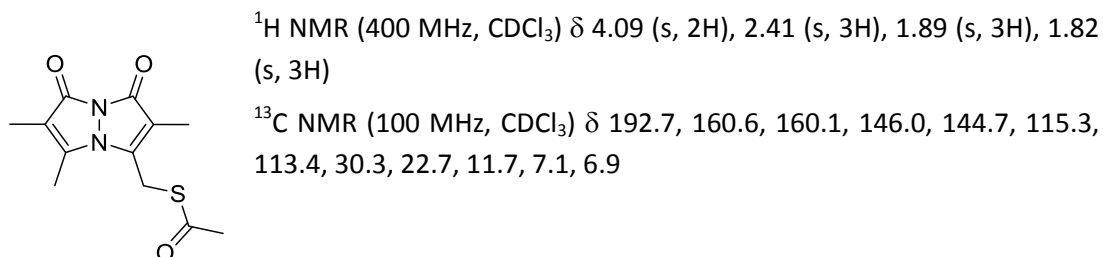
To a solution of CoA (11 mg, 0.014 mmol) and NaHCO_3 (3 mg, 0.036 mmol) in 2 mL of H_2O , mBBr (3.3 mg, 0.012 mmol) in 1 mL CH_3CN was added. The reaction was stirred overnight and the purification was done as described for CySNAcmB and pure CoAmB (3.7 mg, 32%) was obtained.

Sulfite-mB and Thiosulfate-mB

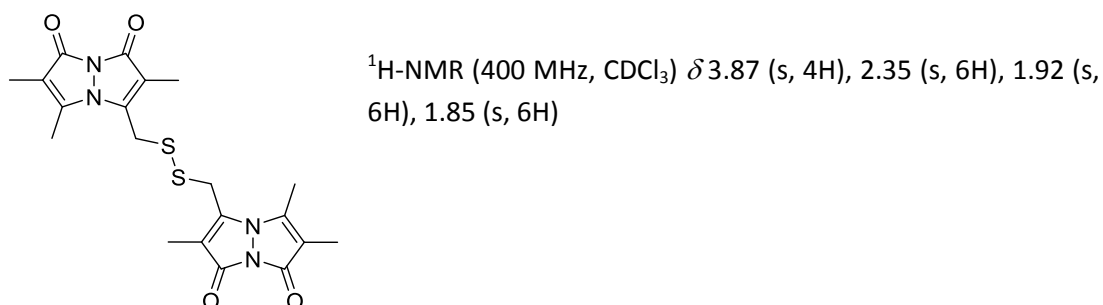
Standards for sulfite and thiosulfate were prepared by reacting their sodium salts (5 mM) with an excess of mBBr (15 mM) in a HEPES buffered solution (20 mM, pH 8) for 15 minutes in the dark at RT. To stop the reaction 25 mM methanesulfonic acid (MeSO_3H) were added and these standards were used without purification.

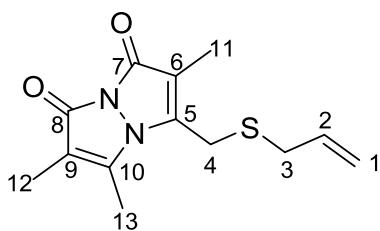
Dibimane-disulfide (mBS)₂**Figure 6.1: Synthesis of dibimane-disulfide (mBS)₂.**

MBBr (15 mg, 0.055 mmol) and thioacetic acid (13.9 μ L, 0.138 mmol) were dissolved in 2.5 mL CH₃CN and Na₂CO₃ (14.7 mg, 0.138 mmol) dissolved in 1 mL H₂O was added. The pH was adjusted to pH 7 with hydrogen chloride (HCl, 6 M stock) and the reaction was stirred in dark at RT for 2 h. Afterwards HCl was added to adjust the solution to pH 3. H₂O and ethyl acetate (5 mL each) were added and the H₂O fraction was extracted 3x with ethyl acetate (1/4 volume) and the combined dried extract gave pure bimane-S-acetate.

Bimane-S-acetate

An aliquot of the dried acetylated product (bimane-S-acetate, 10 mg, 37.6 μ mol) was dissolved in 1 mL MeOH and NH₄HCO₃ (15 mg, 0.19 mmol) was added. The reaction was stirred on ice for 4 h. Purification was performed on a silica solid phase extraction tube (Strata Phenomenex) through gradient elution with hexane and increasing ethyl acetate concentration to obtain pure dibimane-disulfide (mBS)₂. Reduction of this molecule leads to formation of mBSH and mBBr labeling of mBSH leads to formation of mB₂S, both have been used as standards as well.

Dibimane-disulfide (mBS)₂

Allyl mercaptan-bimane (ASmB)

To an aqueous solution (2 mL) of allyl mercaptan (ASH) (4.9 mg, 0.066 mmol) and NaHCO₃ (14 mg, 0.167 mmol), mBBR (14.5 mg, 0.053 mmol) in 1 mL CH₃CN was added and the reaction was stirred in dark for 1.5 h. The product was extracted in hexane and additionally the H₂O phase was again extracted in ethyl acetate. By ¹H-NMR both fractions showed product and impurities.

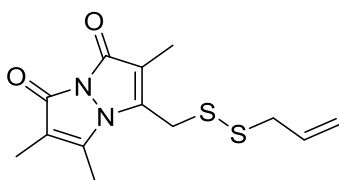
Further purification was done by automated NP flash chromatography (10 g SNAP column) starting with 80% hexane 20% ethyl acetate and increasing ethyl acetate to 99% gave ASmB (7.8 mg, 54%), which was characterised by NMR in CDCl₃.

Table 6.3: ¹H-NMR and ¹³C-NMR data for allyl mercaptan-bimane (ASmB) in CDCl₃.

Position	δ_{H} 400 MHz	δ_{C} 100 MHz ^a
C-1	5.25-5.20 (m, 2H)	118.84
C-2	5.82 (ddt, 17.3, 9.6, 6.9, 1H)	133.13
C-3	3.23 (d, 7.0, 2H)	35.35
C-4	3.58 (s, 2H)	24.49
C-5, C-10		114.33, 112.87
C-6, C-9		146.18, 145.64
C-7, C-8		160.86, 160.35
C-11, C-12	1.87 (s, 3H), 1.84 (s, 3H)	7.43, 7.01
C-13	2.41 (s, 3H)	11.86

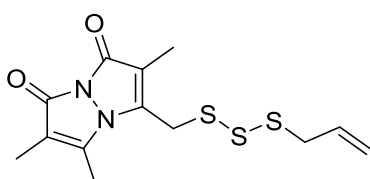
^a ¹³C shifts were assigned according to their HSQC and HMBC correlations.

MS ES⁺: *m/z* calc. for C₁₃H₁₇N₂O₂S [M+H]⁺: 265.1, found 265.0.

Allyl perthiol-bimane (AS2mB)

Prepared as described in section 6.4.1.

MS (ES⁺): *m/z* calc. for C₁₃H₁₇N₂O₂S₂ [M+H]⁺: 297.07, found 296.9.

Allyl hydrotrisulfide-bimane (AS3mB)

Prepared as described in section 6.4.1.3.

MS (ES⁺): *m/z*

calc. for C₁₃H₁₇N₂O₂S₃ [M+H]⁺: 329.04, found 328.9.

calc. for C₁₃H₁₆N₂NaO₂S₃ [M+Na]⁺: 351.03, found 350.9.

6.2.2.2 Preparation of quantitative thiol-mB HPLC standards

Preparation of quantitative standards was done as described by Fahey and Newton⁽¹⁵⁶⁾.

Determination of accurate thiol concentrations by titration with DTNB (5,5'-dithiobis-(2-nitrobenzoic acid))

Stock solutions of thiols were quantified by titration against 2 mM DTNB in phosphate buffer (pH 7.5) and measuring the absorbance increase at 412 nm ($\epsilon = 14,150 \text{ M}^{-1}\text{cm}^{-1}$) due to formation of 5-thio-2-nitrobenzoic acid (TNB)⁽¹⁵⁷⁾.

Reaction of accurately quantified thiol with mBBr

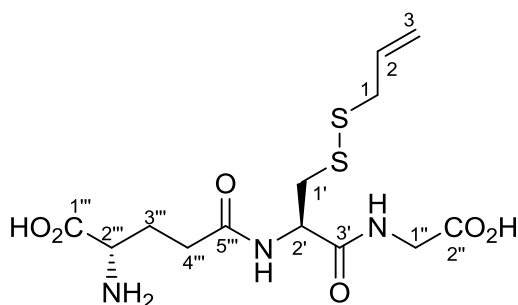
For the reaction with mBBr 50 mM Hepes, 5 mM ethylenediaminetetraacetic acid (EDTA), 3 mM mBBr (dissolved in CH_3CN) were mixed in an aqueous solution in an eppendorf tube and 1 mM final concentration of thiol was added. The reaction was incubated for 15 min at RT in dark and was mixed frequently. After 15 min the colour had turned from bright yellow to bright green-yellow and $\text{Me}_3\text{SO}_3\text{H}$ was added to a final concentration of 25 mM. The solution was aliquotted, dried in a vacuum centrifuge and dry aliquots for single use were stored at -20°C . Good stability for several months was observed for all thiol-mB except for CoAmB, which was prepared freshly for each analysis.

For HPLC analysis the solution was diluted into different concentrations (between 1 μM and 150 μM) and 10 μL were injected into HPLC which corresponds to injections of 10 to 1500 pmol.

6.2.3 Synthesis and characterisation of mixed polysulfides

Allyl-glutathione disulfide (AGS2) ^(84, 158)

GSH (11 mg, 35.8 μmol) dissolved in 1.5 mL NaPO₄ buffer (pH 7, 50 mM) was mixed with DAS2 (55 μL , 379 μmol) in 445 μL MeOH in a round bottom flask to form a milky white suspension, which was then degassed with nitrogen (N₂) and kept under N₂. MeOH was added until DAS2 was dissolved (2.25 mL). The reaction was kept stirring under N₂ at RT overnight and was subsequently concentrated under vacuum and washed with hexane (2 x 2 mL). The reaction gave a colourless, odourless solid (10.5 mg, 77%), which was confirmed to be pure AGS2 by NMR in D₂O.



MS (ES⁺): m/z calc. for C₁₃H₂₂N₃O₆S₂ [M+H⁺]: 380.09, found 380.1

MS (ES⁺): m/z calc. for C₁₃H₂₁N₃NaO₆S₂ [M+Na⁺]: 402.08, found 402.01

MS (ES⁻): m/z calc. for C₁₃H₂₀N₃O₆S₂ [M-H⁺]: 378.08, found 378.1

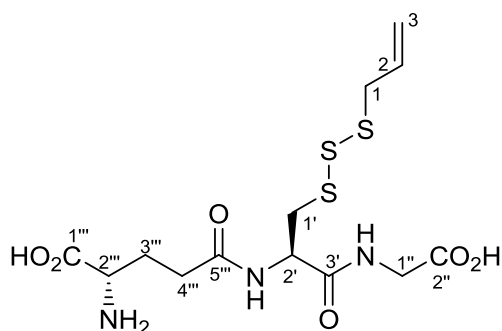
Table 6.4: ¹H-NMR and ¹³C-NMR characterisation for allyl glutathione disulfide (AGS2) in D₂O.

Position	δ_{H} 400 MHz	δ_{C} 100 MHz ^a
Allyl		
1 CH ₂	3.39 (d, 6.9, 2H)	40.9
2 CH	5.90 (ddt, 16.8, 10.1, 7.4, 1H)	133.5
3 CH ₂	5.27-5.19 (m, 2H)	118.9
L-Cysteine		
1' CH ₂	3.26 (dd, 14.3, 4.5, 1H) 2.97 (dd, 14.3, 9.5, 1H)	38.8
2' CH	4.73 (dd, 9.6, 4.5, 1H)	52.8
3' C=O		171.9
Glycine		
1'' CH ₂	3.82-3.72 (m*overlapping with 2''', 2H)	43.4
2'' CO ₂ H		176.2
Glutamic acid		
1''' CO ₂ H		173.9
2''' CH	3.82-3.72 (m* overlapping with 1'', 1H)	54.1
3''' CH ₂	2.16 (q, 7.2, 2H)	26.2
4''' CH ₂	2.60-2.47 (m, 2H)	31.4
5''' C=O		175.0

^a ¹³C shifts were assigned according to their HSQC and HMBC correlations. *A multiplet is reported due to overlapping peaks.

Allyl-glutathione trisulfide (AGS3)

GSH (11 mg, 35.8 μmol) dissolved in 1.5 mL NaPO_4 buffer (50 mM, pH 7) and DAS3 (56 μL , 350 μmol) dissolved in 944 μL MeOH were mixed in a round bottom flask, purged with N_2 and sealed. 3 mL of MeOH were added, to dissolve all DAS3 giving a pale yellow solution and the reaction was stirred under N_2 at RT overnight in the dark. The reaction was then concentrated under vacuum, washed with hexane (3x 2 mL) and dried under vacuum. The NMR solution in D_2O formed a milky white suspension and NMR analysis showed the formation of a mixture of AGS2 and AGS3 (ratio about 2:1). Pure AGS3 (1.1 mg, 7.7%) was isolated by HPLC as described in section 6.3.1.2.



MS (ES^+): m/z

calc. for $\text{C}_{13}\text{H}_{22}\text{N}_3\text{O}_6\text{S}_3$ [$\text{M}+\text{H}^+$]: 412.07, found 412.0

calc. for $\text{C}_{13}\text{H}_{21}\text{N}_3\text{NaO}_6\text{S}_3$ [$\text{M}+\text{Na}^+$]: 434.05, found 434.0

MS (ES^-): m/z

calc. for $\text{C}_{13}\text{H}_{20}\text{N}_3\text{O}_6\text{S}_3$ [$\text{M}-\text{H}^+$]: 410.05, found 410.1

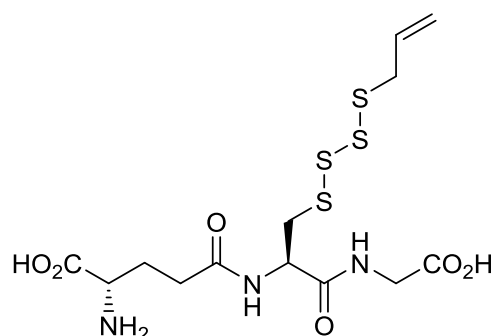
Table 6.5: ^1H -NMR and ^{13}C -NMR characterisation of allyl-glutathione trisulfide (AGS3) in D_2O .

Position	δ_{H} (J in Hz) 400 MHz	δ_{C} 100 MHz ^a
Allyl		
1 CH_2	3.56 (d, 7.3, 2H)	41.53
2 CH	5.94 (ddt, 16.8, 10.2, 7.4, 1H)	133.73
3 CH_2	5.30-5.23 (m, 2H)	119.90
L-Cysteine		
1' CH_2	3.45 (dd, 14.5, 4.9, 1H) 3.18 (dd, 14.2, 9.2, 1H)	40.08
2' CH	4.80**, (m* overlapping with HOD peak, 1H)	53.25
3' C=O		172.27
Glycine		
1'' CH_2	3.82-3.72 (m* overlapping with 2''', 2H)	44.03
2'' CO_2H		182.10
Glutamic acid		
1''' CO_2H		174.6 ***
2''' CH	3.82-3.72 (m* overlapping with 1'', 1H)	54.73
3''' CH_2	2.15 (q, 7.3, 2H)	
4''' CH_2	2.56-2.52 (m, 2H)	
5''' C=O		175.56

^a ^{13}C shifts were assigned according to their HSQC and HMBC correlations. *A multiplet is reported due to overlapping peaks. **confirmed by HSQC ***not visible on ^{13}C , confirmed by HMBC.

Allyl-glutathione tetrasulfide (AGS4)

AGS4 was purified by HPLC (section 6.3.1.2) after reacting DAS3 to DAS6 with GSH (6.4.2.1), however, the amount was not sufficient for NMR characterisation.



MS (ES⁺): *m/z*

calc. for C₁₃H₂₂N₃O₆S₄ [M+H⁺]: 444.04, found 444.0

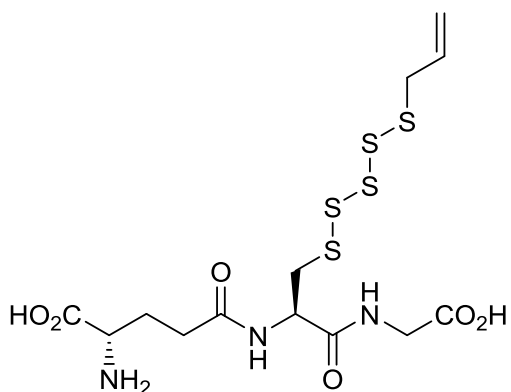
calc. for C₁₃H₂₁N₃NaO₆S₄ [M+Na⁺]: 466.02, found 466.0

MS (ES⁻): *m/z*

calc. for C₁₃H₂₀N₃O₆S₄ [M-H⁺]: 442.02, found 442.1

Allyl-glutathione pentasulfide (AGS5)

AGS5 was purified by HPLC (section 6.3.1.2) after reacting DAS3 to DAS6 with GSH (6.4.2.1), however, the amount was not sufficient for NMR characterisation.



MS (ES⁺): *m/z*

calc. for C₁₃H₂₂N₃O₆S₅ [M+H⁺]: 476.01, found 475.9

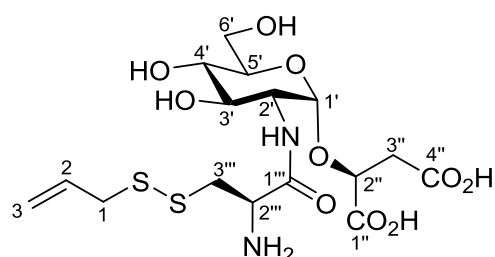
calc. for C₁₃H₂₁N₃NaO₆S₅ [M+Na⁺]: 497.99, found 497.9

MS (ES⁻): *m/z*

calc. for C₁₃H₂₀N₃O₆S₅ [M-H⁺]: 474.00, found 473.9

Allyl-bacillithiol disulfide (ABS2)

BSH (0.239 mg, 0.6 μmol) dissolved in 160 μL NaPO_4 buffer (pH 7, 50 mM) was mixed with DAS2 (1.2 μL , 8 μmol) in 400 μL MeOH in a round bottom flask, which was then purged with N_2 . The reaction was kept stirring under N_2 at RT in dark overnight and was subsequently dried in a vacuum centrifuge to gain a colourless, odourless solid [0.15 mg, 53% (by quantitative NMR)], which was confirmed to be pure ABS2 by ^1H -NMR in D_2O . The isolated quantity was only sufficient for ^1H -NMR, no other NMR spectra could be recorded.



MS (ES^+): m/z

calc. for $\text{C}_{16}\text{H}_{27}\text{N}_2\text{O}_{10}\text{S}_2$ [$\text{M}+\text{H}^+$]: 471.52, found 471.1

calc. for $\text{C}_{16}\text{H}_{26}\text{N}_2\text{NaO}_{10}\text{S}_2$ [$\text{M}+\text{Na}^+$]: 493.50, found 493.1

MS (ES^-): m/z

calc. for $\text{C}_{16}\text{H}_{25}\text{N}_2\text{O}_{10}\text{S}_2$ [$\text{M}-\text{H}^+$]: 469.50, found 469.0

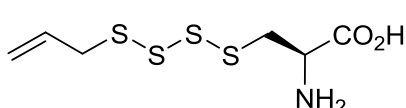
Table 6.6: ^1H -NMR data of allyl-bacillithiol disulfide (ABS2) in D_2O .

Position	δ_{H} 400 MHz	Position	δ_{H} 400 MHz
Allyl		Malate	
1 CH_2S	3.43 (d, 7.3, 2H)	1'' C=O	-
2 =CH	5.94 (ddt**, 16.8, 10.2, 7.4, 1H)	2'' CH	4.14 (dd, 11.4, 2.3, 1H)
3 =CH ₂	5.20-5.40 (m, 2H)	3''CH ₂	2.42 (dd, 15.0, 11.6, 1H) 2.60 (dd, 15.1, 2.1, 1H)
Glucosamine		4'' C=O	-
1'	5.0 (d, 3.3, 1H)	L-Cysteine	
2'	3.84-3.93 (m*, 1H)	1''' C=O	-
3'	3.84-3.93 (m*, 1H)	2''' CH	4.19 (dd, 7.5, 6.1, 1H)
4'	3.84-3.93 (m*, 1H)	3'''CH ₂	3.23 (dd, 14.5, 6.0, 1H) 3.09 (dd, 14.5, 7.7, 1H)
5'	3.51 (dd, 9.7, 8.3, 1H)		
6' CH ₂	3.71 (dd, 12.3, 2.2, 1H) 3.80 (dd, 12.9, 3.9, 1H)		

Assignments were based on previous ^{13}C , COSY, HSQC and HMBC NMR characterisation of BSH and BSSB. *A multiplet is reported due to overlapping peaks. **Peak pattern was established through comparison with NMR spectra of related compounds.

Allyl-cysteine tetrasulfide (ACS4)

ACS4 was synthesised by reacting DAS5 with Cys (section 6.4.2.4) and obtained in analytical quantity after HPLC purification (6.3.1.2).



MS (ES^+): m/z calc. for $\text{C}_6\text{H}_{11}\text{NNa}_2\text{O}_2\text{S}_4^{2+}$ [$\text{M}+2\text{Na}^+$]: 303.38, found 303.1

6.3 Analytical Methods

6.3.1 HPLC

6.3.1.1 HPLC analysis of DAS

DAS were analysed by analytical HPLC using a HiChrom ACE-AR C₁₈ 4.6 x 250 mm, 5 µm column, equilibrated at 37°C and UV detection at 210 nm. As solvent system an isocratic system with 90% MeOH and 10% H₂O was used at a flow-rate of 1.5 mL/min. DAS2 to DAS6 eluted at 3.6, 4.6, 5.9, 7.9 and 10.2 min respectively.

6.3.1.2 HPLC analysis of mixed polysulfides (AGS_n, ACS_n and ABS_n)

Separation of allyl-glutathione (AGS_n), allyl-cysteine (ACS_n) and allyl-bacillithiol (ABS_n) di- and polysulfides was achieved using isocratic conditions with 40, 50 or 60% solvent B (90% MeOH, 10% H₂O, containing 0.25% acetic acid adjusted to pH 4 with NaOH) and solvent A (0.25% acetic acid in H₂O, pH4) at 1.2 mL/min using a HiChrom ACE-AR C₁₈ 4.6 x 250 mm, 5 µm column, equilibrated at 37°C and UV detection at 220 nm. The retention times (rt) for AGS2 to AGS4 were 4.7 min, 9.7 min and 24.5 min respectively, and 3.4 min, 5.2 min and 9.6 min for ACS2 to ACS4 respectively when using 50% solvent B and 3.6 min, 5.6 min, 10.9 min and 22.9 min for AGS2 to AGS5 respectively when using 60% solvent B. Mixed ABS2 to ABS4 were analysed using 40% solvent B and eluted at 3.1 min, 4.8 min, and 9.8 min respectively.

6.3.1.3 HPLC analysis of fluorescent bimane adducts

HPLC analysis for BSmB and CysmB in *B. subtilis* and GSmb, CySmB, CySGlymB, γ-GCmB and homocysteine-monobimane (HCysmB) in nematodes (Method A)

Thiol-mB adducts were separated by HPLC on a HiChrom ACE-AR C₁₈ 4.6 x 250 mm, 5 µm, column, equilibrated at 37 °C with Solvent A (0.25% v/v acetic acid and 10% MeOH, adjusted to pH 4 with NaOH). For analysis of CysmB and BSmB samples were eluted with a gradient of Solvent B (90% MeOH, 10% H₂O) at 1.2 mL/min as follows: 0-5 min, 0% Solvent B; 5-15 min, 0-20% Solvent B; and 15-20 min, 20-100% Solvent B, followed by re-equilibration and re-injection. BSmB and CysmB eluted at 11.8 min and 14.3 min, respectively. For analysis of thiol-mB adducts in nematodes, samples were eluted with the following gradient: 0-25 min, 1-45% solvent B; 25-27 min, 45-100% solvent B, followed by re-equilibration and re-injection. Retention times were 8.9 (CysmB), 9.3 (CysGlymB), 10.5 (γ-GCmB), 11.7 (GSmb) and 12.5 (HCysmB) min. Fluorescence detection was carried out with excitation at 385 nm and emission at 460 nm, and a gain of 1x or 10x, depending on the sample concentration.

HPLC analysis for CoAmB, ASmb, AS2mB and AS3mB (Method B)

CoAmB and AS_nmB were analysed by a different method using a Hichrom ACE C₈ column (4x 150 mm, 5 µm) and a gradient of Solvent C (10 mM tetrabutylammonium phosphate (TBAP) in 90% H₂O, 10% MeOH, adjusted to pH 3.4 with acetic acid) and Solvent D (10 mM TBAP in 90% MeOH, 10% H₂O, adjusted to pH 3.4 with acetic acid). Detection was carried out at 385 nm and emission at 460 nm, and a gain of 1x. To analyse only CoAmB the column was equilibrated with 30% Solvent D at a flow-rate of 1 mL/min at 37 °C and the samples were eluted with the following gradient: 0-10 min, 30-50% Solvent D, 10-17 min, 50-100% Solvent D, followed by re-equilibration and re-injection. CoAmB eluted at 15.4 min.

To analyse ASmB, AS2mB and AS3mB Solvent C and Solvent D were run in two different gradients at 1 mL /min (gradient 1: starting conditions: 35% B, 16 min: 60% B, 19 min: 100% B, re-equilibration and re-injection, gradient 2: starting conditions: 10% B, 16 min: 60% B, 19 min: 100% B, re-equilibration and re-injection). The *rt* were 10 min (ASmB) and 13.7 min (AS2mB) with gradient 1 and 16.2 min (ASmB), 17.9 min (CoAmB), 18.7 min (AS2mB) and 20.6 min (AS3mB) eluting with gradient 2. This method was used for analysis and purification of ASmB, AS2mB and AS3mB and separation of CoAmB and AS_nmB in cell samples.

6.3.2 LC-MS

6.3.2.1 LC-MS analysis of DAS

Pure DAS (DAS2 to DAS6, approx. 2 µg/mL) were dissolved in MeOH and mixed with silver tetrafluoroborate (AgBF₄) (filtered stock solution in MeOH, final concentration in the sample: 20 µg/mL). Masses of the DAS coordinated with silver ions were detected through electrospray ionisation (ESI) in the positive mode by direct injection, eluting with 100% MeOH at a flow-rate of 0.3 mL/min.

6.3.2.2 LC-MS analysis of bimane adducts

LC-MS characterisation of AS_nmB

Collected HPLC fractions of ASmB, AS2mB and AS3mB were analysed by LC-MS using ESI and detection in the positive mode. For ASmB and AS2mB a gradient (20-95% B over 5 min, 95% B for 2 min, followed by re-equilibration and re-injection, flow-rate: 0.3 mL/min) of solvent A (0.05 % formic acid in H₂O) and solvent B (0.05% formic acid in MeOH) was run on an Agilent Zorbax C₁₈ column (2.5x 50mm, 3.5 µm). For analysis of AS3mB formic acid was replaced with acetic acid. *Rt* were 4.1 min (ASmB) and 4.3 min (AS2mB) using formic acid and 4.7 min (ASmB), 5.0 min (AS2mB) and 5.6 min (AS3mB) using acetic acid.

6.3.2.3 LC-MS analysis of mixed polysulfides

LC-MS analysis of AGS_n, ABS_n and ACS_n was done by direct injection of the HPLC purified compounds, ESI and detection in positive and negative mode. The solvent (60% H₂O, 40% MeOH containing 0.05% acetic acid) was used at a flow-rate of 0.2 mL/min or 0.5 mL/min.

6.4 *In vitro* reactions between DAS and LMW thiols

6.4.1 Formation of reduced DAS

6.4.1.1 Reaction of DAS3 with TCEP

From a 1 M stock solution of DAS3 in CH₃CN and a 100 mM stock solution of tris(2-carboxyethyl)phosphine (TCEP) in H₂O, 10 µL of each stock were mixed with 80 µL of CH₃CN (final concentrations: 100 mM DAS3, 10 mM TCEP). 10 µL aliquots of the reaction mixture were added to 90µL mBBr mix (16 mM mBBr, 20 mM Hepes buffer, pH8 in H₂O) at different time points (10 sec, 1 min, 5 min, 10 min, 20 min, 1 h) and incubated at RT in dark for 10 min. A negative control was done for TCEP incubated with mBBr without any DAS3. The reaction was stopped with 1 µL of 5 M MeSO₃H. Bimane labelled products were analysed (after 10-fold

dilution with 10 mM MeSO₃H) and purified by HPLC (section 6.3.1.3), and analysed by MS (section 6.3.2.2)

6.4.1.2 Reduction of AS2mB with TCEP and bimane-labelling of the products

HPLC purified AS2mB was diluted into 20 mM Hepes pH 8 and split in 3 aliquots. Aliquot 1 was left for 20 min at RT in dark (control). Aliquot 2 was reduced by incubation with 10 mM TCEP for 20 min in dark at RT (reduced). Aliquot 3 was treated as aliquot 2, but subsequently the reaction mixture was incubated with 20 mM mBBr (final concentration) for 10 min in the dark at RT (reduced and labelled). All reactions were stopped by adding 50 mM MeSO₃H (final concentration) and analysed by HPLC (section 6.3.1.3).

6.4.1.3 Reaction of DAS3, DAS4 or DAS5 with GSH

1 M stock solutions of DAS3, DAS4 or DAS5 in CH₃CN and 100 mM GSH stock solution in H₂O were diluted 10-fold in 25 mM Hepes pH8 50% CH₃CN. 10 µL aliquots were added to 90 µL mBBr mix (5 mM mBBr, 20 mM Hepes buffer, pH 8 in H₂O) at different time points (10 sec, 1 min, 5 min, 10 min, 20 min, 50 min, 120 min for DAS3 and 10 sec, 1 min, 5 min, 10 min, 25 min and 60 min for DAS4 and DAS5) and incubated at RT in the dark for 10 min. A negative control was done for GSH incubated with mBBr without any DAS3, DAS4 or DAS5. The bimane labelling reactions were stopped with 1 µL of 5 M MeSO₃H. Bimane labelled products were analysed by HPLC (section 6.3.1.3) after 10-fold dilution with 10 mM MeSO₃H and by MS (section 6.3.2.2). Identified products for all reactions were ASmB and AS2mB, additionally for the reaction of DAS4 and DAS5 with GSH AS3mB was identified as a product.

6.4.2 Formation of mixed polysulfides

6.4.2.1 Reaction of DAS3, DAS4, DAS5, DAS6 with GSH

A stock solution of GSH in 50 mM NaPO₄ buffer, pH 7, and 10 mL MeOH were each degassed by bubbling N₂ through the solutions for five to ten minutes. DAS3, DAS4, DAS5 or DAS6 (33 µmol) was dissolved in the N₂ purged MeOH (DAS3: 5.3 µL in 500 µL MeOH, DAS4: 5.7 µL in 900 µL MeOH, DAS5: 6.4 µL in 1100 µL MeOH or DAS6: 7.3 µL in 1300 µL MeOH) and mixed with 150 µL GSH stock solution (1 mg GSH, 3.3 µmol in 50 mM NaPO₄ buffer, pH 7) in 15 mL falcon tubes. After mixing, the reaction mixtures were degassed with N₂ again, sealed and kept stirring under N₂ at RT in the dark overnight. The next day, aliquots were taken out of each reaction for HPLC analysis and to the remaining reaction mixture 500 µL H₂O were added and washed with hexane (5x 1 mL). Reaction mixtures were dried under vacuum and analysed by ¹H-NMR in D₂O.

Reaction aliquots taken before drying and washing with hexane, were analysed by two different HPLC methods (section 6.3.1.1 and 6.3.1.2) to quantify distribution of different DAS and AGS_n in the reaction mixtures.

6.4.2.2 Reaction kinetics of DAS3-DAS5 with GSH analysed by NMR spectroscopy

Stock solutions of GSH in D₂O and DAS in MeOD were prepared and purged with N₂. Appropriate volumes of the stock solutions (Table 6.7) were mixed together and filled up with MeOD (final volumes: 100 μL D₂O and 400 μL MeOD). The pH was measured with a micro pH probe (Jenway 3510 pH Meter) and adjusted by adding small amounts of NaOH or HCl diluted in D₂O. The N₂ purged mixture was transferred into an N₂ purged NMR tube. The tube was sealed and ¹H-NMR spectra were recorded periodically until no further changes in the spectra were observed. Time intervals between NMR experiments were adjusted depending on the speed of the reaction.

Table 6.7: Reactant concentrations for reactions between DAS3 to DAS5 with GSH. *calculations based on a thiol pK_a of 8.93 for GSH.

Reactants	Molar ratio	DAS (mM): GSH (mM)	GS ⁻ (μM)*	pH
DAS3+GSH	1:1	6.4: 6.4	18.56	6.4
DAS3+GSH	1:5	6.4: 32	7.36	5.3
DAS4+GSH	1:1	6.4: 6.4	0.12	4.2
DAS4+GSH	1:5	6.4: 32	0.30	3.9
DAS5+GSH	1:5	6.4: 32	0.03	2.9

For analysis of the spectra and calculation of molar concentrations of the species in the solution, the integral for the multiplet at 2.47-2.60 ppm representing the two protons (CH₂-C=O) of the glutamic acid part of GSH was normalised to the total initial GSH concentration in solution. Accordingly, the doublets between 3 and 4 ppm representing the two protons of the allyl CH₂-S groups were integrated and concentrations for DAS and AGS_n were calculated.

6.4.2.3 Reaction of DAS2 and DAS5 with BSH

DAS2+ BSH

The reaction of DAS2 with BSH yielded pure ABS2 and is described in section section 6.2.3.

DAS5+ BSH

BSH (1 mg, 2 μmol) in 150 μL NaPO₄ buffer (100 mM, pH7) and DAS 5 (4 μL, 20 μmol) in 1 mL MeOH were individually purged with N₂, mixed together and purged with N₂ again. The reaction was sealed and kept stirring at RT overnight in the dark. An aliquot of the crude reaction mixture was analysed on HPLC (section 6.3.1.2) and ABS2 (rt=3.1. min) and two additional peaks at higher retention times were observed (rt=4.8 min and 9.8 min). Subsequently the reaction mixture was washed with hexane (2x 1 mL), dried in a vacuum centrifuge and analysed by ¹H-NMR in D₂O. ¹H-NMR mainly showed ABS2 and repeated HPLC analysis of an aliquot of the NMR sample also showed mainly ABS2. Because of instability of higher ABS_n (n>2), they could not be isolated and characterised, but the observation of two additional peaks at higher retention times by HPLC analysis before work-up of the reaction suggests the formation of ABS3 and ABS4.

6.4.2.4 Reaction of DAS2 and DAS5 with Cys

DAS2+ Cys

Cys (4.4 mg, 36 μmol) in 3.5 mL NaPO_4 buffer (100 mM, pH 7) and DAS2 (110 μL , 720 μmol) in 3.5 mL MeOH were individually purged with N_2 , mixed together and purged with N_2 again. The reaction was sealed and kept stirring at RT overnight in the dark. An aliquot of the crude reaction mixture was analysed on HPLC (section 6.3.1.2) and cystine (CySS) (rt=2.7 min) and an additional peak (rt=3.4 min) were detected. Subsequently, the reaction mixture was dried under vacuum, washed with H_2O (2 x 1 mL, to remove buffer) and dissolved in D_2O containing 300 mM HCl for $^1\text{H-NMR}$ analysis to confirm the formation of CySS and allyl-cysteine disulfide (ACS2).

DAS5+ Cys

Cys (0.44 mg, 3.6 μmol) in 75 μL NaPO_4 buffer (100 mM, pH 7) and DAS5 (4 μL , 20 μmol) in 1 mL MeOH were individually purged with N_2 , mixed together and purged with N_2 again. The reaction was sealed and kept stirring at RT overnight in the dark. An aliquot of the crude reaction mixture was analysed on HPLC (section 6.3.1.2) and CySS (rt=2.7 min), ACS2 (rt=3.4 min) and three additional peaks at higher rt were observed (rt=5.2 min, 9.6 min and 21.1 min). Subsequently the reaction mixture was washed with hexane (3x 2 mL), dried in a vacuum centrifuge and dissolved in D_2O containing 300 mM HCl for $^1\text{H-NMR}$ analysis. The different peaks were isolated through HPLC purification, but not enough material could be collected for NMR analysis of isolated compounds. Only the mass of ACS4 was confirmed by LC-MS.

6.4.2.5 Comparable reactivity of DAS5 with GSH vs. Cys or BSH vs. Cys

Stock solutions of GSH (10 mM, pH 7.2), Cys (10 mM, pH 7.2 and pH 7.7) and BSH (10 mM, pH 7.7) were made up in 50 mM NaPO_4 buffer after DTNB quantification of the thiols. A DAS5 stock solution (10 mM) was prepared in MeOH and all stock solutions were purged with N_2 .

Reactivity of DAS5 with GSH vs. Cys

100 μL of each stock solution (GSH, Cys and DAS5) were mixed with 700 μL NaPO_4 buffer (50 mM, pH 7.2) and purged with N_2 , sealed and kept stirring at RT. Reaction aliquots were analysed by HPLC (section 6.3.1.2) after 10 min, 2 h, 6 h and 20 h using 40% solvent B. Control experiments only using Cys and DAS5 or GSH and DAS5 were performed and analysed by HPLC in the same way.

Reactivity of DAS5 with BSH vs. Cys

100 μL of each stock solution (BSH, Cys and DAS5) were mixed with 700 μL NaPO_4 buffer (50 mM, pH 7.7) and purged with N_2 , sealed and kept stirring at RT. Reaction aliquots were analysed by HPLC (section 6.3.1.2) after 10 min, 2 h, 6 h and 20 h using 40% solvent B. Control experiments only using Cys and DAS5 or BSH and DAS5 were performed and analysed by HPLC in the same way.

6.5 *In vivo* experiments

6.5.1 Bacteria

6.5.1.1 Culturing of *B. subtilis* and *E. coli*

B. subtilis CU1065 WT and *B. subtilis* CU1065 HB11002 *bshA*::*mls*⁽⁵⁵⁾ were received from Prof. J. D. Helmann (Cornell University, USA). Both strains were cultivated either in luria broth (LB) or Belitsky minimal media (BMM) at 37 °C, media for the *bshA*⁻ mutant contained lincomycin (25 mg/L) and erythromycin (1 mg/L).

E. coli K12 was received from Prof. A. J. Slusarenko (RWTH Aachen University, Germany). The strain was grown in LB media at 37 °C.

LB media was made up from 1% tryptone, 1% NaCl, 0.5% yeast extract and 1.7% agar for solid media.

BMM was made up from basal medium [containing 15 mM NH₄SO₄, 8 mM MgSO₄, 27 mM KCl, 7 mM sodium citrate and 50 mM tris(hydroxymethyl)aminomethane hydrochloride (Tris HCl) pH 7.5 (Tris HCl autoclaved separately)] which was autoclaved before use. Supplements (2 mM KH₂PO₄, 2 mM CaCl₂, 10 μM FeSO₄, 10 μM MnSO₄, 4.5 mM glutamic acid, 780 μM tryptophane, 0.2 % glucose) were sterile filtered, stored at 4°C and added to the basal medium immediately before use. For solid media 1.7% agar was added to the basal medium before autoclaving.

6.5.1.2 Culture maintenance and storage of *B. subtilis* and *E. coli*

Bacterial strains were grown on LB plates (containing 25 mg/L lincomycin and 1 mg/L erythromycin for the *bshA*⁻ mutant) at 37°C overnight and afterwards stored at 4°C. They were plated onto fresh plates every fortnight. For long term storage bacteria strains were kept as glycerol stocks at -80°C.

6.5.1.3 *B. subtilis* and *E. coli* growth in liquid culture

Liquid media (LB or BMM) was inoculated with a bacterial colony taken from agar plates and incubated at 37 °C while shaking at 200 revolutions per minute (rpm). For growth experiments fresh media was inoculated with 1 or 1.5% (v/v) of liquid overnight culture and the OD₆₀₀ was measured in regular time intervals.

6.5.1.4 Growth curves of bacterial populations under stress conditions

Tested concentrations against *B. subtilis* WT and *bshA*⁻ mutant (μM): DAS2: 750, 500, 250, 100; DAS3: 250, 200, 150, 100, 50; DAS4: 100, 50, 25; DAS5: 50, 25; DAS6: 50, 25.

To test the influence of DAS on the growth of cultures of *B. subtilis* WT and *bshA*⁻ mutant in BMM, 100-fold concentrated stock solutions of different DAS in EtOH were prepared and added to the culture once it had reached OD₆₀₀=0.5. To an untreated control culture 1% EtOH (final concentration) was added and the population densities of treated and untreated cultures were compared by monitoring the OD₆₀₀ over time. Pure BMM was used as background for OD₆₀₀ measurements and for OD₆₀₀ values >1 the culture was diluted with BMM to get a measurement <1.

6.5.1.5 Determination of Minimum Inhibitory Concentrations (MIC) of DAS against *B. subtilis* WT and the *bshA*⁻ mutant on agar plates

Tested concentrations against *B. subtilis* WT and *bshA*⁻ mutant (mg/L): DAS1: 1024; DAS2: 1024, 512, 256; DAS3: 1024, 512, 256, 128; DAS4: 128, 64, 32, 16, 8; DAS5: 64, 32, 16, 8, 4, 2, 1; DAS6: 64, 32, 16, 8, 4, 2, 1

Overnight cultures of *B. subtilis* WT and *bshA*⁻ mutant in BMM were used to inoculate fresh BMM and grown to an OD₆₀₀ of 1. 100-fold concentrated stock solutions of DAS were prepared in 10% EtOH (DAS were dissolved in 100% EtOH first, then diluted down to 100-fold concentrated stocks containing 10% EtOH). Belitsky Minimal agar was prepared (sterile mineral supplements and Tris were added to the warm agar after autoclaving) and 2970 µL of agar was given into each petri dish (3 cm diameter). 30 µL of the DAS stocks were added and mixed into the agar by stirring with a pipette tip. As controls 30 µL of 10% EtOH or 30 µL of sterile H₂O or 4 mg/L final concentration of chloramphenicol (Cm) was added to the agar. Plates were prepared in triplicates for each compound. After the agar plates were dried, two drops of 2 µL of *B. subtilis* WT and *B. subtilis bshA*⁻ overnight culture (diluted to OD₆₀₀=1) were dropped onto each plate and incubated at 37°C for 16 h.

The plates were observed for growth the next morning and after 4 days, using a microscope if required. For each DAS the lowest concentration that inhibits the growth of the bacteria after 16 h of incubation is reported as the MIC.

6.5.1.6 Determination of MICs of DAS against *B. subtilis* WT and the *bshA*⁻ mutant in liquid media (96 well plates)

Tested concentrations against *B. subtilis* WT and [*bshA*⁻ mutant](mg/L): DAS1: 1024 [1024], DAS2: 1024, 512, 256 [1024, 512, 256]; DAS3: 1024, 512, 256, 128 [1024, 512, 256, 128]; DAS4: 128, 64, 32, 16, 8 [128, 64, 32, 16, 8]; DAS5: 64, 32, 16 [16, 8, 4, 2]; DAS6: 64, 32, 16 [16, 8, 4, 2].

Fresh BMM was inoculated with overnight cultures of *B. subtilis* WT and *bshA*⁻ mutant and grown to an OD₆₀₀=1. The culture was diluted down to 1% in fresh BMM and 180 µL of diluted culture was mixed with 20 µL of 10-fold concentrated stock solutions of DAS (containing 10% EtOH, first dissolved in 100% EtOH and then diluted down in H₂O) into each well. Each concentration was tested in triplicates against each bacterial strain. Only one concentration of DAS was applied (into three wells) in each column and at least one column (only containing bacterial culture) was kept clear between each DAS treatment to avoid DAS contamination of adjacent wells through the gas phase. For each of the DAS at each concentration a blank was mixed into one well, containing only BMM and DAS, no bacteria. These wells were used as the background and were subtracted from the OD₆₀₀-reading of the actual sample. As a control for sterility some wells were only filled with BMM without any DAS and bacteria. As a control for proper application and mixing of the drug Cm was added to some wells at a final concentration of 4 mg/L. All controls were included in each plate and separate plates were used for different bacteria strains. The plates were sealed with parafilm and bacteria were grown at 37°C at 350 rpm for 16 h. Subsequently the OD₆₀₀ was measured in a 96 well plate reader while shaking at 400 rpm and using 50 flashes per well. Each plate was measured twice and averages of the readings were taken. The corresponding blank readings were subtracted from the average of the sample readings. OD₆₀₀ values ≥ 0.1 were interpreted as growth and OD₆₀₀ values <0.1

were interpreted as no growth. For each of the DAS, the lowest concentration used, that inhibited the growth, is reported as the MIC.

6.5.1.7 *In vivo* analysis of DAS and LMW thiols and disulfides and DAS metabolites in *B. subtilis*

6.5.1.7.1 Harvesting of *B. subtilis* cells

Cells were grown in liquid culture and aliquots of the culture were transferred into 50 mL falcon tubes at different time points and centrifuged for 3 min at 12,000 g at 4°C. Afterwards the supernatant was discarded and the cell pellet was re-suspended and transferred into a pre-weighed eppendorf tube. The cell paste was centrifuged again at 12,000 g for 3 min and the supernatant was discarded before freezing the cell pellet in liquid N₂. Cell pellets were stored at -20°C until derivatisation for thiol and disulfide analysis was performed.

6.5.1.7.2 Relationship between the OD₆₀₀ and residual dry weight of *B. subtilis* cultures

LB media was inoculated with 1.5% overnight culture of the *B. subtilis* WT and samples were taken from duplicate cultures at OD₆₀₀ values between 0.4 and 2.8. The samples of known volume were concentrated through centrifugation (12,000 g, 5 min) and the cell pastes were dried in an oven overnight at 60°C. The rdw of the pellets was determined and the rdw/mL of culture was plotted over the OD₆₀₀. In future experiments this relationship was used to calculate the required culture volume at different OD₆₀₀ that results in a rdw of 5 mg.

6.5.1.7.3 Development of labelling conditions for complete thiol labelling

B. subtilis cells were grown to an OD₆₀₀ of 1 and aliquots corresponding to approximately 6 mg rdw were harvested and different volumes of different concentrated mBBr mix (Table 6.8), all containing 20 mM Hepes pH8 and 50% CH₃CN was given to the cell pastes for derivatisation. The samples were vortexed vigourously and incubated for 60°C for different time durations. After cooling on ice, MeSO₃H was added to a final concentration of 25 mM and the reactions were vortexed and centrifuged at 12,000 g for 5 min. The pellets were dried overnight at 60°C and weighed. The supernatant was filtered through a 0.2 µm membrane, and thiol samples were diluted five-fold with 10 mM MeSO₃H prior to analysis by HPLC. HPLC peak areas were converted into mM concentrations for BSmB and CysmB and Table 6.8 shows that all conditions, except 0.5 mM mBBr, led to the same BSmB and CysmB concentrations, within the experimental error.

Table 6.8: Different mBBr labelling conditions used for labelling of cells corresponding to approximately 6 mg rdw. For all samples mBBr was dissolved in 20 mM Hepes (pH8), 50 % CH₃CN and samples were incubated in the dark at 60 °C.

Vol (µl)	mBBr (mM)	EDTA (mM)	Time (min)	BSmB (mM)	CysmB (mM)
120	2	0	15	1.27	0.24
120	2	0	30	1.11	0.21
480	2	0	15	1.36	0.31
120	10	0	15	0.91	0.20
120	2	2	15	1.23	0.23
120	0.5	0	15	0.80	0.06
120	2	0	10	1.37	0.24

6.5.1.7.4 Thiol analysis in *B. subtilis*

Frozen cell pellets (corresponding to approximately 5 mg rdw) were vortexed vigorously in 120 μ l of mBBr mix (20 mM Hepes pH 8, 50% CH₃CN, 2 mM mBBr) and then incubated at 60°C for 15 min in the dark. After cooling on ice, MeSO₃H was added to a final concentration of 25 mM and the reactions were vortexed and centrifuged at 12,000 g for 5 min. The pellets were dried overnight at 60°C and weighed. The supernatant was filtered through a 0.2 μ m membrane, and thiol samples were diluted five-fold with 10 mM MeSO₃H prior to analysis by HPLC.

6.5.1.7.5 Disulfide analysis in *B. subtilis*

Method 1)

For disulfide analysis frozen cell pellets (corresponding to approx. 5 mg rdw) were resuspended in 100 μ L of *N*-ethylmaleimide (NEM) mix (20 mM Hepes, pH 8, 50% CH₃CN, 5 mM NEM) and then incubated at 60°C for 15 min. After centrifugation at 12,000 g for 5 min the supernatant was taken off and treated with 7 mM dithiothreitol (DTT) and incubated for 20 min at RT. Subsequently mBBr was added to a final concentration of 18 mM and incubated for 15 min at RT in the dark before adding MeSO₃H to a final concentration of 50 mM. The pellets were dried overnight at 60°C and weighed. The supernatants were filtered through a 0.2 μ m membrane, and diluted five-fold with 10 mM MeSO₃H prior to analysis by HPLC.

Method 2)

For disulfide analysis frozen cell pellets (corresponding to approx. 30 mg rdw) were resuspended in 1 mL of NEM mix and then incubated at 60°C for 15 min. After centrifugation at 12,000 g for 5 min the supernatant was taken off and 5 mM β -mercaptoethanol (ME) were added to the supernatant and incubated for 10 min at RT. The samples were concentrated to 100 μ L in a vacuum centrifuge and 2 mM DTT were added followed by 15 min incubation at RT. Subsequently 9 mM mBBr were added and incubated for 15 min at RT in the dark before adding MeSO₃H to a final concentration of 100 mM. The pellets were dried overnight at 60°C and weighed. The supernatants were filtered through a 0.2 μ m membrane, and diluted two-fold with 10 mM MeSO₃H prior to analysis by HPLC.

Method 3)

For disulfide analysis frozen cell pellets (corresponding to 10 to 20 mg rdw) were resuspended in 500 μ L of NEM mix and then incubated at 60°C for 15 min. After centrifugation at 12,000 g for 5 min, the supernatant was taken off and excess NEM and DAS were extracted with diethyl ether (Et₂O) (3 x 1 mL). The supernatant (volume reduced to 250 μ L, because 50% CH₃CN were removed with the Et₂O extract) was incubated with 8 mM DTT for 20 min at RT. Subsequently mBBr was added to a final concentration of 20 mM and incubated for 15 min at RT in the dark before adding MeSO₃H to a final concentration of 50 mM. The cell pellets were dried overnight at 60°C and weighed. The supernatants were filtered through a 0.2 μ m membrane, and analysed undiluted or were diluted two-fold with 10 mM MeSO₃H prior to HPLC analysis.

6.5.1.8 Western Blot of *B. subtilis* proteins for detection of bacillithiolated proteins after DAS stress

Buffers and Reagents for Western Blot:

Lysis buffer: 1 mM EDTA, 200 mM Tris-HCl pH 8, Lysozyme 2 mg/mL, Benzonase 3.45 μ L/mL

Electrophoresis buffer: 25 mM Tris-HCl pH 8.3, 250 mM glycine, 0.1% (w/v) sodium dodecyl sulfate (SDS)

Transfer buffer: 2.426 g/L Tris base, 11.26 g/L glycine, 0.1 g/L SDS, 20% (v/v) MeOH

TBS buffer: 3 g/L Tris base, 4.5 g/L NaCl, pH 7.6

TBST buffer: TBS + 0.1% (v/v) polysorbate (Tween) 20

Blotto solution: TBST+2.5% (w/v) milk powder, Blotto solution was prepared fresh on the day and stored at 4°C until used.

BSH antibody: 250-fold dilution in TBS with 5% (w/v) milk powder

The BSH antibody was generously provided by Haike Antelmann (Institute for Microbiology, Ernst-Moritz-Arndt-University of Greifswald, Germany) ⁽⁶³⁾.

IgG antibody: Monoclonal Anti-rabbit IgG (gamma chain specific) –alkaline phosphatase, antibody produced in mouse, Sigma): 1:200,000 dilution in TBST

Alkaline phosphatase buffer (AP buffer): 100 mM NaCl, 5 mM MgCl₂, 100 mM Tris-HCl pH 9.5, (added 0.165 mg/mL 5-bromo-4-chloro-3'-indolylphosphate p-toluidine salt (BCIP), 0.33 mg/mL nitro-blue tetrazolium chloride (NBT) for detection of proteins)

Cell growth and lysis

For Western Blot analysis *B. subtilis* cells were grown in BMM and treated with 200 µM DAS3 or 400 µM or 800 µM DAS2 dissolved in EtOH (final EtOH concentration 1%). To the untreated control only 1% EtOH was added. 10, 30 and 60 min after adding DAS, cells (corresponding to approximately 5 mg rdw) were concentrated by centrifugation (12,000 g, 5 min) and re-suspended in 200 µL lysis buffer. The cells were left on ice in the dark for 1 h and subsequently centrifuged for 30 min at 12,000 g. The supernatant was transferred and the cell pellet was dried overnight at 60°C.

SDS PAGE gel

An aliquot of the supernatant of the lysed cells (10 µL) was mixed with 5 µL Laemmli sample buffer and boiled at 95°C for 5 min. After cooling to RT the samples were loaded onto 4-20% (w/v), denaturing, non-reducing, SDS-Polyacrylamide gel electrophoresis (PAGE) gels. As a positive control bacillithiolated methionine synthase (MetE) and as a negative control native MetE were applied (provided by Dr. Alexandra A. Roberts, School of Pharmacy, University of East Anglia, UK) ⁽⁶⁴⁾. The gel ran at 185 Volt (V) for 30-60 min in electrophoresis buffer and was subsequently stained with Coomassie blue. For Western Blot, another gel was run with the same samples, where the protein content was adjusted depending on the results of the first gel. To perform a Western Blot the gel was not stained after running.

Western Blot

The Western Blot was done in transfer buffer for 1 h at 100 V. The membrane was washed in TBS buffer and incubated in Blotto solution for 90 min. Afterwards the membrane was washed twice in TBST and incubated overnight with BSH antibody. The next day the membrane was washed three times in TBST buffer and incubated for 1 h with IgG antibody. Subsequently it was washed three times with TBST and once with TBS. All washes were done for 10 min while the membrane was shaken gently except for the following staining step. The membrane was incubated in 10 mL staining solution (AP buffer containing BCIP and NBT) and stained until the

bands on the membrane appeared in satisfactory intensity (1-5 min). The staining solution was removed and the membrane was kept in H₂O.

6.5.2 Nematodes

6.5.2.1 Culture maintenance and storage of *Steinernema feltiae* and *Meloidogyne minor*

Steinernema feltiae nematodes (Just Fungus Fly Killer) were purchased from Just Green, Essex, UK and were stored in dry powder for up to three weeks at 4°C. For experimental work a spatula of *S. feltiae* was suspended in lukewarm H₂O in a beaker and stirred occasionally for at least 1 h. Viability of nematodes was checked by observation of nematodes using a Meiji binocular at 45x magnification. Nematode concentrations in solution were adjusted depending on the experimental requirement by counting nematode numbers in several aliquots and subsequent dilution of the suspension with H₂O. To observe nematodes under the binocular 5 to 20 µL drops of nematode suspension were given onto a microscope slide. Nematode suspensions were kept for not more than 48 h and viability was ensured before each experiment.

Meloidogyne minor nematodes were provided by Dr. Colin C. Fleming (Agri-Food and Bioscience Institute (AFBI), Belfast, Northern Ireland) and experiments with *M. minor* were carried out at AFBI.

6.5.2.2 Mortality assay with *S. feltiae*

Nematode suspensions in H₂O were adjusted to approx. 12,000 nematodes/mL. DAS solutions were prepared as 100x stock solutions in EtOH, diluted in H₂O to 10x stock solutions and subsequently 500 µL of nematode suspension were mixed with 100 µL 10x DAS solution and 400 µL H₂O. 1 mL aliquots contained approx. 30 nematodes/5µL and 1% EtOH. A control containing 1% EtOH and no DAS was also prepared. The eppendorf tubes containing nematodes incubated in DAS were coded with random letters to perform a blind experiment. During incubation, the eppendorf tubes were kept slightly open and before taking aliquots for counting, the samples were mixed well. From each sample 3x 5 µL were pipetted onto a microscope slide and nematodes were observed and categorised into live and dead nematodes through observation in a binocular at 45x magnification. Live nematodes move quickly and undulating while dead nematodes are immobile and straight. Live and dead nematodes were counted at different time points and after 24 h, DAS solutions were removed and H₂O was added to the nematodes. Live and dead nematodes were counted again after 24 h in H₂O. The mean percentage of dead nematodes at each time point was plotted against the DAS concentration, which shows the dose dependent mortality of *S.feltiae* after different incubation times.

6.5.2.3 Thiol and Disulfide analysis in *S. feltiae*

6.5.2.3.1 Incubation and harvesting of *S. feltiae*

For thiol analysis nematode suspensions were adjusted to 10,000 nematodes/mL H₂O and for each treatment 900 µL nematode suspension was mixed with 100 µL of 10x concentrated DAS solution in 10% EtOH. The nematodes were incubated and at different time points aliquots (3x 100 µL for thiol analysis, containing 1000 nematodes, 3x 200 µL for total protein analysis,

containing 2000 nematodes), of each treatment were taken and concentrated through 10 min centrifugation at 14,000 rpm. The nematodes were washed 3x with 10 mM Hepes buffer (pH 7.5) and finally all samples were concentrated to 50 μ L.

For disulfide analysis nematode suspensions were adjusted to approx. 20,000 nematodes/mL H₂O and after incubation with DAS, 3x 1.2 mL (containing approx. 80,000 nematodes) were harvested and washed 3x with 10 mM Hepes pH 7.5.

All nematode samples were frozen in liquid N₂ immediately after processing and stored at -20°C until chemical derivatisation.

6.5.2.3.2 Thiol analysis in *S. feltiae*

200 μ L of mBBr mix (20 mM Hepes pH8, 2 mM mBBr, 5 mM EDTA in H₂O) and 100 μ L of zirconium beads (1 mm, Biospec Products, Thistle Scientific) were added to 50 μ L nematode samples. The samples were beaten in a bead beater (Disruptor Gene, Scientific Industries) for 3x 20 sec with 40 sec cooling on ice between the bead beating cycles. Afterwards they were incubated for 10 min at 60°C in the dark. After cooling to RT the supernatant was clarified from cell debris and beads by 10 min centrifugation at 14,000 rpm and the supernatant was acidified with 1 μ L 5 M MeSO₃H. The samples were diluted two-fold in H₂O, filtered through a 0.2 μ m membrane and injected on HPLC using the HPLC method for biman adducts as described in section 6.3.1.3.

6.5.2.3.3 Disulfide analysis in *S. feltiae*

Each sample (containing 80,000 nematodes) was suspended in 1.2 mL 20 mM Hepes pH8 and NEM was added to a final concentration of 5 mM. 600 μ L zirconium beads were added and samples were beaten 3x 20 sec with cooling on ice for 40 sec between the cycles. Afterwards samples were incubated for 10 min at 60°C. After cooling to RT the supernatant was cleared from the cell debris and the beads through centrifugation at 14,000 rpm for 2x 10 min. 50 μ L of the supernatant was incubated with mBBr at a final concentration of 2 mM for 10 min at RT and acidified with 0.5 μ L MeSO₃H to show fluorescent background peaks not derived from thiols. 550 μ L of the supernatant were treated with 5 mM ME and incubated for 10 min at RT. The samples were concentrated to 100 μ L in a vacuum centrifuge and 2 mM DTT were added. After 15 min incubation at RT, 9 mM mBBr were added followed by 15 min incubation at RT in the dark. The samples were acidified with 2 μ L MeSO₃H, filtered through a 0.2 μ m membrane and injected undiluted or two-fold diluted onto the HPLC (method described in section 6.3.1.3).

6.5.2.3.4 Total protein content in *S. feltiae*

Total protein content of nematode extracts was determined using a Pierce® 660 nm Protein Assay Kit (Thermo Fisher) according to the manufacturer's instructions. To each 50 μ L sample 100 μ L Laemmli buffer were added and the samples were boiled for 5 min at 95 °C, immediately frozen in liquid N₂ for 5 min and then kept at 95°C until thawed. 50 μ L zirconium beads were added and the samples were beaten using a bead beater (3x 20 sec, interrupted by 40 sec on ice between each cycle). The samples were spun at 14,000 rpm for 10 min and 50 μ L supernatant was taken off and mixed with 750 μ L Pierce® 660nm Protein Assay reagent. The absorbance at 660 nm was measured with a UV spectrophotometer and protein concentrations were calculated according to a standard curve which was established using

known concentrations of pre-diluted protein (Bovine Serum Albumin), which was delivered as part of the assay kit.

6.5.2.3.5 Analysis of nematode washing solutions

Nematodes were suspended in 2 mL H₂O (approx. 100 nematodes/5 µl) and 750 µM DAS3 were added. The nematodes were incubated for 40 min and subsequently the supernatant was taken off and frozen in liquid N₂. 1 mL of Hepes buffer (20 mM pH 7.5) was added, mixed with the nematodes, vortexed gently, spun down and the supernatant was taken off again. This wash was repeated once more and an additional wash was done in the same way, but 10% CH₃CN was added to the Hepes buffer for washing. All wash solutions were immediately frozen in liquid N₂ and analysed for thiols and disulfides as described below.

6.5.2.3.6 Thiol and disulfide analysis of the incubation media of *S. feltiae*

For thiol analysis of the incubation media of nematodes, an aliquot of 100 µL supernatant was taken and Hepes pH8 (final concentration of 20 mM) and mBBR (final concentration of 2 mM) were added. The samples were incubated for 10 min at RT in the dark and then acidified with 0.6 µL of 5 M MeSO₃H.

For disulfide analysis 20 mM Hepes pH8 and 3 mM NEM were added to 100 µL of supernatant. After 15 min incubation at RT, 5 mM DTT were added and incubated for 20 min at RT. MBBR was added to a final concentration of 12 mM and after 15 min incubation at RT in the dark the sample was acidified with 0.6 µL of 5 M MeSO₃H.

All derivatised supernatants were filtered through a 0.2 µm membrane and injected undiluted onto the HPLC.

6.6 Field trials

All soil sample analyses and determination of nematode populations and egg numbers were performed by Dr. Coiln C. Fleming (Agri-Food and Bioscience Institute (AFBI), Belfast, Northern Ireland).

6.6.1 Carrot trial

The carrot trials were performed on fields in Goole, Yorkshire (M.H. Poskitt Ltd, Kellington, UK) on sandy loam. The carrots (variety Nairobi) were drilled in early April 2012 and all applied nematicides (granule formulations) were applied at a single time point at the time of drilling.

6.6.1.1 Treatments in the carrot trial

Two different garlic-based treatments were included in the trial: NEMguard® (20 kg/ha ECOspray Ltd.) and TDE5 (10 kg/ha or 20 kg/ha, ECOspray Ltd.).

As a positive control Vydate® (20 kg/ha, DuPont) containing oxamyl as active ingredient was used.

6.6.1.2 Carrot sampling and assessment

6.6.1.2.1 Early carrot assessment

17 weeks after drilling two rows of carrots across 1 m length were harvested for each treatment. The total yield (by weight and numbers) and percentage root damage (by weight and numbers) were determined for the different treatments. Additionally, the 30 biggest carrots for each treatment were lined up and photographed for a visual comparison of the treatment effects.

6.6.1.2.2 Late carrot assessment

23 weeks after drilling, two rows of carrots across 1 m length were harvested in 5 replicates for each treatment. The total yield and premium yield (crown diameter of 25-40 mm and minimum length of 14 cm) (by weight) as well as percentage root damage (by weight) were determined for different treatments and the untreated controls.

6.6.1.3 Soil sampling and assessment for nematode numbers in the carrot field

Soil samples were analysed and nematode species and numbers were determined seven weeks after planting.

6.6.2 Potato trial

The potato trial was conducted at Stowbridge Farm, Stretham (Adam Palmer, East of England) on organic soil using Maris Piper potatoes, a potato cultivar with resistance against the yellow potato cyst nematode (yPCN, *Globodera rostochiensis*)⁽¹⁵¹⁾. All applied nematicides are granule formulations and were applied at a single time point at the time of drilling (26/04/13).

6.6.2.1 Treatments in the potato trial

A garlic-based treatment, TDE5 (40, 60, 90 or 120 kg/ha, ECOSpray Ltd.), and two positive control nematicides, Vydate® (55 kg/ha, DuPont) containing oxamyl as active ingredient, and Nemathorin® (35 kg/ha, Syngenta), containing fosthiazate as active ingredient, were used.

6.6.2.2 Potato trial design

6.6.2.2.1 Paired potato trial

The paired trial included two treatments: Nemathorin (35 kg/ha) and TDE5 (60 kg/ha) separated by an untreated control. Each treatment and the untreated control included four rows of potatoes across approx. 200 m length.

6.6.2.2.2 Randomised potato trial

The randomised trial included TDE5 in four different rates (40, 60, 90 and 120 kg/ha), Vydate (55 kg/ha) and an untreated control. The five different treatments and the untreated control were arranged in five completely randomised blocks. Each bed consisted of three to four rows of potatoes at 4 m length.

6.6.2.3 Potato sampling and assessment

6.6.2.3.1 Paired potato trial

For each treatment six replicates (spread 40 m apart from each other across the field) of four plants were harvested six months after drilling and potatoes were size graded (25-35 mm, 35-45 mm, 45-65 mm, 65-80 mm, 80-90 mm) and yields were determined.

6.6.2.3.2 Randomised potato trial

All plots of the randomised trial were harvested completely 6.5 months (13/11/13) after drilling and potato yields (by weight) in different size grades (25-35 mm, 35-45 mm, 45-65 mm, 65-80 mm, 80-90 mm) for the different treatments were determined.

6.6.2.4 Soil sampling and assessment for nematode and egg numbers in the potato trial

Soil samples from the paired trials were taken before drilling and at the time of the harvest from the same positions in the field where potatoes were harvested for yield comparisons. Soil samples from the randomised trial were taken before drilling and at the time of harvest to compare initial and final egg numbers of PCN in the soil.

6.6.3 Statistical analysis

All obtained field trial results were statistically analysed using Microsoft Excel 2010 and a one tailed, type 2 (unpaired and independent, equal variances) t-test was performed.

Appendix 1 : Methodology to quantify LMW thiols and disulfides in cell extracts of *B. subtilis* and *S. feltiae*

1.1 Methodology overview

The methodology for the analysis of *B. subtilis* cell extracts is discussed in detail and the last section (Appendix 1.5) focusses on the differences of low molecular weight (LMW) thiol and disulfide analysis of cell extracts from nematodes. The thiol and disulfide analysis of cell samples involves a number of steps (Figure 1.1). As we investigated the influence of diallyl sulfides (DAS) on LMW thiol and disulfide concentrations in *B. subtilis*, cells were grown in liquid culture in the presence of DAS, growth curves were recorded and cells were harvested at different time points from the DAS treated and untreated control cultures. These cell pellets are used for fluorescent labelling and quantification of thiols and disulfides.

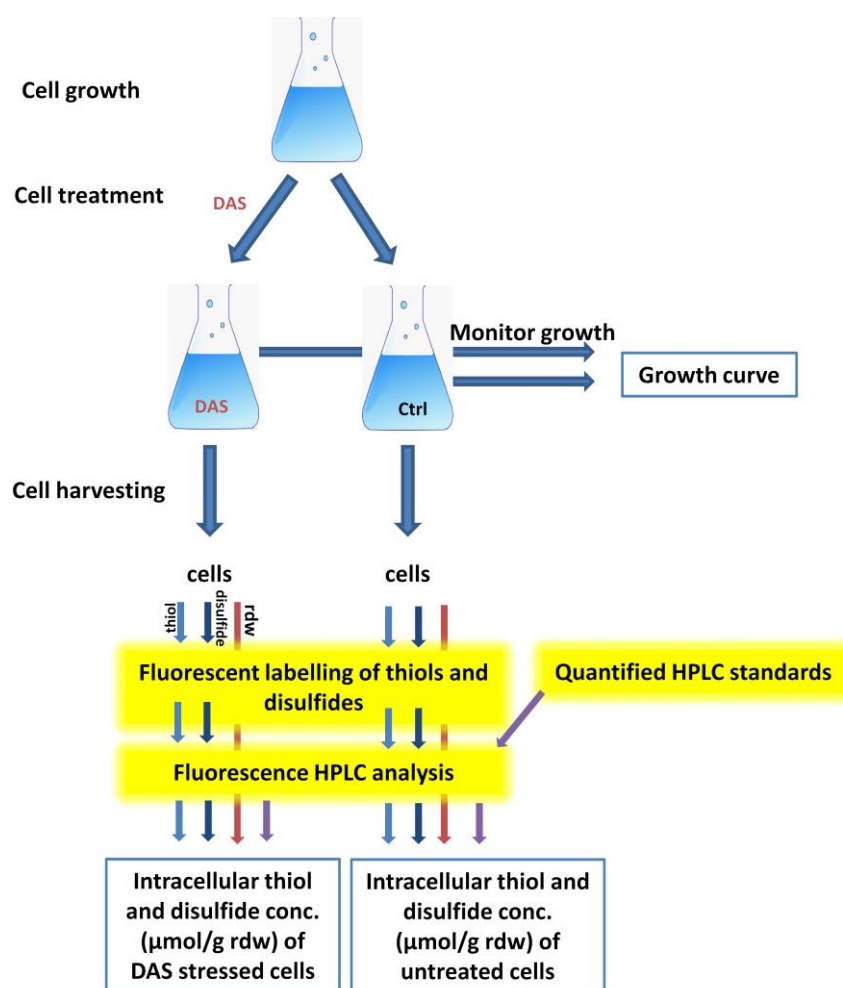


Figure 1.1: Overview of experimental steps involved in thiol and disulfide quantification of cell samples. rdw=residual dry weight.

To quantify intracellular LMW thiol levels, monobromobimane (mBBr) was used as a thiol selective labelling reagent ⁽¹⁵⁹⁾ as described previously ⁽¹⁵⁶⁾. Fluorescent thioethers (mBSR) are formed (Figure 1.2), which can be separated and analysed by fluorescence HPLC. Using this method, it is possible to analyse and quantify different thiols found in one sample/cell extract.

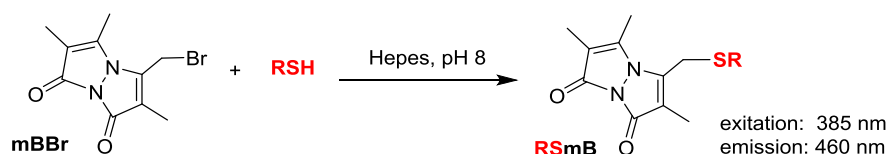


Figure 1.2: Fluorescent labelling of thiols with mBBr.

The disulfide analysis is performed indirectly in several steps: Firstly, all reduced thiols are irreversibly alkylated with *N*-ethylmaleimide (NEM), secondly disulfides are reduced with dithiothreitol (DTT) to form their corresponding thiols and thirdly the resulting thiols (derived from disulfides) are labelled with mBBr (Figure 1.3).

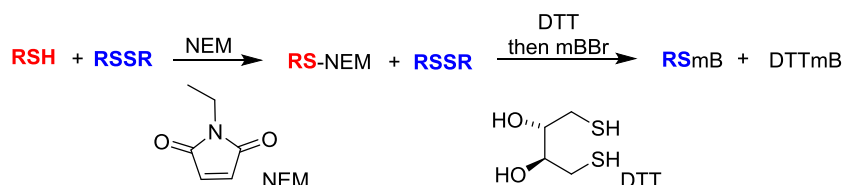


Figure 1.3: Disulfide analysis through irreversible alkylation of thiols, reduction of disulfides and mBBr labelling of reduced disulfides.

This method can be used to quantify picomole levels of thiols and disulfides by HPLC, and enables the quantification of cellular LMW thiol and disulfide concentrations from crude cell extracts.

1.2 Synthesis and characterisation of fluorescent thiol adducts as HPLC standards

Standard thiol-bimane adducts are needed to identify individual thiols from a crude mixture derived from a cell sample (Figure 1.4). Additionally, quantified standards are used to calculate molar concentrations of thiol adducts of unknown concentrations from their peak areas gained by fluorescence HPLC analysis. Cellular thiol content is reported as $\mu\text{mol thiol/g}$ residual dry cell weight (rdw), which can be converted into mM concentrations⁽⁹⁶⁾.

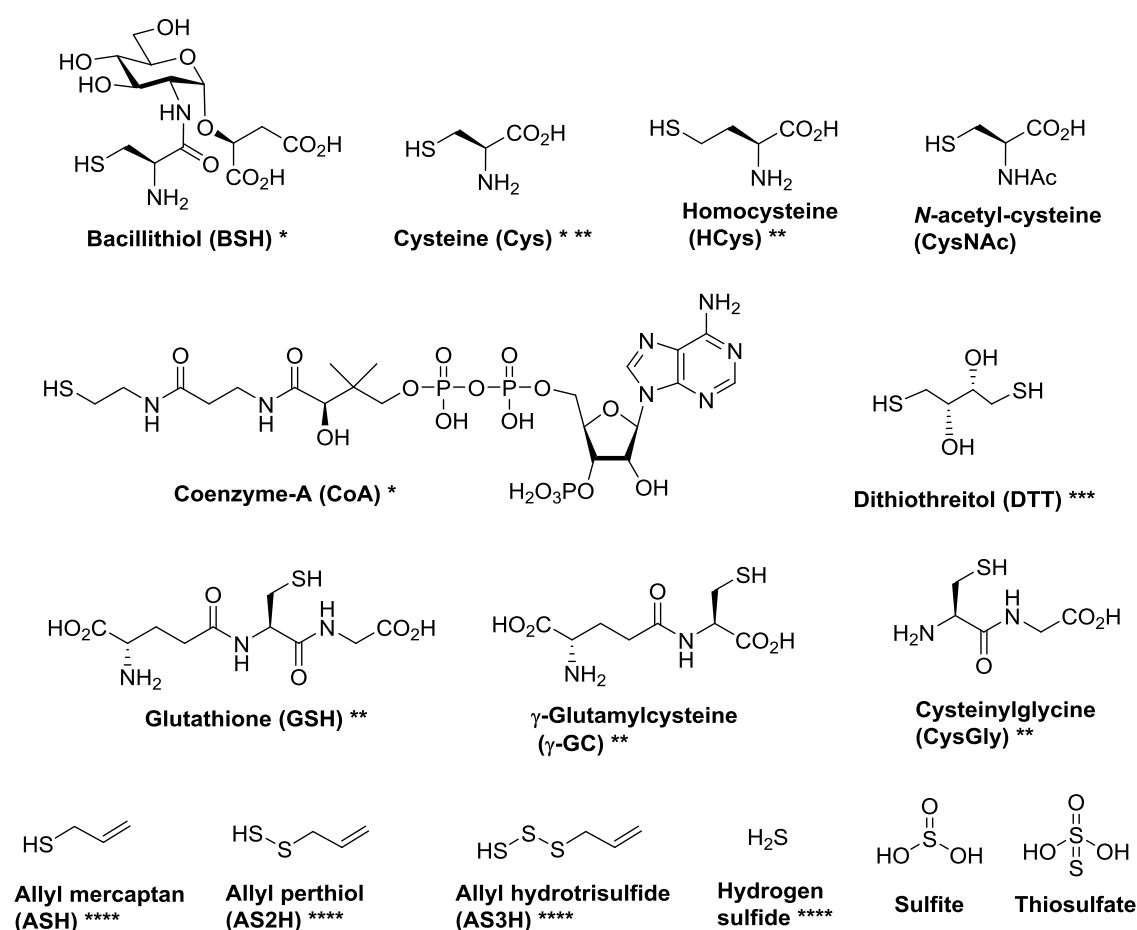


Figure 1.4: Chemical structures of thiols (RSH) reacted with mBBr to use as HPLC standards *for thiol analysis in *B. subtilis*, **for thiol analysis in nematodes, ***for reagent derived peaks, ****for analysis of DAS derived thiols.

Some of the discussed thiol-mB adducts (GSmB, HCysmB, γ -GCmB, CysGlymB), which were prepared as HPLC standards, were not used for comparison with crude cell samples of *B. subtilis*, but for comparison with crude cell samples from GSH utilising nematodes (Appendix 1.5).

Two different types of standards were prepared: Qualitative standards (section 1.2.1), which were purified, and quantitative standards (section 1.2.2), which were accurately quantified using a spectrophotometric method.

1.2.1 Preparation of qualitative standards

One molar equivalent of mBBr was added to 1.2 molar equivalents of thiol in the presence of sodium bicarbonate⁽¹⁶⁰⁾. MBBBr reacts with the thiol in a nucleophilic substitution reaction, where the thiol replaces a bromine and a thioether is formed (Figure 1.5). Purification of the thiol-mB standards was performed on a reverse phase C₁₈ flash column using a H₂O-CH₃CN gradient. DTTmB and DTT(mB)₂ were synthesised as reagent controls, as they are formed as by-products when labelling thiols derived from disulfides.

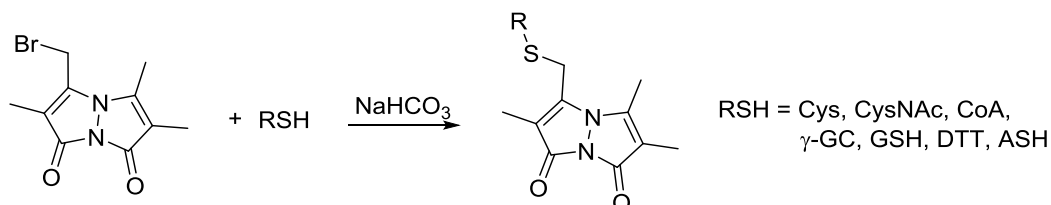


Figure 1.5: Synthesis of thiol-mB standards. Under basic conditions thiolates react with monobromobimane (mBBr) in a nucleophilic substitution reaction to form fluorescent thioethers (mBSR). Br⁻ is liberated and is converted to NaBr in the presence of NaHCO₃.

The mBBr adduct of allyl mercaptan (ASmB) was synthesised as described above, but the purification of the more hydrophobic ASmB adduct was performed on a normal phase flash column eluting with a gradient of hexane and ethyl acetate.

AS2mB and AS3mB were prepared as described in chapter 2. They were only prepared in analytical quantities and characterised by LC-MS.

1.2.2 Preparation of quantitative standards

To quantify thiol peak areas in the crude cell samples, a defined concentration of each thiol was reacted with an excess of mBBr. This reaction resulted in known concentrations of thiol-mB and hydrolysed bimane (mBOH) as a by-product⁽¹⁵⁶⁾.

Determination of thiol concentration by titrating with 5,5'-dithiobis-(2-nitrobenzoic acid) (DTNB)⁽¹⁵⁷⁾.

The thiol concentration was determined by titration with Ellman's reagent (=DTNB)^(157, 161). Thiols react with DTNB by cleaving the disulfide bond to give 2-nitro-5-thiobenzoate (TNB⁻), which ionises to the TNB²⁻ dianion in water at neutral and alkaline pH (Figure 1.6). This TNB²⁻ ion has a yellow color, which can be quantified by measuring the absorbance at 412 nm ($\epsilon=14,150 \text{ mol}^{-1}\text{cm}^{-1}$ ⁽¹⁵⁷⁾). As the reaction is rapid and stoichiometric, and the absorbance is proportional to the thiol concentration, this method can be used for the accurate determination of a thiol concentration in solution when a large excess of DTNB is used.

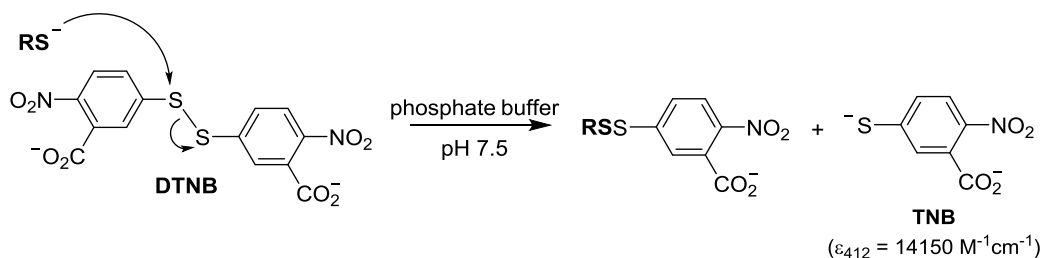


Figure 1.6: Thiol quantification through thiol-disulfide exchange reaction of DTNB with a thiolate (RS⁻) liberates 2-nitro-5-thiobenzoate (TNB⁻) which ionises to the TNB²⁻ dianion in water at neutral and alkaline pH. This TNB²⁻ ion has a yellow colour and can be quantified by measuring the absorption at 412 nm.

Reaction of thiol with mBBr

A three-fold excess of mBBr was reacted with the thiol to ensure the quantitative yield of labelled thiol-mB. The reaction was incubated at RT in the dark (mBBr is light sensitive) and stopped after 15 min by acidification with 25 mM methane sulfonic acid (MeSO₃H). As a by-product, this reaction yields mBOH. Before storage at -20 °C, standard solutions were aliquotted and dried in a vacuum centrifuge to avoid repeated freeze thawing of the standard solutions, which can decrease stability. Dried aliquots were stable for several months at -20°C, except for CoAmB, which became dephosphorylated over time. Therefore, standard solutions of CoAmB were prepared fresh for each analysis. For the quantitative reaction of ASH with mBBr, an aliquot of the ASH solution was quantified simultaneously by DTNB, while initiating the reaction with mBBr, because ASH was found to oxidise rapidly.

All quantitative standards were analysed by fluorescence HPLC at different concentrations to confirm the linear relationship between injection amount and the peak area (Figure 1.7). A thiol-mB standard curve was run during each cell extract analysis to ensure linearity and consistency of the fluorescence intensity.

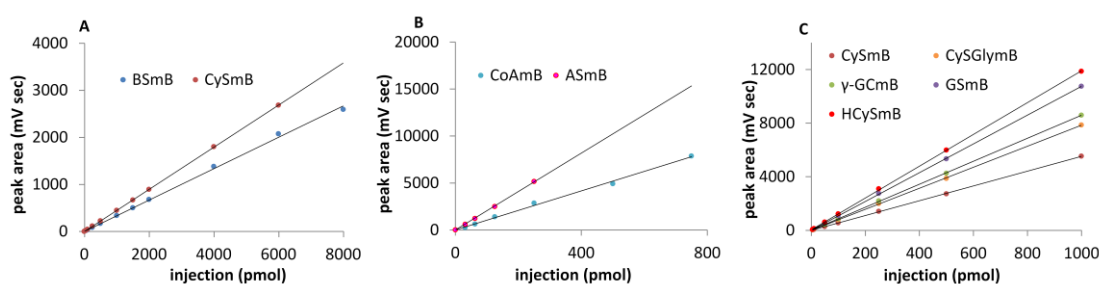


Figure 1.7: Calibration curves for thiol-mB standards recorded by fluorescence HPLC (ex: 385 nm, em: 460 nm). A: BSmB and CysmB analysed by HPLC Method A, 1x gain. B: CoAmB and ASmB analysed on Method B, 10x gain. C: CysmB, CysGlymB, γ-GCmB, GSmB and HCysmB analysed on method A, 10x gain.

1.3 LMW thiol labelling of cell extracts of *B. subtilis*

The thiol and disulfide labeling protocols were based on a method described by Newton *et al.* for LMW thiol quantifications in *Mycobacterium smegmatis*⁽¹⁶²⁾.

For thiol analysis cells were harvested from liquid cultures and cell pellets were immediately frozen in liquid nitrogen (N₂). Subsequently the cells were stored at -20°C until thiol labelling was performed. The frozen cells were resuspended in a buffer/CH₃CN solution (pH8) containing mBBr and incubated at 60°C for 15 min. After stopping the labelling reaction through cooling and acidification, the supernatant is cleared from the cell debris. The samples were then filtered, diluted and injected on the HPLC. After drying the cell pellet to a constant weight, the rdw is determined through weighing the pellet.

In each experiment two control samples were included: the reagent blank, which was treated exactly like the samples, but does not contain any cells. Therefore it gives the HPLC background for all peaks derived from reagents used in the assay protocol. Secondly, the negative control, which is a cell sample alkylated with NEM prior to mBBr labelling to prevent the labelling of thiols. This control shows all non-thiol fluorescent peaks derived from the cell sample.

When labelling thiols from crude cell extracts for quantification purposes, there are a number of things that should be considered:

- 1) confirmation of complete thiol labelling
- 2) minimisation of thiol losses during the sampling and labelling process (oxidation or enzymatic degradation, mBBR degradation through light)
- 3) sample amount/concentration (sufficient thiol concentration for fluorescence HPLC detection and sufficient cell mass for accurate mass determination of the rdw).

1) Confirmation of complete thiol labeling

The efficiency of the bimane labelling process was confirmed by mBBR labelling of pure thiols of known concentrations (determined by DTNB) (Figure 1.8). Concentrations determined by DTNB titration before derivatisation and HPLC analysis after bimane labelling are very similar (difference < 10%) for all BSH and Cys concentrations tested.

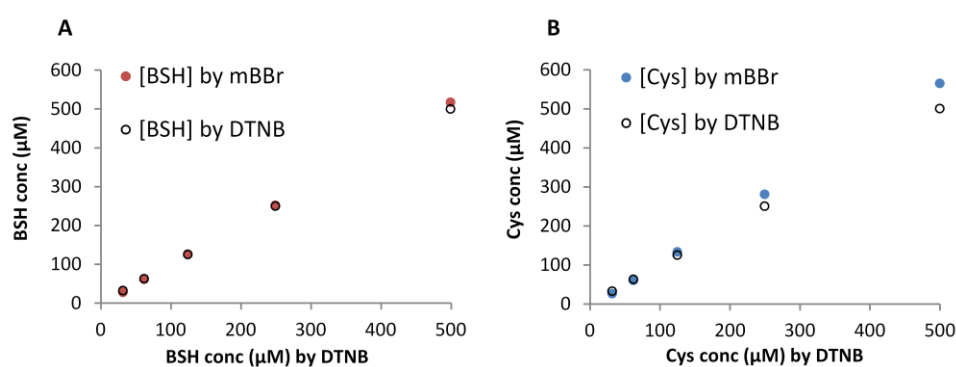


Figure 1.8: MBBR labelling of pure, DTNB quantified samples of A: BSH and B: Cys.

To determine the minimum amount of mBBR needed to accurately quantify thiols in a defined cell pellet, identical amounts of cells were treated with different bimane concentrations. Several *B. subtilis* cell samples corresponding to 6 mg of rdw were incubated with mBBR mix, where extraction volumes, mBBR concentrations, incubation times and ethylenediaminetetraacetic acid (EDTA, metal chelator to prevent metal catalysed oxidation) concentrations were altered. Through this experiment it was determined that 20 μL of mBBR mix (2 mM mBBR in 20 mM Hepes, pH8 in 50% CH₃CN) per mg rdw and an incubation time of 15 min at 60°C gave reproducible results for quantification of BSmB and CysmB of *B. subtilis* cell samples. The presence of EDTA as a metal chelator to prevent metal catalysed oxidation of thiols did not make any difference in this experiment. Therefore the described conditions were used for routine analysis of *B. subtilis* cell samples.

2) Minimisation of thiol losses during the sampling and labelling process

To minimise thiol oxidation during sampling and the labelling process, temperatures were kept low during handling (pelleted in a cooled centrifuge at 4°C and immediately frozen in liquid N₂) and cell pellets were stored at -20 °C until thiol extraction. For the thiol extraction elevated temperature (60°C) and extraction in CH₃CN inactivates enzymes that may lead to the enzymatic reduction of disulfides to thiols during alkylation (as cellular enzymes maintain a thiol-disulfide equilibrium, there is a risk of enzymatic formation of thiol from disulfides, when

the thiol concentration is depleted through alkylation with mBBr). If oxidation of thiols is found to be a problem, EDTA can be used to minimise free metals in the sample. In our analyses, however, metal-catalysed oxidation of thiols was not observed.

Additionally it should be noted that the bimeane moiety is light sensitive, and therefore the exposure to light during sample preparation and storage was minimised. Amber vials were used for HPLC analysis and under these conditions no loss of sample quality was observed during overnight storage at RT in the HPLC autosampler (except for samples containing CoAmB, where dephosphorylation occurred).

3) Sample amount/concentration

20 μ L of mBBr mix /mg rdw was found to yield a good concentration of thiol derivative in samples after five-fold dilution, which was required to minimise the CH₃CN concentration for HPLC analysis.

The relationship between the OD₆₀₀ and rdw of the cell pellet per culture volume was established (Figure 1.9). *B. subtilis* cultures were grown and fixed volumes were harvested at different OD₆₀₀, concentrated and dried. The rdw of the cell pellet per culture volume (mg/mL) was plotted over the optical density (OD₆₀₀). For thiol analysis cell culture volumes corresponding to at least 5 mg rdw were harvested to minimise weighing errors.

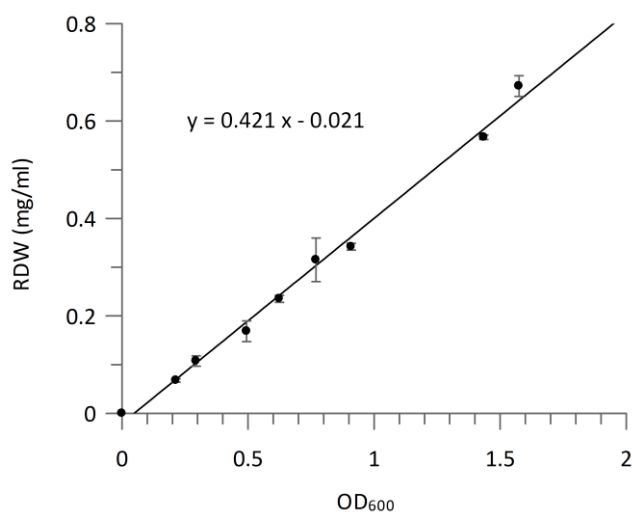


Figure 1.9: Correlation between residual dry weight (rdw) per volume (mg/mL) at different culture densities (OD₆₀₀). Fixed volumes of *B. subtilis* culture were harvested at different OD₆₀₀, concentrated and dried. The rdw of the cell pellet per culture volume (mg/mL) was plotted over the OD₆₀₀. The linear relationship can be used to calculate the culture volume at a certain OD₆₀₀ that gives the required 5 mg rdw. The experiment was performed in duplicate, the mean is plotted and the error bars represent the standard deviation.

1.4 Disulfide analysis of cell extracts from *B. subtilis*

Disulfides are found in the cells in much lower concentrations than their corresponding reduced thiols. The redox ratios (thiol/disulfide) of BSH and Cys in *B. subtilis* have been determined as 400:1 and 120:1 respectively⁽⁵⁴⁾. This low abundance results in some difficulties in the detection and quantification of disulfides, as the method needs to be extremely sensitive. There are no direct detection methods available for disulfides and often disulfide analysis is performed by first blocking thiol, then reducing disulfides to their corresponding thiols, followed by labelling of the resulting thiols with a thiol selective tag (Figure 1.10).

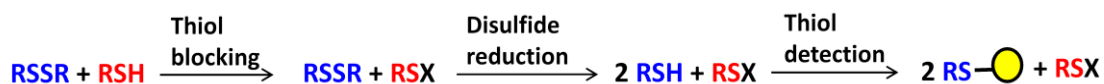


Figure 1.10: Schematic overview of disulfide labelling. Thiols are irreversibly blocked, disulfides reduced and the resulting thiols (derived from disulfides) are modified with a thiol-selective tag.

In vivo disulfide detection is reviewed in Hansen and Winther⁽¹⁶³⁾ and advantages and disadvantages of different reagents for thiol blocking, disulfide reduction and thiol detection are discussed. Disulfides can also be quantified via nicotinamide adenine dinucleotide phosphate (NADPH) dependent enzymatic reduction through disulfide reductases, where the rate of reaction is indirectly measured through the consumption of NADPH (measured at 340 nm)⁽¹⁶⁴⁾. This quantification method requires the corresponding disulfide reductase enzyme, which is not yet characterised for BSH and, furthermore, the method is not suitable for the analysis of multiple cellular disulfides.

The approach in Figure 1.10 possesses some practical issues, such as the cross-reaction between thiol blocking reagents, reducing agents and thiol detection reagents. Another limitation is the inability to differentiate between symmetrical and mixed disulfides or between di- and polysulfides, which would be of special interest in our studies.

1.4.1 Original protocol for disulfide analysis in cell extracts (Method 1)

For disulfide analysis 5 mg rdw/ 100 μ L extraction volume (as described for thiol analysis) were used.

In the first step, all thiols in the cell sample were irreversibly capped with NEM in a Michael-type nucleophilic addition to form a thioether (Figure 1.11 A and B, reaction 1). NEM needs to be in excess over the sum of all thiols to ensure that there is no free thiol left after this step and, therefore, the cell pellet was resuspended and incubated for 15 minutes at 60°C in a buffer/CH₃CN mixture (pH8) containing 5 mM NEM. Under strongly basic conditions the reaction can be reversible, which has to be avoided. Afterwards the sample was clarified from the cell debris by centrifugation and the supernatant transferred for further analyses.

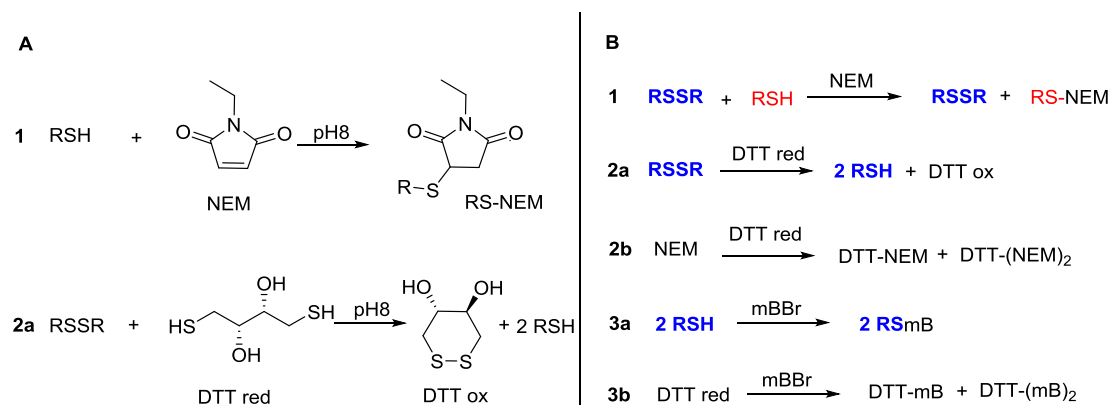


Figure 1.11: A: Chemical reactions: 1) *N*-ethylmaleimide (NEM) blocks thiols irreversibly through nucleophilic addition and 2a) DTT reduces disulfides to thiols and forms an intramolecular disulfide bond. B: Series of reactions required for disulfide analysis of cell samples, including unwanted side-reactions of reagents. Educts and products are not balanced. 1) NEM (used in excess) irreversibly reacts with free thiol. 2a) Dithiothreitol (DTT) reduces disulfides to thiols. 2b) Two molecules of NEM (used in excess in step 1) can irreversibly cap the two thiol groups of one molecule of DTT. 3a) MBBR reacts with thiols to form fluorescent thiol-adducts derived from disulfides. 3b) MBBR reacts with excess DTT to form fluorescent DTTmB or DTT(mB)₂.

In the second step, the reducing agent DTT was added to the supernatant, to reduce all disulfides to the corresponding thiols (Figure 1.11 A and B, reaction 2a). As DTT is a thiol itself it is alkylated by excess NEM that was used in the first step (Figure 1.11 B, reaction 2b). Therefore DTT needs to be used in excess over the sum of NEM and all disulfides, to ensure full reduction of disulfides. Typically, a concentration of 6 mM DTT was used, which corresponds to a minimum of 1 mM free DTT, assuming that all of the initial 5 mM NEM remains and gets monoalkylated by the dithiol DTT. As disulfides are found in the cells in very low concentrations, 1 mM excess of DTT is sufficient to reduce all soluble disulfides. The reduction of disulfides with DTT was performed at pH8 to ensure that enough DTT is in the deprotonated reactive form (pK_{a1}: 9.2, pK_{a2}: 10.1⁽¹⁶⁵⁾). DTT is an effective reducing agent as the formation of a cyclic disulfide is energetically favoured, driving the reaction to completion.

In the third step of the disulfide quantification protocol, mBBr is added to the supernatant (Figure 1.11 B, reaction 3a). The mBBr concentration needs to exceed twice the excess of DTT plus the concentration of free thiol (derived from disulfides), because two molecules of mBBr can react with DTT to form the bilabelled product (Figure 1.11 B, reaction 3b). The reaction was stopped by decreasing the pH and samples were filtered and diluted before HPLC analysis.

Reduction efficiency of DTT *in vitro*

To validate the reduction efficiency of DTT towards disulfides, some *in vitro* experiments were performed, confirming good efficiency of the reduction of BSSB and mixed allyl polysulfides.

Reduction efficiency of DTT towards BSSB

Known concentrations of BSSB (BSH quantified by DTNB and then quantitatively oxidised) were used for reduction with at least 10-fold excess of DTT and subsequent mBBR labelling to test the reduction efficiency of DTT. The initial concentration of BSSB (originally quantified as BSH via DTNB) is in good agreement with the amount detected after DTT reduction and mBBR labelling (Figure 1.12).

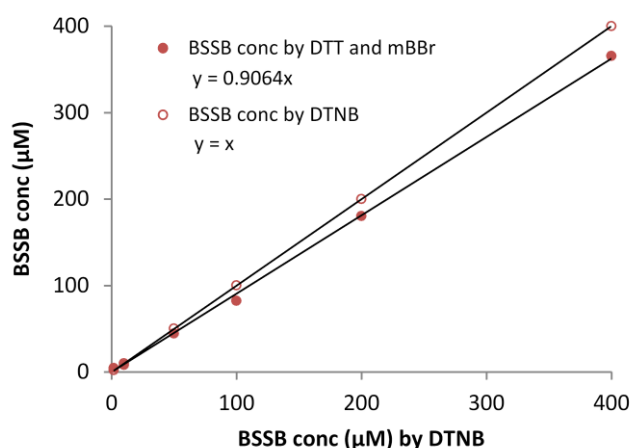


Figure 1.12: Efficiency of BSSB reduction by DTT. BSH was quantified by DTNB and quantitatively oxidised. Known concentrations of BSSB were then reduced with DTT, labelled with mBBR and analysed by HPLC. Concentrations were calculated from fluorescent peak areas of BSMB standards.

Reduction efficiency of DTT towards mixed polysulfides

To investigate whether mixed allyl polysulfides are effectively reduced by DTT, stock solutions of mixed allyl polysulfides of unknown concentration were serially diluted and treated with large excess of DTT, followed by mBBR labelling (Figure 1.13). This experiment confirmed the effective reduction and labelling of mixed allyl-cysteine trisulfide (ACS3), allyl-bacillithiol disulfide (ABS2) and allyl-glutathione tri- and tetrasulfide (AGS3 and AGS4). For all tested compounds, the expected and measured concentrations are in good agreement.

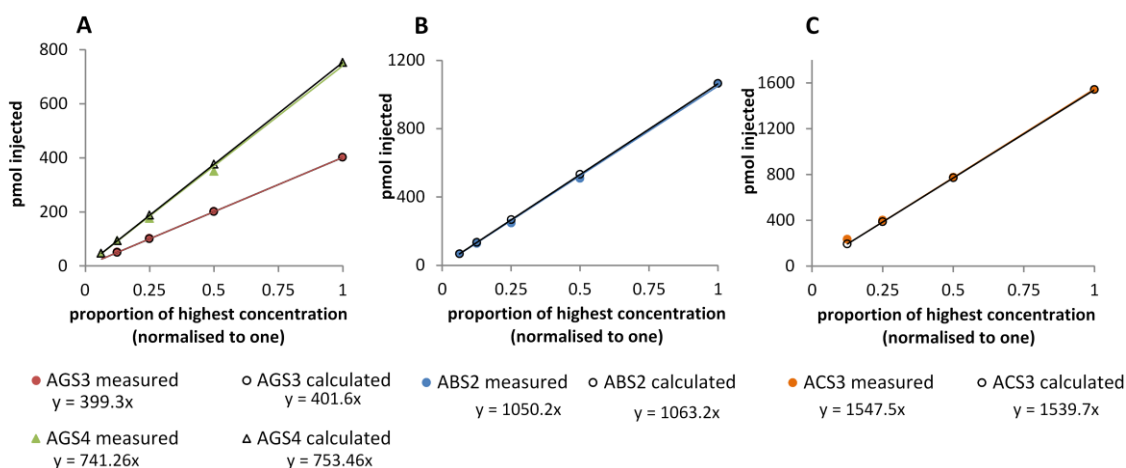


Figure 1.13: Reduction of mixed polysulfides by DTT. Stock solutions of mixed polysulfides of unknown concentration were serially diluted, reduced, labelled and analysed by HPLC. Mixed polysulfide concentrations were calculated by assuming a molar equivalent with the peak areas of GS_mB, BS_mB or CS_mB ("measured"). The actual concentrations of the mixed polysulfide stock solutions were unknown and, therefore, the highest concentration of the serial dilution was normalised to one and the other concentrations were expressed as fractions of one (X-axis, "calculated").

***In vitro* validation of Method 1**

Equal aliquots of BSSB, GSSG, ABS2 and AGS2 were reduced and labeled according to disulfide Method 1 and by a control method (DTT reduction and mBBR labelling, without a thiol blocking step). The control method cannot be used in the analysis of cell samples that contain reduced thiols, but can be used with pure disulfide samples. For all tested disulfides, except for ABS2, the recoveries of disulfide are about 80-87% compared to the control method. The mean recovery for ABS2 is only 54 % and the method is not reproducible for this disulfide (Figure 1.14).

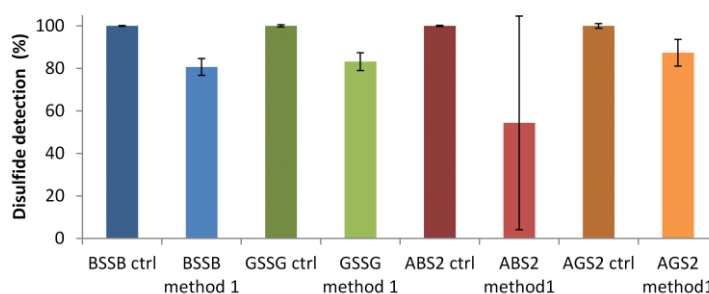


Figure 1.14: *In vitro* verification of disulfide Method 1. Disulfide solutions (approximately 0.5 mM) were divided in six equal aliquots for each disulfide (BSSB, GSSG, ABS2, AGS2). Three aliquots of each disulfide were treated with DTT and mBBR and the remaining three aliquots were analysed with disulfide Method 1. The resulting BS_mB or GS_mB peak areas were used for quantification, and the DTT and mBBR treatment control data was normalised to 100%.

A possible reason for the slightly lower recoveries using Method 1 compared to the control might be the reduction of disulfides while there is still unreacted NEM remaining in the sample. Reduced thiols (originating from disulfides) could then be alkylated by NEM, which is irreversible and leads to the underestimation of disulfides. This might be less of an issue for cell samples where disulfide concentrations are much lower and, therefore, less disulfide may be reduced while there is still unreacted NEM present. The problem seems to be enhanced for ABS2, possibly due to the high reactivity of this molecule for reduction and alkylation.

1.4.2 Improved protocol for disulfide analysis in cell extracts (Method 2) ⁽¹⁶²⁾

There are some practical issues with Method 1:

The concentration of labelled thiol adducts in the samples is very low and by HPLC analysis, peaks are hardly differentiable from the background. The amount of cells and extraction volumes were adjusted to give measurable peaks for thiol analyses and as cellular disulfide concentrations are much lower, we need to adjust the protocol accordingly.

Therefore in an improved protocol, we used cells corresponding to a rdw of 30 mg and resuspended them in a volume of 1 mL, which was partly evaporated before HPLC analysis.

In addition, the concentration of mBBr in Method 1 was very high (13 mM), and leads to high fluorescent background peaks. Furthermore, the mBBr is very expensive and for these reasons it is important to minimise the concentration of mBBr in the sample. To address this issue, another reagent (β -mercaptoethanol, ME) was used to react with excess NEM after the initial alkylation of thiols (Figure 1.15). ME is reported to rapidly react with alkylating agents, essentially without any reduction of disulfides ⁽¹⁶³⁾. This is important, because otherwise thiols derived from disulfides can be irreversibly alkylated by excess NEM. ME was added in equimolar concentration to NEM to ensure all excess NEM reacted with ME.

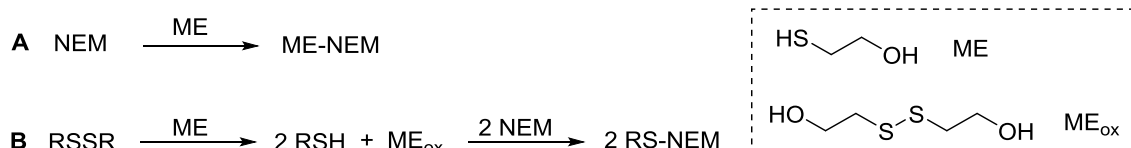


Figure 1.15: A: β -mercaptoethanol (ME) can be alkylated by NEM and B: ME reduces disulfides to thiols, and is subsequently oxidised to ME_{ox} itself. Thiols can be alkylated by excess NEM.

Subsequent concentration in a vacuum centrifuge has two advantages: Firstly, the sample becomes more concentrated and does not need to be diluted before HPLC analysis as CH₃CN evaporates. Secondly, excess of ME evaporates and, therefore, does not interfere in subsequent reactions. Typically, the samples were vacuum dried overnight and reduced with two mM DTT in 100 μ L volume afterwards. In the subsequent labelling step, mBBr is added to a final concentration of six mM, which is in excess of two molar equivalents of DTT plus the thiol concentration (derived from disulfides). Compared to our initial protocol this method increases the sample concentration 30-fold, while using lower concentrations of mBBr.

Disulfide analysis of DAS treated samples was performed without concentration, because DAS molecules are volatile and can evaporate in the vacuum centrifuge. This disulfide labelling method (Method 2) was used for disulfide quantification of untreated *B. subtilis* (section 3.4.2) and DAS3-treated *B. subtilis* (section 3.4.3.1).

***In vitro* validation of Method 2**

A stock solution of ACS3 of unknown concentration was serially diluted and identical samples were treated under cell labelling conditions for disulfides as previously described (Method 2) or treated with DTT and mBBR as a control (without NEM) (Figure 1.16). This experiment highlights a problem with Method 2, as detected polysulfide concentrations are < 50% compared to polysulfide concentrations calculated using the control protocol.

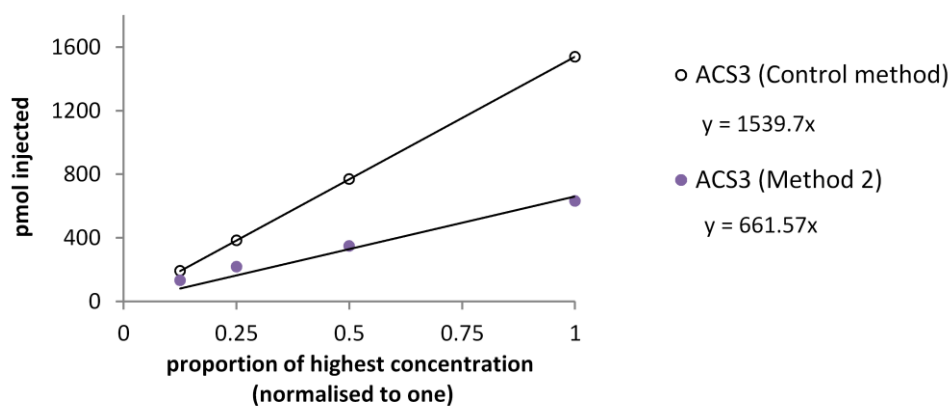


Figure 1.16: *In vitro* test of disulfide Method 2. ACS3 content (pmol) was derived from quantifying the CysmB peak areas from Method 2 and the Control Method. The highest concentration of ACS3 is normalised to one and other concentrations are expressed as fractions of one (X-axis).

1.4.3 Development of disulfide analysis Method 3

There are two possible reasons for the underestimation of disulfide using disulfide Method 2:

1) ME does not evaporate or oxidise completely in the vacuum centrifuge and is left in its free thiol form when labelling cell extracts with mBBr. If this was the case, remaining ME could react with mBBr and reduce the available mBBr for labelling free thiols derived from disulfides. This possibility was eliminated, however, because no MEmB adducts were observed by HPLC. Furthermore, detected thiol-mB did not increase upon repeated reduction and derivatisation of labelled samples, which shows that there are no unlabelled disulfides left in the sample.

2) ME reduces disulfides, which are then capped by free NEM (Figure 1.15). This alkylation is irreversible and therefore disulfides may be underestimated in the assay.

To test the reaction speed of ME with NEM, equimolar concentrations of ME and NEM were reacted, and free thiol (ME) was quantified by DTNB (Figure 1.17). The reaction speed of the reduction of ABS2 by ME under disulfide assay conditions was analysed by mBBr labelling and HPLC analysis (Figure 1.17). Comparison of the reaction rate of the two reactions shows a similar speed for both reactions. For our assay this implies that ME does not only react with NEM, but also reduces disulfides to thiols, which can then react with NEM. This can lead to an underestimation of disulfide concentrations.

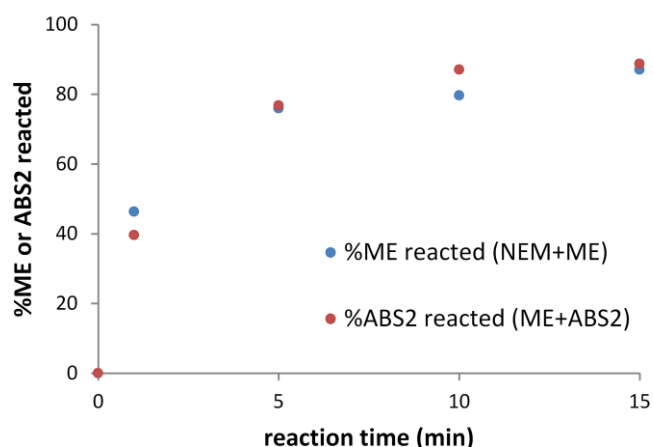


Figure 1.17: Reaction speed of ME with NEM and ABS2 under assay conditions. ME was quantified by DTNB and the initial concentration of ME (5 mM) before adding NEM was normalised to 100%. The reaction speed of 100 μ M ABS2 with 5 mM ME was calculated through quantification of BSMB after mBBr labelling, and the initial concentration of ABS2 was normalised to 100%.

To address this problem, NEM was extracted in diethyl ether (Et_2O , Method 3). After the extraction of NEM, ME addition is not necessary and disulfides can be reduced with DTT and labelled with mBBr. After extraction of NEM with Et_2O , more than 94% of BSSB was detected by DTT reduction and mBBr labelling. Consequently, similar experiments were performed with AGS4 and ABS2 to investigate whether the improved protocol also works for mixed allyl polysulfides. Extraction of NEM leads to the detection of >97% AGS4 and 60% or 83% of ABS2 (with or without concentration in the vacuum centrifuge, respectively). In conclusion, this improved Method 3 works effectively for mixed and symmetric di- and polysulfide analysis *in vitro*, although there still seem to be lower derivatisation efficiencies for ABS2. Due to time limitations, this problem could not be investigated further and as the reduction and labelling

efficiency of ABS2 was increased from 54% (Method1) to 83% (Method 3), it was used for cell extract analysis of DAS4-treated *B. subtilis* cells.

In addition to extracting NEM from the cell extract, the Et₂O extraction process removes DAS (which are very hydrophobic) from the samples. Therefore all allyl-mB detected from the cell sample after extraction and reduction accounts only for mixed polysulfides.

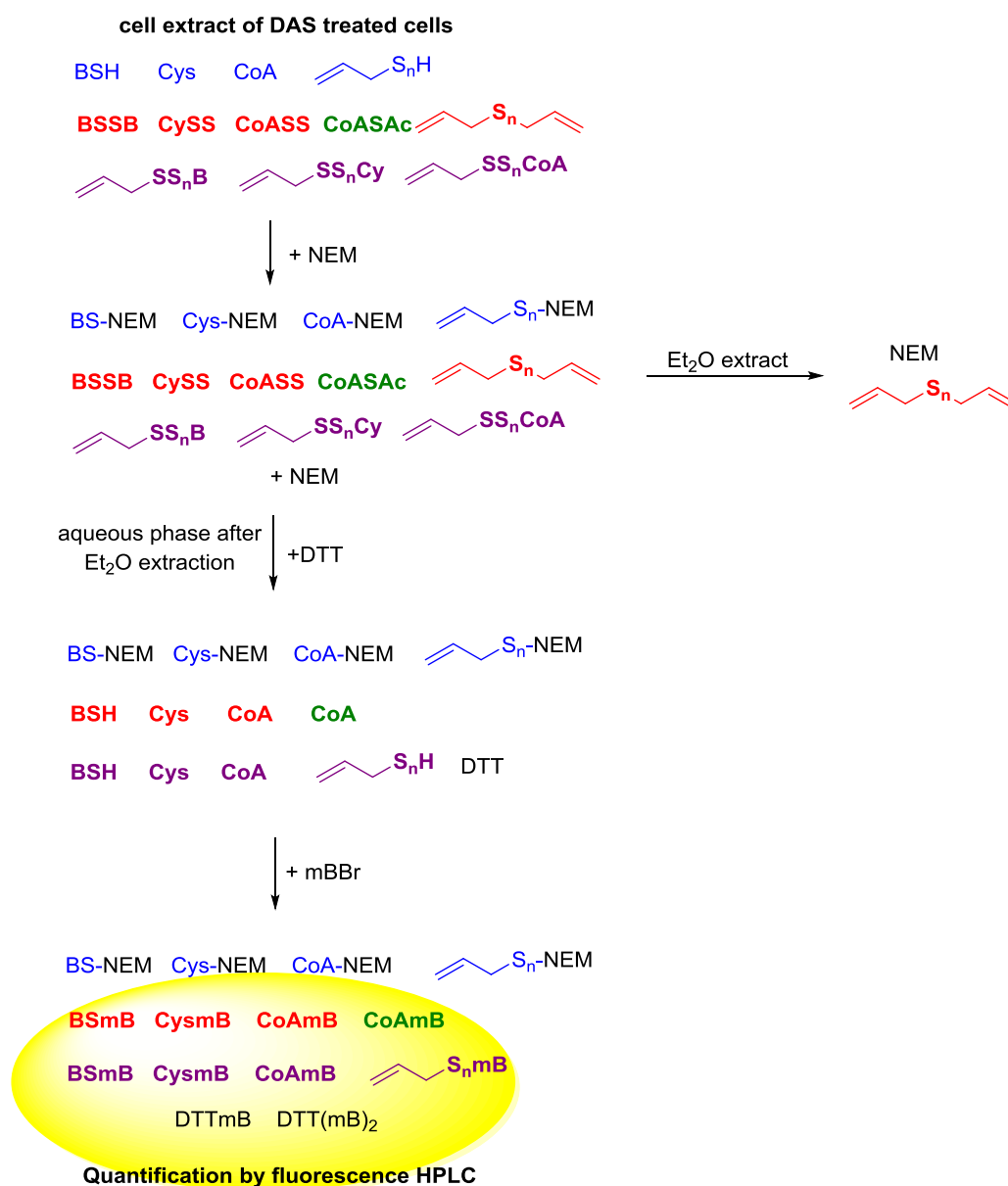
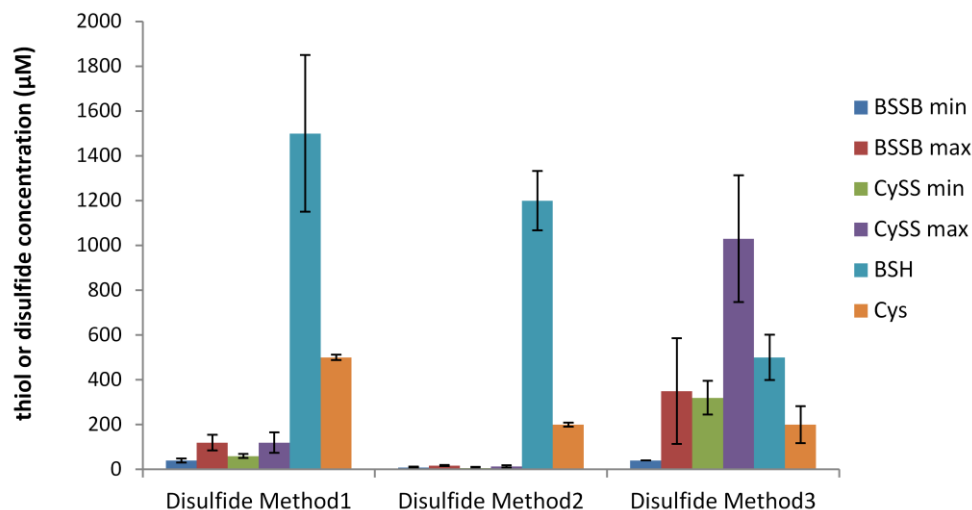


Figure 1.18: Disulfide analysis method for cell samples (Method 3).

1.4.4 *In vivo* comparison of disulfide Methods 1, 2 and 3

Figure 1.19 shows the minimum and maximum concentrations of BSSB and CySS determined by measuring disulfide levels during the whole growth curve in three independent experiments, using disulfide Methods 1, 2 and 3 and the BSH and Cys concentration in the same experiments determined at $OD_{600}=0.8$.

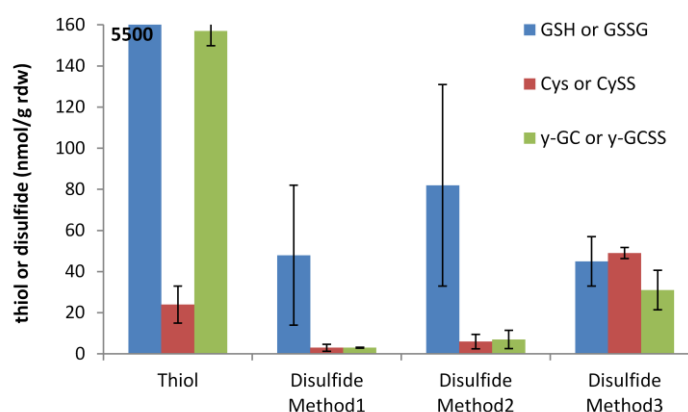


	Disulfide concentrations (µM)				Thiol concentrations (µM)	
	BSSB min ^a	BSSB max ^b	CySS min ^a	CySS max ^b	BSH ^c	Cys ^c
Disulfide Method 1	40 (± 9.2)	120 (± 35.3)	60 (± 8.7)	120 (± 46.3)	1500 (± 350.9)	500 (± 12.1)
Disulfide Method 2	9 (± 3.2)	17 (± 2.3)	7 (± 4.2)	14 (± 4.6)	1200 (± 132.4)	200 (± 9.4)
Disulfide Method 3	40 ^d	350 (± 236.1)	320 (± 75.2)	1030 (± 283.2)	500 (± 101.2)	200 (± 82.6)

Figure 1.19: Comparison of different disulfide analyses methods in *B. subtilis* cell extracts. All thiol and disulfide analyses were performed in triplicates, error bars give the standard deviation, and disulfide values were recorded during the whole growth curve at different OD_{600} . ^aData is shown for the lowest (min) and ^bhighest (max) disulfide concentration measured in each experiment. Data for Method 1 (DTT only) was extracted from ⁽⁶³⁾, data for Method 2 (ME and DTT) was reported in this study ⁽⁵⁹⁾, method previously published in ⁽¹⁶²⁾, and data for Method 3 (Et₂O extraction) was reported in this study. ^cThiol concentrations measured between $OD_{600}=0.8$ and 1.0. ^dNo standard deviation reported, because only a single sample was analysed.

BSSB and CySS concentrations determined by Method 2 are about one order of magnitude lower compared to Method 1. *In vitro* experiments have shown that Method 2 is prone to underestimation of disulfides. BSSB and CySS concentrations determined by Method 3 were up to three and 10-fold higher, respectively, than those determined by Method 1. CySS concentrations determined by Method 3 are even higher than the corresponding reduced Cys concentrations determined in the same experiment. This may be an artefact of the method and we do not have an explanation for the measured high CySS concentrations. It suggests that this method is not reliable for disulfide quantification, although *in vitro* experiments have shown accurate results using this method (section 1.4.3).

As this comparison was performed with cultures from three independent experiments, the three methods cannot be accurately assessed for reliability. Therefore, in another experiment, disulfide concentrations of identical cell samples of *Escherichia coli* were each analysed by the three different methods (Figure 1.20). Analysis with Method 1 and 2 resulted in similar GSSG, CySS and γ -GCSS levels. All three methods detected similar GSSG levels, but CySS and γ -GCSS levels were 10-fold higher using Method 3. These differences in disulfide concentrations have a big influence on the thiol-disulfide redox ratios (Table in Figure 1.20), which are very low for Cys and γ -GC, when disulfide levels are measured with Method 3. Method 3 might be prone to overestimation of disulfides or lead to artificial oxidation of thiols, but a reason for this has not been discovered.



	Disulfide (nmol g ⁻¹ rdw ⁻¹)			Redox ratios (thiol/disulfide)		
	GSSG	CySS	γ -GCSS	GSH/ GSSG	Cys/ CySS	γ -GC/ γ -GCSS
Method 1	48 (\pm 35)	3 (\pm 2)	3 (\pm 0)	115.6 (\pm 93.6)	8.5 (\pm 6.0)	46.5 (\pm 21.7)
Method 2	82 (\pm 49)	6 (\pm 3)	7 (\pm 4)	66.9 (\pm 46.5)	3.9 (\pm 2.7)	22.7 (\pm 17.6)
Method 3	45 (\pm 12)	49 (\pm 27)	31 (\pm 0)	123.3 (\pm 55.4)	0.5 (\pm 0.3)	5.1 (\pm 2.8)

Figure 1.20: Disulfide analysis of *E. coli* using three different methods. *E. coli* cells were grown in liquid broth up to OD₆₀₀=2.8 and thiol and three different disulfide analyses were performed in triplicate from the same *E. coli* cell culture. Disulfide methods 1 to 3 have been described above.

Ultimately we were not able to determine which of the disulfide quantification methods is most reliable and there are certainly difficulties with all described methods. Because of the lack of alternative methods and sensitivity issues with Method 1, Method 2 was used for disulfide analysis of untreated (section 3.4.2) and DAS3-treated (section 3.4.3) cells and Method 3 was used for disulfide quantification of DAS4-treated cells (section 3.4.4).

1.5 Method development for thiol and disulfide analysis in *S. feltiae*

Figure 1.21 provides an overview of the method for LMW thiol and disulfide quantifications in DAS-treated nematodes.

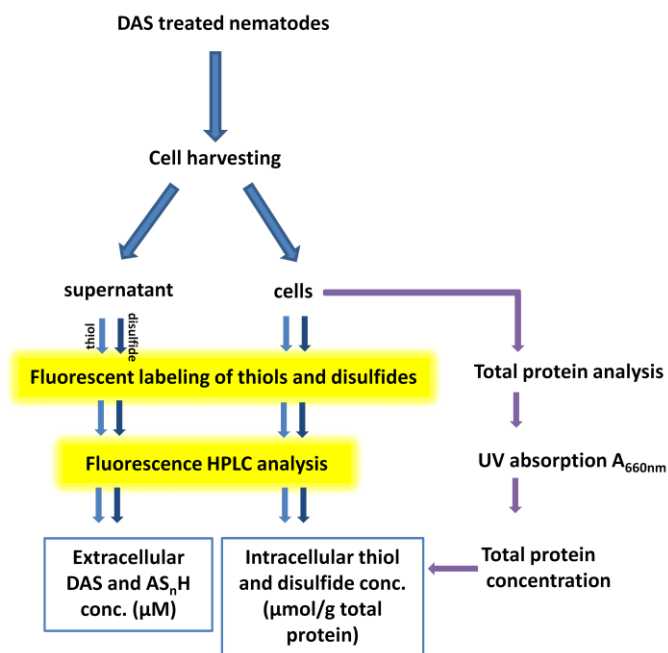


Figure 1.21: Overview of thiol and disulfide analysis methods for DAS treated nematodes.

Nematodes are incubated with DAS and samples are harvested and concentrated at different time points. Cell pellets and supernatants are frozen immediately for thiol and disulfide analysis. For subsequent thiol analysis mBBR was used as a thiol reactive reagent and for disulfide analysis method 2 was used as described for *B. subtilis* in Appendix section 1.4.2, where thiols are blocked with NEM, NEM quenched with ME, disulfides reduced with DTT after concentration of the sample and subsequently thiols derived from disulfides are labelled with mBBR.

One main difference in the protocol for bacteria and nematodes is an additional step, required to break up the cells. For a multicellular organism which has a strong outer cell layer (cuticle), heating to 60°C alone is not enough to permeabilise the cells with the derivatisation reagents. Instead, bead beating can break up the cells and allows the derivatisation reagents to react with intracellular thiols. During the bead beating process nematodes were mixed with the beads in the presence of the derivatisation reagents and mechanically shaken to ensure that the beads destroy the tissue and simultaneously cellular thiols were derivatised. This method is commonly used to lyse tough cells or tissues and material and size of beads needs to be adjusted to the type of tissue.

Another major protocol difference is the reference value for thiol and disulfide quantification. The nematodes (*S.feltiae*) come in a powder carrier, and other particles are suspended in the water with the nematodes. The nematodes cannot be separated from other constituents and therefore the residual dry cell weight (rdw) of the nematodes cannot be determined. Instead, the thiol and disulfide concentrations were referenced to the total protein content of the sample. For total protein analysis, an additional aliquot was taken from a particular sample and analysed with a protein assay according to the supplier's instructions. As the total protein content is proportional to the cell mass, it provides a suitable reference value.

References

1. Block, E., (Ed.) (2010) *Garlic and other Alliums, The Lore and the Science*, RSC Publishing, Cambridge.
2. Cavallito, C. J., and Bailey, J. H. (1944) Allicin, the Antibacterial Principle of *Allium sativum*. I. Isolation, Physical Properties and Antibacterial Action, *Journal of the American Chemical Society* 66, 1950-1951.
3. Ankri, S., and Mirelman, D. (1999) Antimicrobial properties of allicin from garlic, *Microbes and Infection* 1, 125-129.
4. Lawson, L. D. (1993) Bioactive organosulfur compounds of garlic and garlic products - Role in reducing blood-lipids, *Acs Symposium Series* 534, 306-330.
5. Hughes, J., Tregova, A., Tomsett, A. B., Jones, M. G., Cosstick, R., and Collin, H. A. (2005) Synthesis of the flavour precursor, alliin, in garlic tissue cultures, *Phytochemistry* 66, 187-194.
6. Jones, M. G., Hughes, J., Tregova, A., Milne, J., Tomsett, A. B., and Collin, H. A. (2004) Biosynthesis of the flavour precursors of onion and garlic, *Journal of Experimental Botany* 55, 1903-1918.
7. Lancaster, J. E., and Shaw, M. L. (1989) γ -Glutamyl-transferase peptides in the biosynthesis of S-alk(en)yl-L-cysteine sulfoxides (flavour precursors) in allium, *Phytochemistry* 28, 455-460.
8. Shimon, L. J. W., Rabinkov, A., Shine, I., Miron, T., Mirelman, D., Wilchek, M., and Frolov, F. (2007) Two structures of alliinase from *Allium sativum* L.: Apo form and ternary complex with aminoacrylate reaction intermediate covalently bound to the PLP cofactor, *Journal of Molecular Biology* 366, 611-625.
9. Lawson, L. D., Wood, S. G., and Hughes, B. G. (1991) HPLC analysis of allicin and other thiosulfinates in garlic clove homogenates, *Planta Medica* 57, 263-270.
10. Curtis, H., Noll, U., Stormann, J., and Slusarenko, A. J. (2004) Broad-spectrum activity of the volatile phytoanticipin allicin in extracts of garlic (*Allium sativum* L.) against plant pathogenic bacteria, fungi and oomycetes, *Physiological and Molecular Plant Pathology* 65, 79-89.
11. Gruhlke, M. C. H., Portz, D., Stitz, M., Anwar, A., Schneider, T., Jacob, C., Schlaich, N. L., and Slusarenko, A. J. (2010) Allicin disrupts the cell's electrochemical potential and induces apoptosis in yeast, *Free Radic Biol Med* 49, 1916-1924.
12. Miron, T., Mironchik, M., Mirelman, D., Wilchek, M., and Rabinkov, A. (2003) Inhibition of tumor growth by a novel approach: In situ allicin generation using targeted alliinase delivery, *Molecular Cancer Therapeutics* 2, 1295-1301.
13. Block, E., Naganathan, S., Putman, D., and Zhao, S. H. (1993) Organosulfur chemistry of garlic and onion - Recent results, *Pure and Applied Chemistry* 65, 625-632.
14. Block, E. (1992) The organosulfur chemistry of the genus allium - Implications for the organic-chemistry of sulfur, *Angewandte Chemie-International Edition in English* 31, 1135-1178.
15. Rose, P., Whiteman, M., Moore, P. K., and Zhu, Y. Z. (2005) Bioactive S-alk(en)yl cysteine sulfoxide metabolites in the genus Allium: the chemistry of potential therapeutic agents, *Natural Product Reports* 22, 351-368.
16. Capasso, A. (2013) Antioxidant Action and Therapeutic Efficacy of *Allium sativum* L., *Molecules* 18, 690-700.

17. Kaschula, C. H., Hunter, R., and Parker, M. I. (2010) Garlic-derived anticancer agents: Structure and biological activity of ajoene, *Biofactors* 36, 78-85.
18. Benavides, G. A., Squadrito, G. L., Mills, R. W., Patel, H. D., Isbell, T. S., Patel, R. P., Darley-Usmar, V. M., Doeller, J. E., and Kraus, D. W. (2007) Hydrogen sulfide mediates the vasoactivity of garlic, *Proceedings of the National Academy of Sciences of the United States of America* 104, 17977-17982.
19. Münchberg, U., Anwar, A., Mecklenburg, S., and Jacob, C. (2007) Polysulfides as biologically active ingredients of garlic, *Organic & Biomolecular Chemistry* 5, 1505-1518.
20. Shen, J. K., Davis, L. E., Wallace, J. M., Cai, Y., and Lawson, L. D. (1996) Enhanced diallyl trisulfide has *in vitro* synergy with amphotericin B against *Cryptococcus neoformans*, *Planta Medica* 62, 415-418.
21. Tsao, S. M., and Yin, M. C. (2001) *In vitro* activity of garlic oil and four diallyl sulphides against antibiotic-resistant *Pseudomonas aeruginosa* and *Klebsiella pneumoniae*, *Journal of Antimicrobial Chemotherapy* 47, 665-670.
22. O'Gara, E. A., Hill, D. J., and Maslin, D. J. (2000) Activities of garlic oil, garlic powder, and their diallyl constituents against *Helicobacter pylori*, *Appl. Environ. Microbiol.* 66, 2269-2273.
23. Rattanachaikunsopon, P., and Phumkhachorn, P. (2008) Diallyl Sulfide Content and Antimicrobial Activity against Food-Borne Pathogenic Bacteria of Chives (*Allium schoenoprasum*), *Biosci. Biotechnol. Biochem.* 72, 2987-2991.
24. Tsao, S. M., and Yin, M. C. (2001) *In-vitro* antimicrobial activity of four diallyl sulphides occurring naturally in garlic and Chinese leek oils, *J. Med. Microbiol.* 50, 646-649.
25. Lemar, K. M., Aon, M. A., Cortassa, S., O'Rourke, B., Muller, C. T., and Lloyd, D. (2007) Diallyl disulphide depletes glutathione in *Candida albicans*: oxidative stress-mediated cell death studied by two-photon microscopy, *Yeast* 24, 695-706.
26. Antosiewicz, J., Herman-Antosiewicz, A., Marynowski, S. W., and Singh, S. V. (2006) c-Jun NH2-terminal kinase signaling axis regulates diallyl trisulfide-induced generation of reactive oxygen species and cell cycle arrest in human prostate cancer cells, *Cancer Research* 66, 5379-5386.
27. Xiao, D., Herman-Antosiewicz, A., Antosiewicz, J., Xiao, H., Brisson, M., Lazo, J. S., and Singh, S. V. (2005) Diallyl trisulfide-induced G₂-M phase cell cycle arrest in human prostate cancer cells is caused by reactive oxygen species-dependent destruction and hyperphosphorylation of Cdc25C, *Oncogene* 24, 6256-6268.
28. Hosono, T., Fukao, T., Ogihara, J., Ito, Y., Shiba, H., Seki, T., and Ariga, T. (2005) Diallyl Trisulfide Suppresses the Proliferation and Induces Apoptosis of Human Colon Cancer Cells through Oxidative Modification of β -Tubulin, *Journal of Biological Chemistry* 280, 41487-41493.
29. Lee, B. C., Park, B. H., Kim, S. Y., and Lee, Y. J. (2011) Role of Bim in Diallyl Trisulfide-Induced Cytotoxicity in Human Cancer Cells, *J. Cell. Biochem.* 112, 118-127.
30. Iciek, M., Kwiecien, I., Chwatko, G., Sokolowska-Jezewicz, M., Kowalczyk-Pachel, D., and Rokita, H. (2012) The effects of garlic-derived sulfur compounds on cell proliferation, caspase 3 activity, thiol levels and anaerobic sulfur metabolism in human hepatoblastoma HepG2 cells, *Cell Biochemistry and Function* 30, 198-204.
31. Cerella, C., Scherer, C., Cristofanon, S., et al. (2009) Cell cycle arrest in early mitosis and induction of caspase-dependent apoptosis in U937 cells by diallyltetrasulfide (Al₂S₄), *Apoptosis* 14, 641-654.

32. Busch, C., Jacob, C., Anwar, A., *et al.* (2010) Diallylpolysulfides induce growth arrest and apoptosis, *International Journal of Oncology* 36, 743-749.
33. Kelkel, M., Cerella, C., Mack, F., Schneider, T., Jacob, C., Schumacher, M., Dicato, M., and Diederich, M. (2012) ROS-independent JNK activation and multisite phosphorylation of Bcl-2 link diallyl tetrasulfide-induced mitotic arrest to apoptosis, *Carcinogenesis* 33, 2162-2171.
34. Steudel, Y., Wong, M. W., and Steudel, R. (2005) Electrophilic attack on sulfur-sulfur bonds: Coordination of lithium cations to sulfur-rich molecules studied by ab initio MO methods, *Chemistry-a European Journal* 11, 1281-1293.
35. Schneider, T., Ba, L. A., Khairan, K., *et al.* (2011) Interactions of polysulfanes with components of red blood cells, *MedChemComm* 2, 196-200.
36. Tsuchiya, H., and Nagayama, M. (2008) Garlic allyl derivatives interact with membrane lipids to modify the membrane fluidity, *J. Biomed. Sci.* 15, 653-660.
37. Pickering, T. L., Saunders, K. J., and Tobolsky, A. V. (1967) Disproportionation of organic polysulfides, *Journal of the American Chemical Society* 89, 2364-2367.
38. Greer, A. (2001) On the Origin of Cytotoxicity of the Natural Product Varacin. A Novel Example of a Pentathiepin Reaction That Provides Evidence for a Triatomic Sulfur Intermediate, *Journal of the American Chemical Society* 123, 10379-10386.
39. Papageorgiou, C., Corbet, J. P., Menezes-Brandao, F., Pecegueiro, M., and Benezra, C. (1983) Allergic contact dermatitis to garlic (*Allium sativum* L.) identification of the allergens: The role of mono-, di-, and trisulfides present in garlic, *Arch Dermatol Res* 275, 229-234.
40. Munday, R., Munday, J. S., and Munday, C. M. (2003) Comparative effects of mono-, di-, tri-, and tetrasulfides derived from plants of the allium family: Redox cycling in vitro and hemolytic activity and phase 2 enzyme induction in vivo, *Free Radical Biology and Medicine* 34, 1200-1211.
41. Jacob, C., and Anwar, A. (2008) The chemistry behind redox regulation with a focus on sulphur redox systems, *Physiologia Plantarum* 133, 469-480.
42. Chatterji, T., Keerthi, K., and Gates, K. S. (2005) Generation of reactive oxygen species by a persulfide (BnSSH), *Bioorganic & Medicinal Chemistry Letters* 15, 3921-3924.
43. Kimura, H. (2011) Hydrogen sulfide: its production, release and functions, *Amino Acids* 41, 113-121.
44. Lefer, D. J. (2007) A new gaseous signaling molecule emerges: Cardioprotective role of hydrogen sulfide, *Proceedings of the National Academy of Sciences of the United States of America* 104, 17907-17908.
45. Dalle-Donne, I., Rossi, R., Giustarini, D., Colombo, R., and Milzani, A. (2007) S-glutathionylation in protein redox regulation, *Free Radical Biology and Medicine* 43, 883-898.
46. Van Laer, K., Hamilton, C. J., and Messens, J. (2013) Low-Molecular-Weight Thiols in Thiol-Disulfide Exchange, *Antioxidants & Redox Signaling* 18, 1642-1653.
47. Fahey, R. C. (2013) Glutathione analogs in prokaryotes, *Biochimica Et Biophysica Acta-General Subjects* 1830, 3182-3198.
48. Meister, A. (1988) Glutathione metabolism and its selective modification, *Journal of Biological Chemistry* 263, 17205-17208.
49. Meister, A. (1995) [1] Glutathione metabolism, In *Methods in Enzymology* (Lester, P., Ed.), pp 3-7, Academic Press.

50. Masip, L., Veeravalli, K., and Georgioui, G. (2006) The many faces of glutathione in bacteria, *Antioxidants & Redox Signaling* 8, 753-762.
51. Pastore, A., Federici, G., Bertini, E., and Piemonte, F. (2003) Analysis of glutathione: implication in redox and detoxification, *Clinica Chimica Acta* 333, 19-39.
52. Kalinina, E. V., Chernov, N. N., and Saprin, A. N. (2008) Involvement of Thio-, Peroxi-, and Glutaredoxins in Cellular Redox-Dependent Processes, *Biochemistry-Moscow* 73, 1493-1510.
53. Filomeni, G., Rotilio, G., and Ciriolo, M. R. (2002) Cell signalling and the glutathione redox system, *Biochemical Pharmacology* 64, 1057-1064.
54. Newton, G. L., Rawat, M., La Clair, J. J., Jothivasan, V. K., Budiarto, T., Hamilton, C. J., Claiborne, A., Helmann, J. D., and Fahey, R. C. (2009) Bacillithiol is an antioxidant thiol produced in Bacilli, *Nature Chemical Biology* 5, 625-627.
55. Gaballa, A., Newton, G. L., Antelmann, H., Parsonage, D., Upton, H., Rawat, M., Claiborne, A., Fahey, R. C., and Helmann, J. D. (2010) Biosynthesis and functions of bacillithiol, a major low-molecular-weight thiol in Bacilli, *Proceedings of the National Academy of Sciences of the United States of America* 107, 6482-6486.
56. Parsonage, D., Newton, G. L., Holder, R. C., et al. (2010) Characterization of the N-Acetyl-alpha-D-glucosaminyl L-Malate Synthase and Deacetylase Functions for Bacillithiol Biosynthesis in *Bacillus anthracis*, *Biochemistry* 49, 8398-8414.
57. Fang, Z., Roberts, A. A., Weidman, K., Sharma, S. V., Claiborne, A., Hamilton, C. J., and Dos Santos, P. C. (2013) Cross-functionalities of Bacillus deacetylases involved in bacillithiol biosynthesis and bacillithiol-S-conjugate detoxification pathways, *Biochemical Journal* 454, 239-247.
58. Roberts, A. A., Sharma, S. V., Strankman, A. W., Duran, S. R., Rawat, M., and Hamilton, C. J. (2013) Mechanistic studies of FosB: a divalent-metal-dependent bacillithiol-S-transferase that mediates fosfomycin resistance in *Staphylococcus aureus*, *Biochemical Journal* 451, 69-79.
59. Sharma, S. V., Arbach, M., Roberts, A. A., Macdonald, C. J., Groom, M., and Hamilton, C. J. (2013) Biophysical Features of Bacillithiol, the Glutathione Surrogate of *Bacillus subtilis* and other Firmicutes, *ChemBioChem* 14, 2160-2168.
60. Lee, J. W., Soonsanga, S., and Helmann, J. D. (2007) A complex thiolate switch regulates the *Bacillus subtilis* organic peroxide sensor OhrR, *Proceedings of the National Academy of Sciences of the United States of America* 104, 8743-8748.
61. Soonsanga, S., Lee, J.-W., and Helmann, J. D. (2008) Oxidant-dependent switching between reversible and sacrificial oxidation pathways for *Bacillus subtilis* OhrR, *Molecular Microbiology* 68, 978-986.
62. Chi, B. K., Gronau, K., Mäder, U., Hessling, B., Becher, D., and Antelmann, H. (2011) S-Bacillithiolation Protects Against Hypochlorite Stress in *Bacillus subtilis* as Revealed by Transcriptomics and Redox Proteomics, *Molecular & Cellular Proteomics* 10.
63. Chi, B. K., Roberts, A. A., Tran Thi Thanh, H., Baesell, K., Becher, D., Albrecht, D., Hamilton, C. J., and Antelmann, H. (2013) S-Bacillithiolation Protects Conserved and Essential Proteins Against Hypochlorite Stress in Firmicutes Bacteria, *Antioxidants & Redox Signaling* 18, 1273-1295.
64. Gaballa, A., Chi, B. K., Roberts, A. A., Becher, D., Hamilton, C. J., Antelmann, H., and Helmann, J. D. (2013) Redox regulation in *Bacillus subtilis*: the bacilliredoxins BrxA (YphP) and BrxB (YqiW) function in de-bacillithiolation of S-bacillithiolated OhrR and MetE, *Antioxidants & Redox Signaling advanced online publication*.

65. Newton, G. L., Arnold, K., Price, M. S., *et al.* (1996) Distribution of thiols in microorganisms: Mycothiol is a major thiol in most actinomycetes, *Journal of Bacteriology* 178, 1990-1995.
66. delCardayre, S. B., Stock, K. P., Newton, G. L., Fahey, R. C., and Davies, J. E. (1998) Coenzyme A disulfide reductase, the primary low molecular weight disulfide reductase from *Staphylococcus aureus* - Purification and characterization of the native enzyme, *Journal of Biological Chemistry* 273, 5744-5751.
67. Luba, J., Charrier, V., and Claiborne, A. (1999) Coenzyme A-disulfide reductase from *Staphylococcus aureus*: Evidence for asymmetric behavior on interaction with pyridine nucleotides, *Biochemistry* 38, 2725-2737.
68. Mallett, T. C., Wallen, J. R., Karplus, P. A., Sakai, H., Tsukihara, T., and Claiborne, A. (2006) Structure of coenzyme A-disulfide reductase from *Staphylococcus aureus* at 1.54 angstrom resolution, *Biochemistry* 45, 11278-11289.
69. Wallen, J. R., Paige, C., Mallett, T. C., Karplus, P. A., and Claiborne, A. (2008) Pyridine nucleotide complexes with *Bacillus anthracis* coenzyme A-disulfide reductase: A structural analysis of dual NAD(P)H specificity, *Biochemistry* 47, 5182-5193.
70. Keire, D. A., Strauss, E., Guo, W., Noszal, B., and Rabenstein, D. L. (1992) Kinetics and equilibria of thiol/disulfide interchange reactions of selected biological thiols and related molecules with oxidized glutathione, *The Journal of Organic Chemistry* 57, 123-127.
71. Setlow, B., and Setlow, P. (1977) Levels of acetyl coenzyme-A, reduced and oxidized coenzyme-A, and coenzyme-A in disulfide linkage to protein in dormant and germinated spores and growing and sporulating cells of *Bacillus megaterium*, *Journal of Bacteriology* 132, 444-452.
72. Nagy, P. (2013) Kinetics and Mechanisms of Thiol–Disulfide Exchange Covering Direct Substitution and Thiol Oxidation-Mediated Pathways, *Antioxidants & Redox Signaling* 18, 1623-1641.
73. Rabenstein, D. L. (1973) Nuclear magnetic resonance studies of the acid-base chemistry of amino acids and peptides. I. Microscopic ionization constants of glutathione and methylmercury-complexed glutathione, *Journal of the American Chemical Society* 95, 2797-2803.
74. Singh, R., and Whitesides, G. M. (1993) Thiol-disulfide exchange, (Patai, S., and Rappoport, Z., Eds.), John Wiley & Sons Ltd.
75. Everett, S. A., and Wardman, P. (1995) Perthiols as antioxidants: Radical-scavenging and prooxidative mechanisms, In *Methods in Enzymology* (Lester, P., Ed.), pp 55-69, Academic Press.
76. Saidu, N. E. B., Abu Asali, I., Czepukojc, B., Seitz, B., Jacob, C., and Montenarh, M. (2013) Comparison between the effects of diallyl tetrasulfide on human retina pigment epithelial cells (ARPE-19) and HCT116 cells, *Biochimica Et Biophysica Acta-General Subjects* 1830, 5267-5276.
77. Gallwitz, H., Bonse, S., Martinez-Cruz, A., Schlichting, I., Schumacher, K., and Krauth-Siegel, R. L. (1999) Ajoene is an inhibitor and subversive substrate of human glutathione reductase and *Trypanosoma cruzi* trypanothione reductase: Crystallographic, kinetic, and spectroscopic studies, *Journal of Medicinal Chemistry* 42, 364-372.
78. Moutiez, M., Aumercier, M., Teissier, E., Parmentier, B., Tartar, A., and Sergheraert, C. (1994) Reduction of a trisulfide derivative of glutathione by glutathione-reductase, *Biochemical and Biophysical Research Communications* 202, 1380-1386.

79. Hinman, A., Chuang, H.-H., Bautista, D. M., and Julius, D. (2006) TRP channel activation by reversible covalent modification, *Proceedings of the National Academy of Sciences of the United States of America* 103, 19564-19568.
80. (2009) Regulation (EC) No 1107/2009 of the European parliament and of the council of 21 October 2009 concerning the placing of plant protection products on the market and repealing Council Directives 79/117/EEC and 91/414/EEC, In 1107/2009 (Union, E., Ed.), Official Journal of the European Union.
81. Anwar, A. (2009) Natural Polysulfides- Reactive Sulfur Species from Allium with Applications in Medicine and Agriculture, In *Faculty III (Natural Science and Technics)*, Saarland University, Saarbrücken.
82. Derbesy, G., and Harpp, D. N. (1994) A simple method to prepare unsymmetrical disulfide trisulfide and tetrasulfide, *Tetrahedron Letters* 35, 5381-5384.
83. Wang, K., Groom, M., Sheridan, R., Zhang, S., and Block, E. (2013) Liquid sulfur as a reagent: synthesis of polysulfanes with 20 or more sulfur atoms with characterization by UPLC-(Ag⁺)-coordination ion spray-MS, *Journal of Sulfur Chemistry* 34, 55-66.
84. Zhang, G., Li, B., Lee, C.-H., and Parkin, K. L. (2010) Cysteine and Glutathione Mixed-Disulfide Conjugates of Thiosulfates: Chemical Synthesis and Biological Activities, *Journal of Agricultural and Food Chemistry* 58, 1564-1571.
85. Kitko, R. D., Cleeton, R. L., Armentrout, E. I., Lee, G. E., Noguchi, K., Berkmen, M. B., Jones, B. D., and Slonczewski, J. L. (2009) Cytoplasmic Acidification and the Benzoate Transcriptome in *Bacillus subtilis*, *Plos One* 4.
86. Mulhearn, D. C., and Bachrach, S. M. (1996) Selective nucleophilic attack of trisulfides. An *ab initio* study, *Journal of the American Chemical Society* 118, 9415-9421.
87. Steudel, R., Steudel, Y., and Miaskiewicz, K. (2001) Does the interconversion of polysulfur compounds proceed via hypervalent intermediates? - An *ab initio* MO study, *Chemistry-a European Journal* 7, 3281-3290.
88. Chatterji, T., and Gates, K. S. (2003) Reaction of thiols with 7-methylbenzopentathiepin, *Bioorganic & Medicinal Chemistry Letters* 13, 1349-1352.
89. Anwar, A., Burkholz, T., Scherer, C., Abbas, M., Lehr, C.-M., Diederich, M., Jacob, C., and Daum, N. (2008) Naturally occurring reactive sulfur species, their activity against Caco-2 cells, and possible modes of biochemical action (vol 28, pg 251, 2008), *Journal of Sulfur Chemistry* 29, 573-573.
90. Yabroff, D. L. (1940) Extraction of Mercaptans with Alkaline Solutions, *Industrial & Engineering Chemistry* 32, 257-262.
91. Hong, H. A., Khaneja, R., Tam, N. M. K., et al. (2009) *Bacillus subtilis* isolated from the human gastrointestinal tract, *Research in Microbiology* 160, 134-143.
92. Kunst, F., Ogasawara, N., Moszer, I., et al. (1997) The complete genome sequence of the Gram-positive bacterium *Bacillus subtilis*, *Nature* 390, 249-256.
93. Andrews, J. M. (2001) Determination of minimum inhibitory concentrations, *Journal of Antimicrobial Chemotherapy* 48, 5-16.
94. Naganawa, R., Iwata, N., Ishikawa, K., Fukuda, H., Fujino, T., and Suzuki, A. (1996) Inhibition of microbial growth by ajoene, a sulfur-containing compound derived from garlic, *Appl. Environ. Microbiol.* 62, 4238-4242.
95. Yoshida, H., Iwata, N., Katsuzaki, H., Naganawa, R., Ishikawa, K., Fukuda, H., Fujino, T., and Suzuki, A. (1998) Antimicrobial activity of a compound isolated from an oil-macerated garlic extract, *Bioscience, Biotechnology, and Biochemistry* 62, 1014-1017.

96. Bratbak, G., and Dundas, I. (1984) Bacterial dry-matter content and biomass estimations, *Appl. Environ. Microbiol.* **48**, 755-757.
97. Crow, A., Acheson, R. M., Le Brun, N. E., and Oubrie, A. (2004) Structural basis of redox-coupled protein substrate selection by the cytochrome c biosynthesis protein ResA, *Journal of Biological Chemistry* **279**, 23654-23660.
98. Moeller, M., and Hederstedt, L. (2006) Role of membrane-bound thiol-disulfide oxidoreductases in endo spore-forming bacteria, *Antioxidants & Redox Signaling* **8**, 823-833.
99. Tamura, H., Saito, Y., Ashida, H., Inoue, T., Kai, Y., Yokota, A., and Matsumura, H. (2008) Crystal structure of 5-methylthioribose 1-phosphate isomerase product complex from *Bacillus subtilis*: Implications for catalytic mechanism, *Protein Science* **17**, 126-135.
100. Pan, J., and Carroll, K. S. (2014) Chemical Biology Approaches to Study Protein Cysteine Sulfenylation, *Biopolymers* **101**, 165-172.
101. Lo Conte, M., and Carroll, K. S. (2013) The redox biochemistry of protein sulfenylation and sulfinylation, *The Journal of biological chemistry* **288**, 26480-26488.
102. Reddie, K. G., Seo, Y. H., Muse, W. B., III, Leonard, S. E., and Carroll, K. S. (2008) A chemical approach for detecting sulfenic acid-modified proteins in living cells, *Molecular Biosystems* **4**, 521-531.
103. Lo Conte, M., and Carroll, K. S. (2012) Chemoselective Ligation of Sulfinic Acids with Aryl-Nitroso Compounds, *Angewandte Chemie-International Edition* **51**, 6502-6505.
104. Wang, Y., Song, W., Hu, W. J., and Lin, Q. (2009) Fast Alkene Functionalization *In Vivo* by Photoclick Chemistry: HOMO Lifting of Nitrile Imine Dipoles, *Angewandte Chemie-International Edition* **48**, 5330-5333.
105. Yu, Z., Ho, L. Y., and Lin, Q. (2011) Rapid, Photoactivatable Turn-On Fluorescent Probes Based on an Intramolecular Photoclick Reaction, *Journal of the American Chemical Society* **133**, 11912-11915.
106. Houk, K. N., Sims, J., Watts, C. R., and Luskus, L. J. (1973) Origin of reactivity, regioselectivity, and periselectivity in 1,3-dipolar cycloadditions, *Journal of the American Chemical Society* **95**, 7301-7315.
107. Song, W., Wang, Y., Qu, J., and Lin, Q. (2008) Selective functionalization of a genetically encoded alkene-containing protein via "Photoclick Chemistry" in bacterial cells, *Journal of the American Chemical Society* **130**, 9654-+.
108. Song, W., Wang, Y., Yu, Z., Vera, C. I. R., Qu, J., and Lin, Q. (2010) A Metabolic Alkene Reporter for Spatiotemporally Controlled Imaging of Newly Synthesized Proteins in Mammalian Cells, *Acs Chemical Biology* **5**, 875-885.
109. Chen, W., Liu, C., Peng, B., Zhao, Y., Pacheco, A., and Xian, M. (2013) New fluorescent probes for sulfane sulfurs and the application in bioimaging, *Chemical Science* **4**, 2892-2896.
110. Chitwood, D. J. (2003) Nematicides, In *Encyclopedia of Agrochemicals* (Plimmer, J. R., Ed.), pp 1104-1115, John Wiley & Sons, New York.
111. Bridge, J., and Starr, J. L. (2007) *Plant Nematodes of Agricultural Importance - A Colour Handbook*, Manson Publishing Ltd, London.
112. Evans, K., Trudfill, D. I., and Webster, J. M. (1993) *Plant parasitic nematodes in temperate agriculture*.

113. Karszen, G., Bolk, R. J., Van Aelst, A. C., *et al.* (2004) Description of *Meloidogyne minor* n. sp (Nematoda : Meloidogynidae), a root-knot nematode associated with yellow patch disease in golf courses, *Nematology* 6, 59-72.
114. Morris, K., Horgan, F. G., and Griffin, C. T. (2013) Spatial and temporal dynamics of *Meloidogyne minor* on creeping bentgrass in golf greens, *Plant Pathology* 62, 1166-1172.
115. Viaene, N., Wiseborn, D. B., and Karszen, G. (2007) First report of the root-knot nematode *Meloidogyne minor* on turfgrass in Belgium, *Plant Disease* 91, 908-908.
116. Turner, S. J., and Fleming, C. C. (2005) *Meloidogyne minor*: A threat to temperate crops?, *Communications in Agricultural and Applied Biological Sciences* 70, 885-887.
117. Morris, K. S., Horgan, F. G., Downes, M. J., and Griffin, C. T. (2011) The effect of temperature on hatch and activity of second-stage juveniles of the root-knot nematode, *Meloidogyne minor*, an emerging pest in north-west Europe, *Nematology* 13, 985-993.
118. Thoden, T. C., Korthals, G. W., Visser, J., and van Gastel-Topper, W. (2012) A field study on the host status of different crops for *Meloidogyne minor* and its damage potential on potatoes, *Nematology* 14, 277-284.
119. Brewster, C. V. root-knot nematodes disease cycle, American Phytopathological Society.
120. Garthwaite, D. G., Hudson, S., Barker, I., Parrish, G., Smith, L., and Pietravalle, S. (2012) Pesticide usage survey report 250 - Arable crops in the United Kingdom 2012, (Department for Environment, F. a. R. A., Ed.).
121. Byrne, J. T., Maher, N. J., and Jones, P. W. (2001) Comparative responses of *Globodera rostochiensis* and *G. pallida* to hatching chemicals, *Journal of Nematology* 33, 195-202.
122. Anonymous. (2000) Protection of stratospheric ozone: incorporation of Clean Air Act Amendments for reductions in Class I, Group VI controlled substances., (Register, F., Ed.).
123. Thomas, W. B. (1996) Methyl bromide: Effective pest management tool and environmental threat, *Journal of Nematology* 28, 586-589.
124. Eskenazi, B., Bradman, A., and Castorina, R. (1999) Exposures of children to organophosphate pesticides and their potential adverse health effects, *Environmental Health Perspectives* 107, 409-419.
125. Wessels, D., Barr, D. B., and Mendola, P. (2003) Use of biomarkers to indicate exposure of children to organophosphate pesticides: Implications for a longitudinal study of children's environmental health, *Environmental Health Perspectives* 111, 1939-1946.
126. Jaga, K., and Dharmani, C. (2003) Sources of exposure to and public health implications of organophosphate pesticides, *Revista panamericana de salud publica = Pan American journal of public health* 14, 171-185.
127. Slotkin, T. A. (2004) Guidelines for developmental neurotoxicity and their impact on organophosphate pesticides: A personal view from an academic perspective, *Neurotoxicology* 25, 631-640.
128. Abram, M. (2011) British Potato 2011: Nematicide residue warning, <http://www.fwi.co.uk/articles/28/11/2011/130274/british-potato-2011-nematicide-residue-warning.htm>.
129. Chitwood, D. J. (2002) Phytochemical based strategies for nematode control, *Annual Review of Phytopathology* 40, 221 ff.

130. Akhtar, M., and Mahmood, I. (1994) Potentiality of phytochemicals in nematode control: A review, *Bioresource Technology* 48, 189-201.
131. Grewal, P. S. (1989) Nematicidal effects of some plant extracts to *Aphelenchoides composticola* nematoda infesting mushroom *Agaricus bisporus*, *Revue de Nematologie* 12, 317-322.
132. Park, I. K., Park, J. Y., Kim, K. H., Choi, K. S., Choi, I. H., Kim, C. S., and Shin, S. C. (2005) Nematicidal activity of plant essential oils and components from garlic (*Allium sativum*) and cinnamon (*Cinnamomum verum*) oils against the pine wood nematode (*Bursaphelenchus xylophilus*), *Nematology* 7, 767-774.
133. Sukul, N. C., Das, P. K., and De, G. C. (1974) Nematicidal Action of Some Edible Crops, *Nematologica* 20, 187-191.
134. El-Nagdi, W. M. A.-E., and Youssef, M. M. A. (2013) Comparative efficacy of garlic clove and castor seed aqueous extracts against the root-knot nematode, *Meloidogyne incognita* infecting tomato plants, *Journal of Plant Protection Research* 53, 285-288.
135. Hilliard, M. A., Bergamasco, C., Arbucci, S., Plasterk, R. H. A., and Bazzicalupo, P. (2004) Worms taste bitter: ASH neurons, QUI-1, GPA-3 and ODR-3 mediate quinine avoidance in *Caenorhabditis elegans*, *Embo Journal* 23, 1101-1111.
136. Cetintas, R., and Yarba, M. M. (2010) Nematicidal Effects of Five Plant Essential Oils on the Southern Root-Knot Nematode, *Meloidogyne incognita* Race 2, *J. Anim. Vet. Adv.* 9, 222-225.
137. Asamoto, H., Ichibangase, T., Saimaru, H., Uchikura, K., and Imai, K. (2007) Existence of low-molecular-weight thiols in *Caenorhabditis elegans* demonstrated by HPLC-fluorescence detection utilizing 7-chloro-N-[2-(dimethylamino)ethyl]-2,1,3-benzoxadiazole-4-sulfonamide, *Biomedical Chromatography* 21, 999-1004.
138. Luersen, K., Muller, S., Hussein, A., Liebau, E., and Walter, R. D. (2000) The γ -glutamylcysteine synthetase of *Onchocerca volvulus*, *Molecular and Biochemical Parasitology* 111, 243-251.
139. Ajonina, C., Sommer, A., Luersen, K., Liebau, E., and Walter, R. D. (2004) Glutathione synthesis in parasitic nematodes: *Caenorhabditis elegans* as a model system, *International Journal of Medical Microbiology* 293, 109-110.
140. van Rossum, A. J., Brophy, P. M., Tait, A., Barrett, J., and Jefferies, J. R. (2001) Proteomic identification of glutathione S-transferases from the model nematode *Caenorhabditis elegans*, *Proteomics* 1, 1463-1468.
141. Kriksunov, I. A., Schuller, D. J., Campbell, A. M., Barrett, J., Brophy, P. M., and Hao, Q. (2003) Crystallization and preliminary crystallographic analysis of a new class of glutathione transferase from nematodes, *Acta Crystallographica Section D-Biological Crystallography* 59, 1262-1264.
142. Campbell, A. M., Teesdale-Spittle, P. H., Barrett, J., Liebau, E., Jefferies, J. R., and Brophy, P. M. (2001) A common class of nematode glutathione S-transferase (GST) revealed by the theoretical proteome of the model organism *Caenorhabditis elegans*, *Comparative Biochemistry and Physiology B-Biochemistry & Molecular Biology* 128, 701-708.
143. Jones, J. T., Reavy, B., Smant, G., and Prior, A. E. (2004) Glutathione peroxidases of the potato cyst nematode *Globodera rostochiensis*, *Gene* 324, 47-54.
144. Tang, L., Gounaris, K., Griffiths, C. M., and Selkirk, M. E. (1995) Heterologous expression and enzymatic-properties of a selenium-independent glutathione-peroxidase from the parasitic nematode *Brugia pahangi*, *Journal of Biological Chemistry* 270, 18313-18318.

145. Lueersen, K., Stegehake, D., Daniel, J., Drescher, M., Ajonina, I., Ajonina, C., Hertel, P., Woltersdorf, C., and Liebau, E. (2013) The Glutathione Reductase GSR-1 Determines Stress Tolerance and Longevity in *Caenorhabditis elegans*, *Plos One* 8.
146. Baldacci-Cresp, F., Chang, C., Maucourt, M., *et al.* (2012) (Homo)glutathione Deficiency Impairs Root-knot Nematode Development in *Medicago truncatula*, *Plos Pathogens* 8.
147. Ho, N. F. H., Sims, S. M., Vidmar, T. J., Day, J. S., Barsuhn, C. L., Thomas, E. M., Geary, T. G., and Thompson, D. P. (1994) Theoretical perspectives on anthelmintic drug discovery: Interplay of transport kinetics, physicochemical properties, and *in vitro* activity of anthelmintic drugs, *Journal of Pharmaceutical Sciences* 83, 1052-1059.
148. Evans, A. A. F. (1973) Mode of action of nematicides, *Annals of Applied Biology* 75, 469-473.
149. Zanetti, D. G. (2008) Efficacy evaluation of NEMguard against root-knot nematodes (*Meloidogyne* spp.) on carrot, pp 1-20, Centro di Saggio per la Sperimentazione in Agricoltura, Ferrara, Italy.
150. Trudgill, D. L., Elliott, M. J., Evans, K., and Phillips, M. S. (2003) The white potato cyst nematode (*Globodera pallida*) - a critical analysis of the threat in Britain, *Annals of Applied Biology* 143, 73-80.
151. Evans, K. (1993) Changes in the relative proportions of the 2 species of potato cyst nematodes in microplots in which different potato clones were grown for 7 years, *Nematologica* 39, 505-511.
152. Lamondia, J. A., and Brodie, B. B. (1986) Effects of initial nematode density on population-dynamics of *Globodera rostochiensis* on resistant and susceptible potatoes, *Journal of Nematology* 18, 159-165.
153. Whitehead, A. G., Nichols, A. J. F., and Senior, J. C. (1994) The control of potato pale cyst-nematode (*Globodera pallida*) by chemical and cultural methods in different soils, *Journal of Agricultural Science* 123, 207-218.
154. Amonkar, S. V., and Banerji, A. (1971) Isolation and characterization of larvicidal principle of garlic, *Science* 174, 1343-&.
155. Sharma, S. V., Jothivasan, V. K., Newton, G. L., *et al.* (2011) Chemical and Chemoenzymatic Syntheses of Bacillithiol: A Unique Low-Molecular-Weight Thiol amongst Low G+C Gram-Positive Bacteria, *Angewandte Chemie-International Edition* 50, 7101-7104.
156. Fahey, R. C., and Newton, G. L. (1987) Determination of low molecular weight thiols using monobromobimane fluorescent labeling and high performance liquid chromatography, *Methods in Enzymology* 143, 85-96.
157. Riddles, P. W., Blakeley, R. L., and Zerner, B. (1983) [8] Reassessment of Ellman's reagent, In *Methods in Enzymology* (C.H.W. Hirs, S. N. T., Ed.), pp 49-60, Academic Press.
158. Miron, T., Rabinkov, A., Weiner, L., Mirelman, D., and Wilchek, M. (2001) S-allylmercaptogluthathione and uses thereof, In *European Patent Office*.
159. Kosower, E. M., Pazhenchevsky, B., and Hershkowitz, E. (1978) 1,5-Diazabicyclo[3.3.0]octadienediones (9,10-dioxabimanes). Strongly fluorescent syn isomers, *Journal of the American Chemical Society* 100, 6516-6518.
160. Nicholas, G. M., Kovac, P., and Bewley, C. A. (2002) Total synthesis and proof of structure of mycothiol bimane, *Journal of the American Chemical Society* 124, 3492-3493.
161. Ellman, G. L. (1959) Tissue sulfhydryl groups, *Archives of Biochemistry and Biophysics* 82, 70-77.

162. Newton, G. L., Ta, P., and Fahey, R. C. (2005) A mycothiol synthase mutant of *Mycobacterium smegmatis* produces novel thiols and has an altered thiol redox status, *Journal of Bacteriology* 187, 7309-7316.
163. Hansen, R. E., and Winther, J. R. (2009) An introduction to methods for analyzing thiols and disulfides: Reactions, reagents, and practical considerations, *Analytical Biochemistry* 394, 147-158.
164. Anderson, M. E. (1985) [70] Determination of glutathione and glutathione disulfide in biological samples, In *Methods in Enzymology* (Alton, M., Ed.), pp 548-555, Academic Press.
165. Whitesides, G. M., Lilburn, J. E., and Szajewski, R. P. (1977) Rates of thiol-disulfide interchange reactions between mono- and dithiols and Ellmans reagent, *Journal of Organic Chemistry* 42, 332-338.

DOI: 10.1002/cbic.201300404

Biophysical Features of Bacillithiol, the Glutathione Surrogate of *Bacillus subtilis* and other Firmicutes

Sunil V. Sharma,^[a] Miriam Arbach,^[a, b] Alexandra A. Roberts,^[a] Colin J. Macdonald,^[c] Murree Groom,^[b] and Chris J. Hamilton^{*[a]}

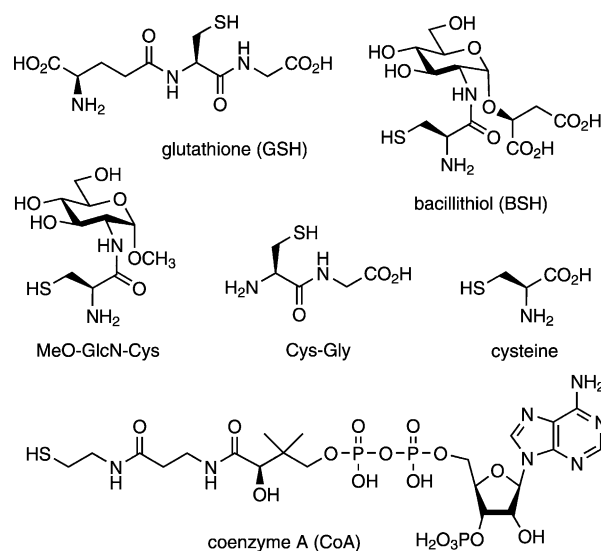
Bacillithiol (BSH) is the major low-molecular-weight (LMW) thiol in many low-G+C Gram-positive bacteria (Firmicutes). Evidence now emerging suggests that BSH functions as an important LMW thiol in redox regulation and xenobiotic detoxification, analogous to what is already known for glutathione and mycothiol in other microorganisms. The biophysical properties and cellular concentrations of such LMW thiols are important determinants of their biochemical efficiency both as biochemical nucleophiles and as redox buffers. Here, BSH has been characterised and compared with other LMW thiols in terms of its thiol pK_a , redox potential and thiol–disulfide exchange reac-

tivity. Both the thiol pK_a and the standard thiol redox potential of BSH are shown to be significantly lower than those of glutathione whereas the reactivities of the two compounds in thiol–disulfide reactions are comparable. The cellular concentration of BSH in *Bacillus subtilis* varied over different growth phases and reached up to 5 mM, which is significantly greater than previously observed from single measurements taken during mid-exponential growth. These results demonstrate that the biophysical characteristics of BSH are distinctively different from those of GSH and that its cellular concentrations can reach levels much higher than previously reported.

Introduction

In eukaryotes and most Gram-negative bacteria, glutathione (GSH, Scheme 1) is the major low-molecular-weight (LMW) thiol cofactor, serving a number of important metabolic functions.^[1,2] GSH plays a critical role in oxidative stress management and in maintaining an intracellular reducing environment. Protein glutathionylation (reversible formation of GS–S–protein disulfides) is also an important post-translational modification for regulating protein function and protecting exposed cysteine (Cys) residues from irreversible damage during oxidative stress.^[3,4] Glutathione-S-transferases mediate the metabolism/detoxification of various electrophilic metabolites/xenobiotics through S-conjugation with GSH, whereas GSH-dependent glyoxalases mediate detoxification of methylglyoxal to lactic acid.^[5]

Instead of GSH, many Gram-positive bacteria produce other, structurally distinct LMW thiols, which serve similar metabolic functions to GSH.^[6–9] In 2009, bacillithiol (BSH, Scheme 1) was discovered as the predominant LMW thiol in many low-G+C Gram-positive Firmicutes, which do not produce GSH or myco-




Scheme 1. Structures of the LMW thiols relevant to this study.

thiol (MSH).^[10] These include bacilli (e.g., *Bacillus subtilis*, *B. anthracis*, *B. cereus*, *B. megaterium*, *B. pumilis*) and some staphylococci (e.g., *Staphylococcus aureus*, *S. saprophyticus*) and streptococci (*Streptococcus agalactiae*). The functions of this recently discovered biothiol, such as its role in detoxification of fosfomycin,^[11] reactive oxidants and methylglyoxal,^[12] as well as the protection and redox regulation of protein function (i.e., protein-S-bacillithiolation during oxidative stress),^[13,14] are now beginning to emerge. As with other LMW thiols,^[15] the thiol pK_a , redox potential and intracellular concentrations of BSH are implicated in its functional efficiency both as a redox buffer and a chemical scavenger of reactive oxidants and electrophiles.

[a] Dr. S. V. Sharma, M. Arbach, Dr. A. A. Roberts, Dr. C. J. Hamilton
School of Pharmacy, University of East Anglia
Norwich Research Park, Norwich NR4 7TJ (UK)
E-mail: c.hamilton@uea.ac.uk

[b] M. Arbach, Dr. M. Groom
ECOSpray Limited
Grange Farm Hilborough, Thetford, Norfolk IP26 5BT (UK)

[c] Dr. C. J. Macdonald
School of Chemistry, University of East Anglia
Norwich Research Park, Norwich NR4 7TJ, (UK)

 Supporting information for this article is available on the WWW under <http://dx.doi.org/10.1002/cbic.201300404>.

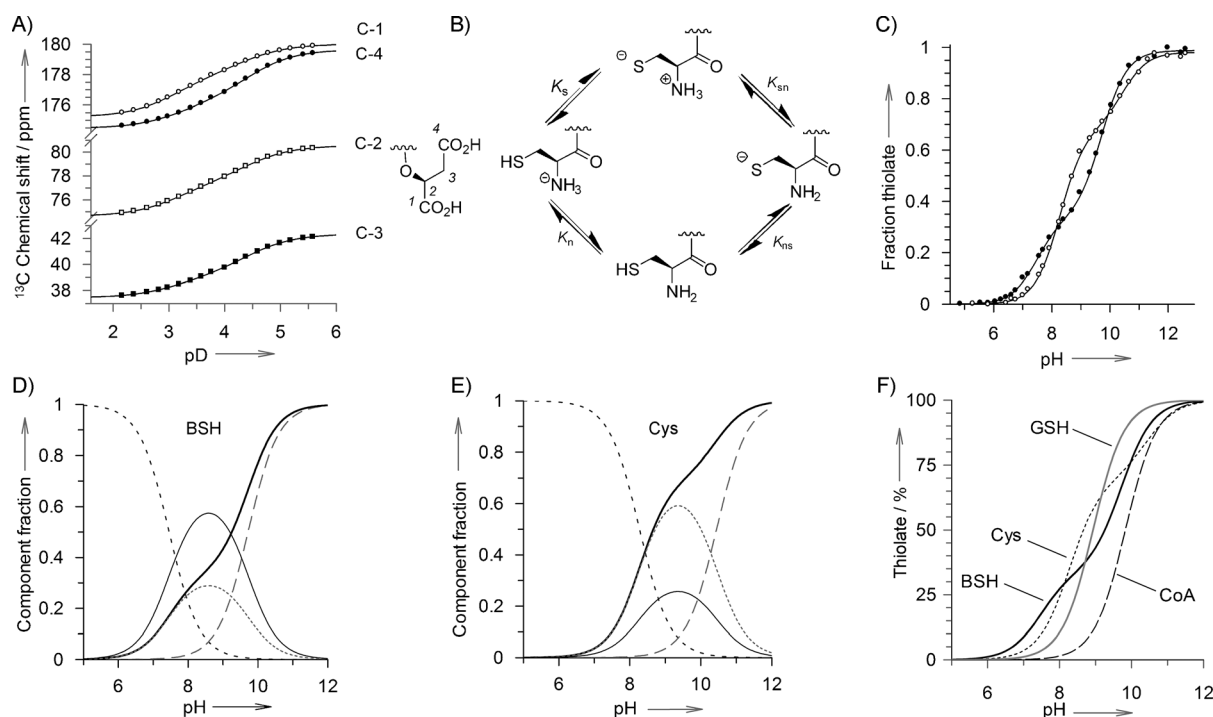


Figure 1. Macro/microscopic pK_a analyses of BSH and Cys. A) Chemical shifts of the malate carbon atoms of BSH C-1 (○), C-4 (●), C-2 (□), C-3 (■) as a function of pD. B) The deprotonation pathways that account for the four microscopic acid dissociation constants for a cysteinyl thiol bearing a free amino group. C) pH-dependent thiolate titration curves for BSH (●) and Cys (○). D) and E) The calculated pH-dependent proportions of different thiol/amino protonation forms [HS–NH₃⁺ (-----), [–]S–NH₃⁺ (.....), HS–NH₂ (—), [–]S–NH₂ (---) and total thiolate (—) of BSH and Cys, respectively. F) The calculated pH-dependent proportions of total thiolate forms of BSH (—), GSH (—), Cys (.....) and CoA (---).

Here the fundamental biophysical properties of BSH have been determined and compared with those of other LMW thiols.

Results

Thiol, amine and carboxylate pK_a values

The macroscopic pK_a values for the malate carboxylate groups of BSH (pK_{a1} and pK_{a2}) were determined from titration curves showing changes in the ¹³C NMR chemical shifts of the malate carbon atoms in the pD 2.1–5.6 range (Figure 1 A). This provided pK_a values of 3.14 and 4.38 (Table 1), which are both lower

than the corresponding pK_a values for malic acid (3.40 and 5.13).^[16]

Macroscopic pK_a values for the thiol and amino groups of BSH and Cys (pK_{a3} and pK_{a4} ; Table 1) were determined by measuring the pH-dependent changes in absorbance at 232 nm for the thiolate anion (Figure 1 C).^[17,18] The methyl glycoside derivative of BSH—MeO-GlcN-Cys (Scheme 1)—was also analysed to gain insight into the influence of the BSH malate aglycone on its thiol and amine acid dissociation constants relative to Cys. The macroscopic pK_a values do not represent the individual (microscopic) pK_a values of the thiol and ammonium groups, because the pK_a of each is influenced by the protonation status of the other.^[19] The sequential deprotonation of the

Table 1. Macroscopic and microscopic pK_a values of different LMW thiols.^[a]

	Cys	BSH	MeO-GlcN-Cys	Cys-Gly ^[18]	Cys ^[18]	GSH ^[41]	CoA ^[42]	Malic acid
pK_{a3}	8.28 ^[b]	7.46	7.02		8.33 ^[b]			
pK_{a4}	10.45 ^[c]	9.72	9.39		10.7 ^[c]			
pK_s	8.38	7.97	7.79	7.87	8.53	8.93	9.83	
pK_n	8.77	7.63	7.10	7.14	8.86			
pK_{ns}	9.94	9.55	9.31	9.48	10.03			
pK_{sn}	10.40	9.21	8.62	8.75	10.36			
pK_{a1}		3.14						3.40 ^[16]
pK_{a2}		4.38						5.13 ^[16]

[a] For clarity, standard errors have been omitted from this table; however, standard deviations for calculated pK values were all < 0.09 pK units. The data errors are provided in the Supporting Information. [b] Cys only contains a single carboxylic acid group, so this value is pK_{a2} . [c] Cys only contains a single carboxylic acid group, so this value is pK_{a3} .

thiol and ammonium groups can proceed by two different routes (Figure 1B). Four different forms of these compounds can therefore exist; their microscopic dissociation constants (pK_s , pK_{nr} , pK_{sn} and pK_{ns} , Table 1) were then calculated from the macroscopic pK_a and pH-dependent thiolate concentrations as described in Equations (2)–(5) in the Experimental Section.

The values obtained for Cys were comparable to those previously determined by similar procedures.^[18] The Cys microscopic pK_a values show that the ammonium group is a weaker acid than the thiol by ≈ 0.4 pK_a units (i.e., $pK_n > pK_s$ and $pK_{sn} > pK_{ns}$). The microscopic pK_a values for BSH were all consistently lower than those determined for Cys. However, contrary to what is observed for Cys, in BSH the ammonium group is more acidic than the thiol by ≈ 0.3 pK_a units (i.e., $pK_n < pK_s$ and $pK_{sn} < pK_{ns}$). Replacing the malate portion of BSH with an uncharged methyl aglycone (MeO-GlcN-Cys) lowers all of the microscopic pK_a values even further, but the effect is most notable for the microscopic acid dissociation constants for the amino group (pK_n and pK_{sn}), which are ≈ 0.5 pK_a units lower than those of BSH. This effect could be due to one (or both) of the negatively charged BSH carboxylate groups helping to stabilise the positively charged ammonium group in its protonated form. Consequently, the loss of this stabilising effect in MeO-GlcN-Cys makes the ammonium group more acidic.

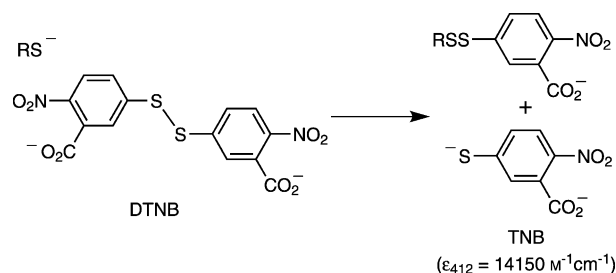
The BSH pK_a values are more comparable to those of Cys-Gly than to those of Cys. Although the inductive effect of the cysteine carboxylate group helps to increase the acidity of the thiol and ammonium groups, this is partially tempered by the electrostatic effect of its negative charge. With both BSH and Cys-Gly the cysteinyl carboxylate is capped with an uncharged amide group, so the inductive effect remains, but the electrostatic effect is removed; hence the acidities of both the amino and thiol functional groups are increased. These observations indicate that, unlike in the case of Cys, the amino and thiol pK_a values of BSH are more strongly influenced by the amide-linked glucosamine motif than by the malate aglycone. Whereas the acidity of the BSH is comparable to that of Cys-Gly, the compound is significantly more acidic than GSH, which lacks a positively charged amino group on its cysteine residue to help stabilise the thiolate anion.

The microscopic pK_a values were used to calculate the proportions of the different protonated forms of BSH and Cys over the pH 6–12 range (Figure 1D and E). The percentage ratios at pH 7.7 are presented in Table 2. A comparison of the pH-dependent proportions of total thiolate forms of BSH, GSH, Cys and CoA is also given in Figure 1F.

Protonation status	Proportion at pH 7.7 [%]		
	BSH	Cys	CoA
HS-NH ₃ ⁺	36.5	79.1	–
[–] S-NH ₃ ⁺	20.9	14.4	–
HS-NH ₂	41.6	6.3	–
[–] S-NH ₂	1.0	0.2	–
total RS [–]	21.9	14.6	0.7

Thiol–disulfide exchange reactivity

Mechanistically, a thiol–disulfide exchange reaction proceeds through a simple S_N2 displacement reaction between a thiolate anion and a disulfide.^[19] The reactivity of the thiolate nucleophile in such a reaction depends on its acidity and the pH of the reaction buffer. The more acidic the thiol, the higher its thiolate concentration will be at physiological pH. To gauge the relative thiol–disulfide exchange reactivities of the thiolate anions of BSH, Cys and CoA, their pH-independent rate constants (k_1) were determined for reaction with 5,5'-dithiobis-(2-nitrobenzoic acid) (DTNB) as a model disulfide (Scheme 2).



Scheme 2. The thiolate reaction with Ellman's reagent used to measure thiol–disulfide exchange reactivity.

The rate constant determined for GSH ($2.02 \times 10^5 \text{ M}^{-1} \text{ s}^{-1}$, Table 3) was comparable to that previously determined under similar conditions ($2.0 \times 10^5 \text{ M}^{-1} \text{ s}^{-1}$).^[20] Whereas k_1 for CoA was comparable to that of GSH, BSH and Cys were two and four

Table 3. Thiol–disulfide exchange reactivities of LMW thiols with DTNB.

Thiol	k_1 [$\text{s}^{-1} \text{ M}^{-1}$]	[RSH] [mM] ^[b]	[RS [–]] [μM] ^[b]	Physiological rate [$\text{s}^{-1} \times 10^6$] ^[b]	relative ^[c]
BSH	$(0.95 \pm 0.04) \times 10^5$	1.22	267	2.54	100
Cys	$(0.49 \pm 0.01) \times 10^5$	0.20	29	0.14	5.5
CoA	$(1.98 \pm 0.08) \times 10^5$	0.46	3	0.06	2.4
GSH ^[a]	$(2.02 \pm 0.14) \times 10^5$	10	556	11.2	441
MeO-GlcN-Cys	$(0.86 \pm 0.03) \times 10^5$				

[a] A typical intracellular GSH concentration of 10 mM in Gram-negative bacteria has been used here for the purpose of comparison. [b] Based on intracellular pH 7.7 in *B. subtilis*^[22] and cellular thiol concentrations measured during mid-exponential growth ($\text{OD}_{600} = 1.40$). [c] Relative to the BSH rate normalised to 100.

times less reactive, respectively. The pH-independent rate constant of MeO-GlcN-Cys is comparable to that of BSH; this indicates that the carboxylate groups of the malate aglycone do not influence the reactivity of BSH in this thiol–disulfide exchange reaction. Although BSH is more sterically hindered, its pH-independent rate constant is 40% faster than that of Cys. The relative reactivities of these thiols with other disulfide substrates might differ depending on complementary/repulsive thiol–disulfide binding interactions that could enhance or deplete reactivity accordingly.

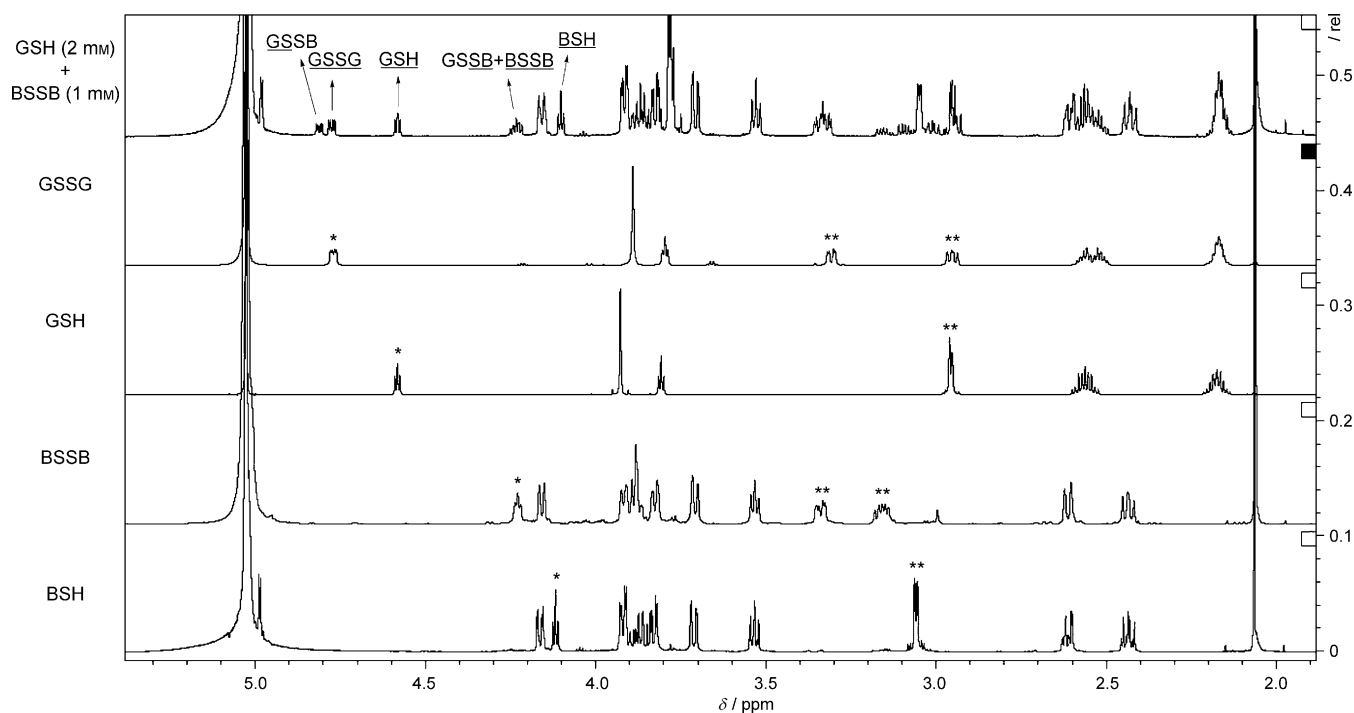


Figure 2. Redox potential determination. Overlay of ^1H NMR spectra (pD 7.0, 5°C , 800 MHz) for reaction between BSSB (1 mM) and GSH (2 mM) after equilibrium, together with pure samples of BSH, BSSB, GSH and GSSG. Cysteinyll protons are indicated as * $\text{CH}\alpha$ and ** $\text{CH}_2\beta$.

However, it is worth noting that the fourfold difference in the relative reactivities of Cys and CoA thiolates with DTNB is comparable to the previously reported ninefold difference in their relative reactivities with GSSG.^[21] This suggests that reactivity with DTNB is a reasonable model for comparing the relative thiol–disulfide exchange reactivities of these LMW thiols.

Although the pH-independent thiol–disulfide exchange reactivity of CoA appears to be greater than for BSH, CoA has a much higher thiol pK_a and lower intracellular abundance than BSH. To illustrate the impact this is likely to have on the relative chemical reactivities of these biothiols in vivo, their k_1 values were corrected for their respective thiolate concentrations during mid-exponential growth and at physiological pH (pH 7.7 for *B. subtilis*,^[22] Table 3). The results of this analysis suggest that, under these physiological conditions, BSH would be 18 and 40 times more chemically reactive than Cys and CoA, respectively. Such differences could vary even more as the relative cellular concentrations of these biothiols change during different stages of growth.

Bacillithiol redox potential

The thiol–disulfide redox potential of BSH ($E_{\text{BSSB}/\text{BSH}}^0$) was determined by measuring the thiol/disulfide equilibrium constants for BSH and GSH in both the forward (BSH/GSSG) and reverse (BSSB/GSH) directions. High-field (800 MHz) proton NMR provided sufficient resolution of the resonances associated with the cysteinyl α -protons for BSH, BSSG, GSH and GSSG for their equilibrium ratios to be quantified (Figure 2). At 25°C , the peaks associated with the α -protons of the cysteine motifs in GSSG and BSSG were obscured by the HOD solvent peak of

the equilibration buffer. However, the temperature dependence of the HOD chemical shift^[23] enabled these to be revealed when NMR spectra were measured at 5°C . Signals for the BSH cysteinyl α -protons in BSSB and BSSG presented a set of overlapping multiplets, so BSSB was quantified indirectly by subtracting the BSSG integral value (4.81 ppm) from the overlapping multiplets (at 4.23–4.29 ppm). These were then used to calculate $E_{\text{BSSB}/\text{BSH}}^0$ relative to the previously calculated GSH redox potential ($E_{\text{GSSG}/\text{GSH}}^0 = -240\text{ mV}$)^[24] by use of the Nernst equation. Thiol redox potentials for Cys and CoA have previously been determined by similar methods,^[21] relative to $E_{\text{GSSG}/\text{GSH}}^0 = -205\text{ mV}$.^[25] Here these literature values have been corrected so they can be compared with $E_{\text{BSSB}/\text{BSH}}^0$ relative to the more accurate $E_{\text{GSSG}/\text{GSH}}^0$ value of -240 mV .^[24] The measured standard thiol redox potential of BSH (-221 mV) is comparable with that of Cys (-223 mV) and higher than those reported for GSH (-240 mV), CoA and γ -glutamylcysteine (-234 mV ; Table 4).

BSH levels in *B. subtilis*

The intracellular LMW thiol and disulfide concentrations were quantified during different stages of growth of *B. subtilis*, from early exponential to late stationary phase (Figure 3A). LMW thiols were analysed by treating cells with the fluorescent thiol labelling reagent monobromobimane, and the bimane-labelled thiols in the cell extracts were then quantified by HPLC. For disulfide analyses, thiols were first capped by treatment of cells with *N*-ethylmaleimide before reduction of the disulfides (with dithiothreitol), so they could then be quantified after bimane labelling. In *B. subtilis* cultured in LB medium, the intracellular

Table 4. Thiol–disulfide redox potentials ($E_{\text{RSSR}/\text{RSH}}^{\circ}$).		
Thiol	$E_{\text{RSSR}/\text{RSH}}^{\circ}$	Ref.
GSH	−240	[24], [43]
γ GC	−234	[44]
CoA	−234 ^[a]	[21]
Cys	−223 ^[a]	[21]
BSH	−221 ± 3	this study

[a] Previously reported values have been corrected relative to $E_{\text{GSH}/\text{GSSG}}^{\circ} = -240 \text{ mV}$.^[24]

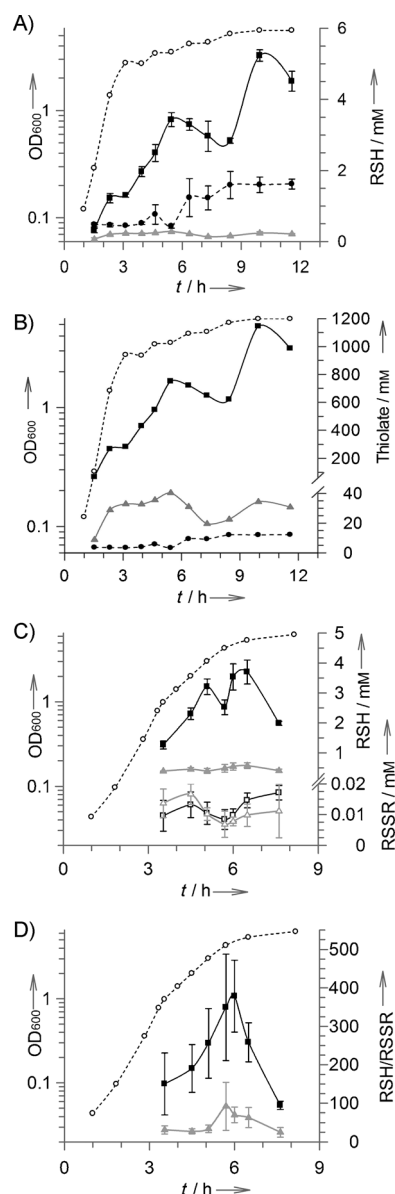


Figure 3. A) Variations in intracellular BSH (■), Cys (▲) and CoA (●) levels* during different growth phases (---) of *B. subtilis*. B) Thiolate levels* of BSH (■), Cys (▲) and CoA (●). C) Thiol and disulfide levels* of BSH (■), Cys (▲), BSSB (□) and (Cys)₂ (Δ). D) Thiol–disulfide redox ratios of BSH/BSSB (■) and Cys/(Cys)₂ (▲). * Intracellular thiol concentrations are derived from the thiol content ($\mu\text{mol g}^{-1}$ rdw) based on previous calculations of 1 μL of intracellular water content per mg rdw in *B. subtilis*^[28] (i.e., 1 $\mu\text{mol g}^{-1}$ rdw = 1 mM).

Cys concentration is maintained at a consistently low level (≈ 0.13 – 0.28 mM) throughout all stages of growth. The CoA concentration remains relatively constant ($\approx 0.5 \text{ mM}$) during exponential growth, but then increases threefold during stationary phase. Interestingly, the BSH level increases during exponential growth and then temporarily decreases in early stationary phase ($\text{OD}_{600} = 3.5$ – 5.2), before rapidly recovering in late stationary phase to a peak value (5.2 mM) ≈ 17 times higher than for Cys and ≈ 3.5 times higher than for CoA at the same time point. However, conversion of these thiol levels into thiolate levels at physiological pH shows how cellular concentrations of Cys thiolate exceed those of CoA thiolate by two to tenfold during different stages of growth (Figure 3B). BSH thiolate levels are consistently higher than the thiolate levels of Cys and CoA by one to two orders of magnitude.

In a separate set of experiments, the thiol/disulfide ratios of BSH and Cys were also determined (Figure 3C). BSSB and cystine concentrations are maintained between 7–17 μM , and are at their lowest levels as the cells approach stationary phase, when a reduction in BSH is also observed. Throughout the growth curve, the thiol/disulfide ratio for BSH (ranging from 100:1 to 400:1) is consistently higher than that for Cys (25:1 to 90:1) (Figure 3D). For both thiols, these redox ratios peak during early stationary phase growth.

Discussion

Unlike in the case of GSH, which in some Gram-negative bacteria can be present in significant excess over Cys (e.g., > 200 -fold in *E. coli*),^[26] previous thiol analyses of BSH-utilising bacteria have reported much lower levels of BSH that are often equivalent to—or no more than six times higher than—those of Cys.^[10,12,13,27] Most of these reported measurements were only taken from cell culture samples at a single time point, usually during mid-exponential growth. The original analyses of BSH content in *B. subtilis*, as well as a number of other Firmicutes, reported BSH levels of 0.2–0.7 $\mu\text{mol g}^{-1}$ residual dry weight (rdw). The intracellular concentrations of BSH were then estimated on the basis of the global assumption that all of the bacteria analysed contained $\approx 3 \mu\text{L}$ of intracellular water per mg of dry weight.^[10] For 0.6 $\mu\text{mol g}^{-1}$ rdw, this equates to an intracellular BSH concentration of approximately 0.2 mM. However, the rdw to intracellular water ratios are not the same in all bacteria. For *B. subtilis* $\approx 50\%$ of cell mass has been calculated as being intracellular water,^[28] so a BSH measurement of 0.6 $\mu\text{mol g}^{-1}$ rdw in *B. subtilis* equates to an intracellular concentration of 0.6 mM (i.e., three times higher than previously reported).

Here, *B. subtilis* BSH concentrations have also been shown to increase significantly during exponential growth (Figure 3A). Collectively, this indicates that BSH levels higher than those previously reported and comparable to GSH levels observed in some Gram-negative bacteria can be attained.^[26] As *B. subtilis* approaches stationary phase there is a temporary decrease in BSH (by $\approx 1 \text{ mM}$) that cannot be accounted for in terms of a compensatory increase in BSSB. Some of this BSH might be diverted into protein bacillithiolation^[13] to help regulate func-

tion during the transition from exponential to stationary phase. Proof of this, and of whether or not such BSH oscillations are observed in other BSH-producing bacteria, remains to be seen. The observed variations in BSH levels in *B. subtilis* do not necessarily represent what will be observed in all other BSH-producing bacteria; recent studies in *S. aureus*, for example, have shown that BSH levels appear to remain constant during exponential growth.^[11] As observed here for *B. subtilis*, a similar decrease in BSH levels is observed during early stationary phase, but those analyses were not continued into late stationary phase, so it is currently not clear if this decrease in BSH levels in *S. aureus* recovers during late stationary phase growth.^[11]

The standard redox potential of BSH (−221 mV) is higher than that of GSH (−240 mV), which implies it has a lower capacity to buffer oxidative stress than GSH does. Redox potentials are a thermodynamic property based on thiol–disulfide exchange equilibria. In living cells, however, although the redox status can be maintained in a steady state, it is never at equilibrium.^[29] Coupled with those of Cys and CoA, knowledge of the BSH/BSSB standard redox potential could prove to be a useful parameter for quantifying disturbances in redox metabolism of BSH-utilising microorganisms. However, the actual redox buffering properties of BSH are likely to be driven by other factors (i.e., cellular abundances and catalytic efficiencies of BSH-specific redox enzymes). A number of BSSB reductases have so far been proposed,^[10,12,30] but none of these has yet been isolated and characterised in detail. In *B. subtilis* the BSH/BSSB ratios are always maintained at a high level in favour of BSH (> 100:1), and these ratios are always greater than those of Cys/Cys₂ (Figure 3C and D).

Interestingly, amongst BSH-producing bacteria, phylogenetic profiling has identified a glutaredoxin-like protein (YphP) as a candidate bacilliredoxin.^[12] YphP also has a remarkably high redox potential (−118 mV)^[31] relative to typical glutaredoxins (−200 mV).^[24] It will be interesting to see whether or not the redox potential differences between BSH and GSH systems are counterbalanced by differences in the kinetics of the enzymes that regulate the intracellular BSH redox status.

During exponential growth, the BSH/BSSB redox ratio continues to increase, but the increases in BSH cannot be accounted for by compensatory reductions in BSSB. The increases in BSH are most likely to arise from BSH biosynthesis, whereas the decreases (in early and late stationary phase) could potentially be accounted for by increased protein bacillithiolation and/or metabolic degradation of BSH. Proof of this, however, remains to be seen.

The thiol group in BSH is more acidic than those in Cys, CoA and GSH (Table 1). At physiological pH (i.e., pH 7.7 in *B. subtilis*),^[22] the percentages of thiolate for BSH, Cys and CoA are 22, 15 and 1%, respectively (Table 2). The significance of this becomes evident when the cellular LMW thiol concentrations in *B. subtilis* are converted into the corresponding thiolate concentrations at physiological pH (Figure 3B). This shows that bacillithiolate levels are significantly higher than the thiolate anion concentrations of Cys and CoA. The predominance of the BS thiolate most probably accounts for enhanced chemical

reactivity of BSH with different electrophilic biomolecules within the cell.

During oxidative stress, protein thiols can be oxidised to their sulfenic acids. Under these conditions, LMW thiols can react with the sulfenic acids to trap them as mixed disulfides (i.e., protein-SOH + RSH → protein-SSR + H₂O), preventing further oxidation to the sulfinic and irreversibly damaged sulfonic acid derivatives. Analogously to the role of GSH in Gram-negative bacteria, protein S-bacillithiolation is now emerging as an important thiol redox mechanism for the regulation of protein function during oxidative stress.^[13,14,32,33] In *B. subtilis* the redox-sensitive peroxiredoxin transcription regulator (OhrR) is bacillithiolated during cumene hydroperoxide stress; this suggests a function for BSH in redox sensing.^[32,33] Interestingly, smaller quantities of Cys-OhrR and CoA-OhrR protein mixed disulfides are also observed during mass spectrometric analysis of OhrR purified from cumene-hydroperoxide-stressed *B. subtilis*. To date, 37 different proteins that are S-bacillithiolated in *B. subtilis* and other BSH-producing microorganisms under hypochlorite (NaOCl) stress have been identified.^[13,14] These include several proteins involved in amino acid, cofactor and nucleotide biosynthesis, as well as some translation factors, chaperones and redox proteins. With some of these proteins (e.g., methionine synthase (MetE)) S-cysteinylation has also been observed as a less abundant redox modification that becomes more prominent in BSH-deficient mutants.^[13,14] Although the chemical rates of reaction between LMW biothiols and physiologically relevant disulfides (e.g., cystine, GSSG) are too slow to be of metabolic significance,^[21,34] their chemical reactivities are much faster with more reactive protein sulfenic acids and sulphenyl chlorides (e.g., produced under peroxide and hypochlorite stress), as well as with S-nitrosylated thiols and thiyl radicals, which react to form protein mixed disulfides.^[35] If the physiologically corrected differences in the reactivities of BSH, Cys and CoA with DTNB (Table 3) are mirrored in their reactivities with sulfenic acids and sulphenyl chlorides, this could explain why mixtures of BS-, Cys- and CoA-protein mixed disulfides have been observed in oxidatively stressed *B. subtilis*, with bacillithiolation being the most abundant protein-S-thiolation process in response to oxidative stress.^[13,14] It will be interesting to see whether or not this is observed in other BSH-producing bacteria such as *S. aureus*, in which thiolate concentrations of BSH and Cys are more comparable. Whereas many LMW-thiol-mediated processes are enzyme-catalysed, the detoxification of reactive carbonyl electrophiles (e.g., methylglyoxal) is dependent on an initial nonenzymatic reaction with the LMW thiol to form a hemithioacetal, which, in GSH-utilising organisms, is converted into lactate by the glyoxalase enzymes (Glx-I-II).^[36] Although no BSH-dependent glyoxalases have yet been characterised, BSH null mutants display increased sensitivity to methylglyoxal.^[12,30] Significantly greater intracellular bacillithiolate concentrations suggest that BSH, rather than Cys, would be the preferential reactant with such electrophiles *in vivo*.

It has been suggested that BSH could function as a metal ion chelator *in vivo*, due to the proximity of the thiol, amino and malate carboxylate groups.^[10] BSH null mutants display

enhanced sensitivity to Cu^{2+} , Cd^{2+} and dichromate ($\text{Cr}_2\text{O}_7^{2-}$) metal ion toxicity.^[30] In vitro, BSH is also able to prevent Zn^{2+} activation of the metallothiol-S-transferase FosB by sequestering the divalent metal cation.^[11] At physiological pH, both malate carboxylate groups of BSH are fully deprotonated (i.e., ideal for bidentate metal coordination). At this pH, most of the thiolate in both BSH and Cys resides is associated with a protonated amine ($-\text{S}-\text{NH}_3^+$; Table 2). Of the total BSH, 37% has both thiol and amino groups protonated ($\text{HS}-\text{NH}_3^+$; 79% for Cys), whereas 42% has an uncharged amine group and a protonated thiol ($\text{HS}-\text{NH}_2$; only 6% for Cys). The propensity to form these different protonation forms of BSH at physiological pH might influence how effectively it can coordinate metal ions in a mono-, di-, tri- or tetradentate manner. The malate aglycone clearly influences the acidities of the thiol and amino groups of BSH. Therefore, if BSH does prove to play a role in metal ion chelation/trafficking in vivo, it will be interesting to see whether or not metal ions influence the thiol acidity (and potential cellular thiolate concentrations).

Conclusions

There are clearly some differences between the biophysical characteristics of BSH and those of other, structurally distinct, and more extensively studied, LMW thiols. It will be interesting to see whether and how these are reflected in the unexplored metabolic functions of BSH (e.g., in redox regulation, xenobiotic detoxification, metal ion homeostasis), which are likely to be driven by its chemical and biophysical properties, as well as those of the enzymes that utilise BSH as a substrate or cofactor to mediate such biochemical processes.

Experimental Section

General: BSH^[37] and MeO-GlcN-Cys^[11] were chemically synthesised as described previously. Stock solutions of all thiols were quantified by titration against DTNB (2 mM) in phosphate buffer (pH 7.5) and measurement of the absorbance increase at 412 nm ($\epsilon = 14150 \text{ M}^{-1} \text{ cm}^{-1}$) due to formation of 5-thio-2-nitrobenzoic acid (TNB).^[38] Accurate stock solutions of DTNB were prepared by quantification of the TNB thiolate anion formed when DTNB was reduced by a large (tenfold) excess of tris-carboxyethyl phosphine (TCEP). Disulfides (BSSB, GSSG) were prepared from titrated quantities of BSH and GSH, which were then oxidised by treatment with aqueous NH_4HCO_3 (33 mM) under aerobic conditions as previously described.^[37] All malate carboxylate, thiol pK_a and thiol–disulfide reaction kinetics data were analysed with the appropriate equations and use of GraFit Version 5 (Erithacus Software, Ltd). NMR spectra were recorded with Varian 800 MHz or Bruker 400 MHz spectrometers. Chemical shifts for NMR are measured in parts per million (δ) relative to HOD (5.03 ppm at 5 °C)^[23] with use of internal standards acetonitrile (2.06 ppm) and dioxane (67.19 ppm) for ^1H and ^{13}C NMR, respectively. Coupling constants (J) are quoted in hertz (Hz). NMR spectra were recorded at 5 °C for redox titrations and 25 °C for pK_a determinations. UV absorbance measurements were performed with a PerkinElmer UV Lambda 25 spectrophotometer and quartz cuvettes (1 cm pathlength). The *B. subtilis* CU1065 wild-type strain was generously provided by Prof. John Helmann (Cornell University).

Carboxylate pK_a measurements for BSH: Macroscopic pK_a values for the malate carboxylate groups of BSH were determined by nonlinear regression analysis of plots of ^{13}C NMR chemical shifts of the malate carbons (δ_{obs}) versus pD with use of Equation (1a), where pK_a and pK_a' are the macroscopic acid dissociation constants, and *Lim* is the inflection point on the biphasic curve.

$$\delta_{\text{obs}} = \frac{\text{lim} \times 10^{(\text{pD}-\text{pK}_a)}}{10^{(\text{pD}-\text{pK}_a)} + 1} - \frac{(\text{lim}-100) \times 10^{(\text{pD}-\text{pK}_a')}}{10^{(\text{pD}-\text{pK}_a')} + 1} \quad (1a)$$

pH determinations were performed with an InLab Flex-Micro pH probe and Jenway 3510 pH meter. pH measurements in D_2O solutions were corrected for the deuterium isotope effect by use of the equation $\text{pD} = \text{pH} + 0.40$.^[39] A solution of BSH (50 mM in D_2O) was acidified to pD 2.1 with DCl (1 M). Stepwise increases in pD were achieved by the addition of NaOD (1 M or 200 mM in D_2O). NMR analyses were carried out at increasing pD values ranging from pD 2.1 to pD 5.6 (at ≈ 0.2 pD increments). The final macroscopic pK_a values were the mean values of those determined from titration curves for each of the four carbons on the malate aglycone.

Thiol and amine pK_a measurements for BSH, MeO-GlcN-Cys and Cys: Macroscopic and microscopic pK_a values were measured by adopting procedures previously described for Cys anion.^[17,18,40] A total of 27 solutions of sodium phosphate buffers (100 mM), ranging from pH 4.85 to pH 12.6 in ≈ 0.25 pH increments, were prepared. These were made from mixtures of mono-/disodium phosphate (pH 4.85–9.74) and disodium phosphate + NaOH (pH 10.04–12.6). Thiol stock solutions were freshly prepared in ultrapure water on the day of use. All experiments were conducted at 25 °C in quartz cuvettes in a final volume of 1 mL. After blanking of the buffer, the thiol (to a final concentration of 40 μM) was added and rapidly mixed, and the UV absorbance at 232 nm (Abs_{232}) was immediately measured to detect the thiolate anion. In control experiments (at pH 12), continuous monitoring of the UV absorbance revealed that the Abs_{232} value decreased by < 5% during the first 10 min under aerobic conditions. This demonstrates that the measurement made immediately after mixing was sufficiently accurate without thiolate measurements being underestimated due to base-catalysed thiol oxidation. The Abs_{232} values at pH 4.85 and 12.6 were normalised to 0% and 100% thiolate content, respectively. The macroscopic pK_a values of the thiol and amino groups of BSH, MeO-GlcN-Cys and Cys were determined by nonlinear regression analysis of a plot of fraction of thiol in its thiolate form (α_s) versus pH fitted to Equation (1b), where pK_a and pK_a' are the macroscopic acid dissociation constants, and *Lim* is the inflection point on the biphasic curve.

$$\alpha_s = \frac{\text{lim} \times 10^{(\text{pH}-\text{pK}_a)}}{10^{(\text{pH}-\text{pK}_a)} + 1} - \frac{(\text{lim}-100) \times 10^{(\text{pH}-\text{pK}_a')}}{10^{(\text{pH}-\text{pK}_a')} + 1} \quad (1b)$$

For the thiol and amino groups, the microscopic acid dissociation constants (k_s , k_n , k_{sn} and k_{ns} , Figure 1B) were calculated from Equations (2)–(5):

$$K_a = k_s + k_n \quad (2)$$

$$\frac{1}{K_{a'}} = \frac{1}{k_{\text{sn}}} + \frac{1}{k_{\text{ns}}} \quad (3)$$

$$K_a K_{a'} = k_{\text{sn}} k_s + k_{\text{ns}} k_n \quad (4)$$

$$k_s = \alpha_s ([\text{H}^+] + K_a) - \frac{K_a K_{a'}}{[\text{H}^+]} (1 - \alpha_s) \quad (5)$$

After Equation (5) had been used to calculate k_g , the other three microscopic constants were calculated from Equations (2) and (4).

Thiol–disulfide exchange rate constants: All reactions were carried out at 30 °C in disposable cuvettes (1 mL final assay volume) in sodium phosphate buffer (100 mM) and at pH 4.58 for all thiols that were analysed, except for CoA, for which reactions were conducted at pH 5.54. Reactions were carried out at pH values well below the thiol pK_a values to ensure that the reactions could proceed at measurable rates. The reactivity of each thiol was monitored at five different concentrations (2–100 μM), and each experiment was carried out in duplicate. Reactions were initiated by the addition of the thiol to a buffered solution of DTNB (40 μM), which was rapidly mixed, and the initial linear rate of TNB production was monitored for 20 s by measuring the increase in absorbance at 412 nm. Under these conditions, the initial rates were measured within the first 2% of total thiol consumption, allowing the assumption that $[\text{RS}^-]_t = [\text{RS}^-]_0$ and enabling the rate Equation (6) for this reaction:

$$\nu = \frac{d[\text{TNB}]}{dt} = k_1[\text{RS}^-][\text{DTNB}] \quad (6)$$

alternatively expressed as Equation (7):

$$\nu = \frac{d[\text{TNB}]}{dt} = k_{\text{obs}}([\text{DTNB}]_0 - [\text{TNB}]_t) \quad (7)$$

and subsequently integrated to give Equation (8), where k_{obs} is the observed reaction rate (s^{-1}) for the specified reaction conditions.

$$\ln \frac{d[\text{TNB}]_0 - [\text{TNB}]_t}{[\text{DTNB}]_0} = k_{\text{obs}} t \quad (8)$$

The k_{obs} values at different thiol concentrations were obtained from the linear fit of $\ln\{([\text{DTNB}]_0 - [\text{TNB}]_t)/[\text{DTNB}]_0\}$ versus time (t). Because $k_{\text{obs}} = k[\text{RS}^-]$, a replot of k_{obs} versus $[\text{RS}^-]$ was then used to obtain the pH-independent rate constant (k_1).

Redox potentials: Deuterated phosphate buffer (50 mM, pD 7.0) was prepared by dissolving monobasic sodium phosphate (0.215 g) and dibasic sodium phosphate (0.133 g) in D_2O (40 mL). The pH was adjusted to 6.6 by addition of a small amount of solid dibasic sodium phosphate. Acetonitrile (100 μL) was added as an internal standard. The buffer was deoxygenated by purging with dry nitrogen gas. The final volume was adjusted to 50 mL with deoxygenated D_2O under nitrogen in a glovebox. The resultant buffer was then stored in the glovebox and used for all the thiol–disulfide exchange experiments.

NMR tubes and solid samples of all thiols and disulfides were kept under nitrogen in a glovebox for at least 24 h prior to the preparation of stock solutions in deoxygenated deuterated buffer. Equilibrium mixtures were prepared with appropriate volumes of the corresponding thiol (BSH or GSH) and disulfide (GSSG or BSSB). The volume was then adjusted to 500 μL with deuterated buffer to obtain final thiol/disulfide ratios of 2:1 or 4:1 (mM). These solutions were transferred to separate NMR tubes and allowed to equilibrate in the glovebox for at least 36 h. The thiol/disulfide ratios were monitored by proton NMR every 8–12 h until equilibrium was reached.

Equilibrated thiol and disulfide ratios were determined by integration of their cysteinyl CH_α protons, the chemical shifts of which were as follows: BSH ($\delta = 4.13$ ppm, t, $J = 5.9$ Hz), BSSB ($\delta =$

4.27 ppm, t, $J = 6.4$ Hz), GSH ($\delta = 4.58$ ppm, t, $J = 5.8$ Hz), GSSG ($\delta = 4.77$ ppm, dd, $J = 9.8, 4.3$ Hz), GSSB ($\delta = 4.81$ ppm, dd, $J = 9.9, 4.3$ Hz), GSSB ($\delta = 4.23$ – 4.29 ppm, m, overlapping the BSSB CH_α signal). These values were used to calculate the equilibrium constant [K_c , Equation (9)], which was then used to calculate the BSH redox potential relative to the previously calculated GSH/GSSG redox potential ($E_{\text{GSSG/GSH}}^{\text{G}} = -240$ mV)^[24] by using the Nernst equation [Equation (10)]. In Equation (10), R is the gas constant ($8.314 \text{ J K}^{-1} \text{ mol}^{-1}$), F is the Faraday constant ($9.65 \times 10^4 \text{ C mol}^{-1}$), T is the absolute temperature (K), and n is the number of electrons transferred = 2.

$$K_c = \frac{[\text{BSSB}][\text{GSH}]^2}{[\text{BSH}]^2[\text{GSSG}]} \quad (9)$$

$$E_{\text{BSSB/BSH}}^{\text{G}} = E_{\text{GSSG/GSH}}^{\text{G}} - \frac{RT}{nF} \ln K_c \quad (10)$$

Thiol quantification in *B. subtilis*: *B. subtilis* CU1065 was grown in triplicate cultures in LB medium. The OD_{600} value was monitored, and samples, corresponding to approximately 5 mg or 30 mg (for thiol or disulfide analysis, respectively) rdw of cells, were harvested from each culture at various times. Cell pellets were frozen at -20 °C until derivatisation with monobromobimane (mBBBr).

Thiol^[13] and disulfide^[26] analyses were performed as described previously, with some minor modifications (see the Supporting Information). BSmB and CySmB were separated by HPLC as previously described^[13] (Method A; see the Supporting Information). CoAmB was analysed by modification of a previously described method^[10] with use of a shortened gradient (Method B; see the Supporting Information). Detection was carried out with a Jasco fluorescence detector (FP-2020 Plus) with excitation at 385 nm and emission at 460 nm, and a gain of $1 \times$. BSmB and CySmB eluted at 11.8 min and 14.3 min, respectively (Method A). CoAmB eluted at 15.4 min (Method B). All samples were quantified by comparison with BSmB, CysmB and CoAmB standards of known concentration, and the results were converted to $\mu\text{mol RSH g}^{-1}$ rdw. For *B. subtilis*, a thiol quantity of $1 \mu\text{mol g}^{-1}$ rdw equates to a cellular concentration of 1 mM .^[28]

Acknowledgements

This work was financially supported by a BBSRC grant BB/H013504/1 and an EU FP-7 ITN grant, number 215009.

Keywords: ionization potentials • NMR spectroscopy • redox chemistry • thiol–disulfide exchange • thiols

- [1] L. Masip, K. Veeravalli, G. Georgioui, *Antioxid. Redox Signaling* **2006**, *8*, 753–762.
- [2] R. C. Fahey, G. L. Newton in *Functions of Glutathione Biochemical, Physiological, Toxicological and Clinical Aspects* (Eds.: A. Larsson, A. Holmgren, B. Mannervik, S. Orrenius), Raven, New York, **1983**, pp. 251–260.
- [3] I. Dalle-Donne, R. Rossi, D. Giustarini, R. Colombo, A. Milzani, *Free Radical Biol. Med.* **2007**, *43*, 883–898.
- [4] For a review, see: P. Ghezzi, *Free Radical Res.* **2005**, *39*, 573–580.
- [5] G. P. Ferguson, S. Totemeyer, M. J. MacLean, I. R. Booth, *Arch. Microbiol.* **1998**, *170*, 209–219.
- [6] V. K. Jothivasan, C. J. Hamilton, *Nat. Prod. Rep.* **2008**, *25*, 1091–1117.
- [7] G. L. Newton, N. Buchmeier, R. C. Fahey, *Microbiol. Mol. Biol. Rev.* **2008**, *72*, 471–494.
- [8] M. Rawat, Y. Av-Gay, *FEMS Microbiol. Rev.* **2007**, *31*, 278–292.
- [9] C. E. Hand, J. F. Honek, *J. Nat. Prod.* **2005**, *68*, 293–308.

- [10] G. L. Newton, M. Rawat, J. J. La Clair, V. K. Jothivasan, T. Budiarto, C. J. Hamilton, A. Claiborne, J. D. Helmann, R. C. Fahey, *Nat. Chem. Biol.* **2009**, *5*, 625–627.
- [11] A. A. Roberts, S. V. Sharma, A. W. Strankman, S. R. Duran, M. Rawat, C. J. Hamilton, *Biochem. J.* **2013**, *451*, 69–79.
- [12] A. Gaballa, G. L. Newton, H. Antelmann, D. Parsonage, H. Upton, M. Rawat, A. Claiborne, R. C. Fahey, J. D. Helmann, *Proc. Natl. Acad. Sci. USA* **2010**, *107*, 6482–6486.
- [13] B. K. Chi, A. A. Roberts, T. T. Huyen, K. Bäsell, D. Becher, D. Albrecht, C. J. Hamilton, H. Antelmann, *Antioxid. Redox Signaling* **2013**, *18*, 1273–1295.
- [14] B. K. Chi, K. Gronau, U. Mäder, B. Hessling, D. Becher, H. Antelmann, *Mol. Cell. Proteomics* **2011**, *10*, M111.009506.
- [15] K. Van Laer, C. J. Hamilton, J. Messens, *Antioxid. Redox Signaling* **2013**, *18*, 1642–1653.
- [16] K. M. Jones in *Data for Biochemical Research* (Ed(s): R. M. C. Dawson, D. C. Elliott, W. H. Elliott), Oxford University Press, London, **1962**, 28–43.
- [17] G. E. Clement, T. P. Hartz, *J. Chem. Educ.* **1971**, *48*, 395–397.
- [18] R. E. Benesch, R. Benesch, *J. Am. Chem. Soc.* **1955**, *77*, 5877–5881.
- [19] P. Nagy, *Antioxid. Redox Signaling* **2013**, *18*, 1623–1641.
- [20] M. Moutiez, D. Mezianecherif, M. Aumercier, C. Sergheraert, A. Tartar, *Chem. Pharm. Bull.* **1994**, *42*, 2641–2644.
- [21] D. A. Keire, E. Strauss, W. Guo, B. Noszal, D. L. Rabenstein, *J. Org. Chem.* **1992**, *57*, 123–127.
- [22] R. D. Kitko, R. L. Cleeton, E. I. Armentrout, G. E. Lee, K. Noguchi, M. B. Berkmen, B. D. Jones, J. L. Slonczewski, *PLoS One* **2009**, *4*, e8255.
- [23] H. E. Gottlieb, V. Kotlyar, A. Nudelman, *J. Org. Chem.* **1997**, *62*, 7512–7515.
- [24] F. Åslund, K. D. Berndt, A. Holmgren, *J. Biol. Chem.* **1997**, *272*, 30780–30786.
- [25] R. P. Szajewski, G. M. Whitesides, *J. Am. Chem. Soc.* **1980**, *102*, 2011–2026.
- [26] G. L. Newton, K. Arnold, M. S. Price, C. Sherrill, S. B. Delcardayre, Y. Aharonowitz, G. Cohen, J. Davies, R. C. Fahey, C. Davis, *J. Bacteriol.* **1996**, *178*, 1990–1995.
- [27] D. Parsonage, G. L. Newton, R. C. Holder, B. D. Wallace, C. Paige, C. J. Hamilton, P. C. Dos Santos, M. R. Redinbo, S. D. Reid, A. Claiborne, *Biochemistry* **2010**, *49*, 8398–8414.
- [28] G. Bratbak, I. Dundas, *Appl. Environ. Microbiol.* **1984**, *48*, 755–757.
- [29] L. Flohé, *Biochim. Biophys. Acta Gen. Subj.* **2013**, *1830*, 3139–3142.
- [30] A. Rajkarnikar, A. W. Strankman, S. R. Duran, D. Vargas, A. A. Roberts, K. Barretto, H. Upton, C. J. Hamilton, M. Rawat, *Biochem. Biophys. Res. Commun.* **2013**, *436*, 128–133.
- [31] U. Derewenda, T. Boczek, K. L. Gorres, M. Yu, L. W. Hung, D. Cooper, A. Joachimiak, R. T. Raines, Z. S. Derewenda, *Biochemistry* **2009**, *48*, 8664–8671. In this paper a YphP redox potential of –130 mV was calculated by using a GSH standard redox potential of –252 mV in the Nernst equation. Here we have adjusted this value to –118 mV relative to the GSH standard redox potential of –240 mV that we used for BSH redox potential calculations.
- [32] J. W. Lee, S. Soonsanga, J. D. Helmann, *Proc. Natl. Acad. Sci. USA* **2007**, *104*, 8743–8748.
- [33] S. Soonsanga, J. W. Lee, J. D. Helmann, *Mol. Microbiol.* **2008**, *68*, 978–986.
- [34] D. P. Jones, Y.-M. Go, C. L. Anderson, T. R. Ziegler, J. M. Kinkade, Jr., W. G. Kirlin, *FASEB J.* **2004**, *18*, 1246–1248.
- [35] M. M. Gallogly, J. J. Mieyal, *Curr. Opin. Pharmacol.* **2007**, *7*, 381–391.
- [36] M. P. Kalapos, *Toxicol. Lett.* **1999**, *110*, 145–175.
- [37] S. V. Sharma, V. K. Jothivasan, G. L. Newton, H. Upton, J. I. Wakabayashi, M. G. Kane, A. A. Roberts, M. Rawat, J. J. La Clair, C. J. Hamilton, *Angew. Chem.* **2011**, *123*, 7239–7242; *Angew. Chem. Int. Ed.* **2011**, *50*, 7101–7104.
- [38] P. W. Riddles, R. L. Blakeley, B. Zerner, *Methods Enzymol.* **1983**, *91*, 49–60.
- [39] D. A. Keire, D. L. Rabenstein, *Bioorg. Chem.* **1989**, *17*, 257–267.
- [40] A. G. Splittgerber, L. L. Chinander, *J. Chem. Educ.* **1988**, *65*, 167–170.
- [41] D. L. Rabenstein, *J. Am. Chem. Soc.* **1973**, *95*, 2797–2803.
- [42] D. A. Keire, J. M. Robert, D. L. Rabenstein, *J. Org. Chem.* **1992**, *57*, 4427–4431.
- [43] J. Rost, S. Rapoport, *Nature* **1964**, *201*, 185–185.
- [44] S. Birtić, L. Colville, H. W. Pritchard, S. R. Pearce, I. Kranner, *Free Radical Res.* **2011**, *45*, 1093–1102.

Received: June 21, 2013

Published online on October 2, 2013